

AD 652415

AN INVESTIGATION OF THE FATIGUE  
AND CREEP PROPERTIES OF GLASS REINFORCED  
PLASTICS FOR PRIMARY AIRCRAFT STRUCTURES

Final Report  
(1 May 1965 to 1 December 1966)  
April 1967

by

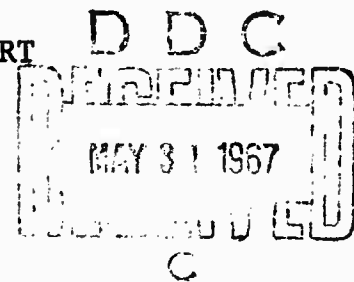
K. E. Hofer, Jr.  
E. M. Olsen

Prepared Under Contract No. NOW 65-0425-f

for

Naval Air Systems Command  
Department of the Navy  
Washington, D. C. 20360

DISTRIBUTION OF THIS REPORT  
IS UNLIMITED



ARCHIVE COPY

AN INVESTIGATION OF THE FATIGUE  
AND CREEP PROPERTIES OF GLASS REINFORCED  
PLASTICS FOR PRIMARY AIRCRAFT STRUCTURES

by

K. E. Hofer, Jr.  
E. M. Olsen

DISTRIBUTION OF THIS REPORT  
IS UNLIMITED

FOREWORD

This is the final report on Research Project M6104 "Investigation of the Fatigue and Creep Properties of Glass Reinforced Plastics for Primary Aircraft Structures" prepared by IIT Research Institute for Naval Air Systems Command under Contract NOW 65-0425-f. The research work described in this report was conducted in the period May 1, 1965 through December 1, 1966. Staff who have made substantial contributions to the work reported herein include J. Anderson, L. C. Bennett, C. K. Cole, K. E. Hofer, E. Koeller, H. Lane and E. M. Olsen.

Respectfully submitted,

IIT RESEARCH INSTITUTE

*K. E. Hofer, Jr.*

K. E. Hofer, Jr.  
Manager, Materials Engineering  
and Building Technology

APPROVED:

*R. H. Cornish*

R. H. Cornish  
Assistant Director  
Mechanics Research Division

KEH/cy

## ABSTRACT

Fatigue of glass reinforced epoxy composite materials is examined from several points of view. High cycle and low cycle fatigue and the effects of frequency, moisture, and state of stress on the fatigue life are included. The effects of creep and strain rate are also studied with a view toward their effect on fatigue life. Cumulative fatigue damage studies include nondestructive ultrasonic techniques applied to damage levels and application of phenomenological theory to the results of two stress level testing. Appendices accompanying the report include 1) a survey of GRP fatigue literature, and 2) a survey of existing cumulative fatigue damage theories with potential application to GRP. Two types of reinforcement were used, uniaxial roving and glass cloth.



## TABLE OF CONTENTS

<u>Section</u>	<u>Page</u>
I. INTRODUCTION	1
II. MATERIALS AND LAMINATE PREPARATION	3
III. SPECIMEN CODING AND IDENTIFICATION	9
IV. STATIC MATERIAL PROPERTIES	11
V. FATIGUE TESTS	27
A. Specimen Configuration	27
B. Frequency and Amplitude Studies	29
C. Effect of Repeated Load Application at an Angle of 45 Deg to Weave - 181/S901 Glass Reinforced Epoxy	41
D. Comparison of Amplitude Fatigue Results of Tests on Similar Epoxy Materials and with Those of Other Investigators	54
E. Fatigue Tests of 143/S901 Glass Cloth Reinforced Epoxy	61
F. Torsional Fatigue: Shear Stress Fatigue of S994 Glass Roving Reinforced Epoxies	61
G. Discussion of Frequency and Amplitude Studies	67
VI. CREEP AND STRAIN RATE TESTS	73
A. Specimens and Testing Procedures: Creep Tests	73
B. Results of Creep Testing	78
C. Strain Rate Effects on 181/S901 Glass Cloth and S994 Uniaxial Roving Reinforced Epoxies	79
VII. EFFECT OF MOISTURE AND COATINGS ON FATIGUE LIFE	97
VIII. CUMULATIVE DAMAGE STUDIES	105
A. Nondestructive Damage Observations - Ultrasonic Tests	105
B. Sequential Amplitude Studies	129

## TABLE OF CONTENTS (Contd)

<u>Section</u>	<u>Page</u>
IX. SUMMARY, CONCLUSIONS AND RECOMMENDATIONS	149
<u>Appendix</u>	
A. LAMINATE BLANKING	153
B. REVIEW OF GRP COMPOSITES FATIGUE TECHNOLOGY	167
C. REVIEW OF CUMULATIVE FATIGUE DAMAGE THEORIED FOR POTENTIAL APPLICATION TO GRP MATERIALS	173
D. TORSIONAL FATIGUE TESTING OF CARBON-FILAMENT REINFORCED PLASTIC TUBE	197
E. STRAIN RATE CALCULATIONS FROM GRIP MOVEMENT OF THE INSTRON UNIVERSAL TESTING MACHINE	199
F. FATIGUE MACHINES AND EQUIPMENT USED IN GRP STUDIES	205
REFERENCES	229

## ILLUSTRATIONS

<u>Figure</u>	<u>Page</u>
1. Fabrication of Test Plates	4,5
2. S994 Glass Rovings Wound onto Plate Mandrel	7
3. Uniaxial Tensile Specimens	12
4. Tension Specimen Optimization Tests	13
5. Stress Concentration Factor, $K_T$ , for Flat Bar with Circular Shoulder Fillet in Tension, from Peterson	16
6. Tension Specimen Used in Static and Fatigue Tests	17
7. Uniaxial Roving Glass Reinforced Epoxy Tab-Ended Specimen	18
8. Uniaxial Glass Roving, Tension Specimen Failures in Static and Fatigue Loading	19
9. Tab-Ended Reduced Section Tensile Specimen Used in Testing 143/S901 Glass Cloth Reinforced Epoxy	22
10. Compression Fixture for Static and Creep Loading of Thin Sheet Laminates (Specimen of 181/S901 Glass Reinforced Epoxy Is Shown in Greatly Exaggerated Exposure)	23
11. Compression Fixture Details	24
12. Bending Fatigue Specimens	28
13. Alternating Stress Versus Cycles to Failure at Several Frequencies for Fully Reversed ( $R = -1$ ) Loading for 181/S901 Glass Cloth Reinforced Epoxy	34

## ILLUSTRATIONS (Contd)

<u>Figure</u>		<u>Page</u>
14.	Alternating Stress Versus Cycles to Failure at Two Frequencies for Fully Reversed ( $R = -1$ ) Loading for S994 Uniaxial Glass Roving Reinforced Epoxy	35
15.	Maximum Stress Versus Cycles to Failure at Several Frequencies for Tension-Zero-Tension ( $R = 0.05$ ) Loading for 181/S901 Glass Cloth Reinforced Epoxy	39
16.	Maximum Stress Versus Cycles to Failure at Several Frequencies for Tension-Zero-Tension ( $R = 0.05$ ) Loading for S994 Glass Roving Reinforced Epoxy	40
17.	Maximum Compressive Stress Versus Cycles to Failure at Three Frequencies for Compression-Zero-Compression ( $R = -10$ ) Loading for 181/S901 Glass Cloth Reinforced Epoxy	44
18.	Maximum Compressive Stress Versus Cycles to Failure at Several Frequencies for Compression-Zero-Compression ( $R = -10$ ) Loading for S994 Glass Roving Reinforced Epoxy	45
19.	Alternating Bending Stress Versus Cycles to Failure at Three Frequencies for Fully Reversed Out-of-Plane Bending ( $R = -1$ ) Loading for 181/S901 Glass Cloth Reinforced Epoxy	48
20.	Alternating Bending Stress Versus Cycles to Failure at Several Frequencies for Fully Reversed Out-of-Plane Bending ( $R = -1$ ) Loading of S994 Glass Roving Reinforced Epoxy	49

## ILLUSTRATIONS (Contd)

<u>Figure</u>		<u>Page</u>
21.	Maximum Bending Stress Versus Cycles to Failure at Three Frequencies for Out-of-Plane Bending with a Mean Bending Stress Equal to the Alternating Bending Stress ( $R = 0.05$ ) for 181/S901 Glass Cloth Reinforced Epoxy	52
22.	Maximum Bending Stress Versus Cycles to Failure at Three Frequencies for Out-of-Plane Bending with a Mean Bending Stress Equal to the Alternating Bending Stress ( $R = 0.05$ ) for S994 Uniaxial Roving Reinforced Epoxy	53
23.	Specimens Used for Testing 181/S901 Glass Cloth Reinforced Epoxy at 45 Deg to Weave Blanking Schedule	55
24.	Tension Fatigue Curve, Stress Versus Cycles to Failure ( $R = 0.05$ ) for 181/S901 Glass Cloth Reinforced Plastic Loaded at 45 Deg to the Weave - 1800 cpm	57
25.	Tension-Zero-Tension ( $R = 0.05$ ) Fatigue Results for Vacuum-Bagged 181/S994 Glass Cloth Reinforced Epoxy - Glass Content = 60.35 Percent	59
26.	Fatigue Results for Vacuum Bagged 181/S994 Glass Cloth Reinforced Epoxy at Three Stress Ratios, Tested at Room Temperature - NAA Results	60

## ILLUSTRATIONS (Contd)

<u>Figure</u>		<u>Page</u>
27.	Maximum Stress Versus Cycles to Failure for 143/S901 Glass Cloth Reinforced Epoxy Tested in Tension-Zero-Tension ( $R = 0.05$ ) in the Preferential Strong Direction: Tested at Room Temperature at 1800 cpm	63
28.	Typical Unfailed Torsion Specimens and Grips	64
29.	Typical Torque-Angle of Rotation Plot from Hydro-Mechanical Torque Machine for Basket-Woven S994 Glass Roving Reinforced Epoxies	68
30.	Torque Versus Cycles to Failure for Basket-Woven S994 Uniaxial Glass Roving Epoxy Composites	70
31.	Log N Versus Normal Probability for 181/S901 Glass Cloth Reinforced Epoxy $\sigma = 43,000$ psi	72
32.	Creep Testing Machines with Bending, Compression and Tension Creep Tests in Progress	74
33.	Test Fixture, Tension Creep with 181/S901 Glass Cloth Reinforced Constant Radius Plastic Specimen in Position	75
34.	Test Fixture - Compression Creep with 181/S901 Glass Cloth Reinforced Rectangular Specimen in Position	76
35.	Test Fixture - Bending Creep with 181/S901 Glass Cloth Reinforced Plastic Reduced Section Bending Specimen in Position	77
36.	Tension Strain-Time Curves, 181/S901 Glass Cloth Reinforced Epoxy Resin Composite	82

## ILLUSTRATIONS (Contd)

<u>Figure</u>		<u>Page</u>
37.	Compression Strain-Time Curves, 181/S901 Glass Cloth Reinforced Epoxy Resin Composite	83
38.	Bending Strain-Time Curves, 181/S901 Glass Cloth Reinforced Epoxy Resin Composite (Ultimate Bend Strength, $\sigma_{BV} = 67.5$ ksi)	84
39.	Stress Versus Time to Rupture Plot for Tension, Compression and Bending of an 181/S901 Glass Cloth Reinforced Epoxy Resin Composite	86
40.	Average Stress at Failure Versus Strain Rate for 181/S901 Glass Cloth Reinforced Epoxies	94
41.	Average Stress at Failure Versus Strain Rate for S994 Uniaxial Roving Reinforced Epoxies	95
42.	Water Encapsulation System for Environmental Test on 181/S901 Glass Cloth Reinforced Epoxy Tested in Tension-Zero-Tension ( $R = 0.05$ )	102
43.	Probable Curves Showing Effect of Prior Exposure to Water Environment for Various Exposure Lengths for 181/S901 Glass Cloth Reinforced Epoxy (Very High Life Values Not Plotted)	103
44.	Probable Curves Showing Effect of Prior Exposure Lengths for S994 Uniaxial Roving Reinforced Epoxy (Very High Life Values Not Plotted)	104
45.	Schematic of the Flat Composite Specimen Ultrasonic Inspection Unit	106
46.	Ultrasonic Inspection Equipment for Flat Composite Specimens	108

## ILLUSTRATIONS (Contd)

<u>Figure</u>		<u>Page</u>
47.	Ultrasonic X-Y Recorder	109
48.	Ultrasonic Inspection at Different Cyclic Levels for 181/S901 Glass Cloth Reinforced Epoxy Specimen 5-T-12 Tested in Tension-Zero-Tension ( $R = 0.05$ ), $\sigma_{Max} = 47,500$ psi, Failure at 3415 Cycles	110
49.	Ultrasonic Inspection at Different Cyclic Levels for 181/S901 Glass Cloth Reinforced Epoxy Specimen 2-T-15 Tested in Tension-Zero-Tension ( $R = 0.05$ ), $\sigma_{Max} = 65,000$ psi, Failure at 93 Cycles	111
50.	Ultrasonic Inspection at Different Cyclic Levels for 181S/901 Glass Cloth Reinforced Epoxy Specimen 2-T-20 Tested in Tension-Zero-Tension ( $R = 0.05$ ) $\sigma_{Max} = 35,000$ psi, Failure at 205,000 Cycles	112
51.	Average Attenuation Measurement of an Ultrasonic Trace	114
52.	Wide Specimen with Three Available Trace Paths to be Used in Weighted Attenuation Measurements	115
53.	Maximum Attenuation Measurement of an Ultrasonic Trace	117
54.	Weighting of Maximum Attenuation along Parallel Paths	118
55.	Example of Weighted Maximum Attenuation along Single Scan Path	119
56.	Shear Failure Load Versus Maximum Ultrasonic Attenuation for 3-Point Beam Specimens	121



# ILLUSTRATIONS (Contd)

<u>Figure</u>		<u>Page</u>
57.	Shear Failure Load Versus Average Ultrasonic Attenuation for 3-Point Beam Specimens	122
58.	Attenuation Versus Stress Cycles to Failure for 181/S901 Glass Cloth Reinforced Epoxy Specimens Tested in Tension-Zero-Tension ( $R = 0.05$ ) at $\sigma_{Max} = 43,000$ psi at 6 cpm	126
59.	Attenuation in db Versus Percent of Life Expended for 181/S901 Glass Cloth Reinforced Epoxy Specimens Tested in Tension ( $R = 0.05$ ) and Bending ( $R = -1$ ) Fatigue	127
60.	Attenuation Versus Cycles, Specimen 5-T-12 181/S901 Glass Cloth Reinforced Epoxy Tested in Tension-Zero-Tension at 47,5000 psi	128
61.	Two Stress Level Cumulative Damage Method	130
62.	Ranges for Two Cyclic Rate Fatigue Machines for Application in Cumulative Damage Study	131
63.	Example of the Determination of d from Experimental Data	134
64.	Example of Freudenthal-Heller Fictitious S-N Curve	137
65.	Intersection of Corten-Dolan and Freudenthal-Heller Fictitious S-N Curves	142
66.	Laminates 1-6, Blanking Schedule	154
67.	Laminates 7-12, Blanking Schedule	155
68.	Laminates 9A-11A, Blanking Schedule	156
69.	Laminates 13-16, Blanking Schedule	157
70.	Laminates 17-22, Blanking Schedule	158

# ILLUSTRATIONS (Contd)

<u>Figure</u>		<u>Page</u>
71.	Laminates 23-26, Blanking Schedule	159
72.	Laminates 27-30, Blanking Schedule	160
73.	Laminates 31-33, Blanking Schedule	161
74.	Laminates 35-37, Blanking Schedule	162
75.	Laminates 34 and 38, Blanking Schedule	163
76.	Laminates 39 and 40, Blanking Schedule	164
77.	Laminates 41-44, Blanking Schedule	165
78.	Stress-Dependent and Stress-Independent Cumulative Damage Theories	174
79.	Stress-Interaction-Free and Stress-Interaction Cumulative Damage Theories	175
80.	Two Stress Level Cumulative Damage Curve	177
81.	Grover's Cumulative Damage Theory	183
82.	Valluri's Cumulative Damage Theory	186
83.	Shanley's Stress-Dependent Interaction Cumulative Damage Theory	193
84.	Fabrication of Carbon-Filament Torsional Fatigue Specimen	198
85.	Constant Radius Tensile Specimen Gage Section (Used to Evaluate 181/S901 Glass Cloth Rein- forced Epoxy)	200
86..	Test Beam under Constant Moment in Center Gage Section	203
87.	Sonntag SF-1-U Fatigue Machine and 4-Point Bending Fixture	206

## ILLUSTRATIONS (Contd)

<u>Figure</u>		<u>Page</u>
88.	Bending Fixture for Fatigue of 181/S901 Glass Cloth and S994 Uniaxial Roving Reinforced Epoxies	207
89.	Uniaxial Tension and Compression Fatigue Grips Used for Testing Sheet Coupons of 181/S901 Glass Cloth Reinforced Epoxies	208
90.	Hydraulic-Mechanical Prime Mover Capable of 6 to 60 cpm and $\pm 10,000$ lb Alternating Load at a Mean Load of 0 to 10,000 lb	210
91.	Low Cyclic Rate Flexural Fatigue Console Load Capabilities are $\pm 1,000$ lb	211
92.	Hydraulic-Mechanical Fatigue Machine Capable of Both Constant Stress and Constant Strain Amplitudes to $\pm 10,000$ lb Load	212
93.	Hydro-Mechanical Beam Fatigue Machine Power Supply and Rams	213
94.	Schematic of Hydraulic-Mechanical Prime Movers	215
95.	Uniaxial Fatigue Grips with Optimum 181/S901 Glass Cloth Reinforced Epoxy Tensile Specimen and Alignment Fixture	216
96.	Test Results, Fatigue Fixture Calibration	217
97.	Strain Distribution over Specimen Cross Section as Produced by Hydraulic-Mechanical Fatigue Machine No. 1	218
98.	Test Results, Fatigue Console Calibration	219
99.	Closeups of Uniaxial Grips Employed in Testing 181/S901 Glass Cloth and S994 Roving Reinforced Epoxies in Low Cyclic Rate Fatigue Machines	220

## ILLUSTRATIONS (Contd)

<u>Figure</u>		<u>Page</u>
100.	Load Cycles, Tension-Zero-Tension	221
101.	Schematic of Torsion Fatigue Equipment	223
102.	Power Supply, Test Standard Prime Mover, and Servac Control System for Hydraulic-Mechanical Torsional Fatigue of Epoxy-Glass Composites	224
103.	Actuator Test Specimen and Load Frame Torsional Fatigue of Epoxy-Glass	226
104.	Epoxy-Woven Glass Roving Composite Torsional Specimen	227
105.	Dead Weight Calibration System for Torsional Fatigue System	230

## LIST OF TABLES

<u>Number</u>		<u>Page</u>
1.	Resin Content of Individual Sheets of Material	8
2.	Specimen Identification Code	9
3.	Coupon Tensile Tests on 181/S901 Glass Cloth Reinforced Epoxy - Specimen D	14
4.	Coupon Tensile Tests on 181/S901 Glass Cloth Reinforced Epoxy - Specimen B	15
5.	Static Tensile Tests on Uniaxial S994 Glass Roving Reinforced Epoxy	20
6.	Static Tensile Tests on 143/S901 Glass Cloth Reinforced Epoxy	20
7.	Results of Static Compression Tests on 181/S901 Glass Cloth Reinforced and S994 Glass Roving Reinforced Epoxy	25
8.	Material Properties for Vacuum Bagged 181/S994 Glass Reinforced Epoxy Laminates	26
9.	Fatigue Life at 6, 60 and 1800 cpm ( $R = 1.0$ ) for 181/S901 Glass Cloth Reinforced Epoxy	32
10.	Fatigue Life at 50 and 1800 cpm ( $R = 1.0$ ) for S994 Uniaxial Roving Reinforced Epoxy	33
11.	Effect of Mean Tensile Stress on Fatigue Life at 5 cpm Mean Stress = Alternating Stress ( $R = 0.05$ ) for 181/S901 Glass Cloth Reinforced Epoxy	36
12.	Effect of Mean Tensile Stress on Fatigue Life at 50 and 1800 cpm Mean Stress = Alternating Stress ( $R = 0.05$ ) for 181/S901 Glass Cloth Reinforced Epoxy	37

# LIST OF TABLES (Contd)

<u>Number</u>		<u>Page</u>
13.	Effect of Mean Tensile Stress on Fatigue Life at 6, 50 and 1800 cpm; Mean Stress = Alternating Stress ( $R = 0.05$ ) for S994 Uniaxial Glass Roving Reinforced Epoxy ( $\sigma_{ult} = 250$ ksi)	38
14.	Effect of Mean Compressive Stress on Fatigue Life at 50 and 1800 cpm: Mean Compressive Stress = Alternating Stress ( $R = 10$ ) for 181/S901 Glass Cloth Reinforced Epoxy	42
15.	Effect of Mean Compressive Stress on Fatigue Life at 6, 50 and 1800 cpm: Mean Compressive Stress = Alternating Stress ( $R = 10$ ) for S994 Uniaxial Roving Reinforced Epoxy	43
16.	Bending Fatigue Life at 6, 50 and 1800 cpm ( $R = -1$ ) for 181/S901 Glass Cloth Reinforced Epoxy	46
17.	Bending Fatigue Life at 6 and 1800 cpm ( $R = -1$ ) for S994 Uniaxial Glass Roving Reinforced Epoxy	47
18.	Effect of Mean Bending Stress on Fatigue Life at 6, 50 and 1800 cpm: Out-of-Plane Bending with Mean Bending Stress Equal to Alternating Bending Stress ( $R = 0.05$ ) for 181/S901 Glass Cloth Reinforced Epoxy	50
19.	Effect of Mean Bending Stress on Fatigue Life at 6 and 1800 cpm: Out-of-Plane Bending with Mean Bending Stress ( $R = 0.05$ ) for S994 Glass Roving Reinforced Epoxy	51
20.	Fatigue Life of 181/S901 Glass Cloth Reinforced Epoxy Loaded at 45 Deg Angle to Weave in Uniaxial Tension-Zero-Tension Fatigue ( $R = 0.05$ ) - 1800 cpm	56

# LIST OF TABLES (Contd)

<u>Number</u>		<u>Page</u>
21.	Tension-Zero-Tension Fatigue Test Results on Vacuum-Bagged 181/S994 Glass Cloth Reinforced Epoxy ( $R = 0.05$ ) Tested at 1800 cpm, Static Strength = 74,700 psi	58
22.	Tension-Zero-Tension ( $R = 0.05$ ) Fatigue Test Results on 143/S901 Glass Cloth Reinforced Epoxy, Tested at 1800 cpm Static Strength = 123,000 psi, Percent Glass = 70 Percent	62
23.	Results of Torsional Fatigue Tests on Basket- Woven S994 Glass Roving Reinforced Epoxy	69
24.	Strain Versus Time for Specimen 16-CrT-17 Loaded in Tension for 1000 Hrs at 77.5 Percent $\sigma_{TU}$ (64,000 psi)	80
25.	Strain Versus Time for Specimen 15-CrC-9 Loaded in Compression for 1000 Hrs at 75 Percent $\sigma_{CU}$ (40,500 psi)	80
26.	Strain Versus Time for Specimen 31-CrB-13 Loaded in Bending for 1000 Hrs at 87.5 Percent $\sigma_{BU}$ (59,500 psi)	81
27.	Stress Level Versus Time to Rupture for Several Loading Modes 181/S901 Glass Cloth Reinforced Epoxy	85
28.	Stress Level Versus Time to Rupture for Compression and Bending Modes S994 Uniaxial Roving Reinforced Epoxy	87
29.	Strain Rate Tests on 181/S901 Glass Cloth Reinforced Epoxy - Tensile Loading	88
30.	Strain Rate Tests on 181/S901 Glass Cloth Reinforced Epoxy - Compressive Loading	89

# LIST OF TABLES (Contd)

<u>Number</u>		<u>Page</u>
31.	Strain Rate Tests on 181/S901 Glass Cloth Reinforced Epoxy - Bending Loading	90
32.	Strain Rate Tests on S994 Uniaxial Roving Reinforced Epoxy - Tensile Loading	91
33.	Strain Rate Tests on S994 Uniaxial Roving Reinforced Epoxy - Compressive Loading	92
34.	Strain Rate Tests on S994 Uniaxial Roving Reinforced Epoxy - Bending Loading	93
35.	Effect of Moisture and Painting on the Fatigue Life of 181/S901 Glass Cloth Reinforced Epoxies; Tested after Exposure to 100 Percent Relative Humidity and 95°F (1800 cpm, R = -1)	99
36.	Effect of Moisture and Painting on the Fatigue Life of S994 Uniaxial Glass Roving Reinforced Epoxies; Tested after Exposure to 100 Percent Relative Humidity and 90°F (1800 cpm, R = -1)	100
37.	Maximum Attenuation at a Single Flaw - 181/S901 Glass Cloth Reinforced Epoxy Specimen 9-CuT-5 Tested in Tension (R = 0.05) Fatigue to $\sigma_{Max} = 43,000$ psi at 6 cpm	123
38.	Maximum Attenuation at a Single Flaw - 181/S901 Glass Cloth Reinforced Epoxy Specimen 14-CuT-3 Tested in Tension (R = 0.05) Fatigue to $\sigma_{Max} = 43,000$ psi at 6 cpm	123
39.	Maximum Attenuation at a Single Flaw - 181/S901 Glass Cloth Reinforced Epoxy Specimen 15-CuT-2 Tested in Tension (R = 0.05) Fatigue to $\sigma_{Max} = 43,000$ psi at 6 cpm	124



# LIST OF TABLES (Contd)

<u>Number</u>		<u>Page</u>
40.	Maximum Attenuation at a Single Flaw - 181/S901 Glass Cloth Reinforced Epoxy Specimen 16-CuT-1 Tested in Tension ( $R = 0.05$ ) Fatigue to $\sigma_{Max} = 43,000$ psi at 6 cpm	124
41.	Maximum Attenuation at a Single Flaw - 181/S901 Glass Cloth Reinforced Epoxy Specimen 10-CuT-4 Tested in Tension ( $R = 0.05$ ) Fatigue to $\sigma_{Max} = 43,000$ psi at 6 cpm	125
42.	Cumulative Damage Two Step Stress Level Tests Results with Miner's Rule Summation - 181/S901 Glass Cloth Reinforced Epoxy Loaded in Tension- Zero-Tension ( $R = 0.05$ ) at 6 cpm, (Average Life $N_1$ at $\sigma_1 = 43,000$ psi was 1150 cycles; Average Life $N_2$ at $\sigma_2 = 31,000$ psi was 29,200 Cycles)	135
43.	Cumulative Damage Two-Step Stress Level Test Results with Corten-Dolan Exponent Compressions of Theoretical and Experimental Values 181/S901 Glass Cloth Reinforced Epoxies Loaded in Tension- Zero-Tension was ( $R = 0.05$ ) at 6 cpm (Average Life at $\sigma = 43,000$ psi was 11,500 Cycles; Average Life at $\sigma_2 = 31,000$ psi was 29,200 Cycles	137
44.	Miner's Summations for Freudenthal-Heller Fictitious S-N Curve from Tensile Fatigue Data on 181/S901 Glass Cloth Reinforced Epoxy	141
45	Comparison of Cumulative Damage Constants	144

## LIST OF TABLES (Contd)

<u>Number</u>		<u>Page</u>
46.	Summary of Results of Two-Step Stress Level Tests with Miner's Rule Applied for S994 Uniaxial Glass Roving Reinforced Epoxy Tested at 1800 cpm in Tension-Zero-Tension ( $R = 0.05$ ). (Average Life at 75,000 psi = 9,000 Cycles, Average Life at 45,000 psi = 2,500,000 Cycles	145
47.	Three-Step Stress Level Tests - Using Miner's Summation for S994 Uniaxial Roving Reinforced Epoxy-Cycles in Fully Reversed and Compression Axial Fatigue at 1800 cpm	147
48.	Residual Static Strength of 181/S901 Glass Cloth Reinforced Epoxy after Cycling in Tension-Zero-Tension ( $R = 0.05$ ) at 60 cpm for Various Fractions of the Average Life at two Stress Levels ( $\sigma = 43,000$ psi and $N = 1150$ Cycles; for $\sigma = 31,000$ psi, $N = 29,200$ Cycles) Average Static Strength of 181/S901 Specimens was 90,200 psi	148
49.	Summary of Selected Fatigue and Creep Properties References	171

## SECTION I

### INTRODUCTION

In the past few years, the application of glass reinforced plastic (GRP) has shifted from a secondary to a primary role as a load carrying material. This shift has required a closer look at material properties such as static strength, fatigue strength, environmental effects, frequency effects, creep, stress rupture, and reinforcement configuration. Perhaps the most important consideration to the aircraft designer and GRP user is a knowledge of the fatigue limit of the material being considered along with criteria for deciding when excessive fatigue damage has taken place. Aircraft technology has reached the stage where major aircraft components are designed to meet specific fatigue conditions. The designer of metal aircraft has access to a wealth of excellent literature dealing with the mechanism of fatigue, fatigue properties, fatigue strength of joints, cumulative damage theories, influence of stress concentration factors, and full scale fatigue tests on structural components and airframes. The designer of composite aircraft, however, has little if any directly applicable information on these various aspects of fatigue. The basic mechanism of composite failure has been firmly established in certain static stress fields but is still open to considerable question in cyclic stress fields.

In addition to this lack of data on the phenomenological behavior of composites, the problem of quality control consistently has appeared. Nondestructive test methods, though frequently sought, were not readily available for composite materials. A desirable goal would be the development of NDT tests which insure that all structural members fall within a category of acceptance. Standard acceptance methods such as testing a composite panel in static flexure are insufficient to describe phenomena such as voids, crack propagation, and cumulative fatigue damage.

Therefore, it would seem that in order to make glass reinforced plastic a more useful and reliable primary load carrying material, the types of tests and the correlation of these test results with mechanistic studies simultaneously performed, must be analyzed in detail and placed on a firm basis. Since the fatigue and creep properties of glass reinforced plastics, isolated from the influences of prior static loading and environmental conditions, are somewhat academic in nature, the interaction of these influences with creep and fatigue must be determined. Finally, the sites of potential composite failure must be given careful scrutiny in order to assess damage and to establish a portion of the cumulative damage criteria for GRP in aircraft design. This report describes the work performed over the past year toward the accomplishment of these objectives for a single resin system and two types of reinforcement.

First the fatigue and creep properties of reinforced plastics were determined at frequencies and amplitudes designed to give realistic results within the time framework allowed. The material samples used in these studies were laminates of glass cloth and uniaxial roving reinforced epoxy.

Next the frequency results were analyzed and representative frequencies were selected for cumulative damage studies. These studies included ultrasonic and macroscopic assessment of damage accrued in the course of a fatigue test. These studies also included determination of the reduction in fatigue life at a given stress level by initially prefatiguing at lower or higher stress levels. In addition, the residual static load-carrying capability of prefatigued materials was determined. Where applicable, these cumulative damage data were correlated with the appropriate ultrasonic attenuation data and various theoretical bases commonly employed in metal damage predictions.

SECTION II  
MATERIALS AND LAMINATE PREPARATION

Two types of reinforcement were selected for this investigation. These reinforcements included two varieties of glass cloth: 181 and 143 weaves in which the glass fabric was prepared from S-901 yarn. In addition to these fabric reinforcements, uniaxial 20-end fiber glass rovings of S994 glass were used as the reinforcements.

The resin used was a three-component mix of the following elements:

Resin	83.4 percent (by weight) Jones and Dabney Epirez 510
Hardener	14.1 percent Apco 320
Silane Coupling Agent	2.5 percent Dow Corning 26040

No other resin treatment or post treatment was employed.

Plates of both the 181 and 143 glass cloth reinforcements were press-laminated from stacks of cloth which had been prepared by a wet lay-up process. After cutting, resin was troweled onto each stacked sheet with a wood spatula. Squeeze-out was accomplished in the laminating press which effected a purge of the air entrapped between plies. The 181 cloth reinforcement was crosslaid, i.e., alternating layers were turned 90 deg to the principal bolt direction thus giving rise to a warp-fill-warp, etc., pattern through the thickness. The 143 cloth reinforcements were, of course, laid up parallel thus yielding a material with a preferential strong direction. (143 cloth is 8 fibers in the warp direction to 1 in the fill direction. See Fig. 1 for details of the process.) Plates were fabricated, in large, to two thicknesses: 1/10 in. and 1/4 in.



a) Glass Fabric Sheets Cut to Size



b) Mixed Resin Poured onto Individual Sheets



c) Resin Troweled over Each Sheet

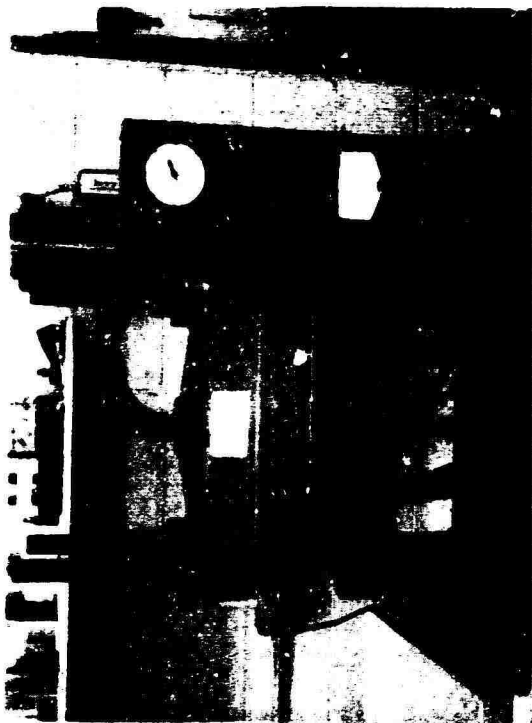


d) Next Sheet Laid in Place

Fig. 1 FABRICATION OF TEST PLATES



e) Aluminum Cover Plate



f) Laminating Press



g) Final Plate Trimmed to Shape

Fig. 1 (Contd)

The unidirectional material prepared from glass rovings was prepared by wet-winding the rovings on an 18 x 12 in. flat aluminum plate mandrel, and then press-laminating to the same schedule used in preparing the cloth-reinforced epoxy plates. Figure 2 shows the filament-winding equipment winding a plate by this process.

The cure schedule for the cloth and roving plates was as follows:

1. Precure	$170 \pm 10^{\circ}\text{F}$	60 min (minimum)	2 tons
2. Cure	$260 \pm 10^{\circ}\text{F}$	30 min (minimum)	2 tons
3. Postcure	$325 \pm 10^{\circ}\text{F}$	120 min (minimum)	2 tons
4. Cool Down	$170 \pm 10^{\circ}\text{F}$	with the use of water	2 tons
5. Final Cure	$260 \pm 10^{\circ}\text{F}$	120 min (minimum)	Ambient

Following the final cure, each sheet was then blanked according to specimen dimensions (see Appendix A) by a diamond blade cutoff wheel cooled by water pickup. Each blank was final machined to specimen configuration by a high speed router using three levels of tungsten-carbide rotary router bits. A total of six passes with this router was used to remove material at the periphery of the specimens. The final three passes removed 0.005 in. per pass from the edges of the specimen.

#### Resin Content Determination

Control of the ratio of glass weight to resin weight is important from several standpoints. The nominal strength of the composite based upon cross-sectional area depends critically upon the percent of resin present. Burnout tests were, therefore, conducted on each sheet of material prior to testing. The results of these tests and other geometrical plate measurements are shown in Table 1.



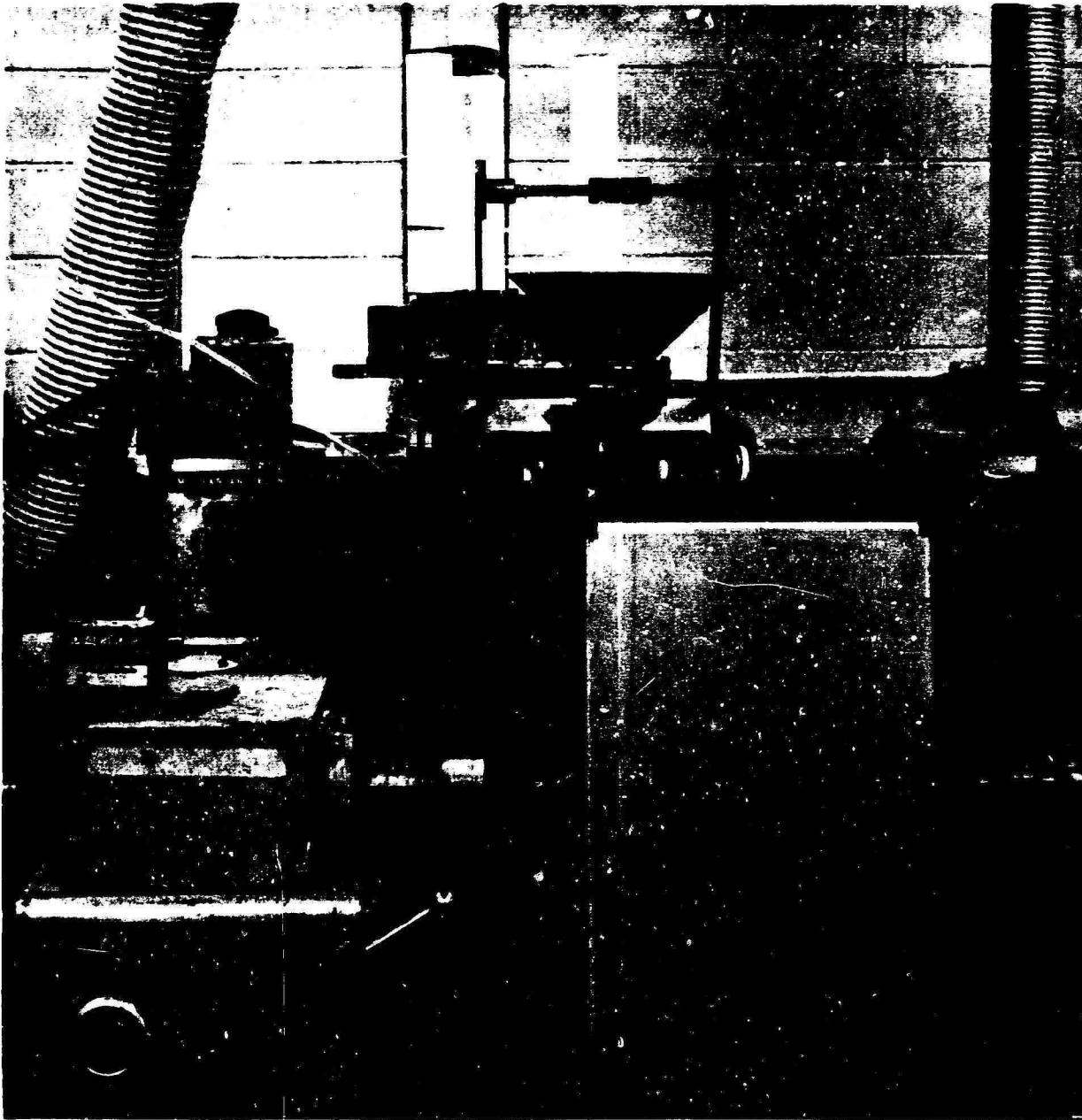


Fig. 2 S994 GLASS ROVINGS WOUND ONTO PLATE MANDREL

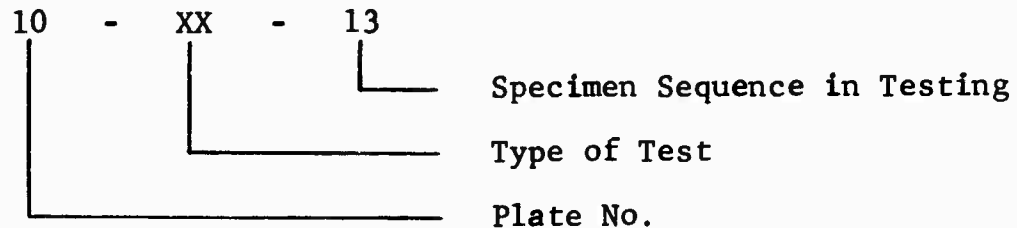
**Table 1**  
**RESIN CONTENT OF INDIVIDUAL SHEETS OF MATERIAL**

Sheet No.	Reinforcement Type	Nominal Plate Dimension (in x in x in)	Number of Specimens	Initial Sample Weight $W_i$ (GMS)	Burnout Wt., $W_f$ (GMS)	Percent Resin by Wt.	Percent Glass by Wt.
1	181 S Glass Cloth	11 x 17 x 0.090	22	4.10	2.85	30.5	69.5
2	181 S Glass Cloth	11 x 17 x 0.090	23	5.25	3.74	28.7	71.3
3	181 S Glass Cloth	11 x 17 x 0.090	19	4.34	3.20	26.4	73.6
4	181 S Glass Cloth	11 x 17 x 0.090	20	4.05	3.39	16.1	83.9
5	181 S Glass Cloth	11 x 17 x 0.090	20	4.07	2.80	31.1	68.9
6	181 S Glass Cloth	11 x 17 x 0.090	18	3.64	2.02	44.4	55.6
7	181 S Glass Cloth	11 x 17 x 0.090	20	3.31	2.30	30.6	69.4
8	181 S Glass Cloth	11 x 17 x 0.090	19	2.85	2.00	29.7	70.3
9	181 S Glass Cloth	11 x 17 x 0.090	22	5.04	3.66	27.4	72.6
10	181 S Glass Cloth	11 x 17 x 0.090	16	4.57	3.20	30.0	70.0
11	181 S Glass Cloth	11 x 16 x 0.090	20	3.77	2.48	34.2	65.8
12	181 S Glass Cloth	11 x 17 x 0.090	12	5.09	2.94	42.2	57.8
13	181 S Glass Cloth	11 x 17 x 0.090	12	5.08	3.59	29.3	70.7
14	181 S Glass Cloth	11 x 17 x 0.090	20	4.70	3.41	27.4	72.6
15	181 S Glass Cloth	11 x 17 x 0.090	20	5.70	3.90	31.6	68.4
16	181 S Glass Cloth	11 x 17 x 0.090	20	5.01	3.44	31.3	68.7
17	Uniaxial Rovings	11 x 17 x 1/8	22	2.51	1.95	22.3	77.7
18	Uniaxial Rovings	11 x 17 x 1/8	21	4.10	2.91	29.2	70.8
19	Uniaxial Rovings	11 x 17 x 1/8	20	5.20	3.72	28.4	71.6
20	Uniaxial Rovings	11 x 17 x 1/8	21	3.19	2.14	32.8	67.2
21	Uniaxial Rovings	11 x 17 x 1/8	21	3.15	2.30	26.9	73.1
22	Uniaxial Rovings	11 x 17 x 1/8	10	4.00	2.91	27.3	72.7
23	Uniaxial Rovings	11 x 17 x 1/8	16	4.05	3.11	23.2	76.8
24	Uniaxial Rovings	11 x 17 x 1/8	17	6.04	4.19	30.7	69.3
25	Uniaxial Rovings	11 x 17 x 1/8	13	3.01	2.09	30.5	69.5
26	Uniaxial Rovings	11 x 17 x 1/8	13	4.15	2.80	32.6	67.4
27	181 S Glass Cloth	10 x 16 x 1/4	24	9.19	6.72	26.7	73.3
28	181 S Glass Cloth	10 x 16 x 1/4	24	10.49	7.51	28.3	71.7
29	Uniaxial Rovings	10 x 14 x 1/4	20	9.28	6.61	28.7	71.3
30	Uniaxial Rovings	10 x 14 x 1/4	20	5.41	3.86	28.7	71.3
31	181 S Glass Cloth	10 x 16 x 1/4	24	8.60	6.71	22.0	78.0
32	181 S Glass Cloth	10 x 16 x 1/4	24	9.49	6.25	34.1	65.9
33	Uniaxial Rovings	10 x 14 x 1/4	20	6.65	4.74	28.7	71.3
34	Uniaxial Rovings	10 x 16 x 0.060	42	2.84	2.35	17.6	82.4
35	Uniaxial Rovings	10 x 13 x 1/4	20	2.11	1.51	28.4	71.6
36	Uniaxial Rovings	10 x 13 x 1/4	20	1.78	1.26	30.2	69.8
37	Uniaxial Rovings	10 x 13 x 1/4	20	9.28	6.35	31.5	68.5
38	Uniaxial Rovings	10 x 16 x 0.60	40	3.19	2.49	22.0	78.0
39	Uniaxial Rovings	10 x 16 x 0.60	40	2.44	1.85	24.0	76.0
40	Uniaxial Rovings	10 x 16 x 0.60	40	7.10	5.02	29.0	71.0
41	143 S Glass Cloth	11 x 18 x 0.090	30	4.59	3.34	27.2	72.8
42	143 S Glass Cloth	11 x 18 x 0.090	30	4.74	3.41	28.0	72.0
43	143 S Glass Cloth	11 x 18 x 0.090	30	3.61	2.63	27.1	72.9
44	143 S Glass Cloth	11 x 18 x 0.090	30	6.02	4.23	30.0	70.0
9A	181 S Glass Cloth	11 x 17 x 0.090	20	4.76	3.39	29.0	71.0
10A	181 S Glass Cloth	11 x 17 x 0.090	20	4.78	3.33	30.0	70.0
11A	181 S Glass Cloth	11 x 17 x 0.090	20	4.82	3.34	31.0	69.0

SECTION III  
SPECIMEN CODING AND IDENTIFICATION

To quickly identify source and physical properties of a specimen, the following coding was used throughout the testing phase:

Typical



Individual tests were identified as shown in Table 2.

Table 2  
SPECIMEN IDENTIFICATION CODE

Fatigue

T	Tension-Zero-Tension Axial (R = 0.05)
C	Compression-Zero-Compression Axial (R = -10)
F	Fully Reversed Axial (R = -1)
B1	Moment-Zero-Moment Bending (R = 0.05)
B2	Fully Reversed Bending (R = -1)

Static

ST	Static Tension
SC	Static Compression
SB	Static Bending
CrC	Compression Creep
CrB	Bending Creep
STT	Tension Strain Rate
STC	Compression Strain Rate
STB	Bending Strain Rate

Appendix A shows the detailed location of all specimens used as they were blanked from the laminates. In addition to the regular numbering system employed throughout the test, series of specimens appear on the figures in Appendix A which were used in preliminary tests and evaluations. In general, these specimens proved fixture validity but were not judged suitable for further testing.

## SECTION IV

### STATIC MATERIAL PROPERTIES

A base from which fatigue tests could be scrutinized was established from static tension, compression, and bending tests. The tests were performed on the 181/S901 and 143/S901 glass cloth and S994 uniaxial roving reinforced epoxy laminates prepared as described earlier.

For the 181/S901 glass cloth tensile specimens, laminate No. 1 was selected to be used in some specimen optimization studies. Specimens shown in Fig. 3 appeared particularly attractive at the outset. The laminate was blanked as shown schematically in Fig. 4.

Two specimens were selected from these candidates for more extensive testing, Specimen B and Specimen D. Nineteen B specimens and 26 D specimens were drawn from laminates 1 to 15. Tables 3 and 4 show the values of tensile strength obtained from these tests. Specimen B, showing superior strength, was selected for fatigue, creep, and strain rate testing as well as static tensile values. The lower values obtained from Specimen D are attributed to a higher stress concentration factor present. ( $1.0 < S.C.F. < 1.4$ ) see Fig. 5 in this report from Peterson.<sup>1\*</sup> Extrapolated values from this chart show that Specimen B stress concentration factor is approximately 1.03. Figure 6 shows finish dimensions for this specimen.

For the tensile tests on uniaxial rovings, the specimen shown in Fig. 7 was designed. This specimen is prepared by cementing tabs onto the edges of the sheet, curing the adhesive and cutting the laminate (with tabs) into 1/2 in. wide specimens. The best results are obtained when the elastic modulus of the tabs is approximately 1/4 to 1/2 of the elastic modulus of the material being tested. Scrap material from the 181/S901 glass cloth laminates was used for the glass roving specimens. Figure 8 shows typical static and fatigue specimen failures using this specimen. Table 5 shows the results of some static tensile tests using this specimen.

\* Superscript numbers refer to references listed at the end.

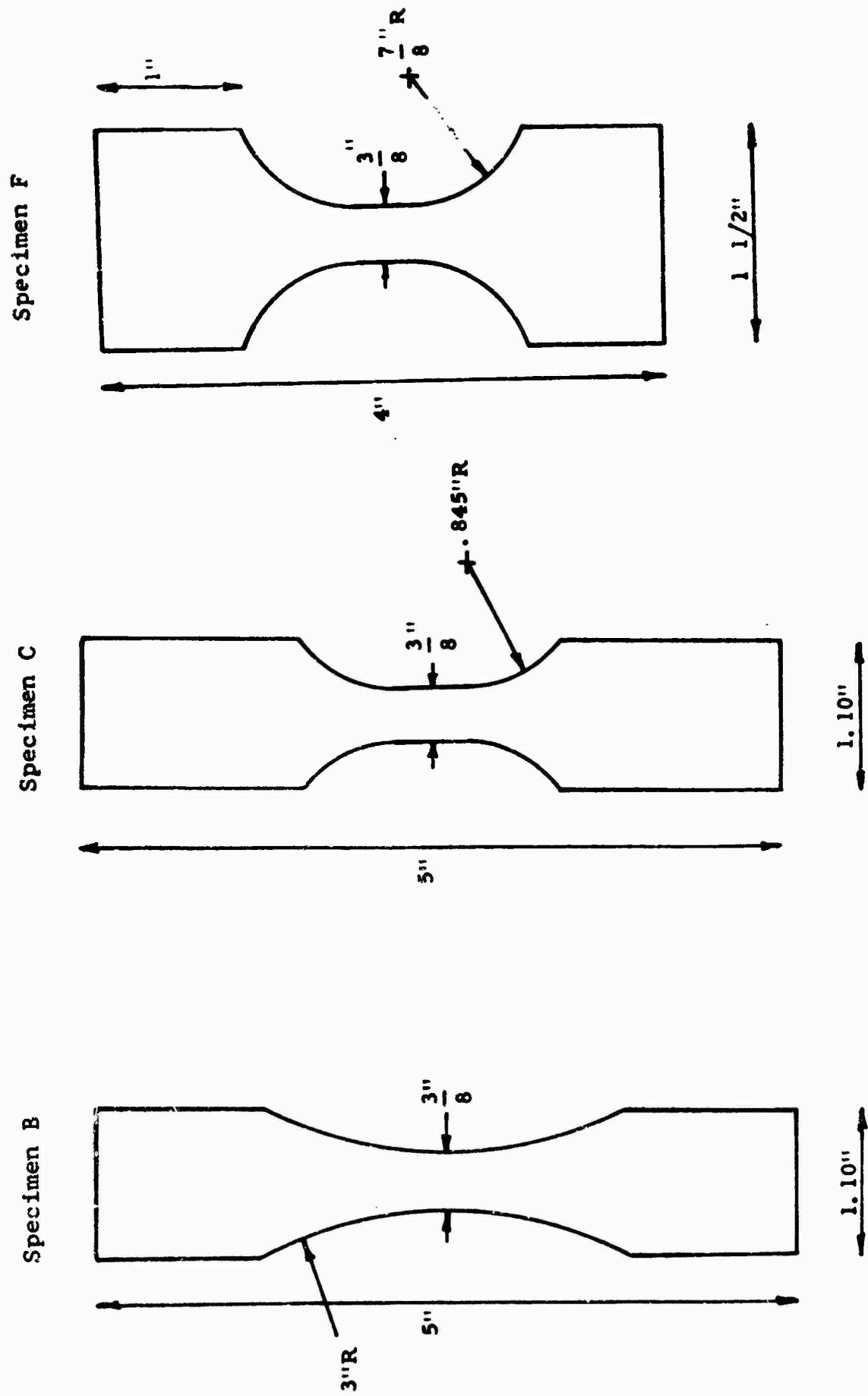
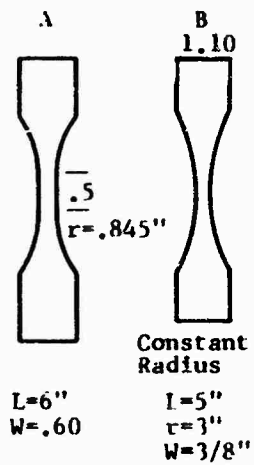
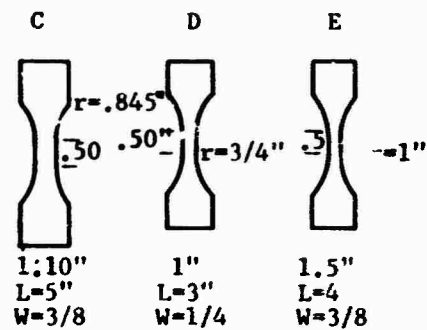


Fig. 3 UNIAXIAL TENSILE SPECIMENS



E		D	
E		B (Compression Test)	
D		F	
B	C		D
		Not Used	
		Not Used	
		E	B
			F
A			
C		Not Used Here	
E			
C			







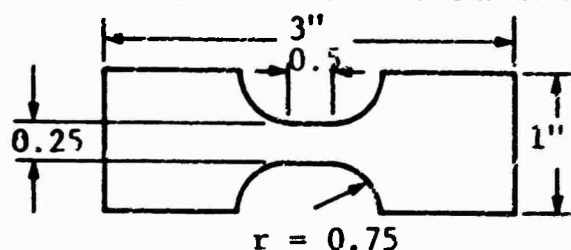
65,800		80,000	
71,000		49,000	
79,500		C	
79,000	66,800		73,600
			
		75,500	
		74,700	
84,400			
77,600			
64,400			
66,800			

Fig. 4 TENSION SPECIMEN OPTIMIZATION TESTS - SPECIMEN B WAS SELECTED

Table 3

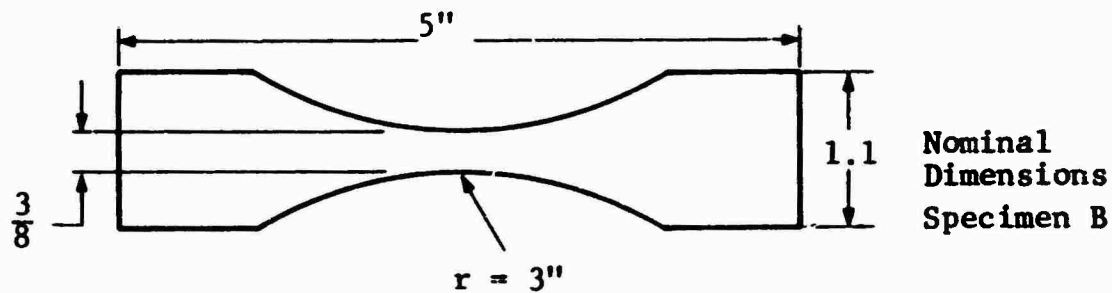
COUPON TENSILE TESTS ON 181/S901 CLASS CLOTH  
REINFORCED EPOXY - SPECIMEN DNominal  
Dimensions  
Specimen D

Specimens tested at 0.02 in/min

Specimen Number	Thickness t (in)	Width w (in)	Failure Load P (lbs)	Ultimate Strength $\sigma_{ult}$ (psi)	Percent Glass (%)
2-STT-50	0.088	0.262	2010	87,200	71.3
2-STT-51	0.085	0.262	1915	86,000	71.3
3-STT-52	0.090	0.258	1770	76,200	73.6
3-STT-53	0.090	0.258	1870	80,400	73.6
4-STT-54	0.086	0.256	1920	87,200	83.9
4-STT-55	0.086	0.257	1965	88,800	83.9
5-STT-56	0.087	0.259	1740	77,200	68.9
5-STT-57	0.087	0.259	1750	77,600	68.9
6-STT-58	0.086	0.260	1790	80,200	55.6
6-STT-59	0.087	0.260	1765	78,200	55.6
7-STT-60	0.085	0.264	1600	71,400	69.4
7-STT-61	0.086	0.269	2070	90,800	69.4
8-STT-62	0.090	0.260	1825	78,000	70.3
8-STT-63	0.085	0.260	1725	78,200	70.3
9A-STT-64	0.084	0.268	1980	88,200	71.0
9A-STT-65	0.084	0.268	1710	76,200	71.0
9A-STT-75				77,000	71.0
10A-STT-66	0.087	0.261	1745	77,000	70.0
10A-STT-67	0.089	0.261	1890	81,300	70.0
11A-STT-68	0.089	0.262	1445	61,600	69.0
11A-STT-69	0.089	0.262	1770	75,600	69.0
11A-STT-70	0.087	0.260	1905	84,200	69.0
12-STT-71	0.091	0.265	2065	85,800	57.8
12-STT-72	0.087	0.263	1950	85,200	57.8
13-STT-73	0.089	0.259	1765	76,700	70.7
13-STT-74	0.092	0.261	1930	80,300	70.7
Average	-	-	-	80,300	-



Table 4  
COUPON TENSILE TESTS ON 181/S901 GLASS CLOTH  
REINFORCED EPOXY - SPECIMEN B



Specimens tested at 0.02 in./min

Specimen Number	Thickness $t$ (in)	Width $w$ (in)	Failure Load $P$ (lbs)	Ultimate Strength $\sigma_{ult}$ (psi)	Percent Glass (%)
14-STT-30	0.089	0.375	2780	83,500	72.6
15-STT-31	0.089	0.375	2720	81,500	68.4
15-STT-32	0.088	0.384	3050	90,400	68.4
2-STT-33	0.088	0.384	3070	90,800	71.3
3-STT-34	0.090	0.382	3040	88,400	73.6
4-STT-35	0.088	0.383	3430	101,500	83.9
5-STT-36	0.090	0.385	3490	100,500	68.9
6-STT-37	0.087	0.380	3240	97,600	55.6
7-STT-38	0.090	0.383	3400	98,600	69.4
8-STT-39	0.092	0.389	3130	88,500	70.3
2-STT-40	0.089	0.379	3100	91,700	71.3
4-STT-41	0.088	0.380	2850	85,400	83.9
1-STT-42	0.105	0.380	3500	87,800	69.5
7-STT-43	0.088	0.379	2950	88,400	69.4
8-STT-44	0.091	0.379	2750	79,700	70.3
5-STT-45	0.088	0.379	2950	88,500	68.9
3-STT-46	0.088	0.379	2700	81,000	73.6
6-STT-47	0.084	0.380	2950	92,500	55.6
2-STT-48	0.085	0.384	3150	96,500	71.3
Average	-	-	-	90,200	-

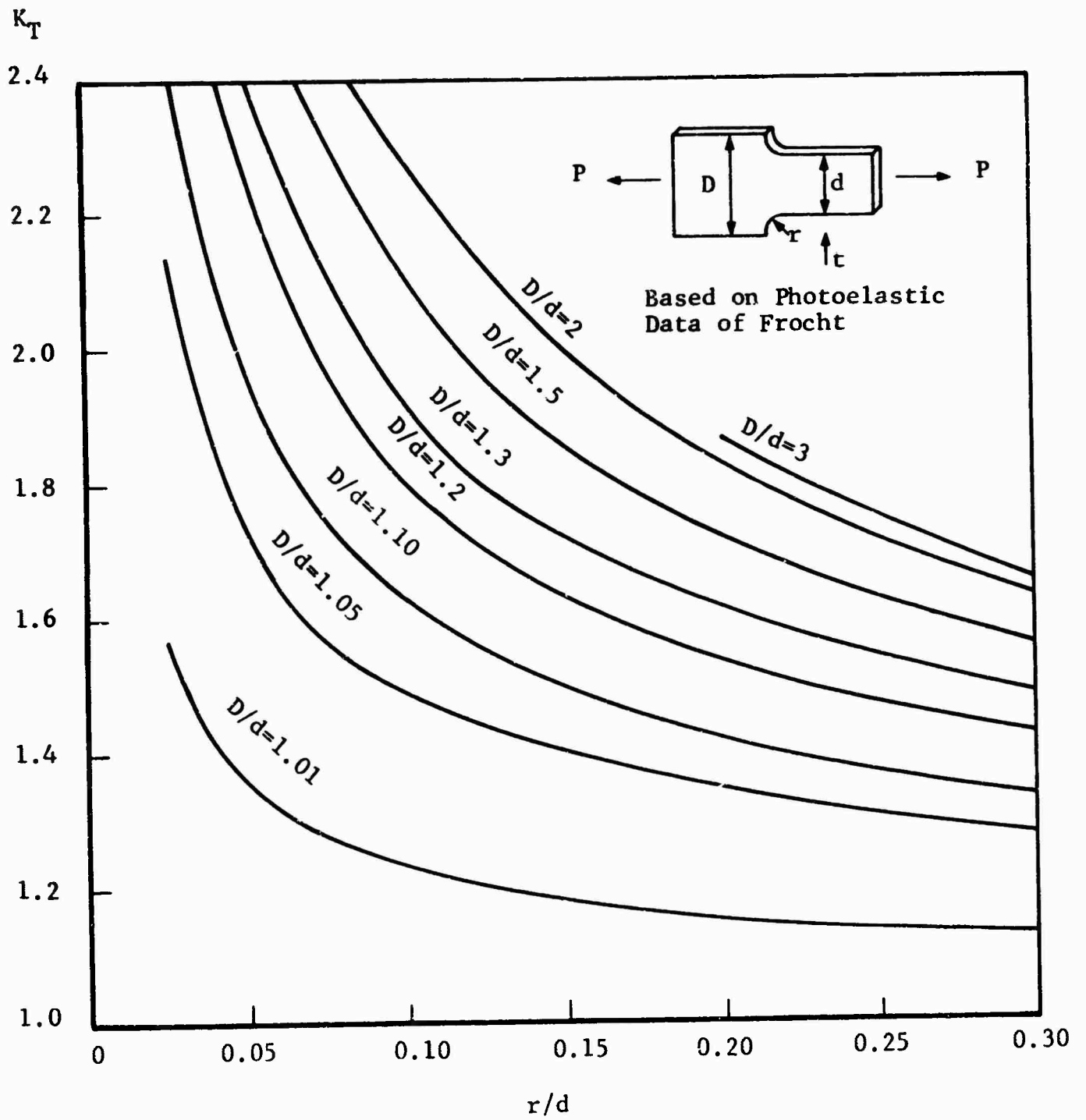


Fig. 5 STRESS CONCENTRATION FACTOR,  $K_T$ , FOR FLAT BAR WITH CIRCULAR SHOULDER FILLET IN TENSION, FROM PETERSON

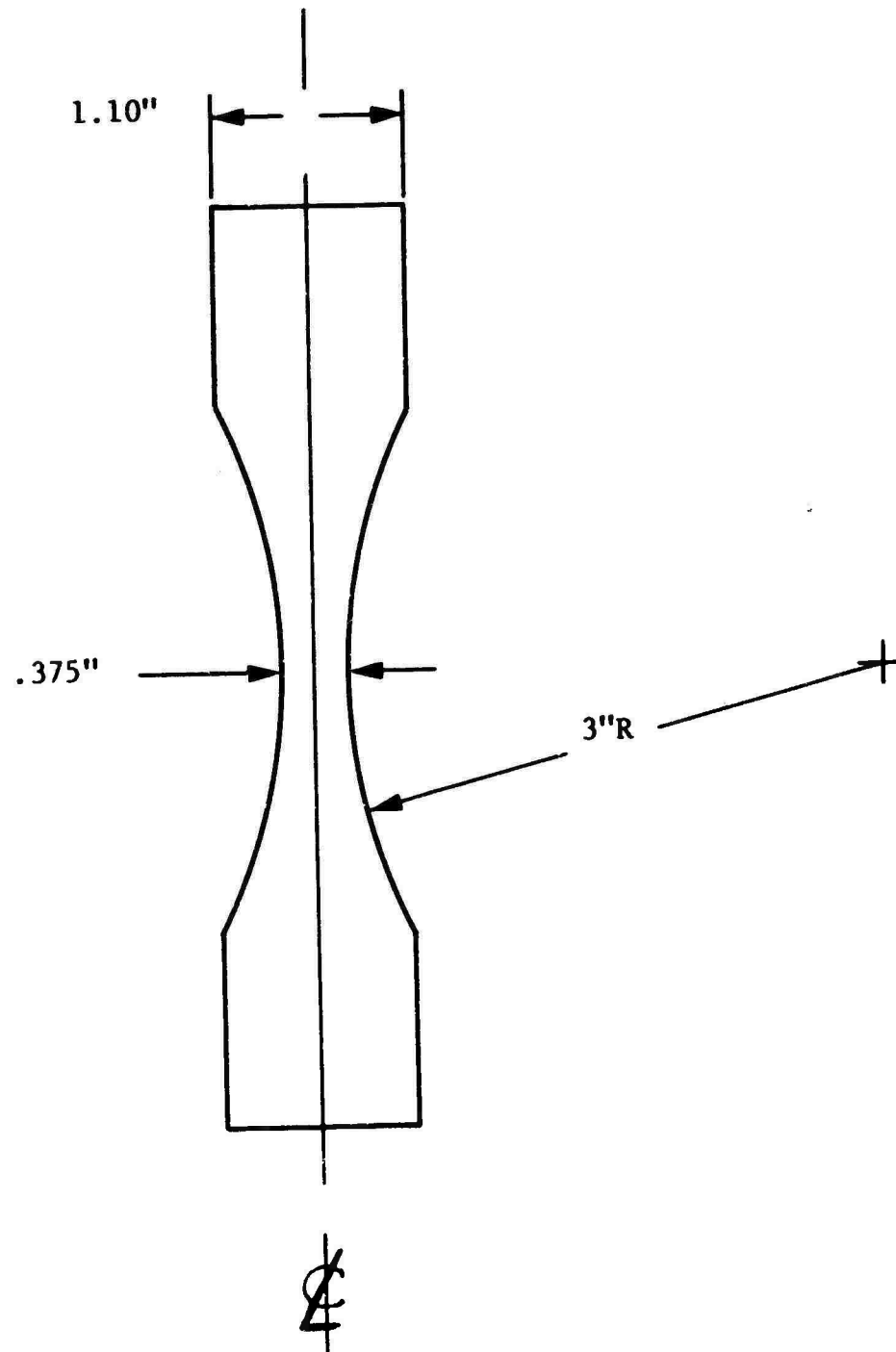


Fig. 6 TENSION SPECIMEN USED IN STATIC AND FATIGUE TESTS



Fig. 7 UNIAXIAL ROVING GLASS REINFORCED EPOXY TAB-ENDED SPECIMEN



Fig. 8 UNIAXIAL GLASS ROVING, TENSION SPECIMEN FAILURES  
IN STATIC AND FATIGUE LOADINGS

**Table 5**  
**STATIC TENSILE TESTS ON UNIAXIAL S994 GLASS ROVINGS REINFORCED EPOXY**

Specimen Number	Width (in)	Thickness (in)	Strength (psi)	Percent Glass (%)
34-T-41	0.470	0.061	255,000	82.4
34-T-42	0.508	0.062	245,000	82.4
34-T-43	0.502	0.063	214,000	82.4
34-T-44	0.506	0.063	226,000	82.4
Average	-	-	235,000	-

**Table 6**  
**STATIC TENSILE TESTS ON 143/S901 GLASS CLOTH REINFORCED EPOXY**

Specimen Number	Width (in)	Thickness (in)	Strength (psi)	Percent Glass (%)
43-ST-8	0.126	0.254	145,000	72.9
44-ST-7	0.114	0.277	109,810	70.0
44-ST-22	0.111	0.273	115,510	70.0
Average	-	-	123,400	-

The 143/S901 glass cloth tensile specimens were a combination of the tab-ended and reduced section specimens as shown in Fig. 9. The results of tensile tests using this specimen are shown in Table 6.

Static compression testing was also performed using a compression fixture similar to the one recommended by the ASTM for thin metal sheet compression tests. The fixture accommodates a 1-in. maximum width specimen and has set screws which align the specimen in the vertical direction. The ends of the specimen are clamped to give a fixed-end column effect. (See Figs. 10 and 11.) The results of the static tests are presented in Table 7.

As a means of comparing these values with previous values for a similar material, Table 8 shows material parameters similar to the ones obtained here and also includes interlaminar shear values. The data presented in Table 8 were obtained on laminates similar to those used on this program where the cloth had been woven from S994 yarn instead of S901 yarn and the laminates prepared by vacuum bagging techniques. The tests were performed by Aeronautical Materials Laboratory in accordance with Fed. Test STD No. 406-Method 1042B.

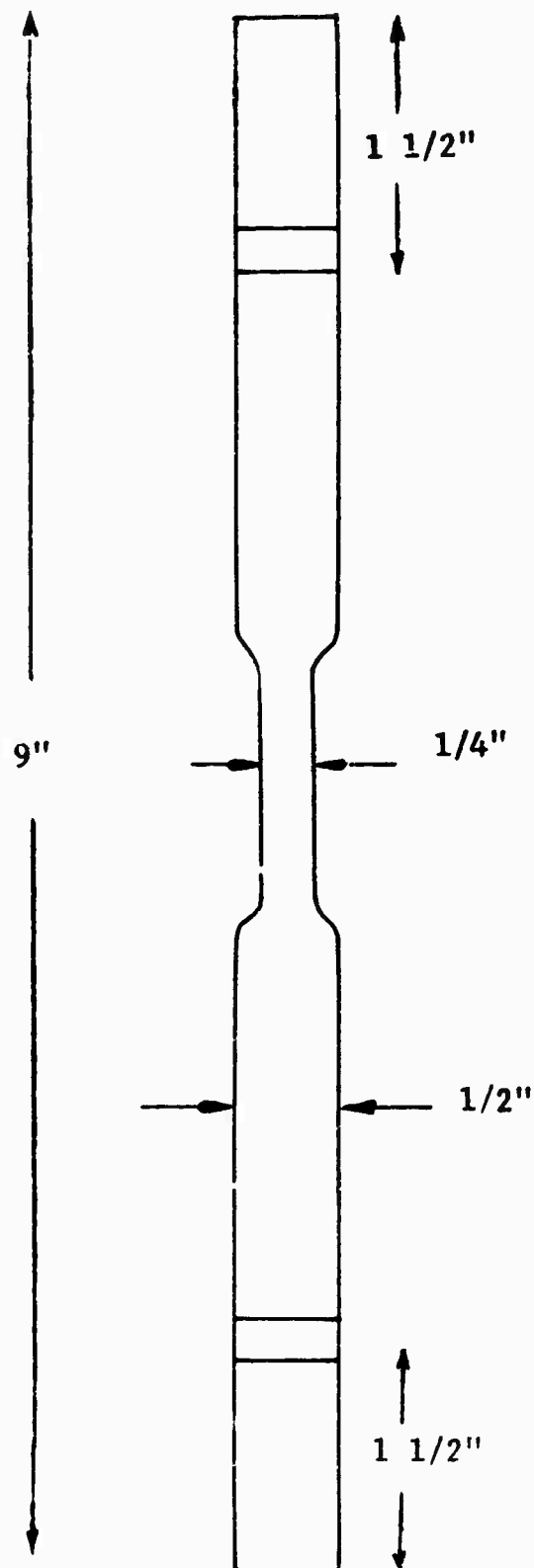
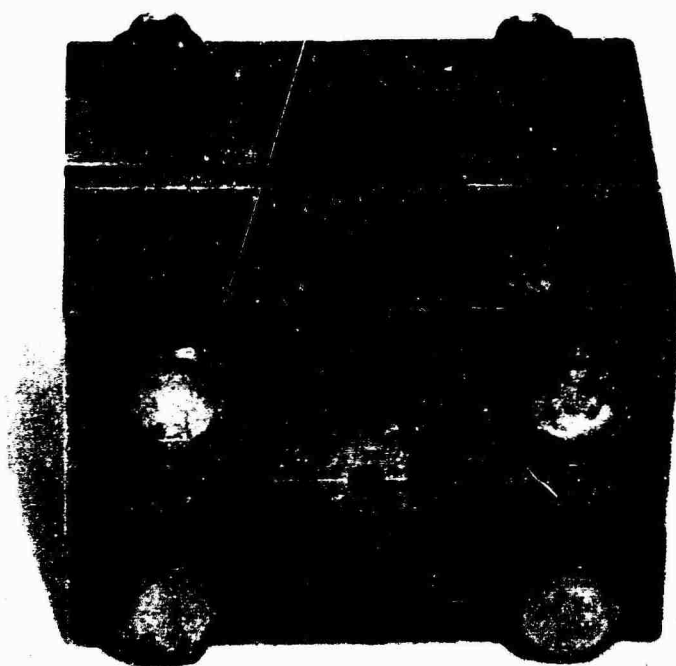


Fig. 9 TAB-ENDED REDUCED SECTION TENSILE SPECIMEN USED IN TESTING 143 S901 GLASS CLOTH REINFORCED EPOXY





**Fig. 10 COMPRESSION FIXTURE FOR STATIC AND CREEP LOADING OF THIN SHEET LAMINATES (SPECIMEN OF 181/S901 GLASS REINFORCED EPOXY IS SHOWN IN GREATLY EXAGGERATED EXPOSURE)**

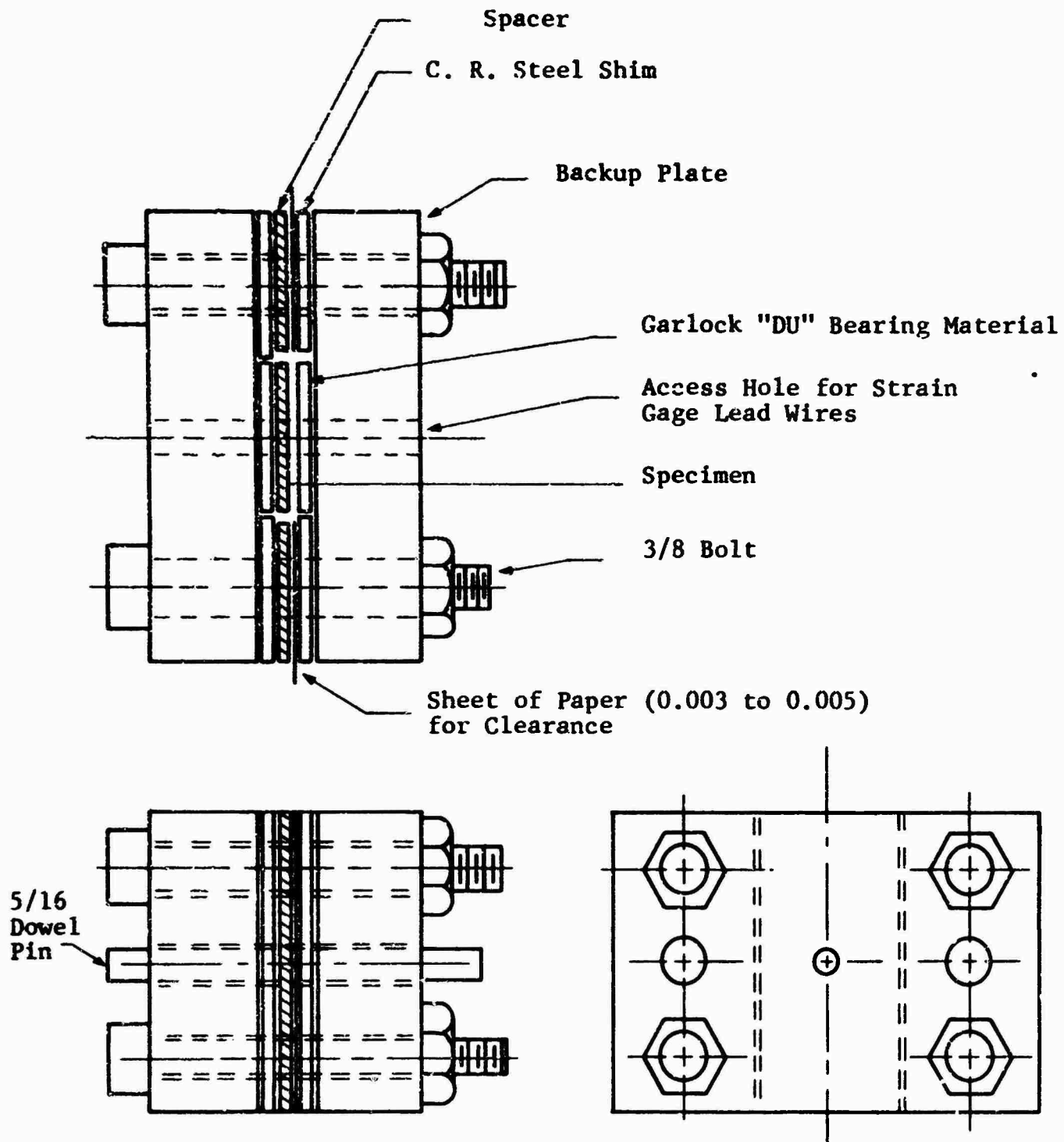


Fig. 11 COMPRESSION FIXTURE DETAILS

Table 7

RESULTS OF STATIC COMPRESSION TESTS ON 181/S901 GLASS CLOTH  
REINFORCED AND S994 GLASS ROVING REINFORCED EPOXY

Specimen Number	Reinforcement Type	Strength (psi)	Percent Glass (%)	Strength Based on 70% Glass Content (psi)
17-STC-1	Uniaxial Roving	65,000	77.7	58,000
21-STC-2	Uniaxial Roving	62,300	73.1	59,800
18-STC-3	Uniaxial Roving	58,400	70.8	58,000
17-STC-4	Uniaxial Roving	87,100	77.7	78,000
Average	Uniaxial Roving	68,200	-	-
1-STC-1	181/S901 Glass Cloth	48,100	69.5	48,500
2-STC-3	181/S901 Glass Cloth	58,400	71.3	57,000
3-STC-2	181/S901 Glass Cloth	55,000	73.6	52,300
4-STC-4	181/S901 Glass Cloth	59,000	83.9	49,400
Average	181/S901	55,100	-	-

Table 8  
MATERIAL PROPERTIES FOR VACUUM BAGGED 181/S994 GLASS REINFORCED EPOXY LAMINATES

Test Condition	Edgewise Compression (ksi)	Tensile Strength (ksi)	Interlaminar Shear (Supported) (psi)	Resin Content (%)
Room Temperature	62.3	93.2	3380	32.7
Room Temperature after 2 hr boil	61.5	89.5	3830	32.7
160°F after 1/2 hr @ 160°F	57.6	78.0	4020	32.7
-65°F after 1/2 hr @ -65°F		106.3	4700	32.7
Room Temperature	55.8	76.1	3700	45.2
Room Temperature after 2 hr boil	45.0	81.6	3680	45.2
160°F after 1/2 hr @ 160°F	48.5	70.3	3430	45.2
-65°F after 1/2 hr @ -65°F	72.1	84.6	3570	45.2
Room Temperature*	56.6	79.1	3360	45.2
Room Temp. after 2 hr boil*	56.2	76.8	3400	45.2
160°F after 1/2 hr @ 160°F*	43.5	71.0	3240	45.2
-60°F after 1/2 hr @ -65°F*	74.9	88.2	3350	45.2

\* Last four series of tests subjected to 400 hr weatherometer accelerated aging prior to conditioning and testing.

## SECTION V

### FATIGUE TESTS

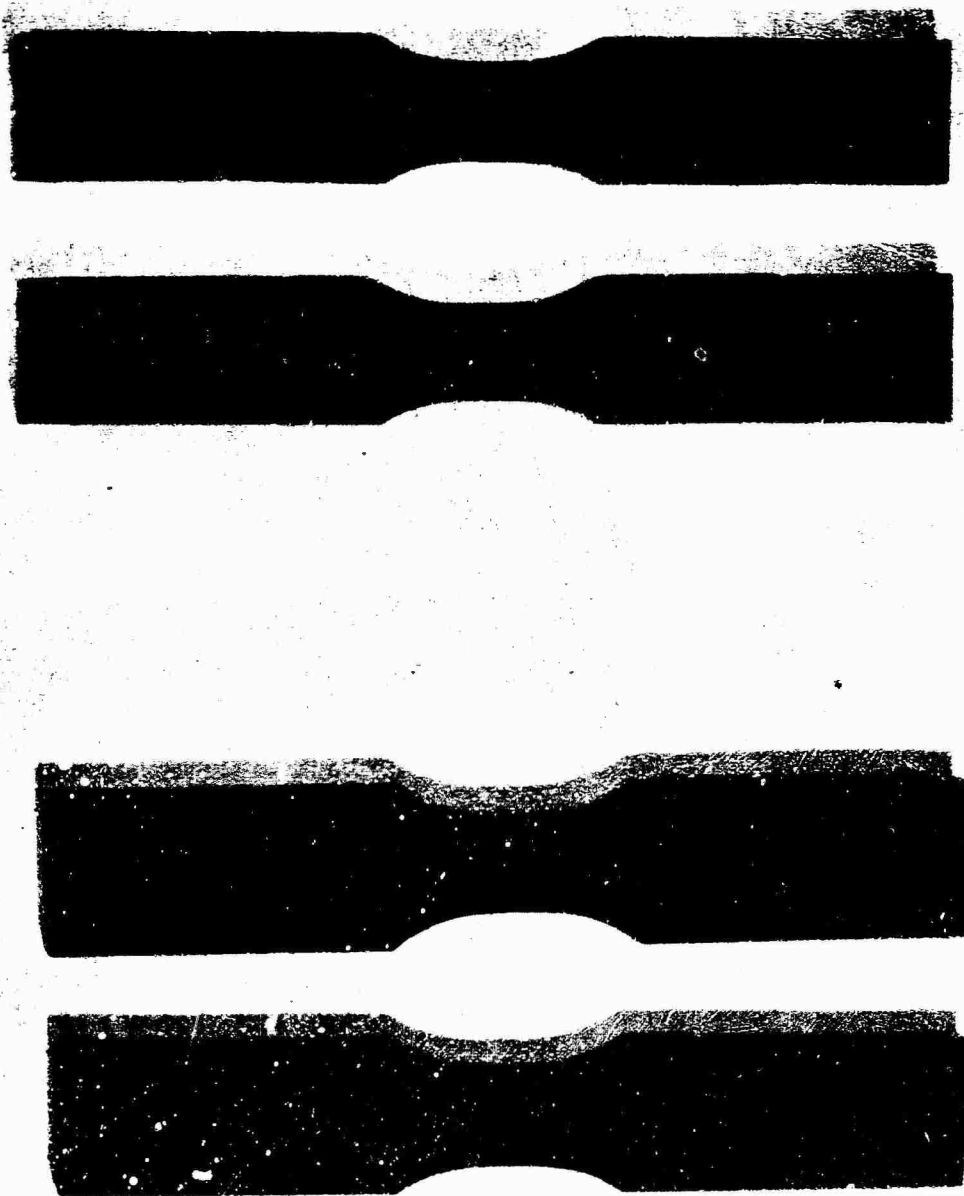
#### A. SPECIMEN CONFIGURATION

Fatigue tests at different R ratios call for different specimen configurations. In fact, the factors which contribute major portions of the error in test results are specimen shape and specimen grips. The shape of the specimen is important because stress concentrations greater than 1.05 can be sufficiently influential to reduce the apparent strength and shade the results in the same proportions. The specimen grips are important because the axially of the loading must be maintained; small eccentricities of load result in bending in the specimens and again this element can significantly reduce apparent strengths.

The static tensile specimen optimization studies were used to solve both problems simultaneously. Two conditions were set up for the fatigue tension ( $R = 0.1$ ) specimens. These conditions were, 1) the stress concentration factor must be less than 1.05 and 2) the grip must introduce less than 5 percent bending stress to provide specimen-grip compatibility.

For the 181/S901 glass cloth reinforced epoxy specimens, the specimen fulfilled both conditions. The 143/S901 glass cloth and uniaxial S994 rovings reinforced tensile specimens similarly met the grip compatibility condition. The S994 glass rovings specimen had an unknown stress concentration factor but since the majority of failure occurred in the central section, no problems in this regard are anticipated. The 143/S901 glass cloth reinforced epoxy specimen (see Fig. 9) possessed a stress concentration factor somewhat less than 1.10 and most probably less than 1.05.

Bending specimens consisted of a strip of nominally 1/4 in. thick with a central reduced section to permit failures at relatively low fatigue machine loads. Typical specimens of the 181/S901 glass cloth and S994 glass roving reinforced epoxies are shown in Fig. 12.



b) S994 Glass Roving  
Reinforced Epoxy

a) 181/S901 Glass Cloth  
Reinforced Epoxy

Fig. 12 BENDING FATIGUE SPECIMENS

Compression fatigue ( $R = +10$ ) and fully reversed ( $R = -1$ ) specimens were simply the tensile specimens with grip modifications to reduce the effective unsupported length. Other special specimens, such as torsional fatigue, will be described later as appropriate.

## B. FREQUENCY AND AMPLITUDE STUDIES

### Cyclical Aircraft Loadings

The utilization of glass reinforced plastics for primary aircraft structures cannot be accomplished reliably without a characterization of GRP under cyclic or fatigue loading. From a basic point of view, the fatigue properties of the materials employed in the primary structure of an aircraft are of paramount importance. A variety of sources for inducing fatigue in aircraft structures exist, including those imposed during takeoff and landing, by wind gust and by engines during flight. The frequency and amplitudes of these fatigue loadings being distinctly different, each must be separately understood as to its contribution to the total spectrum. For propeller and/or turbo-prop driven aircraft, these can be categorized as follows:

1. For pressure cabins, undercarriages and other major design entities, where during takeoff, climb, descent, and landing, fluctuating loads are imposed at approximately once or at most a few times per flight. These are stressed at low cyclic frequencies probably in the range of  $10^{-4}$  to  $10^{-3}$  cps.
2. On wing structures and control surfaces, gust loadings are encountered over a wide frequency spectrum. A typical frequency range for the most damaging gust type, presupposing the cruising height for a typical flight plan to be between 25,000 and 40,000 ft, would be from  $3 \times 10^{-4}$  to  $3 \times 10^{-3}$  cps.

3. The presence of power and auxiliary machinery in flight structures is responsible for vibrations introduced to the airframe, whereby resonance conditions sometimes induce quite large fatigue stresses in various structural members. These vibrations usually fall into the frequency range from 20 to 200 cps.
4. Finally, the use of pure jet and turbo-prop aircraft have introduced a new high frequency structural loading phenomenon. Fatigue problems of this type are due to the noise levels associated with fatigue producing acoustical noise range from 10 to 10,000 cps and even higher. Although the pressure levels are low, a great number of cycles ( $10^{10}$ ) can be accumulated during the life of an aircraft. Also, structural interaction with the acoustical excitation sometimes aggravates the situation.

Thus, it is clear from the three instances cited that the frequencies ranging from  $10^{-4}$  to  $1 \times 10^3$  cps enter into the fatigue problem of aircraft. Although testing over this wide range of frequencies for several parametric changes in material is seen to be desirable, it is rather obvious that the length of time required to do so quickly is inflated. By narrowing the range somewhat (from  $10^{-1}$  to  $10^2$ ), a great deal of information may yet be obtained and the fatigue strength obtained at one frequency can be extended over the frequency spectrum obtained in the structure.

### Test Results

Implementation of the studies of frequency effects described was accomplished through the use of both hydraulic-mechanical and electromechanical prime movers. The details of the equipment used and constructed for use on this program are to be found in Appendix F.



Fatigue tests were performed at several stress amplitude levels and at several frequencies. In general, two specimens were tested at each stress level for each type of stress-time profile investigated. For statistical purposes, occasionally as many as 12 specimens were tested at a single stress level.

Failure of axial specimens was defined as separation into two or more pieces. It was far more difficult to define failure for out-of-plane bending fatigue specimens. Failure progresses by a series of delaminations and local tensile failures which lead to increasingly greater deflections as the test progresses. As has been deemed appropriate in the past, failure of the out-of-plane bending specimens was defined as deflection exceeding some prescribed limit. As occasionally happened, the specimen fractured in two, but the microswitch arrangement for marking excessive deflection was always triggered and the correct number of cycles to failure was detectable in all cases. A loss of stiffness of approximately 50 percent was selected as the failure criterion for both 181/S901 glass cloth and S994 glass roving reinforced epoxy.

#### Zero Mean Stress Tests, Axial Loading

The results for specimens tested in the fully reversed axial loading state are shown in Tables 9 and 10. Plots of stress amplitude versus cycles to failure are shown in Fig. 13 for the 181/S901 glass cloth reinforced epoxy and in Fig. 14 for the S994 glass roving reinforced epoxy.

#### Mean Stress (Tensile) Equal to Alternating Stress-Axial Loading

The results for specimens tested in tension-zero-tension axial loading state are shown in Tables 11 through 13. The plot of stress amplitude versus cycles to failure are shown in Figs. 15 and 16 for the 181/S901 glass cloth and S994 uniaxial roving reinforced epoxies respectively.

Table 9  
FATIGUE LIFE AT 6, 50 AND 1800 CPM, (R = -1.0)  
FOR 181/S901 GLASS CLOTH REINFORCED EPOXY

Specimen Number	Loading Frequency (cpm)	Alternating Stress (ksi)	Cycles to Failure
6-F-13	6	35.0	721
15-F-17	6	31.0	2,385
8-F-11	6	20.0	44,000*
5-F-22	50	45.0	44
16-F-24	50	40.0	237
15-F-25	50	37.5	1,300
4-F-21	50	35.0	5,500
14-F-26	50	32.5	1,389
6-F-23	50	30.0	4,010
11-F-27	50	25.0	3,537
11-F-28	50	25.0	9,553
7-F-29	50	20.0	205,594
6-F-32	1800	22.4	40,000
1-F-34	1800	22.0	33,000
2-F-35	1800	20.0	6,000
16-F-36	1800	20.0	349,000
14-F-37	1800	18.5	93,000
15-F-38	1800	15.0	15,000
15-F-39	1800	15.0	103,000
1-F-40	1800	12.0	10,000,000*
16-F-41	1800	13.5	3,937,000

\* Runout, no failure.

Table 10  
FATIGUE LIFE AT 50 AND 1800 CPM, (R = -1.0) FOR S994  
UNIAXIAL ROVING REINFORCED EPOXY

Specimen Number	Loading Frequency (cpm)	Alternating Stress (ksi)	Cycles to Failure
25-F-43	1800	50.0	1,000
23-F-40	1800	45.0	31,000
24-F-39	1800	42.5	35,000
19-F-38	1800	40.0	61,000
19-F-41	1800	40.0	254,000
23-F-37	1800	37.5	764,000
24-F-36	1800	35.0	1,017,000
24-F-35	1800	32.5	1,482,000
19-F-34	1800	30.0	1,891,000
17-F-33	1800	27.5	3,348,000
26-F-42	1800	25.0	8,569,000
17-F-31	1800	17.5	10 <sup>7</sup> *
22-F-32	1800	23.5	10 <sup>7</sup> *
17-F-11	50	70.0	2
18-F-12	50	60.0	9
19-F-13	50	50.0	26
20-F-14	50	45.0	356

\* Runout, no failure at 10<sup>7</sup> cycles

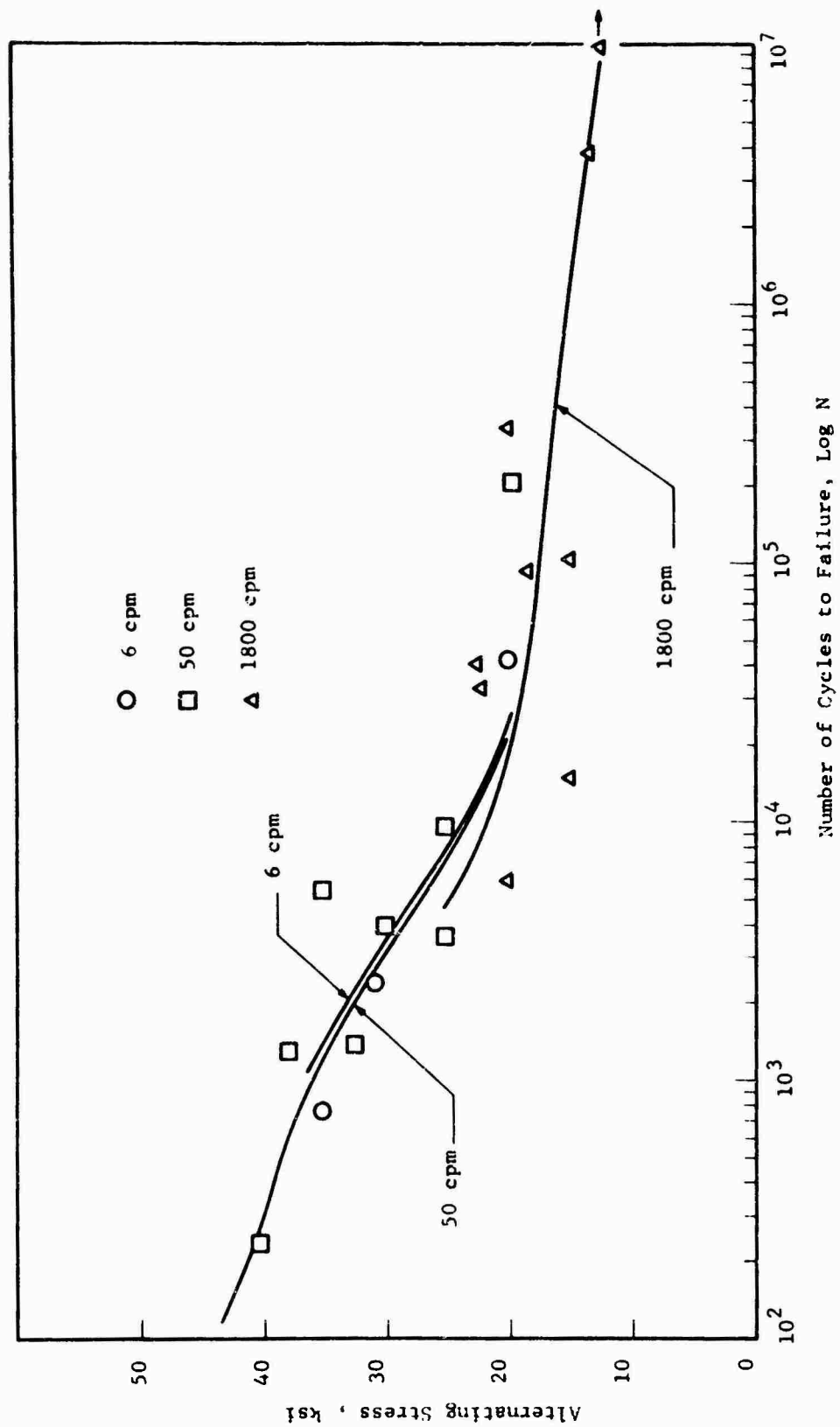


Fig. 13 ALTERNATING STRESS VERSUS CYCLES TO FAILURE AT SEVERAL FREQUENCIES FOR FULLY REVERSED ( $R = -1$ ) LOADING FOR 181/S901 GLASS CLOTH REINFORCED EPOXY

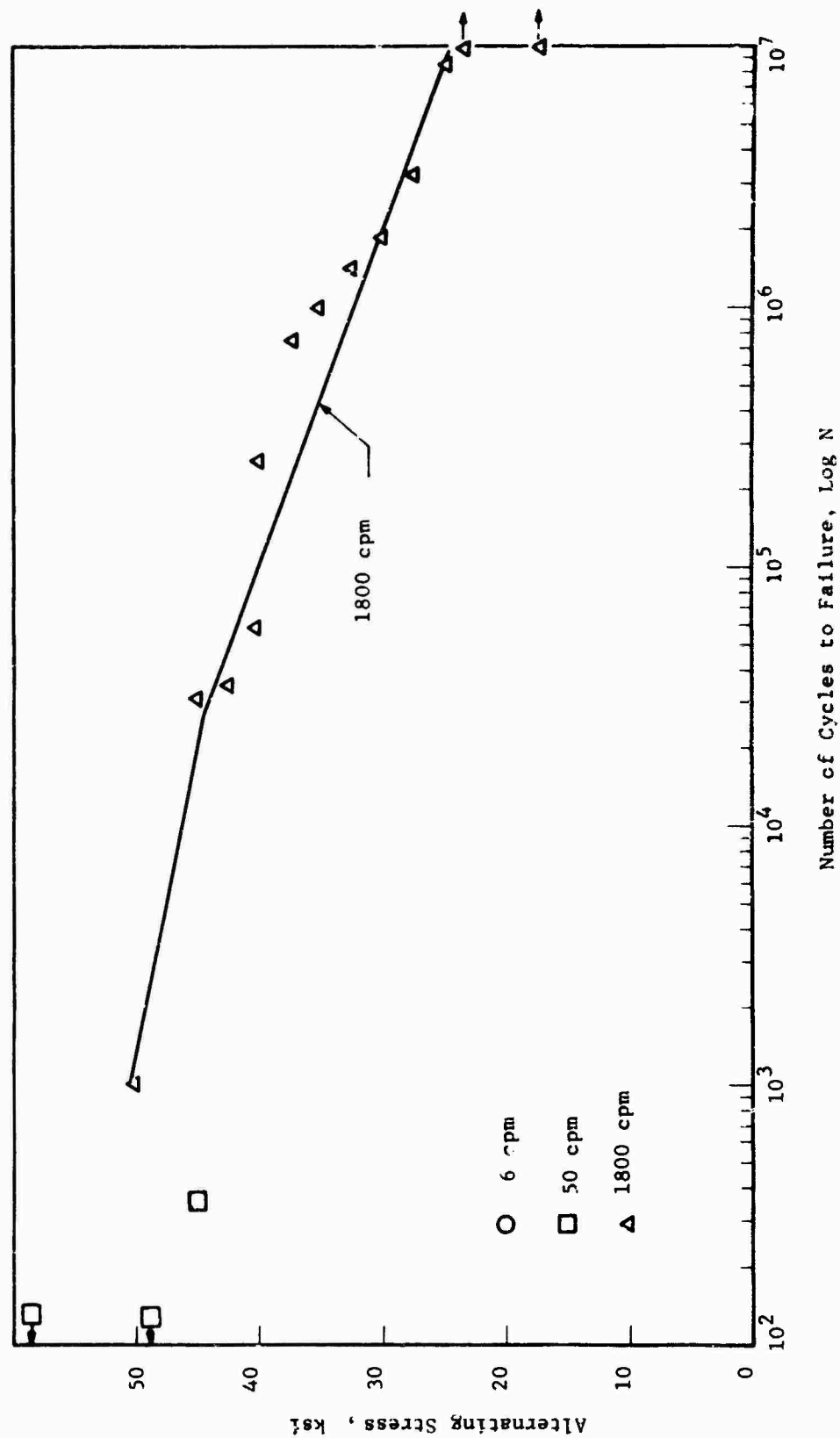


Fig. 14 ALTERNATING STRESS VERSUS CYCLES TO FAILURE AT TWO FREQUENCIES FOR FULLY REVERSED (R = -1) LOADING FOR S994 UNIAXIAL GLASS ROVING REINFORCED EPOXY

**Table 11**  
**EFFECT OF MEAN TENSILE STRESS ON FATIGUE LIFE AT 6 CPM MEAN**  
**STRESS = ALTERNATING STRESS (R = 0.05) FOR 181/S901 GLASS**  
**CLOTH REINFORCED EPOXY**

Specimen Number	Loading Frequency (cpm)	Maximum Stress (ksi)	Cycles to Failure
14-T-14	6	70.0	32
10A-T-11	6	69.5	67
2-T-15	6	65.0	93
2-T-16	6	60.0	337
1-T-17	6	55.0	280
5-T-12	6	47.5	3,415
15-T-67	6	43.0	663
9-T-70	6	43.0	937
14-T-68	6	43.0	1,080
10-T-69	6	43.0	1,331
16-T-66	6	43.0	1,550
1-T-19	6	40.0	68,000
2-T-20	6	35.0	205,000
8-T-13	6	33.0	28,712
3-T-73	6	31.00	21,400
8-T-72	6	31.0	25,266
9-T-75	6	31.0	29,190
4-T-71	6	31.0	30,097
7-T-76	6	31.0	31,720
7-T-74	6	31.0	104,573

Table 12

EFFECT OF MEAN TENSILE STRESS ON FATIGUE LIFE AT 50 AND 1800 CPM  
 MEAN STRESS = ALTERNATING STRESS (R = 0.05) FOR 181/S901 GLASS  
 CLOTH REINFORCED EPOXY

Specimen Number	Loading Frequency (cpm)	Maximum Stress (ksi)	Cycles to Failure
10-T-41	1800	43.0	3,000
13-T-31	1800	40.0	12,000
6-T-42	1800	40.0	11,000
8-T-43	1800	40.0	67,000
6-T-44	1800	40.0	53,000
9-T-45	1800	40.0	7,000
1-T-46	1800	40.0	115,000
3-T-47	1800	40.0	18,000
10-T-48	1800	40.0	37,000
14-T-49	1800	40.0	113,000
10-T-50	1800	40.0	186,000
4-T-51	1800	40.0	49,000
9-T-52	1800	40.0	6,000
9-T-53	1800	40.0	5,000
7-T-54	1800	40.0	45,000
9-T-55	1800	31.0	36,000
7-T-32	1800	30.0	79,000
5-T-56	1800	30.0	696,000
9-T-57	1800	30.0	23,000
3-T-58	1800	30.0	186,000
2-T-59	1800	30.0	$2.84 \times 10^6$
15-T-60	1800	30.0	13,000
15-T-61	1800	30.0	14,000
15-T-62	1800	30.0	38,000
9-T-63	1800	30.0	338,000
9-T-64	1800	30.0	12,000
8-T-65	1800	30.0	753,000
4-T-21	50	55.0	1,365
6-T-22	50	50.0	5,209
4-T-24	50	45.0	683
3-T-23	50	40.0	20,483
2-T-25	50	35.0	142,634

Table 13

EFFECT OF MEAN TENSILE STRESS ON FATIGUE LIFE AT 6, 50  
AND 1800 CPM; MEAN STRESS = ALTERNATING STRESS (R = 0.05)  
FOR S994 UNIAXIAL GLASS ROVING REINFORCED EPOXY ( $\sigma_{ULT}$  = 250 KSI)

Specimen Number	Loading Frequency (cpm)	Maximum Stress (ksi)	Cycles to Failure
39-T-2	6	180.0	20
38-T-4	6	180.0	102
38-T-2	6	160.0	121
38-T-3	6	140.0	604
38-T-1	6	100.0	94,464
38-T-5	6	120.0	760
38-T-9	50	100.0	1,261
38-T-13	50	80.0	14,194
38-T-14	50	70.0	152,983
38-T-15	50	50.0	500,000
34-T-32	1800	200.0	150
34-T-33	1800	125.0	690
34-T-34	1800	100.0	2,000
34-T-35	1800	162.0	330
34-T-36	1800	100.0	2,000
34-T-37	1800	75.0	13,000
34-T-38	1800	50.0	57,000
34-T-39	1800	62.5	15,000
34-T-40	1800	25.0	10,005,000*
34-T-41	1800	37.7	10,055,000*
34-T-42	1800	45.2	596,000
34-T-44	1800	45.2	5,053,000
34-T-45	1800	62.5	756,000
34-T-47	1800	75.0	6,000
34-T-48	1800	45.0	1,871,000
34-T-49	1800	75.0	8,000

\* Specimen did not fail, runout.



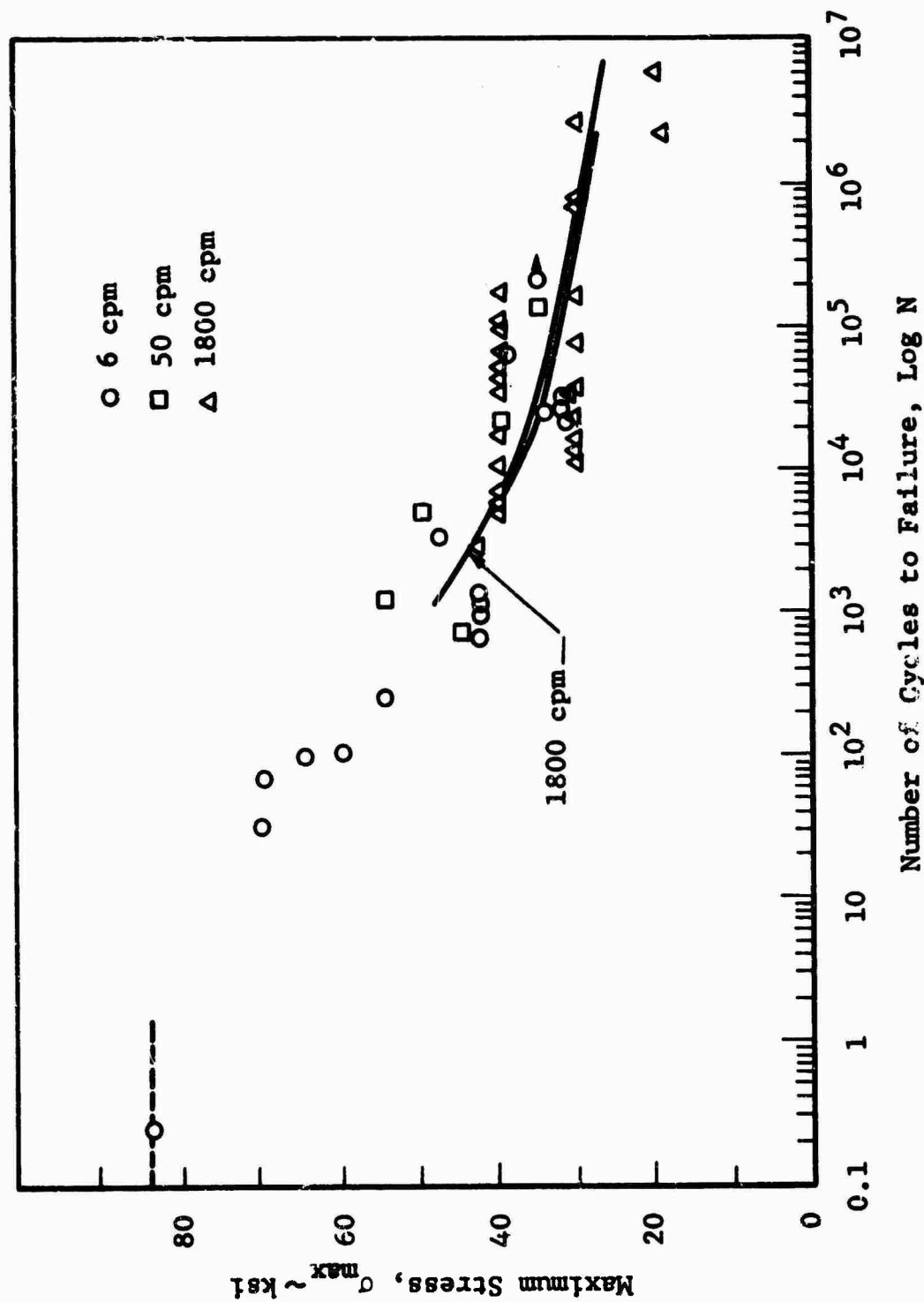


Fig. 15 MAXIMUM STRESS VERSUS CYCLES TO FAILURE AT SEVERAL FREQUENCIES FOR TENSION-ZERO-TENSION (R=0.05) LOADING FOR 181/S901 GLASS CLOTH REINFORCED EPOXY

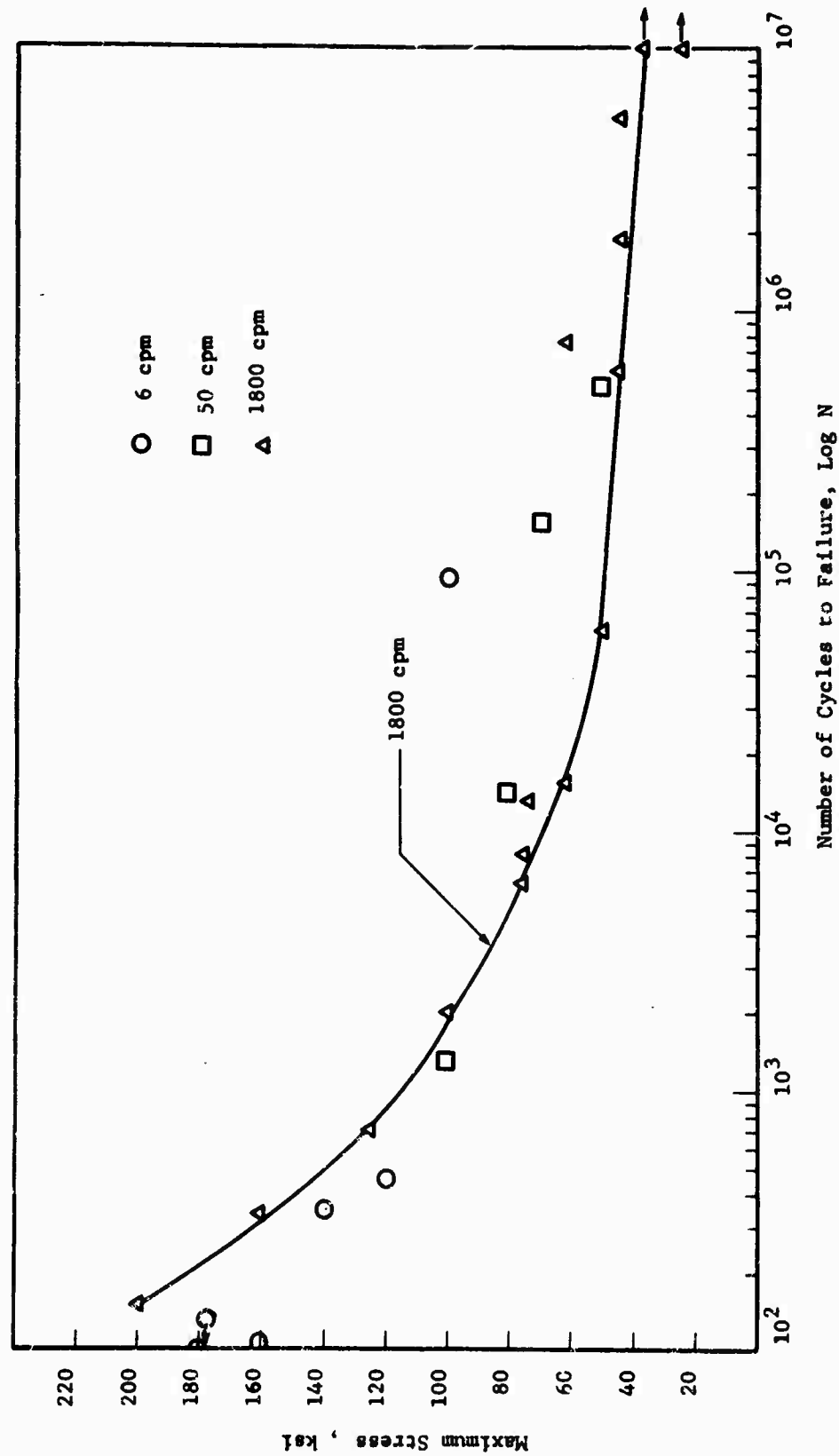


Fig. 16 MAXIMUM STRESS VERSUS CYCLES TO FAILURE AT SEVERAL FREQUENCIES FOR TENSION-ZERO-TENSION ( $R = 0.05$ ) LOADING FOR S994 GLASS ROVING REINFORCED EPOXY

#### Mean Stress (Compressive) Equal to Alternating Stress-Axial Loading

The results for specimens tested in compression-zero-compression axial loading state are shown in Tables 14 and 15. The plots of stress amplitude versus cycles to failure are shown in Figs. 17 and 18 for the 181/S901 glass cloth and S994 uniaxial roving reinforced epoxies respectively.

#### Zero Mean Stress, Out-of-Plane Bending

Results for specimens tested in fully reversed pure bending are presented in Tables 16 and 17. Figures 19 and 20 for 181/S901 glass cloth and S994 uniaxial roving reinforced epoxy, respectively, show the plot of stress amplitude versus cycles to failure.

#### Mean Stress (Bending) Equal to Alternating Stress Out-of-Plane Bending

Results for specimens tested in bending at a mean bending moment equal to the alternating bending moments are shown in Tables 18 and 19 and in Figs. 21 and 22 for 181/S901 glass cloth and S994 uniaxial roving reinforced epoxy respectively.

#### C. EFFECT OF REPEATED LOAD APPLICATION AT AN ANGLE OF 45 DEG TO WEAVE - 181/S901 GLASS REINFORCED EPOXY

The reduction in static strength that occurs when uniaxial load is applied in a direction of 45 deg to the fibers in a 1:1 cloth such as 181 weave is well-known. The fatigue strength reduction is less well-established. To supplement data on the 181/S901 glass cloth reinforced epoxy obtained for axial tension, compression, and fully reversed fatigue lives, it was decided to perform a single series of tests in tension-zero-tension ( $R = 0.05$ ) on the 181/S901 glass cloth reinforced epoxy sheet material.

Table 14

EFFECT OF MEAN COMPRESSIVE STRESS ON FATIGUE LIFE AT 6,  
50 AND 1800 CPM; MEAN COMPRESSIVE STRESS = ALTERNATING  
STRESS (R = 10) FOR 181/S901 GLASS CLOTH REINFORCED EPOXY

Specimen Number	Loading Frequency (cpm)	Maximum Compressive Stress (ksi)	Cycles to Failure
12-C-11	6	-42.0	10,988
5-C-12	6	-55.0	1
5-C-13	6	-29.5	19,101*
5-C-14	6	-52.5	1
6-C-15	6	-36.0	198
7-C-16	6	-33.0	28,815*
3-C-17	6	-32.0	1,436
3-C-18	6	-36.0	385
7-C-19	6	-47.0	38
4-C-20	6	-35.0	13,300*
4-C-21	6	-38.0	210
1-C-11	6	-39.0	60
14-C-12	6	-37.0	22
16-C-13	6	-35.0	364
14-C-14	6	-33.0	302
15-C-15	6	-31.0	7,000
11-C-30	50	-45.0	5
11-C-41	50	-40.0	17
11-C-42	50	-35.0	9,986
6-C-26	50	-32.5	1,460
11-C-43	50	-30.0	296,270
8-C-31	1800	-28.0	55,000
2-C-32	1800	-25.0	9,501,000
1-C-33	1800	-24.5	23.8 x 10 <sup>6</sup>

\* Runout, no failure.

Table 15

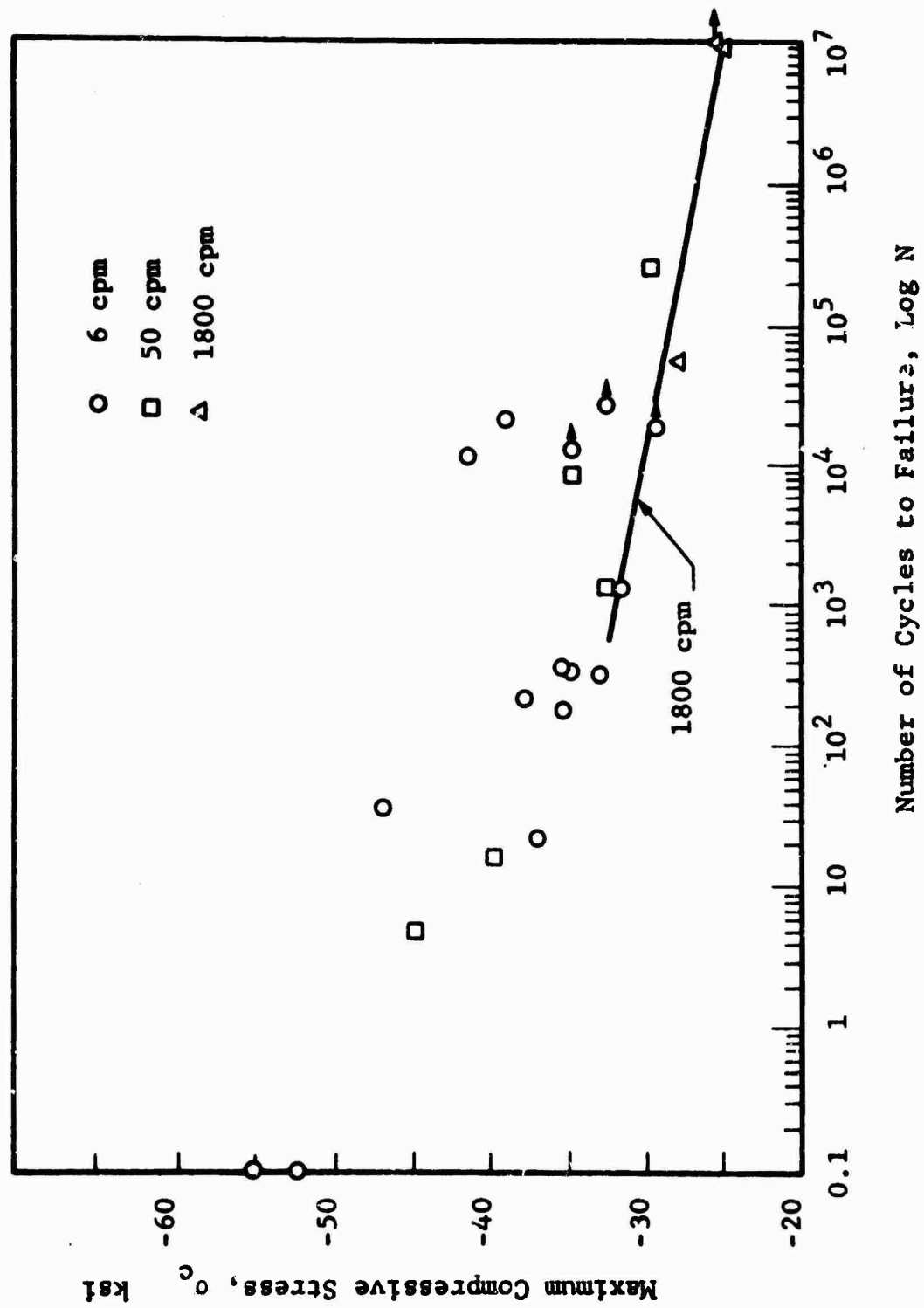
EFFECT OF MEAN COMPRESSIVE STRESS ON FATIGUE LIFE AT 6,  
50 AND 1800 CPM; MEAN COMPRESSIVE STRESS = ALTERNATING  
STRESS (R = 10) FOR S994 UNIAXIAL ROVING REINFORCED EPOXY

Specimen Number	Loading Frequency (cpm)	Maximum Compressive Stress (ksi)	Cycles to Failure
39-C-11	6	-60.0	10
39-C-12	6	-65.0	8
39-C-14	6	-55.0	148
39-C-15	6	-50.0	1,384
39-C-16	6	-50.0	429
20-C-21	50	-65.0	2
21-C-22	50	-60.0	81
22-C-23	50	-55.0	195
39-C-24	50	-55.0	95
20-C-31	1800	-35.0	11,312,000*
26-C-32	1800	-55.0	111,000
25-C-33	1800	-60.0	1,000
23-C-34	1800	-57.5	108,000
24-C-35	1800	-52.5	2,000**
26-C-36	1800	-52.5	401,000
17-C-37	1800	-52.5	9,000***
20-C-38	1800	-50.0	326,000
18-C-39	1800	-45.0	669,000
25-C-40	1800	-40.0	5,604,000

\* No failure, runout.

\*\* Low cyclic life attributed to clamping stress at minimum  
section - not plotted.

\*\*\* Buckling noted - not plotted.



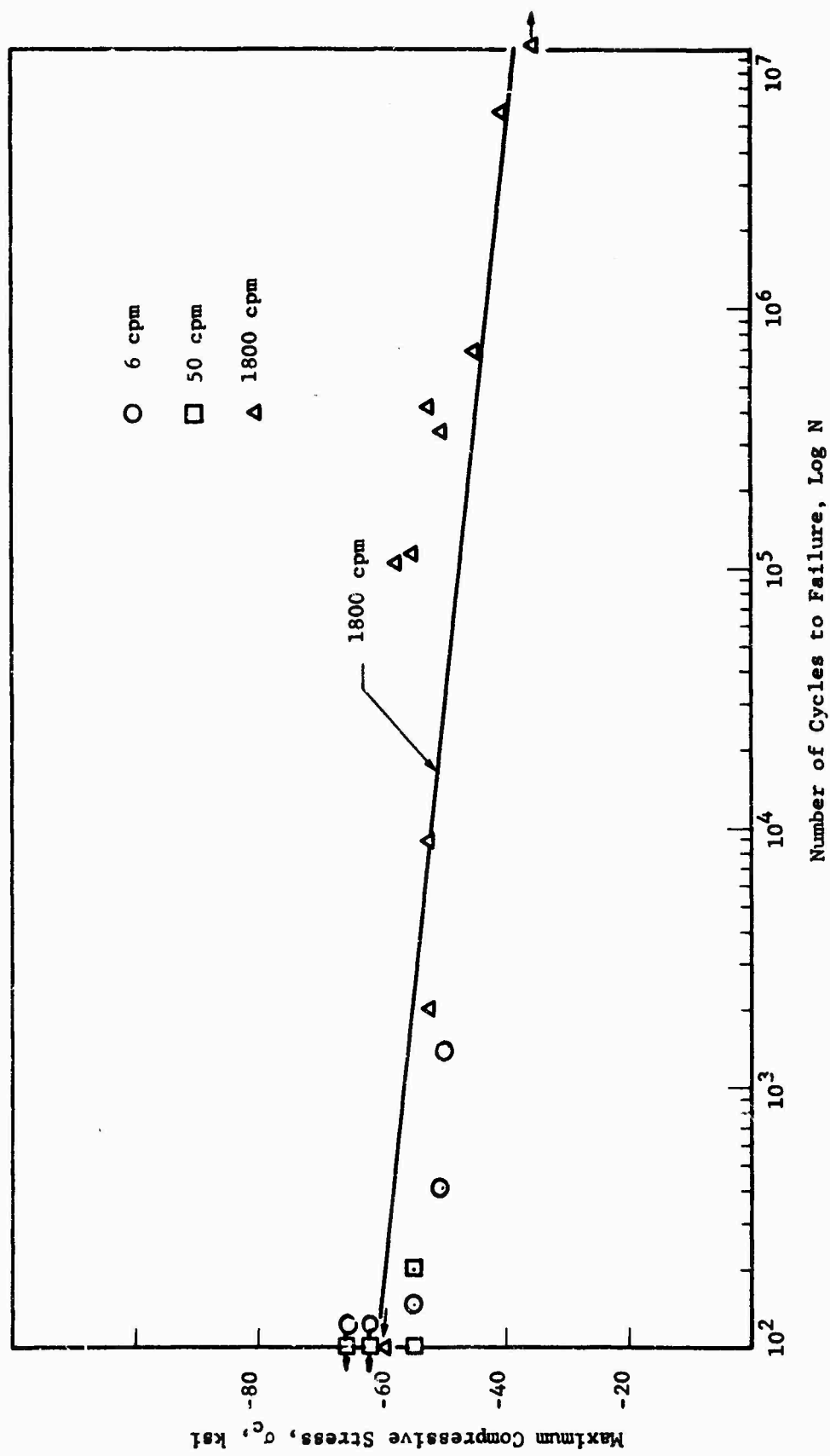


Fig. 18 MAXIMUM COMPRESSIVE STRESS VERSUS CYCLES TO FAILURE AT SEVERAL FREQUENCIES FOR COMPRESSION-ZERO-COMPRESSION ( $R = -10$ ) LOADING FOR S994 GLASS ROVING REINFORCED EPOXY

**Table 16**  
**BENDING FATIGUE LIFE AT 6, 50 AND 1800 CPM (R = -1)**  
**FOR 181/S901 GLASS CLOTH REINFORCED EPOXY**

Specimen Number	Loading Frequency (cpm)	Alternating Bending Stress (ksi)	Cycles to Failure
28-B1-11	6	50.0	73
28-B1-12	6	32.4	14,067
28-B1-13	6	27.0	13,875
28-B1-14	6	60.0	18
28-B1-15	6	70.0	69
28-B1-16	6	40.0	2,050
31-B1-8	6	60.0	160
31-B1-37	6	40.0	936
27-B1-21	50	32.4	297
27-B1-22	50	27.0	50,000*
27-B1-23	50	50.0	1,149
27-B1-31	1800	32.4	29,000
27-B1-32	1800	27.0	54,000
27-B1-33	1800	23.4	371,000
27-B1-34	1800	18.0	824,000
27-B1-35	1800	45.0	3,000
27-B1-36	1800	27.5	16,000
27-B1-37	1800	18.0	8,936,000
27-B1-38	1800	20.0	971,000
27-B1-39	1800	35.0	8,000

\* Runout, no failure



**Table 17**  
**BENDING FATIGUE LIFE AT 6 AND 1800 CPM (R = -1)**  
**FOR S994 UNIAXIAL GLASS ROVING REINFORCED EPOXY**

Specimen Number	Loading Frequency (cpm)	Alternating Bending Stress (ksi)	Cycles to Failure
33-B1-11	6	55.0	24,728
29-B1-12	6	45.0	51,022
29-B1-13	6	65.0	420
37-B1-14	6	60.0	857
37-B1-15	6	40.0	23,500
29-B1-32	1800	25.0	180,000
29-B1-33	1800	27.0	122,000
29-B1-34	1800	25.0	1,051,000
29-B1-35	1800	30.0	11,000
29-B1-36	1800	23.0	379,000

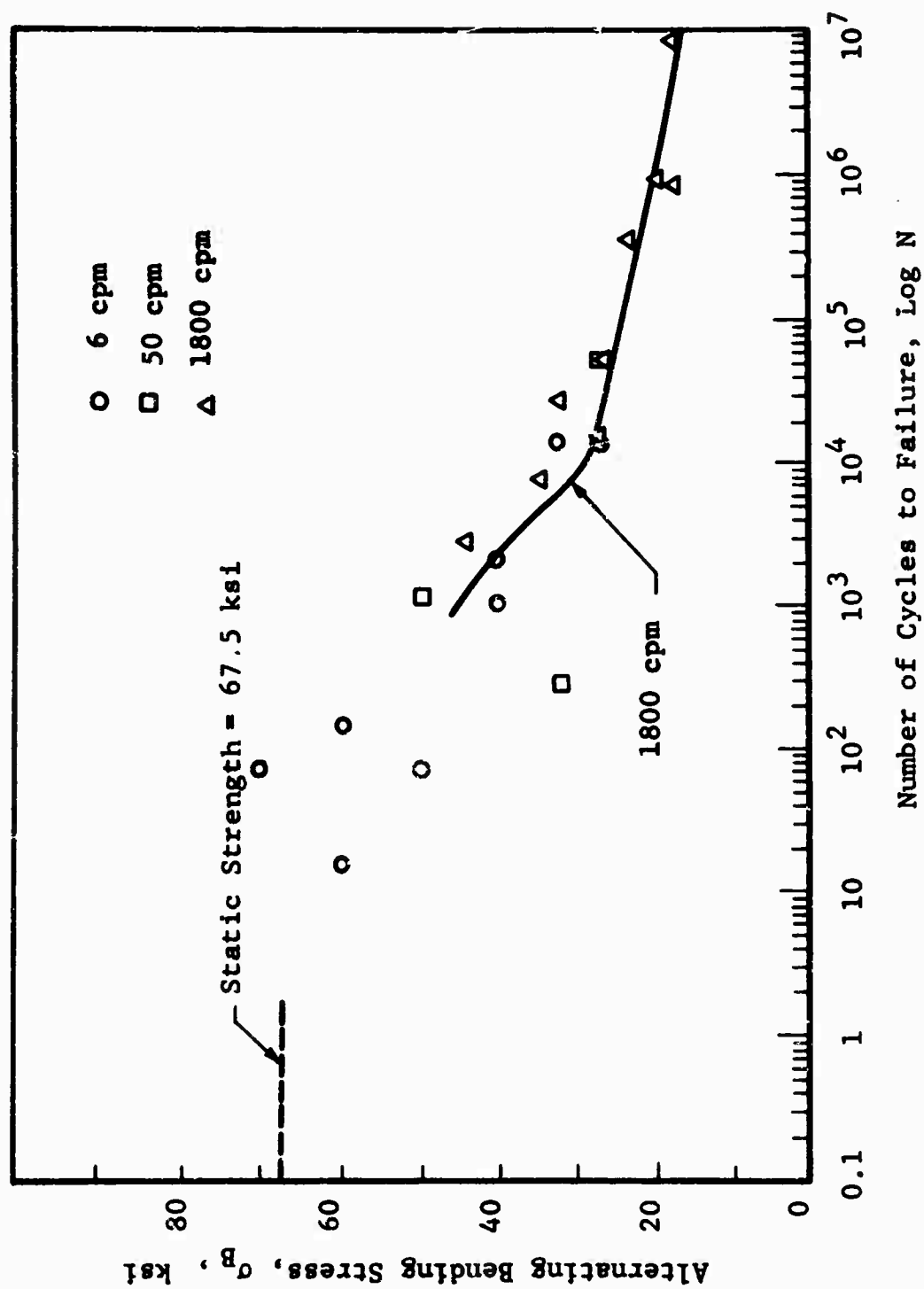


Fig. 19 ALTERNATING BENDING STRESS VERSUS CYCLES TO FAILURE AT THREE FREQUENCIES FOR FULLY REVERSED OUT OF PLANE BENDING (R=-1) LOADING FOR 181/S901 GLASS CLOTH REINFORCED EPOXY

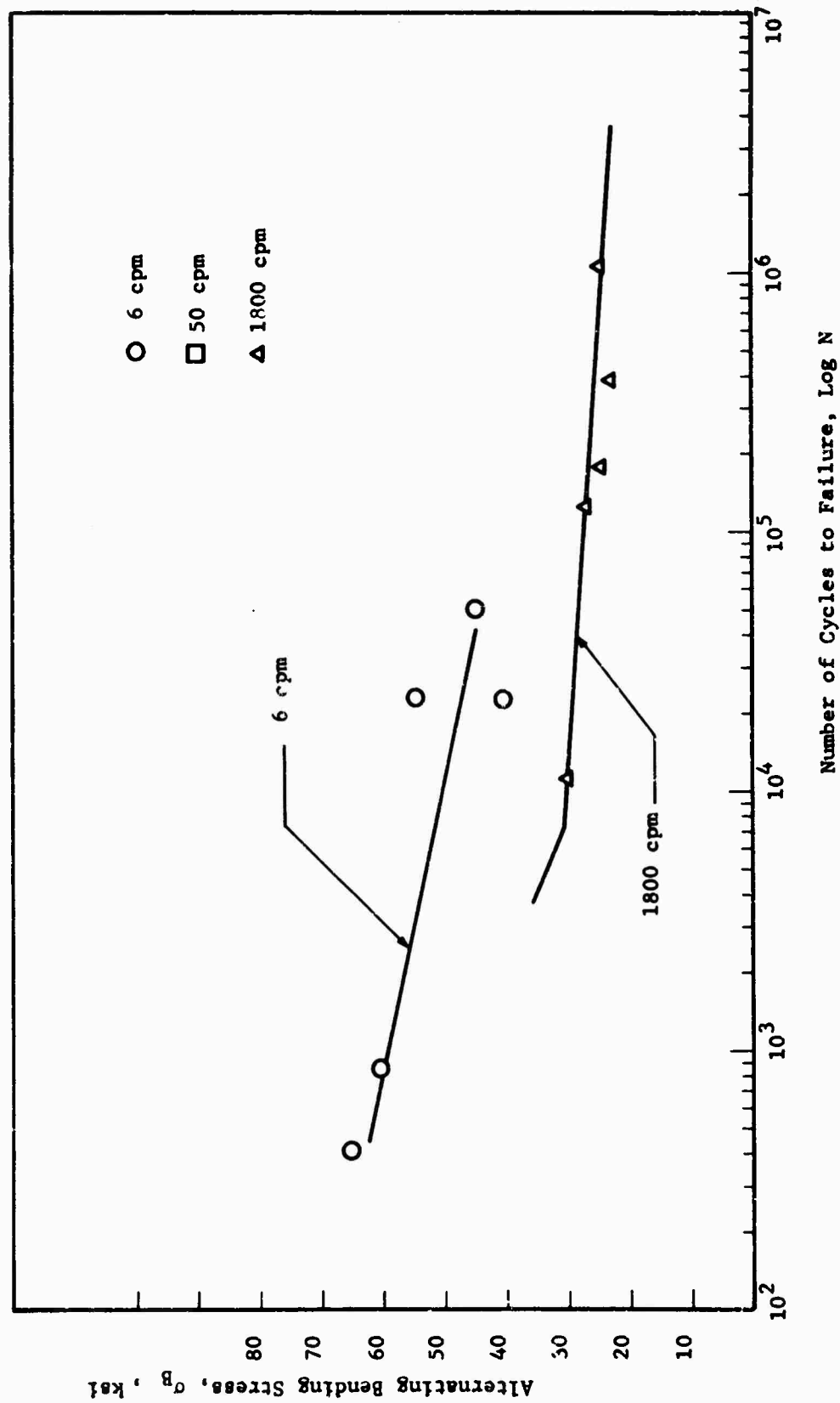


Fig. 20 ALTERNATING BENDING STRESS VERSUS CYCLES TO FAILURE AT SEVERAL FREQUENCIES FOR FULLY REVERSED OUT-OF-PLANE BENDING (R = -1) LOADING OF S994 GLASS ROVING REINFORCED EPOXY

Table 18

EFFECT OF MEAN BENDING STRESS ON FATIGUE LIFE AT 6, 50  
AND 1800 CPM; OUT OF PLANE BENDING WITH MEAN BENDING  
STRESS EQUAL TO ALTERNATING BENDING STRESS ( $R = 0.05$ )  
FOR 181/S901 GLASS CLOTH REINFORCED EPOXY

Specimen Number	Loading Frequency (cpm)	Maximum Bending Stress (ksi)	Cycles to Failure
28-B2-11	6	75.0	2
28-B2-12	6	70.0	5
28-B2-13	6	60.0	121
28-B2-14	6	50.0	55,281
27-B2-21	50	38.7	28,355
27-B2-23	50	40.0	10,977
27-B2-24	50	35.0	143,840
27-B2-25	50	60.0	98
27-B2-26	50	50.0	4,882
27-B2-31	1800	32.4	16,000,000*
27-B2-32	1800	40.5	197,000
27-B2-33	1800	58.5	8,000
27-B2-34	1800	54.0	4,000
27-B2-35	1800	45.0	14,000
27-B2-36	1800	38.7	1,420,000
27-B2-37	1800	49.5	14,000
32-B2-39	1800	62.5	1,000

\* No failure, runout.

Table 19

EFFECT OF MEAN BENDING STRESS ON FATIGUE LIFE AT 6 AND 1800 CPM:  
OUT OF PLANE BENDING WITH MEAN BENDING STRESS = ALTERNATING BENDING  
STRESS (R = 0.05) FOR S994 GLASS ROVING REINFORCED EPOXY

Specimen Number	Loading Frequency (cpm)	Maximum Bending Stress (ksi)	Cycles to Failure
33-B2-11	6	70.0	42,448
33-B2-12	6	90.0	3
33-B2-13	6	80.0	2,576
37-B2-14	6	60.0	7,810
37-B2-15	6	72.0	724
29-B2-31	1800	80.0	4,000
29-B2-32	1800	48.0	7,900,000
29-B2-33	1800	46.0	1,091,000
29-B2-34	1800	52.0	40,000
29-B2-35	1800	50.0	1,169,000
29-B2-36	1800	50.0	20,000
29-B2-37	1800	52.0	12,300,000

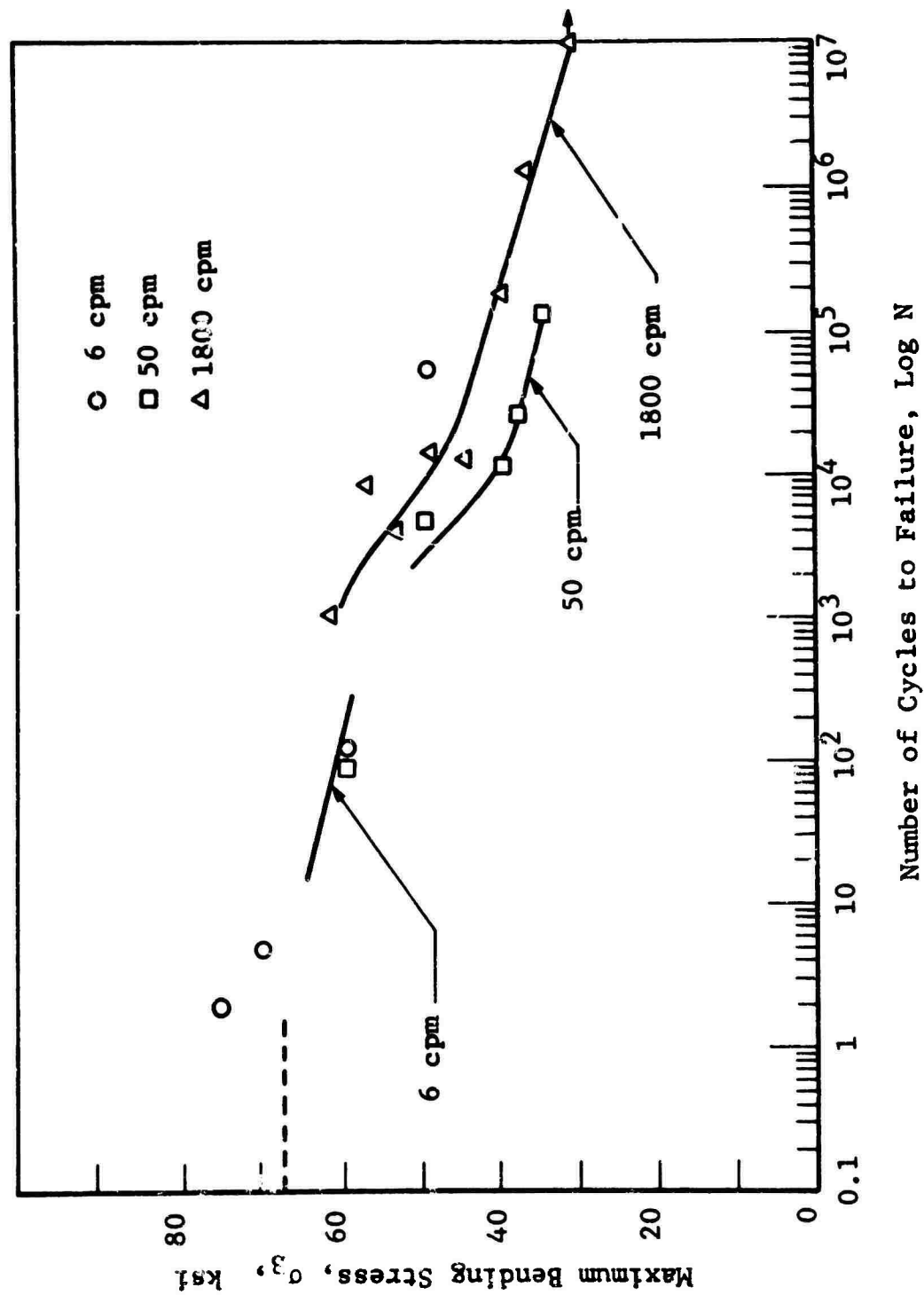
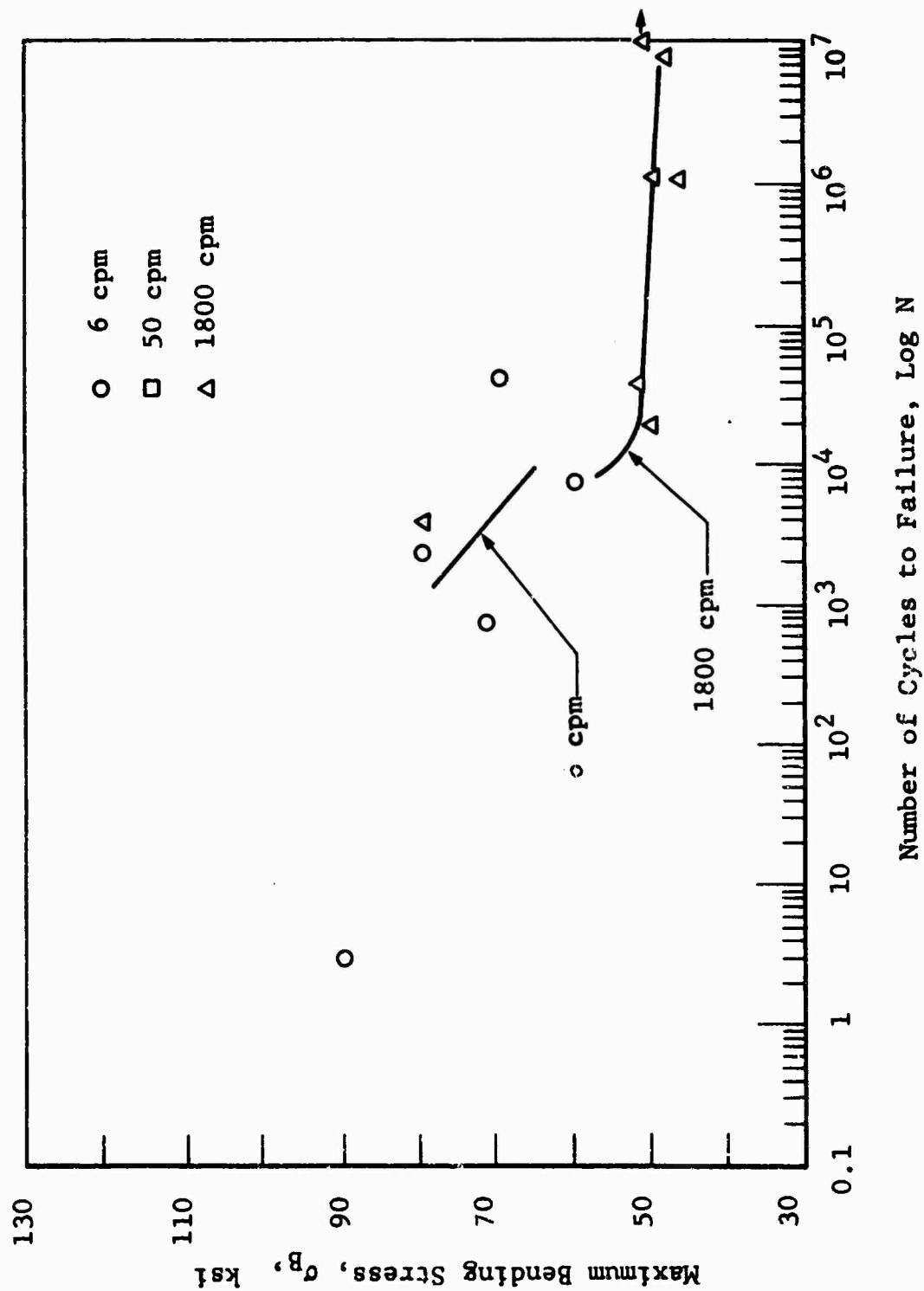


Fig. 21 MAXIMUM BENDING STRESS VERSUS CYCLES TO FAILURE AT THREE FREQUENCIES FOR OUT OF PLANE BENDING WITH A MEAN BENDING STRESS EQUAL TO THE ALTERNATING BENDING STRESS ( $R=0.05$ ) FOR 181/S901 GLASS CLOTH REINFORCED EPOXY



Specimens were removed from blanks as shown in Fig. 23. Table 20 shows the results of this series of tests and Fig. 24 is a plot of the maximum stress versus cycles to failure.

D. COMPARISON OF AMPLITUDE FATIGUE RESULTS WITH RESULTS OF TESTS ON SIMILAR EPOXY MATERIALS AND WITH THOSE OF OTHER INVESTIGATORS

A 6 by 20 in. section of 1/8 in. laminate made from 16 layers of 181/S994 glass cloth reinforced Jones-Dabney 510 with metaphenylene-diamine was forwarded to IITRI from the Naval Air Engineering Center. The material was, of course, similar to the resin-reinforcement system extensively tested as described earlier. The laminate was, however, produced by vacuum-bagging rather than press-laminating. This difference resulted in a satiny appearance and a much higher resin content. The particular plate tested had a resin content of 39.6 percent and a tensile strength of 74,700 psi (average of two specimens).

Twelve constant radius fatigue specimens (see Fig. 6) were prepared and subjected to uniaxial tension-zero-tension ( $R = 0.05$ ) fatigue. The results are presented in Table 21 and Fig. 25.

A review of the literature showed that tests had also been conducted on this 181/S994 glass cloth reinforced epoxy at North American Aviation, Inc.\* using a constant 1 1/4 in. radius specimen 6 in. long. Specimens were 23 plies thick. Specimens were tested in the fully reversed, tension-zero-tension and compression-zero-compression modes ( $R = -1, 0.05$  and 10 respectively). Figure 26 shows the results found by North American.

\* NA64H-1283



9-S2-11-3	9-S2-11-2	9-S2-11-1	
-----------	-----------	-----------	--

Blank No. 9-S2-11

9-S2-21-1	9-S2-21-2	9-S2-21-3	
-----------	-----------	-----------	--

Blank No. 9-S2-21

9-S2-23-1	9-S2-23-2	9-S2-23-3	
-----------	-----------	-----------	--

Blank No. 9-S2-23

13-S2-9-1	13-S2-9-2	13-S2-9-3	
-----------	-----------	-----------	--

Blank No. 13-S2-9

Fig. 23 SPECIMENS USED FOR TESTING 181/S901 GLASS CLOTH  
REINFORCED EPOXY AT 45 DEG TO WEAVE BLANKING-SCHEDULE

Table 20  
 FATIGUE LIFE OF 181/S901 GLASS CLOTH REINFORCED EPOXY  
 LOADED AT 45 DEG ANGLE TO WEAVE IN UNIAXIAL TENSION-  
 ZERO-TENSION FATIGUE (R = 0.05) - 1800 CPM

Specimen Number	Maximum Stress (ksi)	Percent Ult (%)	Cycles to Failure	Remarks
9-S2-33-3	32,850	100.0		Static Test
9-S2-11-3	21,360	65.0	150	
9-S2-21-1	14,780	45.0	2,000	
9-S2-33-1	12,390	37.0	4,000	
9-S2-21-2	11,830	36.0	7,000	
9-S2-21-3	11,500	35.0	6,000	
9-S2-33-2	11,500	35.0	10,000	
9-S2-11-1	11,500	35.0	3,113,000	
9-S2-11-2	9,855	30.0	10 <sup>7*</sup>	
13-S2-9-1	6,600	20.0	10 <sup>7*</sup>	

\*  
 No failure, runout.

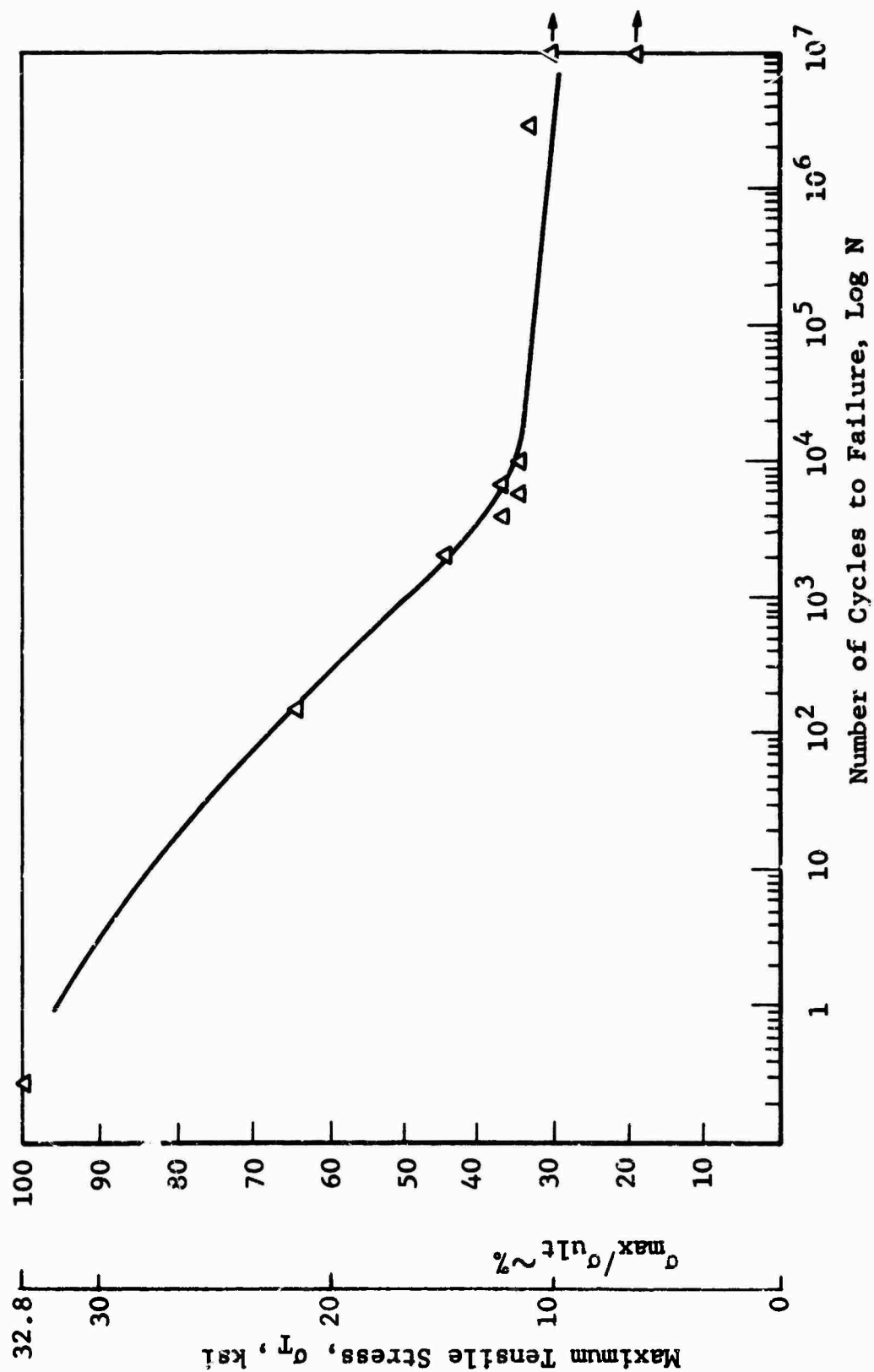


Fig. 24 TENSION FATIGUE CURVE, STRESS VERSUS CYCLES TO FAILURE ( $R=0.05$ ) FOR 181/S901 GLASS CLOTH REINFORCED PLASTIC LOADED AT 45 DEG TO THE WEAVE - 1800 CPM

Table 21

TENSION-ZERO-TENSION FATIGUE TEST RESULTS ON VACUUM-BAGGED  
181/S994 GLASS CLOTH REINFORCED EPOXY - ( $R = 0.05$ ) TESTED  
AT 1800 CPM, STATIC STRENGTH = 74,700 PSI

Specimen Number	Maximum Tensile Stress (ksi)	Cycles to Failure
NA-T-1	36.0	326,000
NA-T-2	14.4	14,880,000
NA-T-3	54.0	990
NA-T-4	32.4	15,000
NA-T-5	36.0	4,000
NA-T-6	36.0	14,000
NA-T-7	32.4	8,000
NA-T-8	30.6	12,000
NA-T-9	21.6	
NA-T-10	25.2	408,000
NA-T-11	18.0	8,880,000
NA-T-12	39.6	4,000

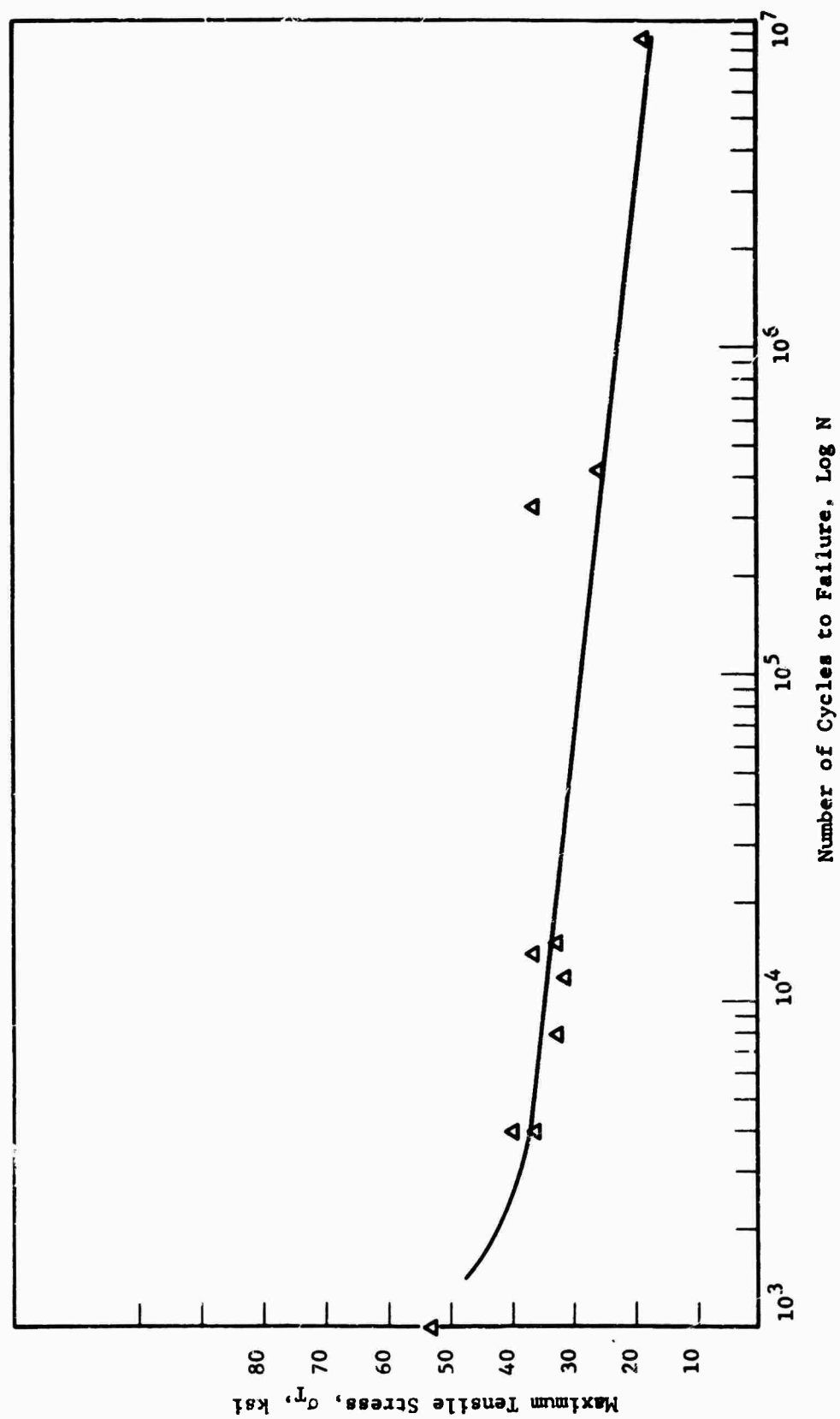


Fig. 25 TENSION-ZERO-TENSION ( $R = 0.05$ ) FATIGUE RESULTS FOR VACUUM-BAGGED 181/S994 GLASS CLOTH REINFORCED EPOXY - GLASS CONTENT = 60.35 PERCENT

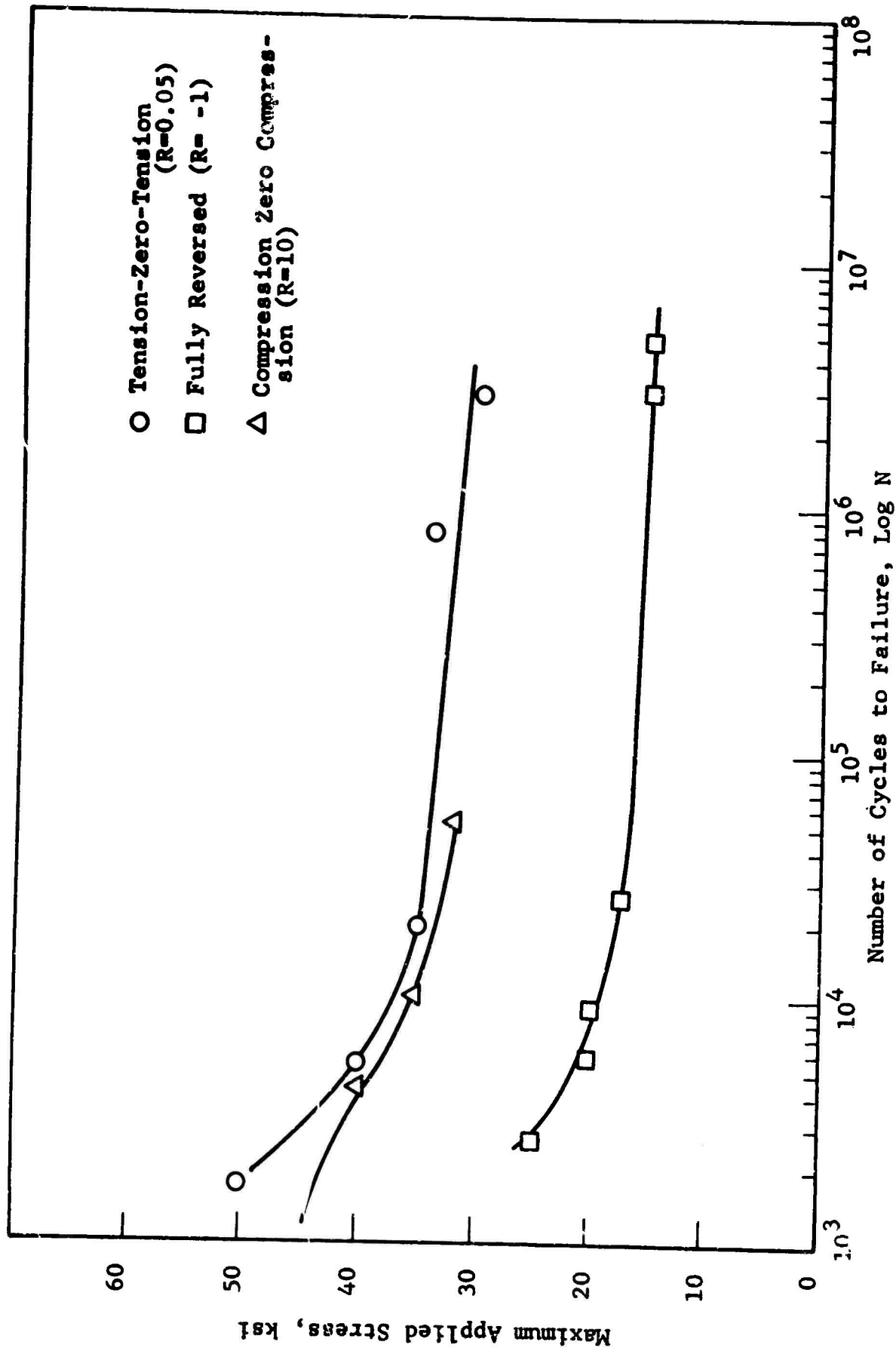


Fig. 26 FATIGUE RESULTS FOR VACUUM BAGGED 181/S994 GLASS CLOTH REINFORCED EPOXY AT THREE STRESS RATIOS, TESTED AT ROOM TEMPERATURE - NAA RESULTS

#### E. FATIGUE TESTS OF 143/S901 GLASS CLOTH REINFORCED EPOXY

As a means of comparing one type of glass fabric reinforced epoxy with another, as well as identification of the similarities and differences between two forms of strongly preferentially oriented reinforcement (i.e. glass rovings and fabric), 143/S901 glass fabric was selected. A series of tension-zero-tension ( $R = 0.05$ ) fatigue tests were performed at 1800 cpm. The results are shown in Table 22 and are plotted as maximum stress versus cycles to failure in Fig. 27.

#### F. TORSIONAL FATIGUE; SHEAR STRESS FATIGUE OF S994 GLASS ROVING REINFORCED EPOXIES

Fatigue tests were performed with a closed loop materials torquing machine described in Appendix F. The torque tube specimen was designed to be shear failure critical rather than compressive or tensile failure critical and to fail at or near 6,000 in-lb of torque.

The composite specimen is the tubular shaped piece described in Appendix F and shown unbroken in Fig. 28. The ends of the specimen are built-up to cause the failure to occur in the gage length. The inside diameter of the ends is maintained while the outside diameter is increased to 2 in. at each end for 1 in. The built-up end is simply a radial wind with the angle of wind nearly zero. On the other hand, the main tube of the specimen is wound with a 45 deg helix angle.

The built-up ends were then cemented with epoxy adhesive to end grips made of aluminum. To assure proper bonding of the specimen to the grip, the grips were acid etched. The etching serves two functions, 1) to degrease the metal surface, and 2) to provide an active bond surface. Surfaces of metal with finger prints from handling or oil from machining decrease bond effectiveness or eliminate it entirely. The shear strength of this bond was indeed exceeded during one of the tests. To carry load over and above the bond strength, subsequent specimens were

Table 22

TENSION-ZERO-TENSION (R = 0.05) FATIGUE TEST RESULTS ON  
143/S901 GLASS CLOTH REINFORCED EPOXY, TESTED AT 1800 CPM  
STATIC STRENGTH = 123,000 PSI, PERCENT GLASS = 70 PERCENT

Specimen Number	Maximum Tensile Stress (ksi)	Cycles to Failure
43-T-2	56.0	1,000
43-T-17	35.0	71,000
43-T-19	56.0	5,000
43-T-9	56.0	4,000
43-T-4	28.0	134,000
44-T-3	42.0	6,000
44-T-10	16.9	8,171,000
44-T-2	33.8	58,000
44-T-5	28.2	223,000
44-T-8	22.5	503,000
44-T-9	33.8	40,000
44-T-11	45.1	3,000
44-T-15	56.4	1,500
44-T-16	56.4	1,000
44-T-19	73.3	369
44-T-21	73.3	330
44-T-1	16.9	10,737,000
44-T-17	28.2	346,000
44-T-18	22.5	784,000



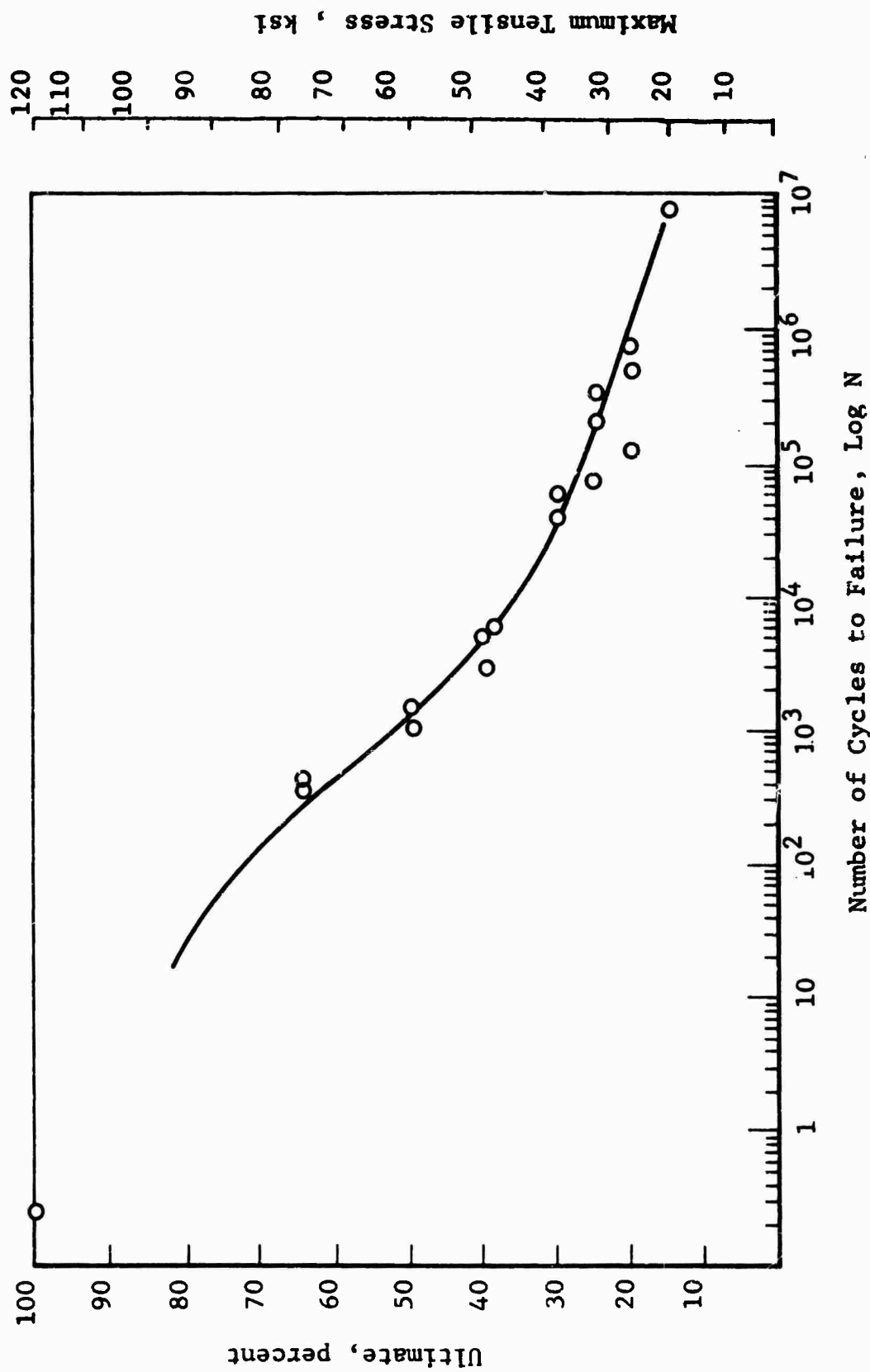


Fig. 27 MAXIMUM STRESS VERSUS CYCLES TO FAILURE FOR 143/S901 GLASS CLOTH REINFORCED EPOXY TESTED IN TENSION-ZERO-TENSION ( $R=C.05$ ) IN THE PREFERENTIAL STRONG DIRECTION, TESTED AT ROOM TEMPERATURE AT 1800 CPM

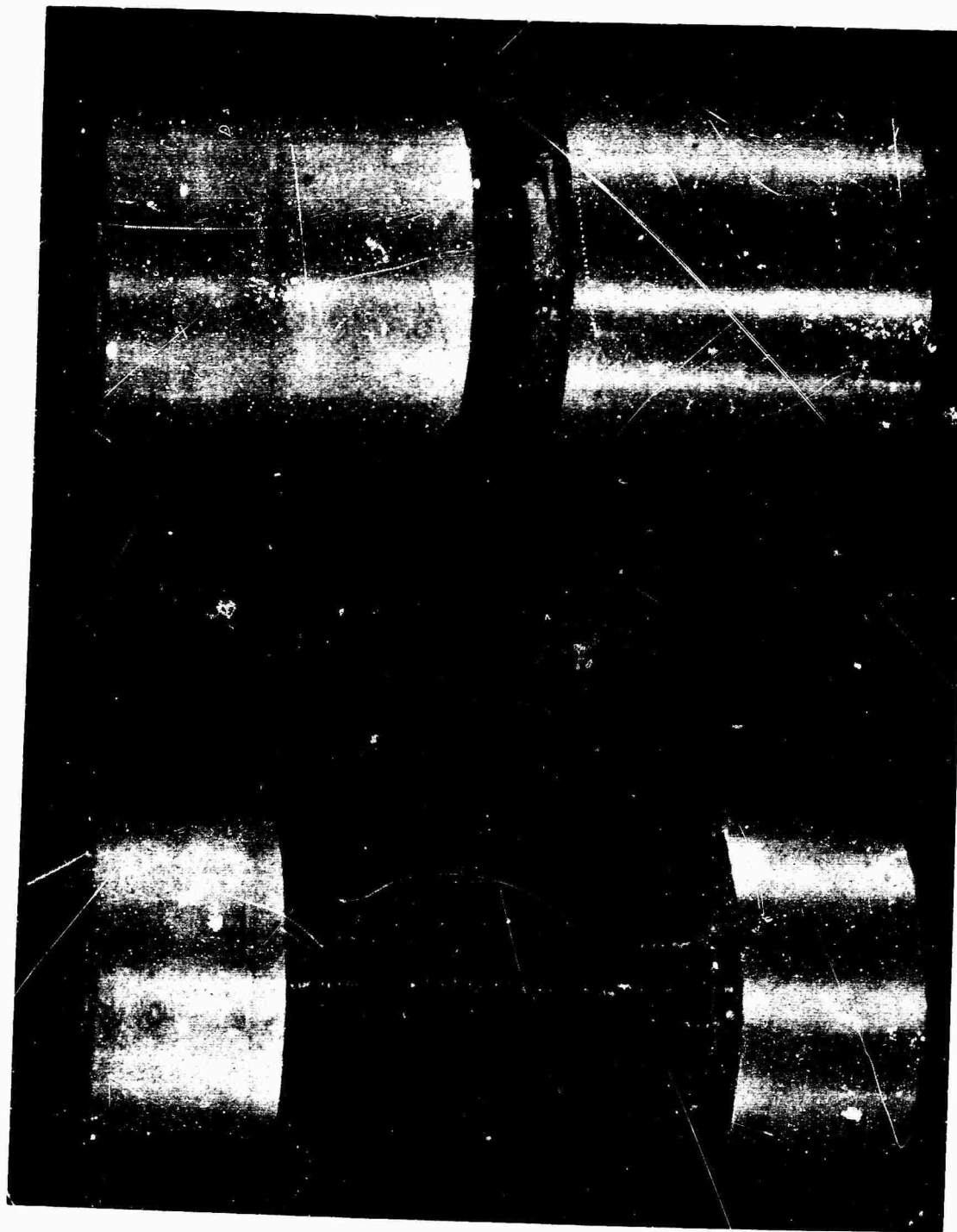


Fig. 28 TYPICAL UNFAILED TORSION SPECIMENS AND GRIPS  
(FOR TESTING OF SPECIMEN ON RIGHT, SEE APPENDIX D)

pinned with a dowel through the grip. This was done in addition to cementing. The combination of cement and pin was sufficient to carry the entire load.

Clearance between the specimen and grip was held to 0.005-0.010 in. This provides ample room for the epoxy to flow evenly in the joint bonding both surfaces. To maintain this close tolerance, both the grip and specimen were machined.

Once the specimen was bonded in place, the aluminum grips were attached to the splined hub of the actuator at one end and to the load cell on the other end. The attachment on the actuator end was made with bolts through the grip. At the load cell, coupling was made by bolts passing through the attachment point and screwed into tapped holes in the grip (see Fig. 103).

The testing procedure for fatigue specimens is divided into three distinct operations.

1. The specimen is placed in the testing frame, making certain that proper alignment is maintained.
2. The test specimen is statically or dynamically loaded until failure occurs. For static tests, the appropriate loading rate is selected and programmed. For dynamic tests, the appropriate maximum and minimum torque levels and the frequency of load application are fixed.
3. The specimen is removed from the load frame and the data is evaluated by means of both visual inspection of the test specimen and reduction of the recorded information.

To collect meaningful data in a torque test system, the first requisite is good specimen circumferential alignment. Special attention is given to reduce the bending that would result as load is applied to the specimen. The test fixture mentioned previously was designed to produce a simple pure torque.

The load measuring system is insensitive to all loads except the couple which is produced by the specimen in pure torsion, and hence, the addition of other stress components reduces the validity of the data.

Before actual testing, the load system was calibrated. The calibration loading of the load cell is accomplished with the loading fixture described earlier. As the calibrating weights are added to the loading fixture, the output from the load cell is observed. The output is a linear analog signal in the millivolt range. To actually determine the output voltage, a digital voltmeter (DVM) was used. The DVM was read to the nearest 0.01 mv. Total or maximum output was 20 mv which corresponds to 8,000 in-lb. Maximum resolution of the calibration was  $\pm 2$  in-lb or 0.025 percent of full scale.

After load cell calibration, the specimen was placed in the test fixture. Load cell output was recorded on an X-Y recorder. The output load signal was recorded to  $\pm 10$  in-lb. This is the load accuracy for all tests. Load was recorded on the Y-axis of the recorder and angular rotation of the actuator on the X-axis.

For fatigue testing an additional step was required prior to testing. The feedback signal from the load cell was reset before the specimen was installed in the test fixture. This produced a mechanical closed loop prior to load application. The closed loop consisted of a path from the load cell to the servac amplifier, to the servo valve, to the actuator closed by the specimen and the load cell. In an effort to avoid overload of the test specimen, a substitution blank was used to complete the loop. The loads were set at  $1/2$  and  $2/3$  ultimate shear load for the actual specimen. Once the loads were inputted, the tests were performed.

The load-time history for cyclic fatigue was a sine function with a frequency of 50 cpm. The command signal for the test program was obtained from a low frequency function generator capable of 0.01 to 5,000 cps.

Figure 29 shows a typical record of torque versus angle of rotation. Table 23 shows the values of torque and cycles to failure for specimens tested and is also plotted in Fig. 30.

#### G. DISCUSSION OF FREQUENCY AND AMPLITUDE STUDIES

The results described in the previous section were examined to establish the influence of frequency on endurance strength and on life at a given stress level.

Examination of the S-N curves shows that there is no appreciable effect of frequency for the tensile axial fatigue conditions, a small effect is present in the fully reversed condition and a somewhat greater effect is present for the bending and axial compression fatigue conditions. The effects appear to be related to the compressive portion of the cyclic loading.

Such effects are not surprising in view of the fact that it is well known that by loading and unloading polymeric materials, a slight hysteresis loop is noted even at low frequencies. In such a stress-strain diagram, the hysteresis loop has an area  $\Delta_w$ .  $\Delta_w$  represents energy lost per unit volume for each cycle of stress. In general,  $w$  is dependent upon the amplitude of the stress according to a relationship of the form:

$$w = C_1 (\sigma *)^n$$

where

$C_1$  is a proportionality constant

$n$  is a power exponent usually between 2 and 3  
for metallic materials (for GRP materials,  
it may be higher)

The area enclosed by the hysteresis loop,  $\Delta_w$ , is significant in that it represents energy that is converted into heat within the specimen during each cycle of stress. This heat must be conducted to the surface of the polymer and dissipated to the atmosphere by convection. Since polymers are relatively poor conductors of heat, higher frequencies of load application

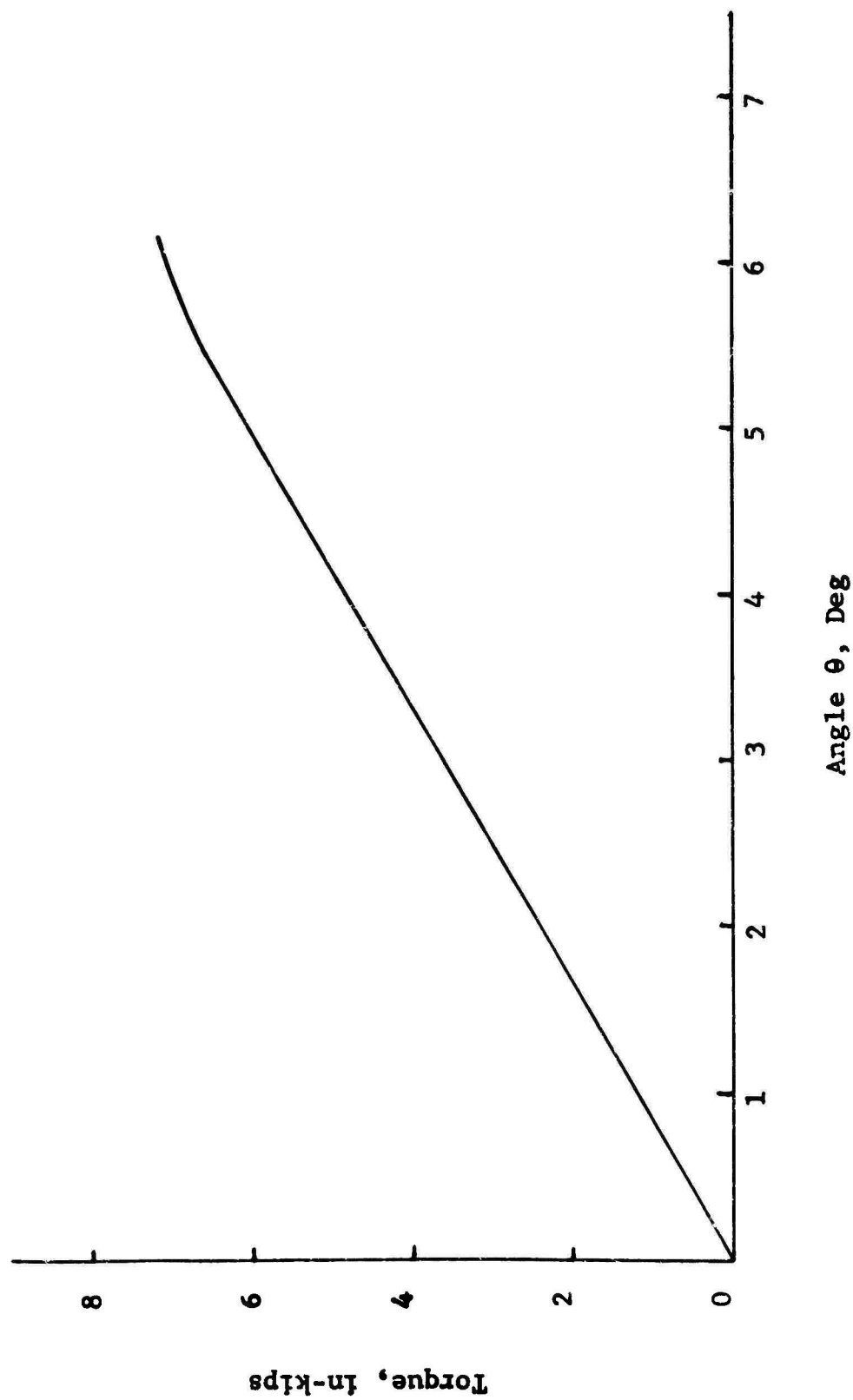


Fig. 29 TYPICAL TORQUE-ANGLE OF ROTATION PLOT FROM HYDRO-MECHANICAL TORQUE MACHINE  
FOR BASKET-WOVEN S994 GLASS ROVING REINFORCED EPOXIES

Table 23  
RESULTS OF TORSIONAL FATIGUE TESTS ON BASKET-WOVEN  
S994 GLASS ROVING REINFORCED EPOXY

Torque (in-lbs)	Shear Stress (ksi)	Cycles to Failure (n)
7200	76.5	Static Test
3600	38.2	648
3000	31.8	23,538

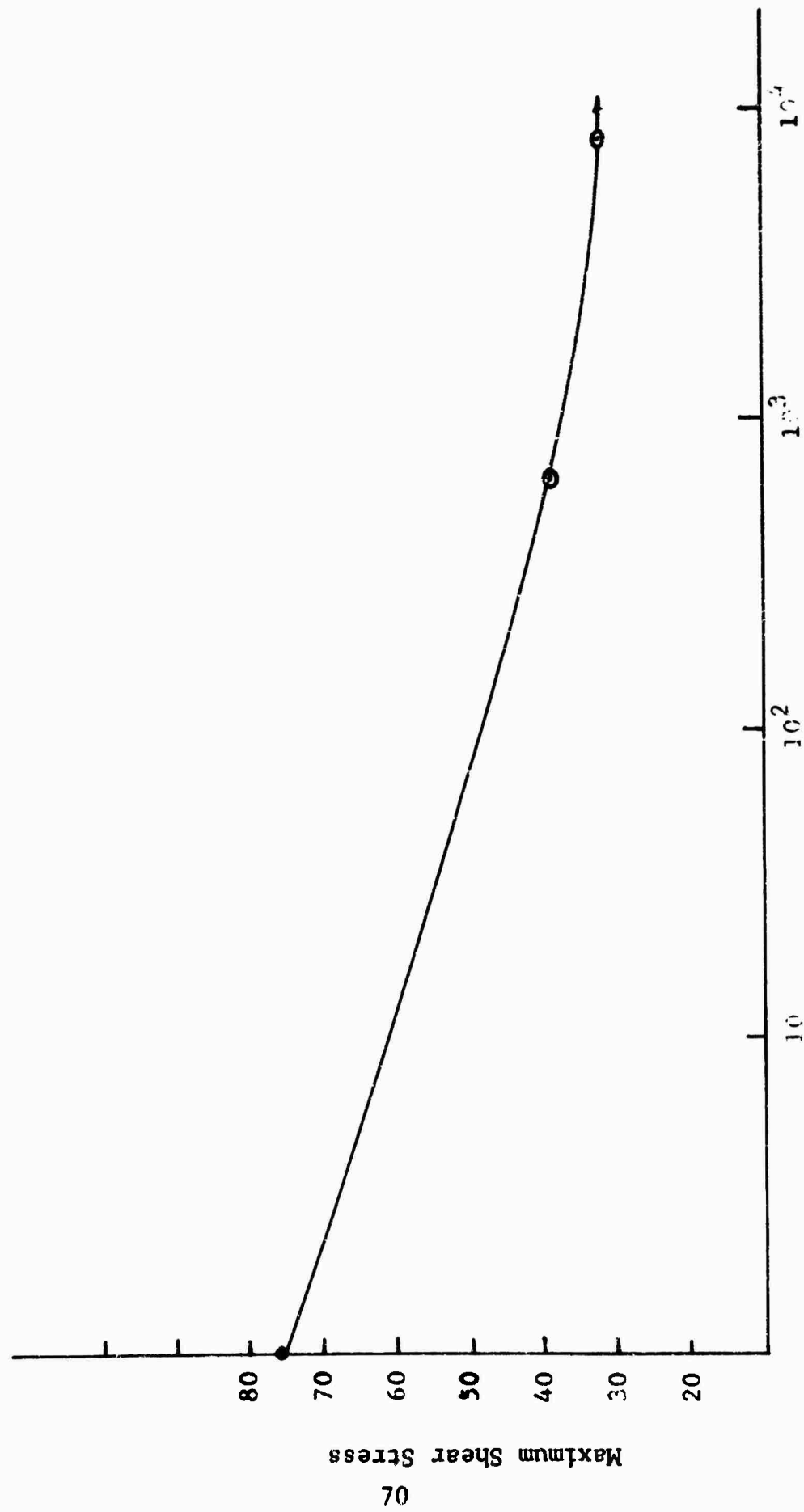


Fig. 30 TORQUE VERSUS CYCLES TO FAILURE FOR BASKETWOVEN S994  
UNIAXIAL GLASS ROVINGS EPOXY COMPOSITES



could produce temperature increases in the specimen at modest stress levels. Increasing the stress level should, of course, increase the specimen temperature according to the power law:

$$T = T_0 (\sigma *)^n$$

This temperature change may work to the detriment of the fatigue life of the glass reinforced plastic, as the properties of the resin matrix material can be altered appreciably by increases in temperature of the order of magnitude that occur in fatigue testing. In tension fatigue, the role of the resin matrix is not as prominent as is its role in compression loading. Thus as might be expected, the tension fatigue results show little if any effect of cyclic rate over the entire life range. However as the specimen experiences increasingly more substantial compressive loadings, the role of the matrix increases, and consequently, the effects of cyclic rate are more prominent.

Since the employment of relatively high speed fatigue testing equipment may considerably shorten the testing time and thereby permit a greater number of specimens to be tested in a relatively short time, this lack of frequency effect over the entire range is particularly advantageous in tension fatigue. This lack of frequency effect also appeared to be present in the intermediate cyclic life range ( $10^4$  to  $10^6$  cycles). The effect of cyclic rate appears to be variable in the sense that for fully reversed axial type loadings the lower cyclic rates indicate higher performance, i.e. longer life at the same stress level, while for the bending loadings poorer performances, i.e. shorter life at the same stress level are indicated. The effect of frequency is much more pronounced for the uniaxial roving type composite than it was for the woven fabric as is indicated by the alternating bending tests as shown in Figs. 19 and 20.

Figure 31 shows a plot of log cycles to failure versus cumulative probability of failure for 181/S901 glass cloth reinforced epoxy tested at  $\sigma = 43,000$  psi in tension-zero-tension ( $R = 0.05$ ). The curve is fairly straight suggesting strongly that the failures are normally distributed about the S-N curve at constant stress.

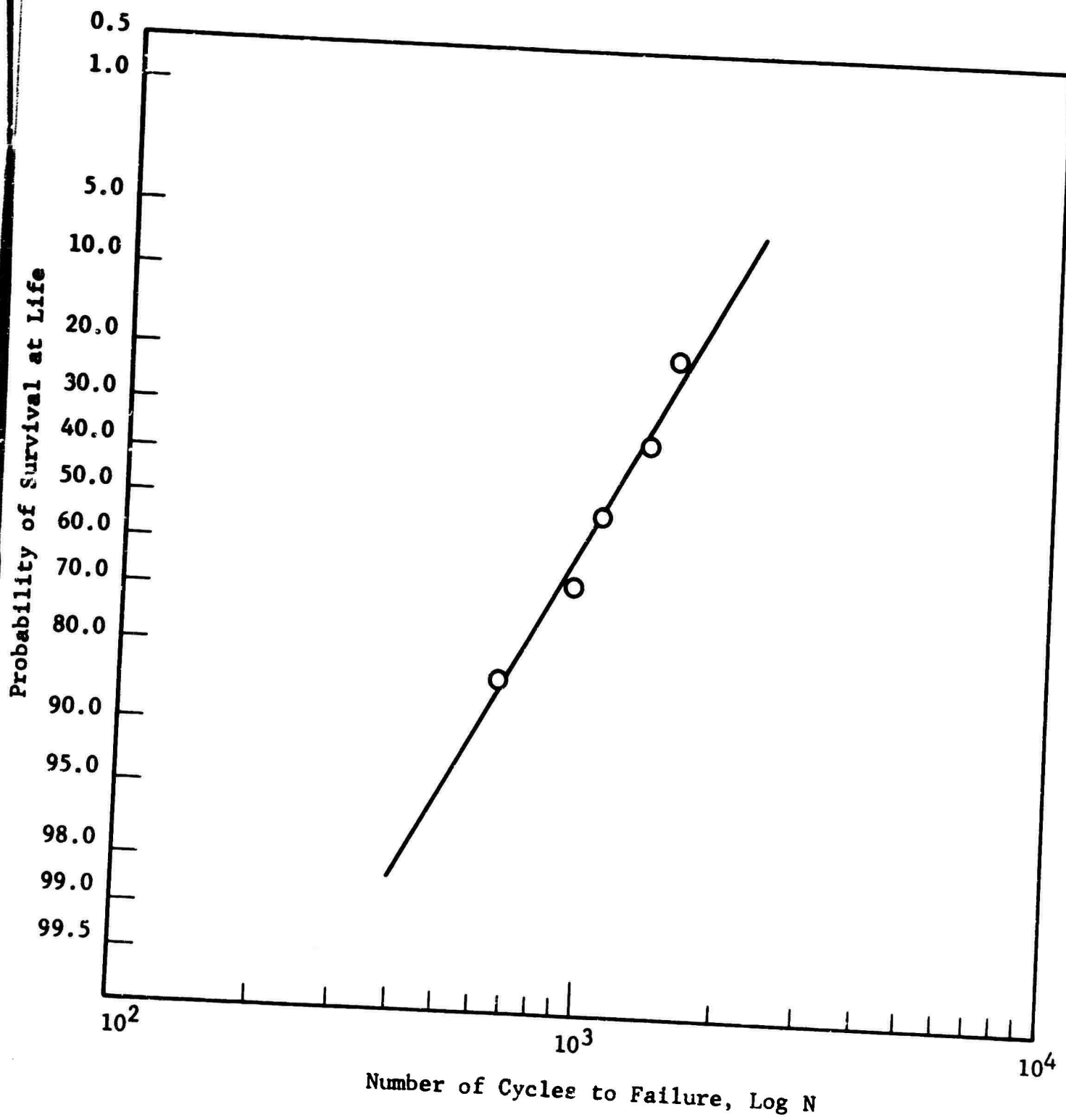


Fig. 31 LOG N VERSUS NORMAL PROBABILITY FOR 181/S901 GLASS CLOTH REINFORCED EPOXY -  $\sigma=43,000$  PSI

## SECTION VI

### CREEP AND STRAIN RATE TESTS

We have already examined one aspect (frequency) of time dependent mechanical properties of glass reinforced plastics. Two others spring to mind rather quickly: creep effects and strain rate dependencies. These effects were also studied and are reported herein.

#### A. SPECIMENS AND TESTING PROCEDURES: CREEP TESTS

Creep testing in tension, compression and bending was performed on 20:1 lever type testing equipment as shown in Fig. 32. The machine, originally designed for only tension creep testing, required a special jig fixture for compression tests. Figures 33 through 35 show the tensile, compressive and bending fixtures respectively.

Testing was primarily restricted to 181/S901 glass cloth reinforced epoxy. To simulate aircraft application conditions, loading was applied to 1,000 hr. Three test conditions were employed: room temperature, 75°F, and 30 percent relative humidity. The tension specimens were the fatigue specimen configuration. The compression specimens were the 1 in. wide, 1.25 in. long and 0.090 in. thick rectangular specimens. The bending specimens were the 6.5 in. long, 1/4 in. thick, 1 in. wide reduced section types. Strain monitorization for the tension and compression specimens was performed using electrical resistance foil gages.

To eliminate zero drift in these strain gage readings resulting from a possible electrical instability in the strain gage indicator, the following procedure was employed:

1. Two strain gage readings were taken for each active gage by switching the lead wires connected to the strain gage indicator.
2. The average of these readings gave the zero drift for the indicator.

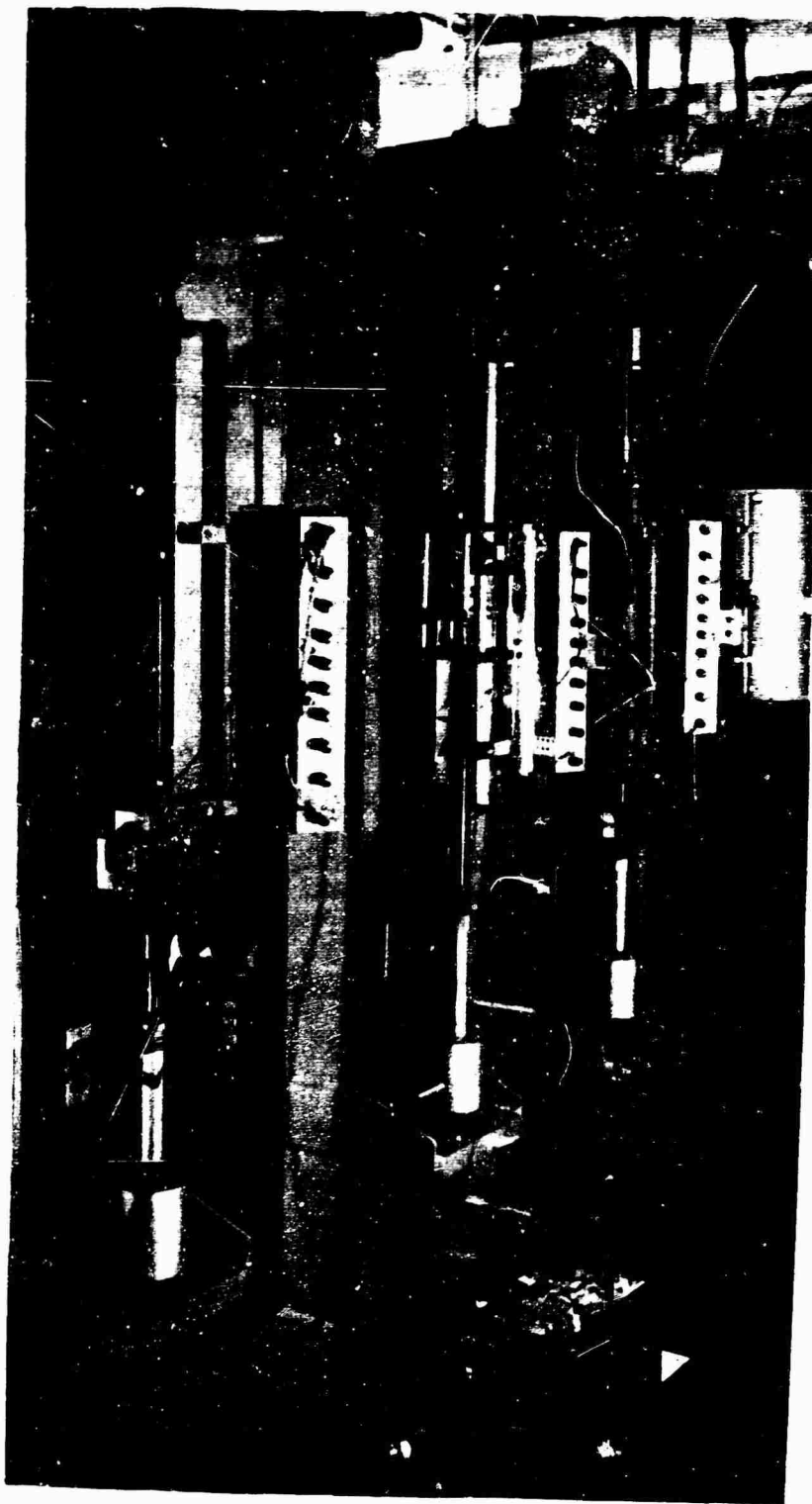


**Fig. 32 CREEP TESTING MACHINES WITH BENDING, COMPRESSION  
AND TENSION CREEP TESTS IN PROGRESS**

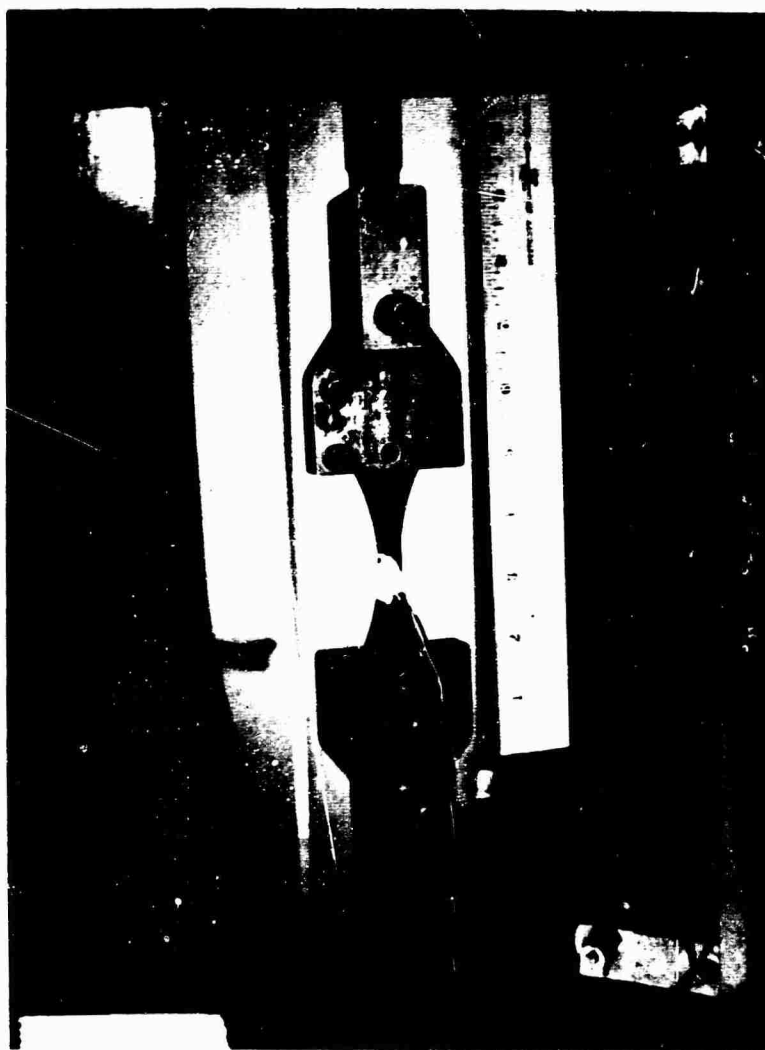


**Fig. 33 TEST FIXTURE, TENSION CREEP WITH 181/S901 GLASS CLOTH  
REINFORCED CONSTANT RADIUS PLASTIC SPECIMEN IN POSITION**

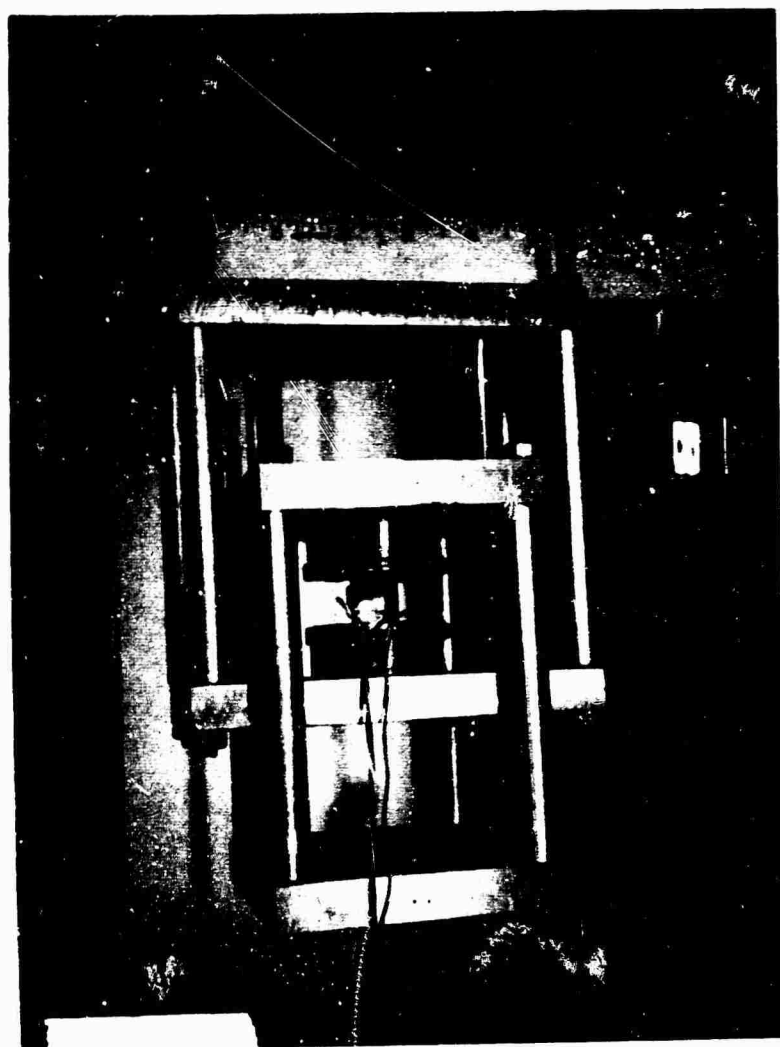


Fig. 34 TEST FIXTURE - COMPRESSION CREEP WITH 181/S901 GLASS  
CLOTH REINFORCED RECTANGULAR SPECIMEN IN POSITION

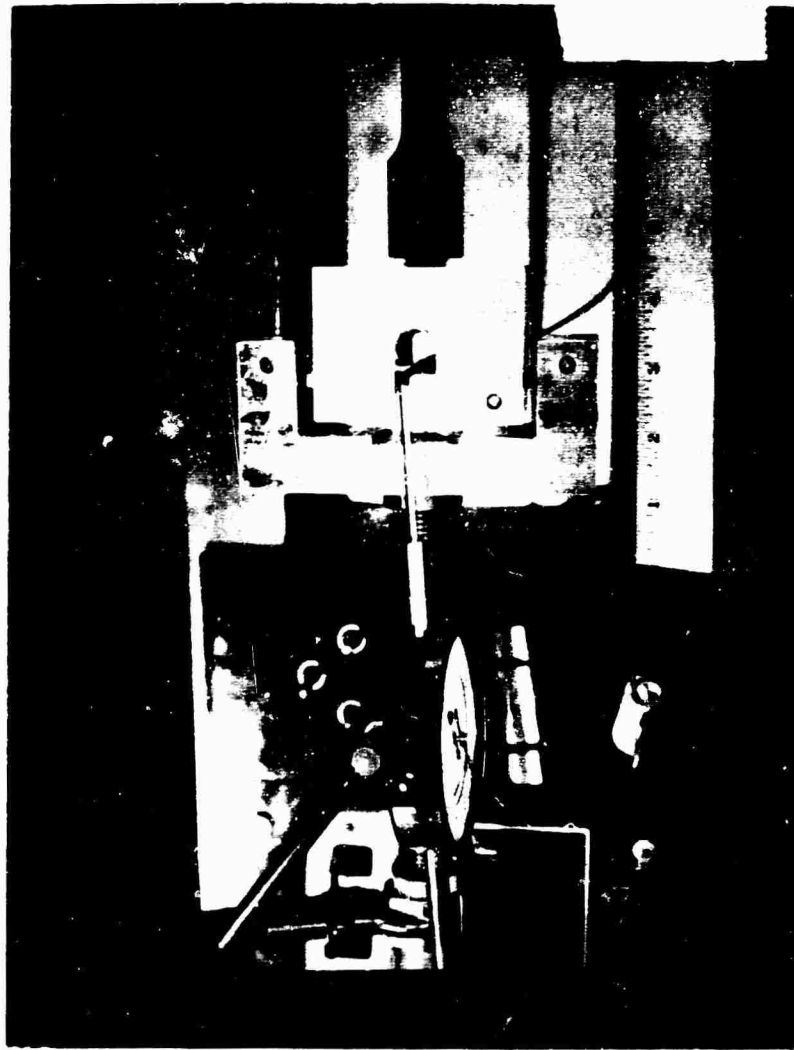


Fig. 35 TEST FIXTURE - BENDING CREEP WITH 181/S901 GLASS  
CLOTH REINFORCED PLASTIC REDUCED SECTION BENDING  
SPECIMEN IN POSITION

3. This value was then subtracted from the initial readings to give the actual strain reading.

This method is based on the fact that the resistance changes in adjacent bridge arms produce a bridge unbalance of opposite sign.

For the bending specimens, deflection readings were taken by a dial gage and the equivalent strain obtained through the use of standard deflection equations. For all test series, loading was initiated at 95 percent of ultimate. The tension and compression specimens failed in the first 6 min and the bending specimen in 138 hr. Subsequent bending loads were decreased in 5 percent increments; the last specimen being tested at 80 percent of static ultimate. This specimen still supported load after 800 hr. Tension testing was continued at 80 percent of static ultimate with failure in 44.2 hr. Subsequent specimens were tested at 5 percent reductions in applied stress. A total of five was tested in each loading mode.

#### B. RESULTS OF CREEP TESTING

For the tension and compression creep evaluations, testing was initiated at 90 percent of ultimate and both specimens failed within the first 6 min. The initial bending specimen was tested at 95 percent of ultimate and failure occurred after 138 hr. The loads were continually decreased until the specimen was removed. For the compression testing, the 1,000 hr specimen was obtained at 60 percent of ultimate. Subsequent testing at 70 and 75 percent of ultimate also went out to 1,000 hr. But for three tests at 80 percent of ultimate, failure occurred within the first 12 min. The same difficulty in obtaining intermediate test points also occurred for the bending specimens, but not to the same degree as in pure compression. The first 1,000 hr bending specimen runout occurred at 80 percent of ultimate. Subsequent tests at 85 and 87.5 percent of ultimate also went out to 1,000 hr and at 90 percent of ultimate, failure occurred at 46.1 hr. In tension intermediate test points with a runout specimen at 70 percent of ultimate and intermediate points at 75, 77.5 and 80 percent of ultimate were obtained.



Tables 24 through 26 present the highest stress level, with 1,000 hr runout obtained, strain versus time data for tension, compression and bending respectively. Figures 36 through 38 show the results for all tests in strain versus log time plots. Table 27 and Fig. 39 summarized stress versus time to rupture for the three types of tests. Values reported by other investigators for other glass cloth reinforced epoxies show similar trends.

To establish some preliminary data on the stress level versus time to rupture for S994 uniaxial roving reinforced epoxy, several specimens were tested in compression and bending. The results of these tests are shown in Table 28.

C. STRAIN RATE EFFECTS ON 181/S901 GLASS CLOTH AND S994 UNIAXIAL ROVING REINFORCED EPOXIES

Strain rate evaluations were performed on an Instron 10,000 lb universal testing machine. Various crosshead speeds were chosen from the slowest at 0.02 in./min to a high speed of 5 in./min. Standard Instron tension file grips were used for all tension tests. Compression and bending tests employed grips described earlier in Section IV. Tests conducted at higher Instron speeds were uninterpretable due to inability of the recording instruments to follow the maximum load at failure. The two highest rates listed on the Instron, 12 and 20 in./min, could not be utilized since the limit of the Instron recording response time was approximately 8.5 in./min for this particular material and specimen configuration (see Appendix E).

Results are shown in Tables 29 through 34 for the 181/S901 glass cloth and S994 uniaxial roving reinforced epoxies respectively. Figures 40 and 41 show the average failure stress versus strain rate for the two reinforcement systems. In the bending tests, two types of failures were observed. The first and more prevalent was interlaminar shear failure resulting in excessive deformation causing the test to be concluded.

Table 24  
STRAIN VERSUS TIME FOR SPECIMEN 16-CrT-17 LOADED IN TENSION  
FOR 1000 HOURS AT 77.5 PERCENT  $\sigma_{TU}$  (64,000 PSI)

Time (hr)	Total Strain Corrected ( $\mu$ -in./in.)
0	14,250
0.1	14,387
0.7	14,540
21.0	15,965
165.0	16,400
314.0	17,480

Table 25  
STRAIN VERSUS TIME FOR SPECIMEN 15-CrC-9 LOADED IN COMPRESSION  
FOR 1000 HOURS AT 75 PERCENT  $\sigma_{CU}$  (40,500 PSI)

Time (hr)	Total Strain Corrected ( $\mu$ -in./in.)
0	9,735
0.1	9,815
1.0	10,100
23.4	10,545
48.3	10,635
192.0	10,878
500.0	11,148
900.0	11,495
1012.0	11,573

Table 26

STRAIN VERSUS TIME FOR SPECIMEN 31-CrB-13 LOADED IN BENDING  
FOR 1000 HOURS AT 87.5 PERCENT  $\sigma_{BU}$  (59,500 psi)

Time (hrs)	Dial Gage Displacement (in.)	Creep Strain Corrected ( $\mu$ -in./in.)
0	0.277	-
0.1	0.277	17,600
1.0	0.281	17,800
23.0	0.291	18,450
163.7	0.302	19,150
311.2	0.307	19,450
481.0	0.313	19,900
1000.0	0.318	20,200

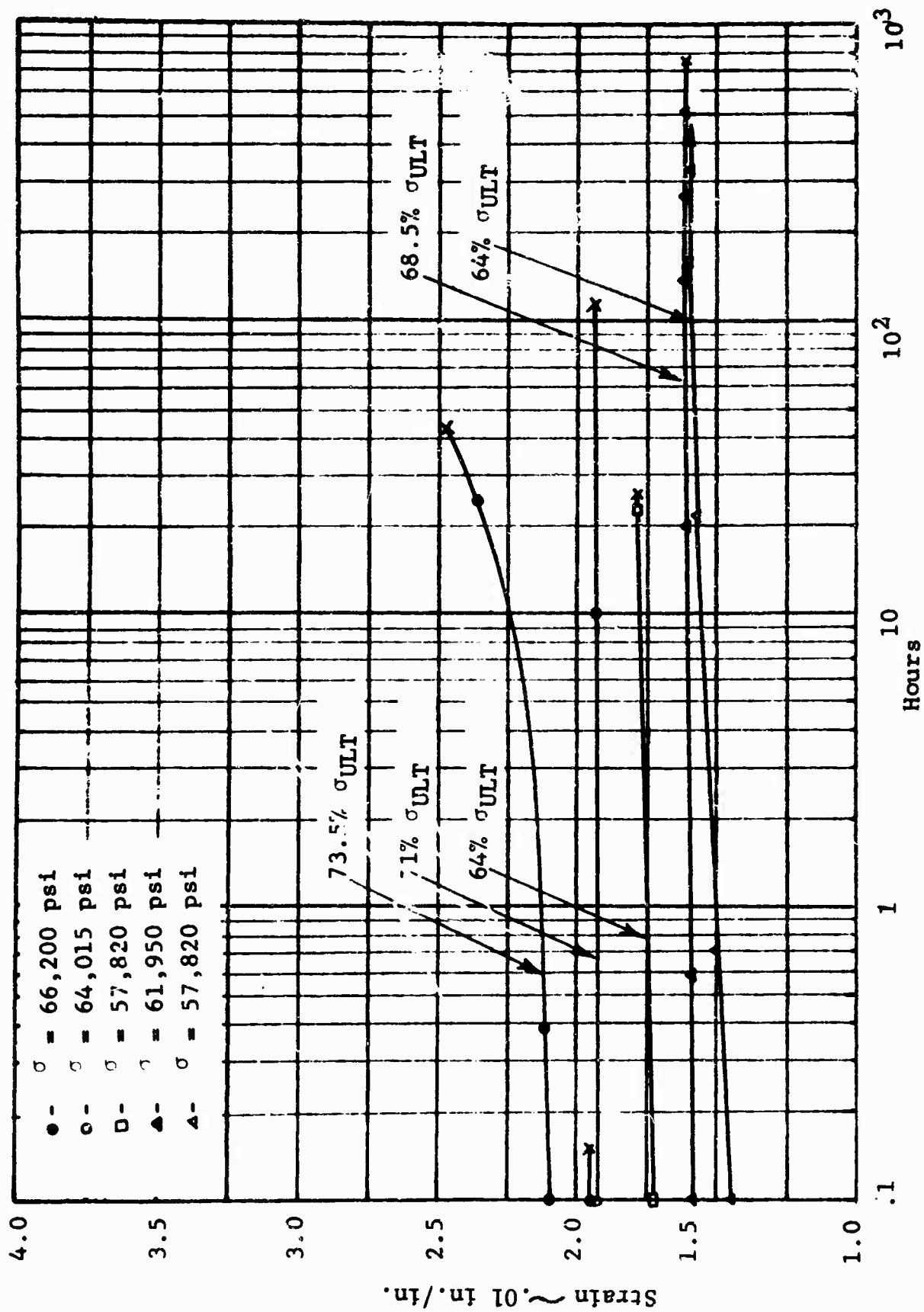


Fig. 36 TENSION STRAIN-TIME CURVES, 181/S901 GLASS CLOTH REINFORCED EPOXY RESIN COMPOSITE

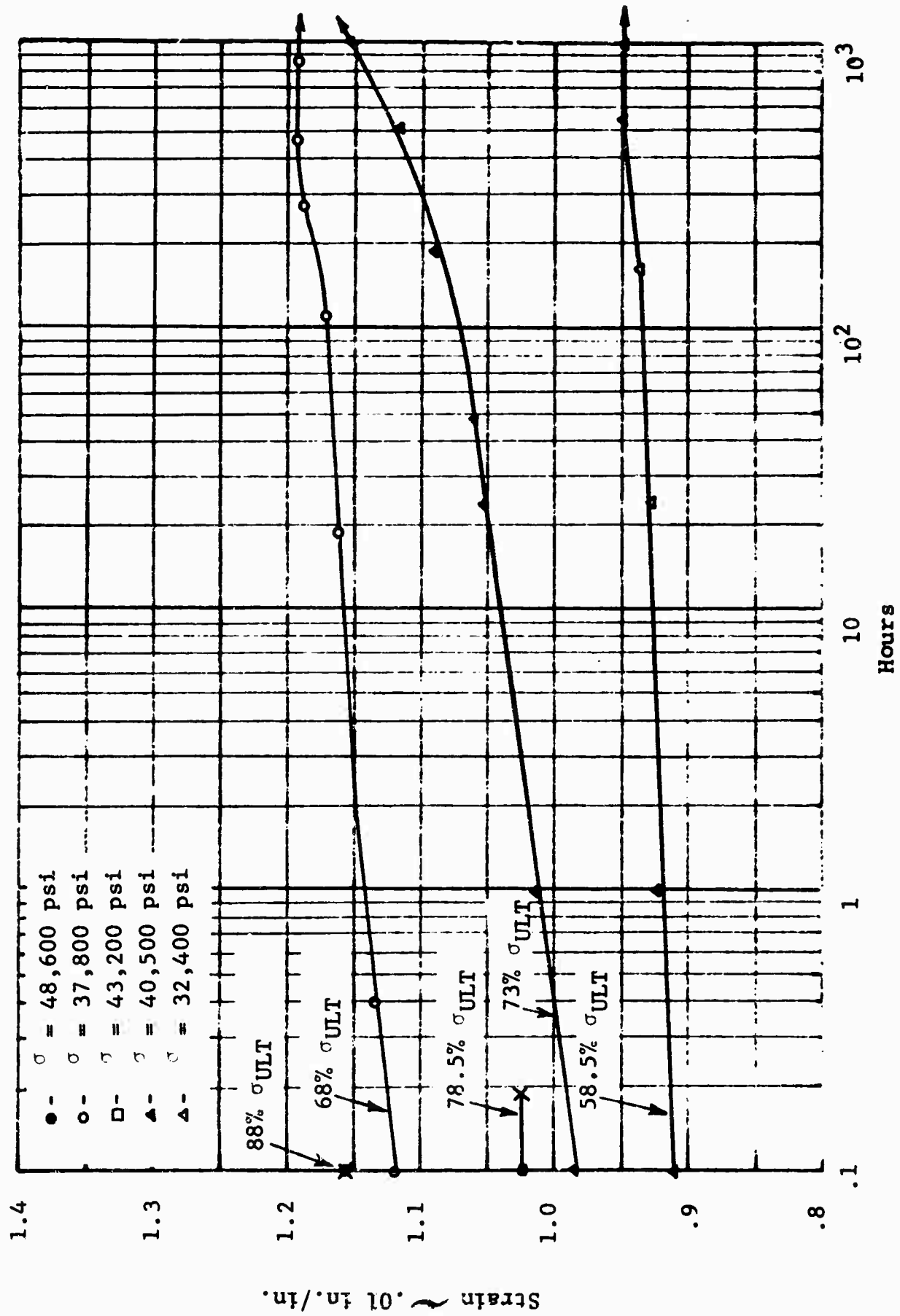


Fig. 37 COMPRESSION STRAIN-TIME CURVES, 181/S901 GLASS CLOTH REINFORCED EPOXY RESIN COMPOSITE

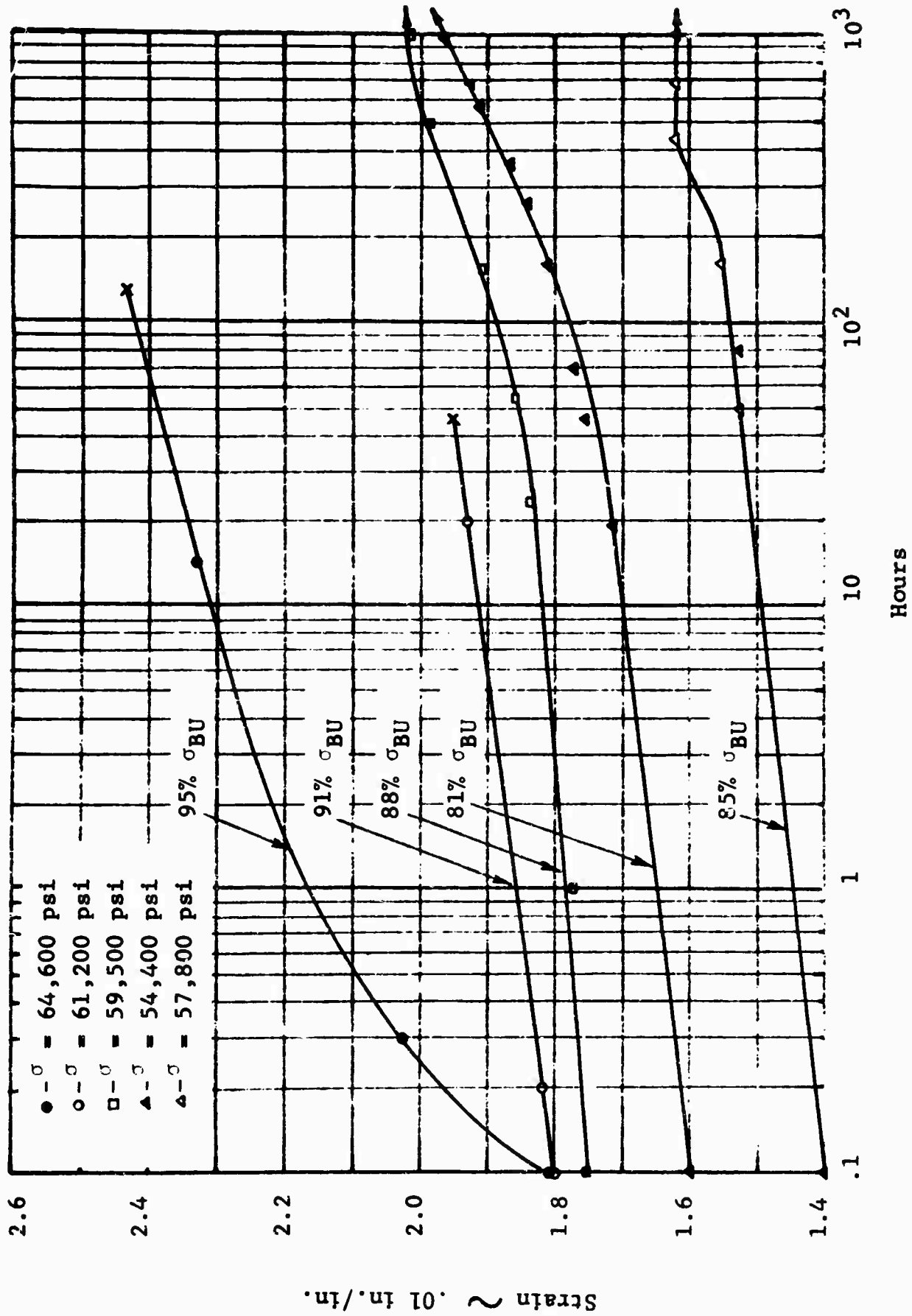


Fig. 38 BENDING STRAIN-TIME CURVES, 181/S901 GLASS CLOTH REINFORCED EPOXY RESIN COMPOSITE (ULTIMATE BEND STRENGTH,  $\sigma_{BU} = 67.5$  KSI)

Table 27  
STRESS LEVEL VERSUS TIME TO RUPTURE FOR SEVERAL LOADING MODES  
181/S901 GLASS CLOTH REINFORCED EPOXY

Specimen Number	Type of Loading	Stress Level (psi)	Strain @0.1 hr (μ-in/in)	ε <sub>T</sub> =Strain @ Rupture (μ-in/in)	t = Rupture Time (hrs)	Percent σ <sub>Ult</sub>
16-CrT-1	Tension	74,400	**		.10	90.0
10-CrT-2	Tension	66,200	20,820	24,700	44.20	80.0
9-CrT-3	Tension	61,950	15,700	16,180	755.20	75.0
7-CrT-4	Tension	57,820	17,300	17,900	24.70	70.0
1-CrT-5	Tension	64,015	19,360	19,360	0.16	77.5
16-CrT-16	Tension	64,015	19,220	19,500	118.00	77.5
16-CrT-17	Tension	57,820	14,387	---	---	70.0
1-CrC-6	Compression	48,600	11,500	11,500	0.10	90.0
2-CrC-7	Compression	32,400	9,070	9,570	1386.00	60.0
14-CrC-8	Compression	37,800	11,140	12,010	1629.00	70.0
15-CrC-9	Compression	40,500	9,815	11,573	1012.00	75.0
9-CrC-10	Compression	43,200	10,200	10,200	0.20	80.0
12-CrC-18	Compression	43,200	**	---	0.10	80.0
12-CrC-19	Compression	43,200	**	---	0.10	80.0
*28-CrB-11	Bending	64,600	18,100	24,300	138.10	95.0
28-CrB-12	Bending	61,200	18,100	19,600	46.10	90.0
31-CrB-13	Bending	59,500	17,600	20,200	1000.00	87.5
31-CrB-14	Bending	54,400	16,000	19,700	1055.00	80.0
31-CrB-15	Bending	57,800	13,900	16,300	1000.00	85.0

\*  $\epsilon = \frac{CTR(d)}{4.00}$

d = specimen thickness

\*\*

Gage lost at loading of specimen

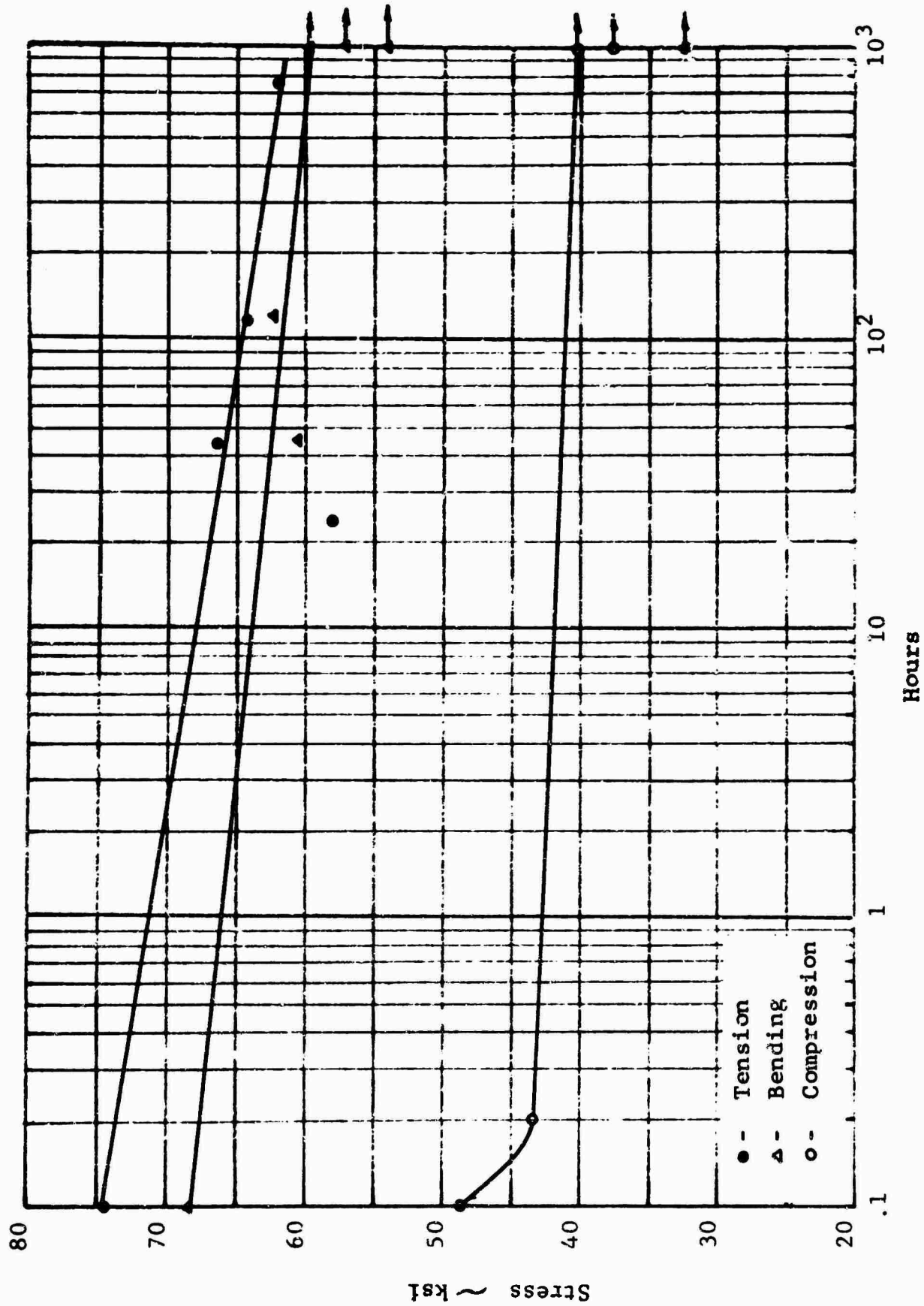


Fig. 39 STRESS VERSUS TIME TO RUPTURE PLOT FOR TENSION, COMPRESSION AND BENDING OF A 181/S901 GLASS CLOTH REINFORCED EPOXY RESIN COMPOSITE



Table 28  
STRESS LEVEL VERSUS TIME TO RUPTURE FOR COMPRESSION AND BENDING MODES  
S994 UNIAXIAL ROVING REINFORCED EPOXY

Specimen Number	Type of Loading	Stress Level (psi)	Time to Rupture (hrs)	Percent $\sigma_{ult}$ (%)
17-CrC-6	Compression	49,500	3575*	80
17-CrC-7	Compression	46,300	3575*	75
29-CrB-11	Bending	132,500	0.3	85
29-CrB-12	Bending	141,000	0.2	90
29-CrB-13	Bending	93,500	5306	60
29-CrB-14	Bending	125,000	0.1	80
29-CrB-15	Bending	109,000	1285*	70

Note:  $\sigma_{CU} = 61,950$  psi,  $\sigma_{BU} = 156,000$  psi

\* Specimen did not fail

Table 29  
STRAIN RATE TESTS ON 181/S901 GLASS CLOTH REINFORCED EPOXY - TENSILE LOADING

Specimen Number	Cross Head Speed (in./min)	Specimen Strain Rate ( $\mu$ -in./in./sec)	Ultimate Strength (psi)	Average Strength (psi)
16-STT-1	0.02	167	86,400	
6-STT-2	0.02	167	85,400	
14-STT-3	0.02	167	76,000	82,600
15-STT-4	0.05	418	102,000	
8-STT-5	0.05	418	95,000	
1-STT-6	0.05	418	92,500	96,500
2-STT-7	0.50	4,180	85,000	
15-STT-8	0.50	4,180	100,000	
4-STT-10	0.50	4,180	96,600	93,700
10-STT-11	5.00	41,800	100,000	
14-STT-12	5.00	41,800	101,500	100,700

Table 30  
STRAIN RATE TESTS ON 181/S901 GLASS CLOTH REINFORCED EPOXY - COMPRESSIVE LOADING

Specimen Number	Cross Head Speed (in./min)	Specimen Strain Rate ( $\mu$ -in./in./sec)	Ultimate Strength (psi)	Average Strength (psi)
1-STC-1	0.02	167	48,100	
3-STC-2	0.02	167	55,000	
2-STC-3	0.02	167	58,400	53,800
4-STC-4	0.05	418	59,000	
8-STC-5	0.05	418	55,400	
15-STC-6	0.05	418	56,400	56,900
16-STC-7	0.50	4,180	60,500	
7-STC-8	0.50	4,180	58,000	
6-STC-9	0.50	4,180	54,800	57,800
5-STC-10	5.00	41,800	66,000	
10-STC-11	5.00	41,800	67,600	
9-STC-12	5.00	41,800	58,300	64,000

Table 31  
STRAIN RATE TESTS ON 181/S901 GLASS CLOTH REINFORCED EPOXY - BENDING LOADING

Specimen Number	Cross Head Speed (in./min)	Specimen Strain Rate ( $\mu$ -in./in./sec)	Ultimate Strength (psi)	Average Strength (psi)
32-STB-1	0.02	23	63,000	
32-STB-2	0.02	23	73,900	
32-STB-3	0.02	23	67,000	68,000
32-STB-4	0.05	56	65,000	
32-STB-5	0.05	56	69,000	
32-STB-6	0.05	56	70,000	68,000
32-STB-7	0.50	565	65,200	
32-STB-8	0.50	565	70,200	
32-STB-9	0.50	565	82,700	72,700
32-STB-10	5.00	5,650	77,600	
32-STB-11	5.00	5,650	82,600	
32-STB-12	5.00	5,650	83,800	81,300

Almost all failures appeared to occur on the compression side of the beam.

Table 32  
STRAIN RATE TESTS ON S994 UNIAXIAL ROVING REINFORCED EPOXY - TENSILE LOADING

Specimen Number	Cross Head Speed (in./min)	Specimen Strain Rate ( $\mu$ -in./in./sec)	Ultimate Strength (psi)	Average Strength (psi)
40-STT-3	0.1	279	172,000	
40-STT-4	0.1	279	178,500	
40-STT-5	0.1	279	173,500	174,700
40-STT-6	0.5	1,380	213,000	
40-STT-7	0.5	1,380	188,500	
40-STT-8	0.5	1,380	195,500	199,000
40-STT-9	1.0	2,790	198,500	
40-STT-10	1.0	2,790	210,000	
40-STT-11	1.0	2,790	220,000	209,500

Table 33  
STRAIN RATE TESTS ON S994 UNIAXIAL ROVING REINFORCED EPOXY - COMPRESSIVE LOADING

Specimen Number	Cross Head Speed (in./min)	Specimen Strain Rate ( $\mu$ -in./in./sec)	Ultimate Strength (psi)	Average Strength (psi)
17-STC-1	0.02	167	65,029	
21-STC-2	0.02	167	62,390	
18-STC-3	0.02	167	58,430	
17-STC-4	0.02	167	87,100	68,230
20-STC-5	0.05	418	86,000	
21-STC-6	0.05	418	77,200	
19-STC-7	0.05	418	58,200	73,800
23-STC-8	0.10	835	64,800	
24-STC-9	0.10	835	50,200	
25-STC-10	0.10	835	91,400	68,800
17-STC-11	0.20	1,670	61,900	
19-STC-12	0.20	1,670	55,930	
20-STC-13	0.20	1,670	56,500	61,440
17-STC-17	1.00	8,350	79,700	
19-STC-18	1.00	8,350	61,400	
20-STC-19	1.00	8,350	89,500	76,800
26-STC-14	2.00	16,700	63,650	
17-STC-15	2.00	16,700	62,437	
18-STC-16	2.00	16,700	62,630	62,900
19-STC-20	5.00	41,800	52,200	
20-STC-21	5.00	41,800	80,400	
21-STC-22	5.00	41,800	90,000	
18-STC-23	5.00	41,800	65,200	
18-STC-24	5.00	41,800	65,760	
19-STC-25	5.00	41,800	67,200	70,130

Table 34  
STRAIN RATE TESTS ON S994 UNIAXIAL ROVING REINFORCED EPOXY - BENDING LOADING

Specimen Number	Cross Head Speed (in./min)	Specimen Strain Rate ( $\mu$ -in./in./sec)	Ultimate Strength (psi)	Average Strength (psi)
33-STB-7	0.10	113	147,000	147,000
33-STB-4	0.50	565	168,000	
33-STB-5	0.50	565	146,000	
33-STB-6	0.50	565	159,000	158,000
33-STB-10	1.00	1,130	176,500	
33-STB-11	1.00	1,130	117,000	
33-STB-12	1.00	1,130	179,000	157,500
33-STB-1	5.00	5,650	106,500	
33-STB-2	5.00	5,650	112,000	
33-STB-3	5.00	5,650	193,000	137,000

**Note:**

Specimens 3, 4, 5, 6, 7, 10 and 12 failed in interlaminar shear.

Specimens 1, 2 and 11 failed as fiber failures.

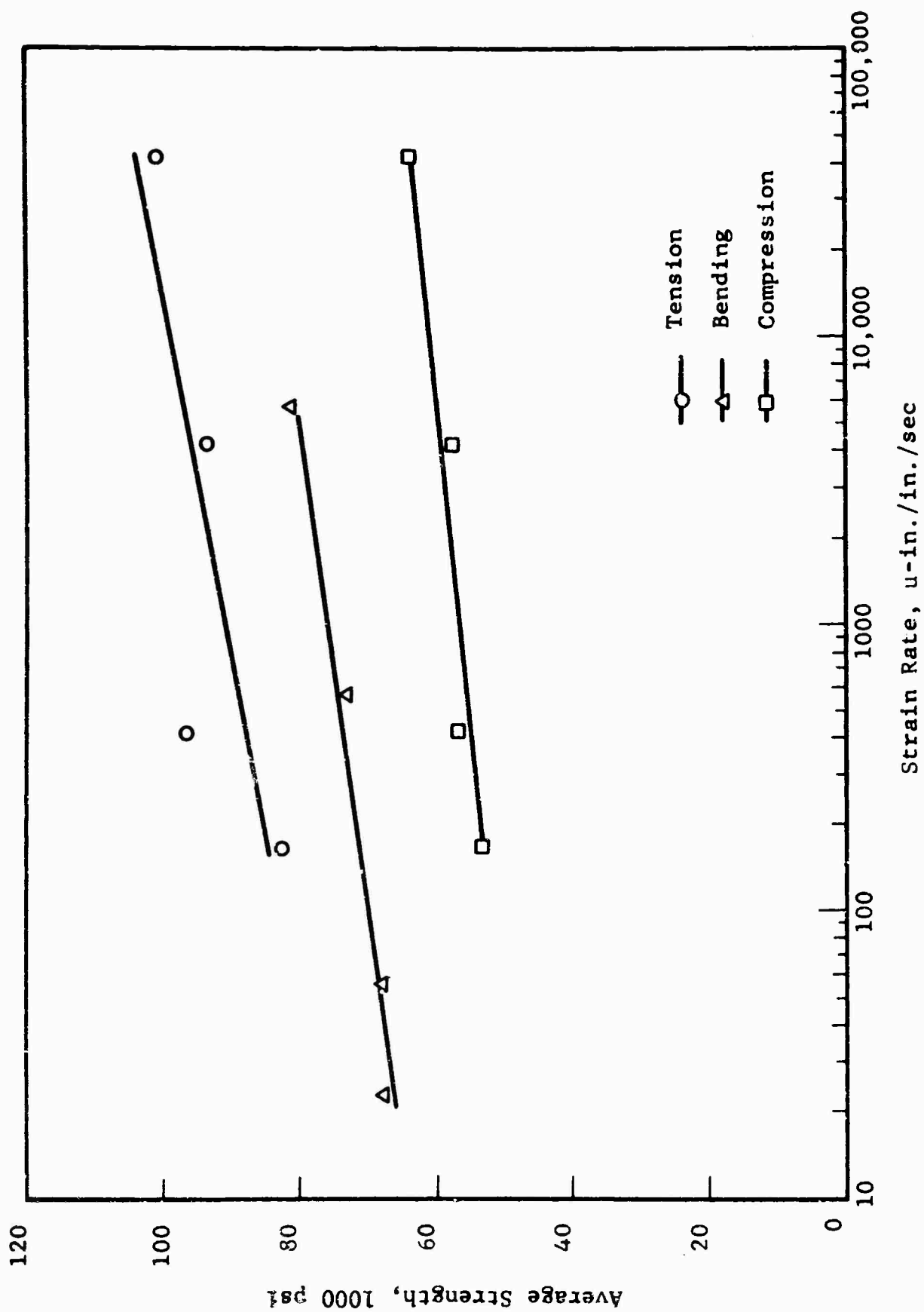


Fig. 40 AVERAGE STRESS AT FAILURE VERSUS STRAIN RATE FOR 181/S901 GLASS CLOTH REINFORCED EPOXIES



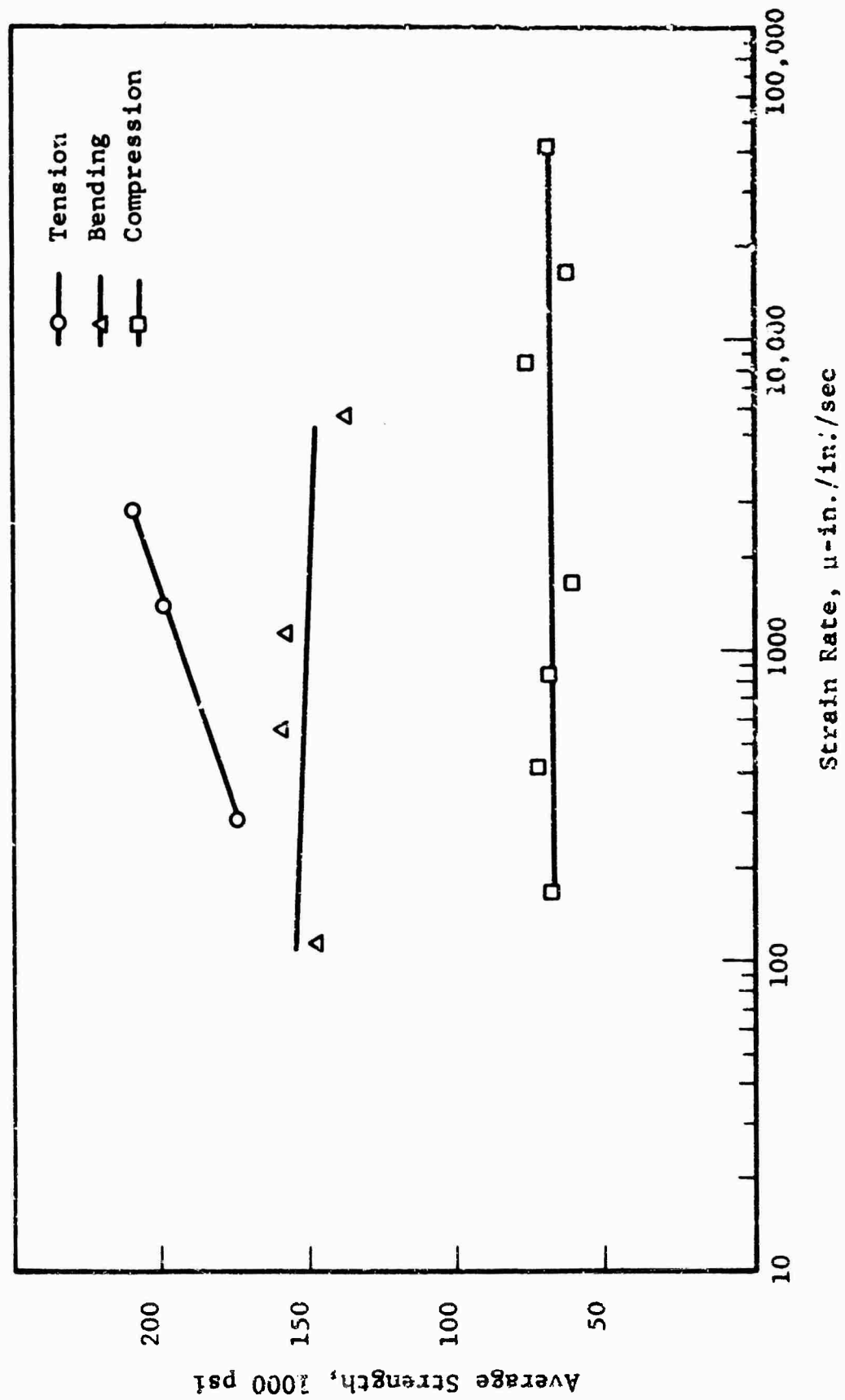


Fig. 41 AVERAGE STRESS AT FAILURE VERSUS STRAIN RATE FOR S994 UNIAXIAL ROVING REINFORCED EPOXIES

The second type was failure of the fibers occurring first on the compression side and progressing until complete fracture of the test specimen. The two types of failures are indicated in Table 34. The interlaminar shear failure specimens gave higher breaking strength with a slight increase due to cross-head speed.

## SECTION VII

### EFFECT OF MOISTURE AND COATINGS ON FATIGUE LIFE

One very important factor or group of factors which influences the performance of a GRP composite structure is the environmental conditions experienced during service life. By themselves, extremes of temperature and humidity characteristics of naval propeller aircraft operating conditions do not pose a serious threat to the static performance of GRP; however, coupled with cyclic and static loading, moisture particularly has become an important consideration. Repeated fatiguing of a GRP structure has been theorized as opening paths at glass resin interfaces for moisture penetration.

Previous work performed to investigate the effect on compressive fatigue life from immersion in fresh water did not show conclusively either a reduction in fatigue life or noticeable water penetration. However, it was initially suspected that a GRP airplane skin might be more susceptible to water corrosion due to the requirements of long fatigue life and to its relative thinness and probable exposure to direct shear and abrasion in areas of high tension. For this reason, some of the effort expended here was devoted to an investigation of the effect of moisture on fatigue life of the the composites. In addition, the effect of typical coatings on preventing such effects was also investigated. Both 181/S901 glass cloth and uniaxial roving reinforcements were used. Specimens were tested in both fully reversed bending and tension fatigue modes.

The stress level chosen for testing the 181/S901 glass cloth reinforced epoxy was 22,000 psi or 34.4 percent of static ultimate. Specimens were tested in bending fatigue with  $R = -1$ . The environmental conditions were 90°F at 100 percent relative humidity. Four exposure times were chosen, 1 wk, 2 wk, 3 wk and 4 mo.

The protective coating used was one used extensively by the U. S. Rubber Co. prepared with the following ingredients:

Dow Epoxy Resin D.E.R. 331	70 parts
Dow Epoxy Resin D.E.R. 732	30 parts
Tetraethylenepentamine, tech. grade	14 parts

Specimens painted with this mixture were cured for 2 hr at 212°F. At this point the coating generally gives an elongation at yield of 10 percent and a tensile strength of 6,500 psi. The resin is brush coated on the finished specimens and allowed to gelate in air at a temperature of approximately 150°F. Coatings remain constant at approximately 0.004 in. per pass. Surface air bubbles were broken by gently heating with a low flame apparatus.

Results of fatigue tests showed a decrease in cyclic life for the unpainted specimens as the exposure time increased. The painted specimens showed no apparent decrease in cyclic life until the 3 mo exposure specimens which showed a substantial decrease in cyclic life. The test results are summarized in Table 35.

Environmental fatigue of the S994 uniaxial roving reinforced epoxy specimens was also performed on bending type specimens with  $R = -1$ . The stress level chosen was 25,000 psi or 17.4 percent of static ultimate. Exposure times similar to those of the 181/S994 glass cloth reinforced epoxy specimens were used.

Test results for the S994 uniaxial roving reinforced epoxy are tabulated in Table 36. As can be seen, the 10 wk unpainted specimens showed a substantial decrease in cyclic life while no change was indicated for painted specimens. The range in cyclic life for some groups is typical of the behavior as demonstrated earlier in Section V. Specimen 30-E-9, having a cyclic life of 4,000 cycles, could have been a bad specimen or was just on the low end of the frequency distribution curve for this particular stress level.

Table 35

EFFECT OF MOISTURE AND PAINTING ON THE FATIGUE LIFE  
OF 181/S901 GLASS CLOTH REINFORCED EPOXIES:  
TESTED AFTER EXPOSURE TO 100 PERCENT RELATIVE  
HUMIDITY AND 95°F (1800 CPM, R = -1)

Specimen Number	Condition	Exposure Time (Weeks)	Alternating Stress- Bending (psi)	Cycles to Failure
28-E1-1	Bare	1	22,000	25,000
31-E1-2	Bare	1	22,000	9,000
32-E1-9	Bare	1	22,000	20,000
32-E1-10	Bare	1	22,000	21,000
28-E2-1	Painted	1	22,000	16,000
31-E2-2	Painted	1	22,000	13,000
32-E2-9	Painted	1	22,000	151,000
32-E2-10	Painted	1	22,000	21,000
31-E1-3	Bare	2	22,000	8,000
31-E1-4	Bare	2	22,000	12,000
31-E2-3	Painted	2	22,000	32,000
31-E2-4	Painted	2	22,000	285,000
28-E1-5	Bare	3	22,000	95,000
31-E1-6	Bare	3	22,000	8,000
28-E2-5	Painted	3	22,000	67,000
31-E2-6	Painted	3	22,000	182,000
31-E1-7	Bare	12	22,000	5,000
31-E1-8	Bare	12	22,000	2,000
28-E2-7	Painted	12	22,000	3,000
28-E2-8	Painted	12	22,000	6,000

Table 36  
EFFECT OF MOISTURE AND PAINTING ON THE FATIGUE LIFE  
OF S994 UNIAXIAL GLASS ROVING REINFORCED EPOXIES:  
TESTED AFTER EXPOSURE TO 100 PERCENT RELATIVE  
HUMIDITY AND 90°F (1800 CPM, R = -1)

Specimen Number	Condition	Exposure Time (wks)	Alternating Stress- Bending (psi)	Cycles to Failure
30-E1-1	Bare	1	25,000	254,000
30-E1-3	Bare	1	25,000	145,000
30-E2-2	Painted	1	25,000	146,000
30-E2-4	Painted	1	25,000	579,000
30-E1-5	Bare	3	25,000	256,000
30-E1-7	Bare	3	25,000	467,000
30-E2-6	Painted	3	25,000	236,000
30-E2-8	Painted	3	25,000	3,021,000
30-E1-9	Bare	4	25,000	4,000
30-E1-11	Bare	4	25,000	3,758,000
30-E2-10	Painted	4	25,000	2,579,000
30-E2-12	Painted	4	25,000	5,104,000
30-E1-13	Bare	10	25,000	1,000
30-E1-15	Bare	10	25,000	2,000
30-E2-14	Painted	10	25,000	617,000
30-E2-16	Painted	10	25,000	747,000

Two unpainted specimens were also tested in continuous contact with water throughout the cycling by encasing them in a silastic RTV capsule filled with water. (See Fig. 42.) The results of these two tests for tension-zero-tension ( $R = 0.05$ ) at 1800 cpm are shown below:

<u>Specimen</u>	<u>Stress Level</u>	<u>Cycles to Failure</u>
Sample 1	40,000 psi	12,000
Sample 2	20,000 psi	$10^7$ runout, no failure

Comparison of these results with Fig. 15 shows that the first sample failed at the low end of the scatter distribution for the particular load levels used. The second specimen survived the repeated cycling to runout. This could hardly be interpreted as decisive but does indicate the possibility of some detrimental damage occurring as a result of the water environment.

It is evident that a great deal more testing would be required to distinguish quantitatively meaningful results among the vast statistical variability in the individual tests performed. Figures 43 and 44 are proposed as probable candidates for the behavior of bare and painted environmental fatigue results. They are drawn dashed to indicate a lack of substantive statistical reliability.

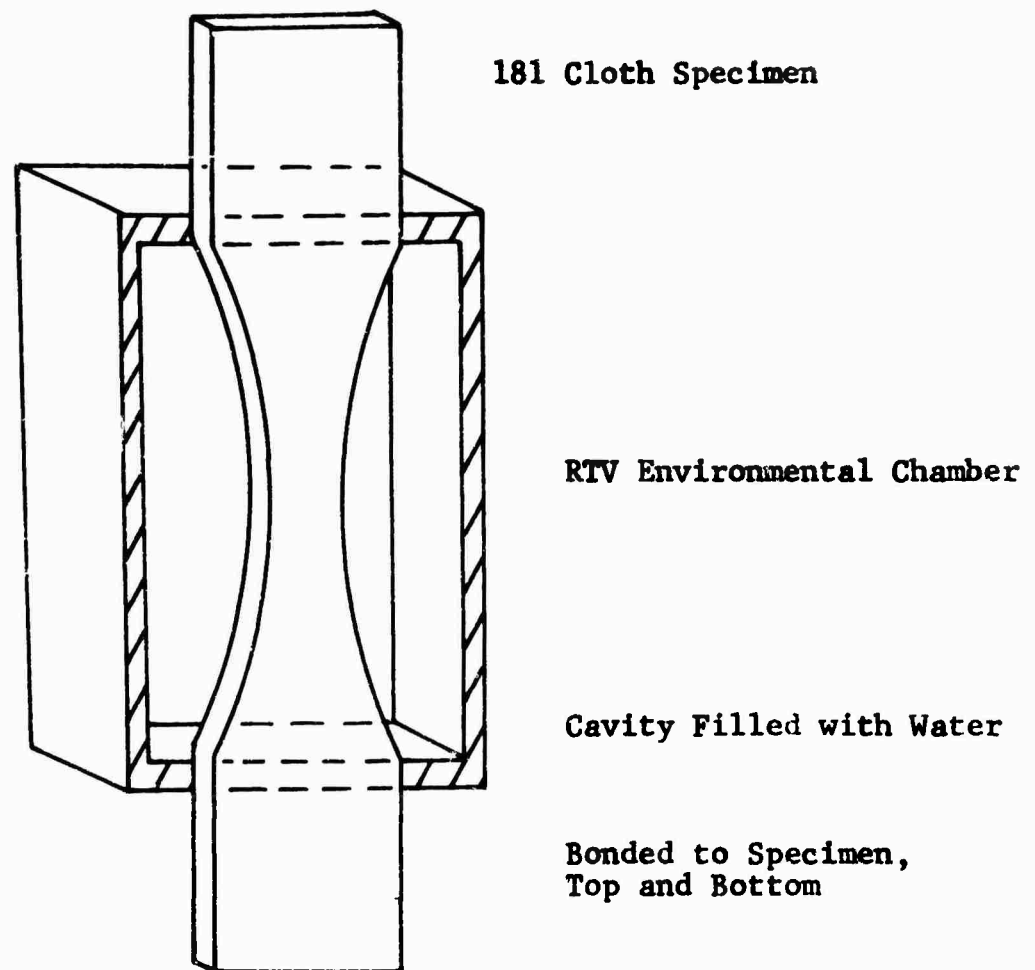


**Fig. 42 WATER ENCAPSULATION SYSTEM FOR ENVIRONMENTAL TEST  
ON 181/S901 GLASS CLOTH REINFORCED EPOXY TESTED  
IN TENSION-ZERO-TENSION ( $R = 0.05$ )**



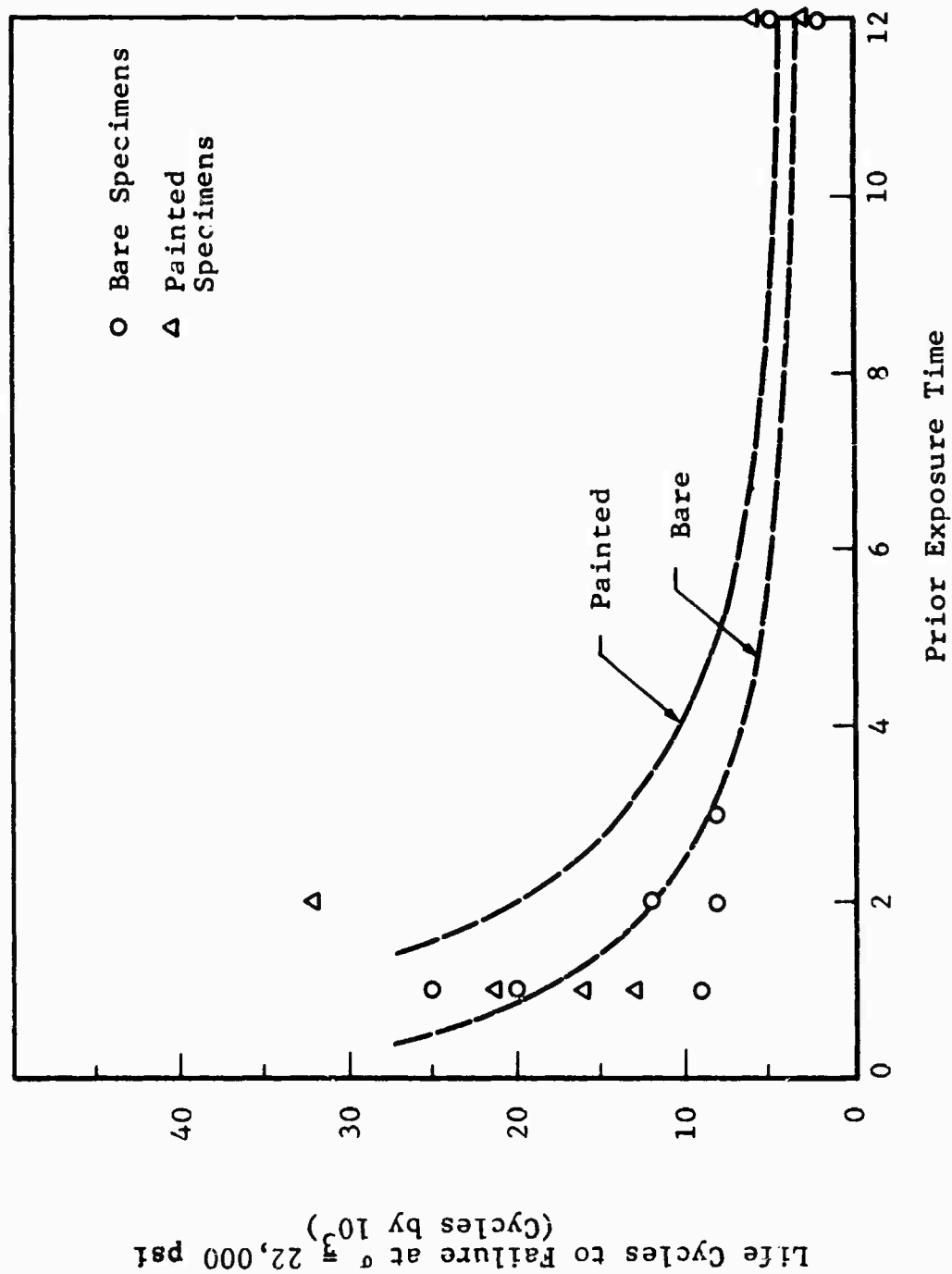


Fig. 43 PROBABLE CURVES SHOWING EFFECT OF PRIOR EXPOSURE TO WATER ENVIRONMENT FOR VARIOUS EXPOSURE LENGTHS FOR 181/S 901 GLASS CLOTH REINFORCED EPOXY (VERY HIGH LIFE VALUES NOT PLOTTED)

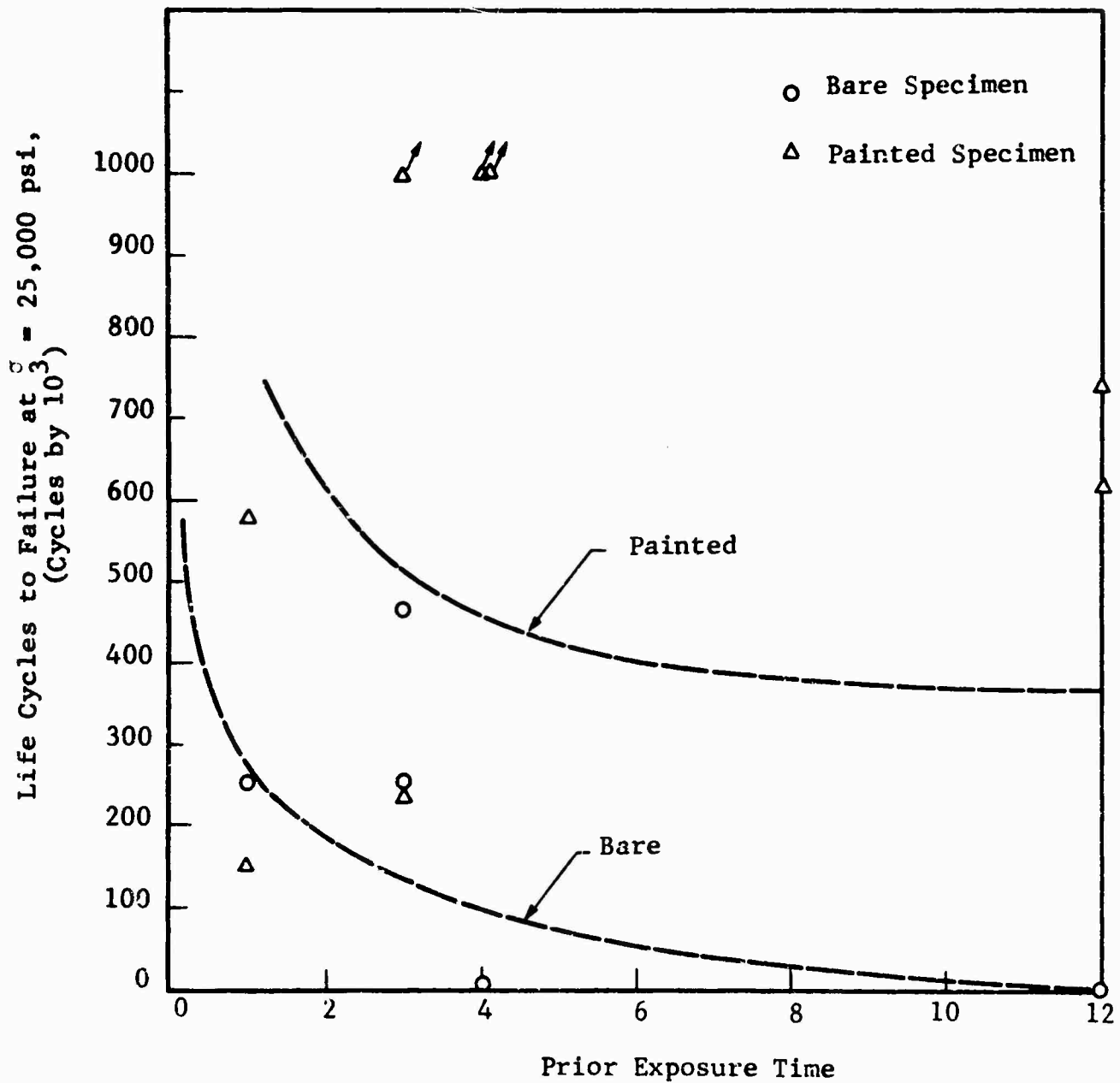


Fig. 44 PROBABLE CURVES SHOWING EFFECT OF PRIOR EXPOSURE TO WATER ENVIRONMENT FOR VARIOUS EXPOSURE LENGTHS FOR S994 UNIAXIAL ROVING REINFORCED EPOXY (VERY HIGH LIFE VALUES NOT PLOTTED)

## SECTION VIII

### CUMULATIVE DAMAGE STUDIES

#### A. NONDESTRUCTIVE DAMAGE OBSERVATIONS - ULTRASONIC

Several previous investigations on the detection and quantitative evaluation of flaws through the use of ultrasonic techniques have been performed. It is also well established that these flaws present serious implications for the static strength and fatigue lives of glass reinforced plastic composites. Ultrasonic techniques immediately offer considerable promise not only as a screening technique for quality control but as a tool, which when properly utilized, can lead to a quantitative assessment of the useful life of a composite material or structural component.

The system used for ultrasonic inspection of flat composite specimens (see Fig. 45) essentially consists of a point focused transmission transducer and a field transducer reception unit. This particular arrangement was selected after careful consideration since it seems to possess the following advantages:

1. Small void areas appear to be readily discernable. In contrast, a line or field transducer transmitter tends to damp-out the effects of individual small flaws by averaging over a larger volume of material.
2. Should a slight scattering of the ultrasonic signal occur, the field transducer reception unit will not misinterpret the signal as voids. The field transducer presents a target to the transmittal signal large enough to pick up all scatter within a conical angle of 22 deg.

The key to the ultrasonic inspection system is the accurate and repeatable repositioning of the flat composite specimens relative to the ultrasonic transducers. The mechanical system developed

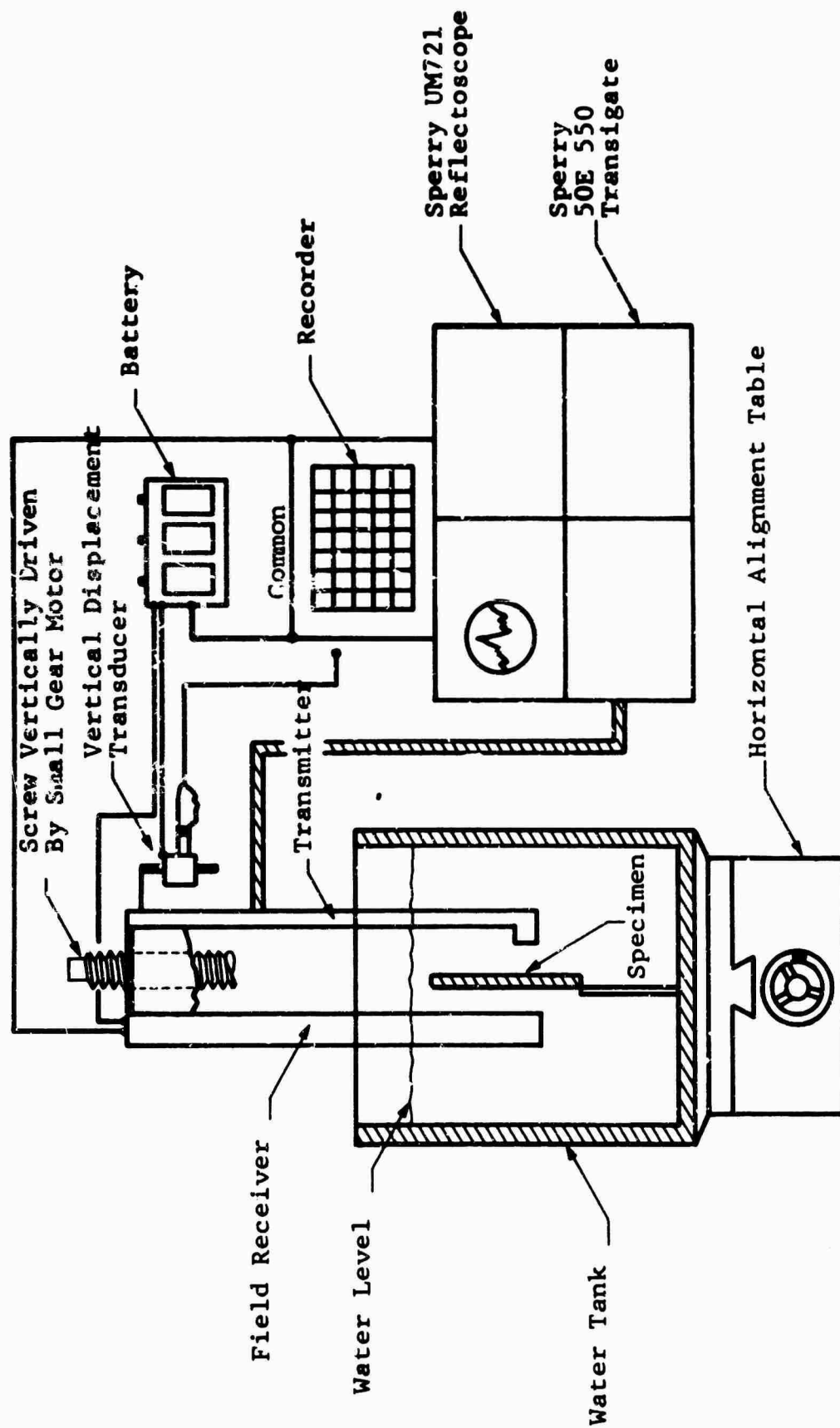


Fig. 45 SCHEMATIC OF THE FLAT COMPOSITE SPECIMEN ULTRASONIC INSPECTION UNIT (SEE FIG. 46)

specifically for these flat laminates is one similar to earlier IITRI devices described in Appendix B (see references 40, 41, 53, 59 and 62 at the end of this report) in which the ultrasonic transducer rather than the specimen is the active (or mobile) element during the scan. This is possible by affixing the carriage of the ultrasonic transducer to a lead screw which is rotated by a small motor (see Fig. 46). Both vertical and horizontal specimen alignments are accomplished by a small milling machine table which permits specimen traverse repositioning to 0.001 in. as well as regulation of constant specimen-to-ultrasonic transducer distances.

During the scan, vertical translation of the ultrasonic transducer relative to the specimen, which is also aligned vertically, is accomplished by rotation of the lead screw which moves the carriage. The particular traverse line in the specimen is maintained by forward or rearward adjustment of the milling machine table. The position of the ultrasonic transducer along the length of the specimen is monitored by a linear potentiometer fixed relative to the movable carriage.

The voltage from the variable tap of the potentiometer is the signal which drives the X-axis arm of an X-Y recorder shown in Figs. 45 and 47. The gate circuit of this particular ultrasonic pulser-scanner is set to monitor the reflected pulse from the ultrasonic transducer. This voltage is used as the signal which drives Y-axis or pen servo of the X-Y recorder. This system thus provides a plot of ultrasonic input signal attenuation (in voltage rather than db) versus position along the specimen. Typical plots for some particular specimens of interest are shown in Figs. 48 through 50.

From such a plot, the attenuation (db) may be calculated through the following relationship:

$$db = 20 \log \frac{E_1}{E_2}$$

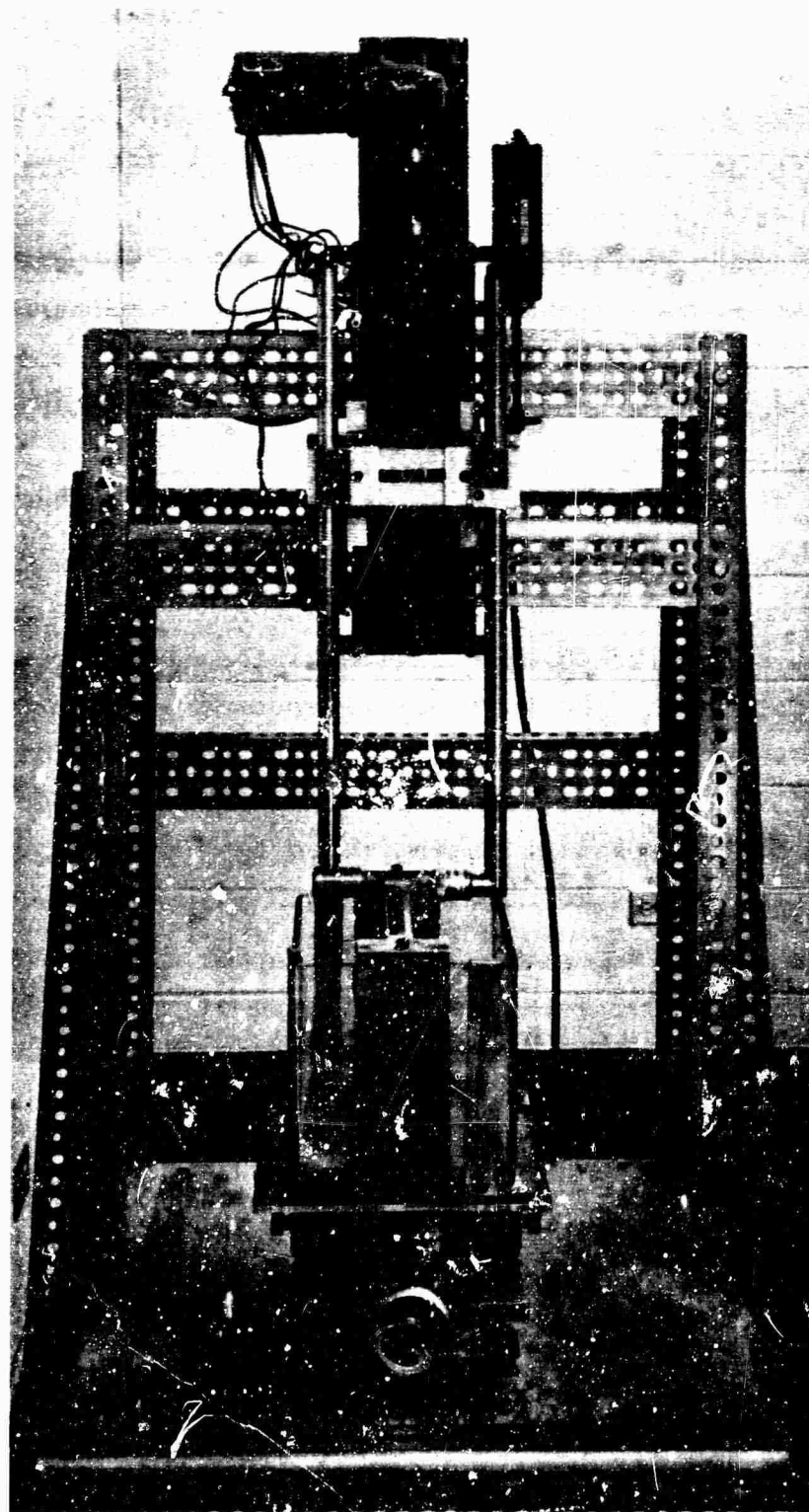


Fig. 46 ULTRASONIC INSPECTION EQUIPMENT FOR FLAT  
COMPOSITE SPECIMENS



Fig. 47 ULTRASONIC X-Y RECORDER

0.1 V  
Ref.

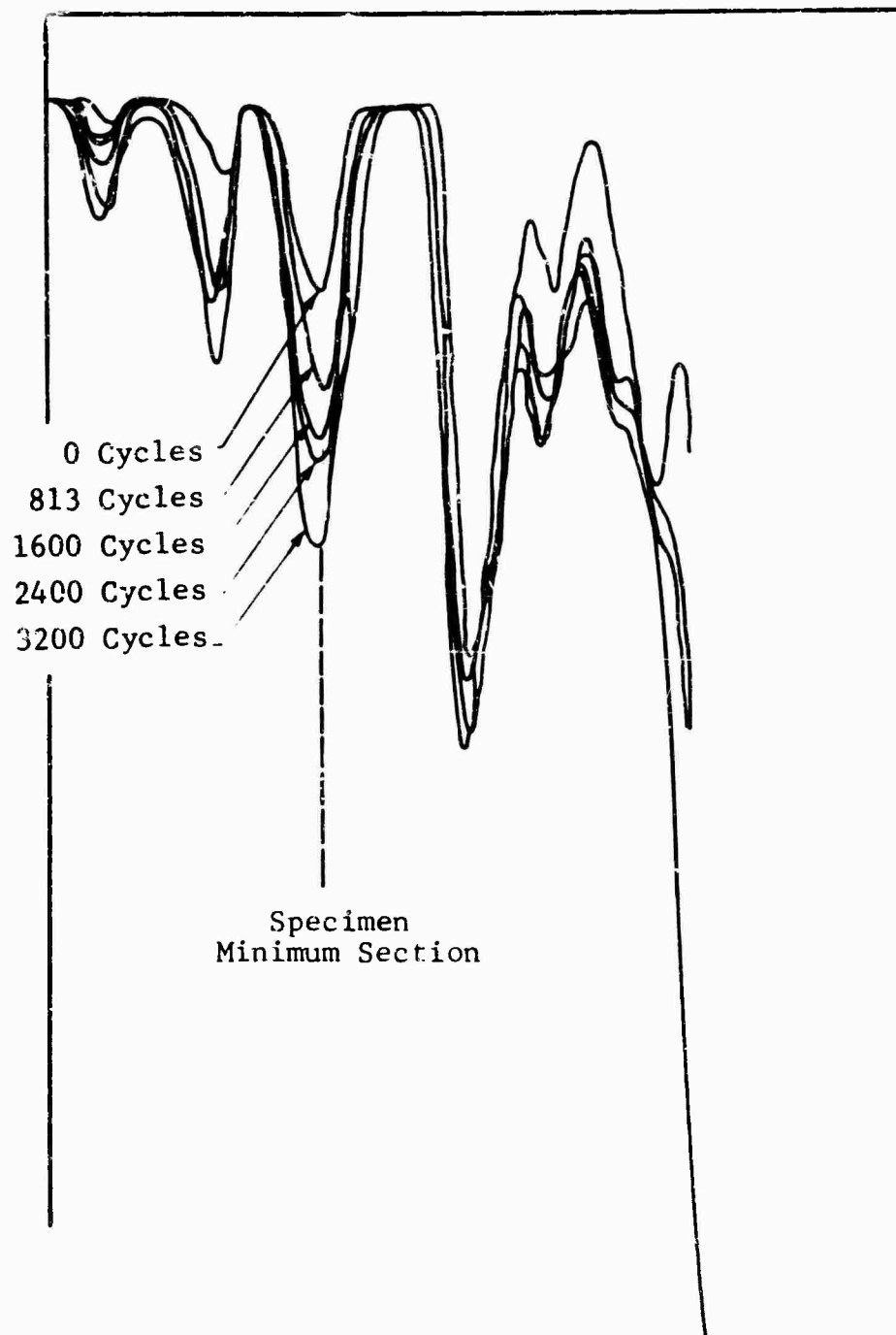


Fig. 48 ULTRASONIC INSPECTION AT DIFFERENT CYCLIC LEVELS  
FOR 181 S-GLASS CLOTH REINFORCED EPOXY SPECIMEN  
5-T-12 TESTED IN TENSION-ZERO-TENSION ( $R = 0.05$ ),  
 $\sigma_{MAX} = 47,500$  PSI FAILURE AT 3415 CYCLES



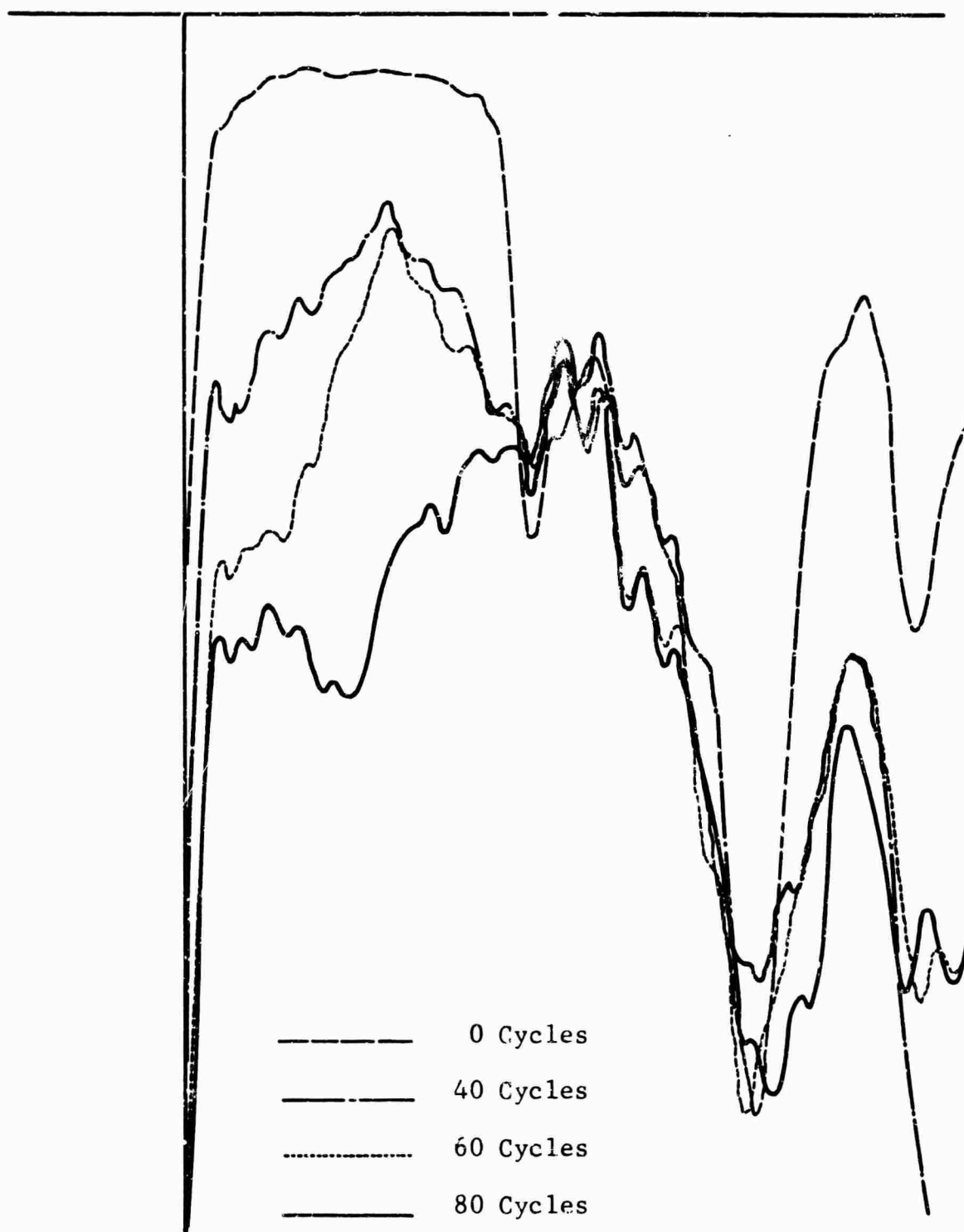


Fig. 49 ULTRASONIC INSPECTION AT DIFFERENT CYCLIC LEVELS FOR  
 181/S901 GLASS CLOTH REINFORCED EPOXY SPECIMEN NO. 2-T-15  
 TESTED IN TENSION-ZERO-TENSION ( $R=0.05$ ),  $\sigma_{MAX} = 65,000$  PSI,  
 FAILURE AT 93 CYCLES

0.1 V  
Ref.

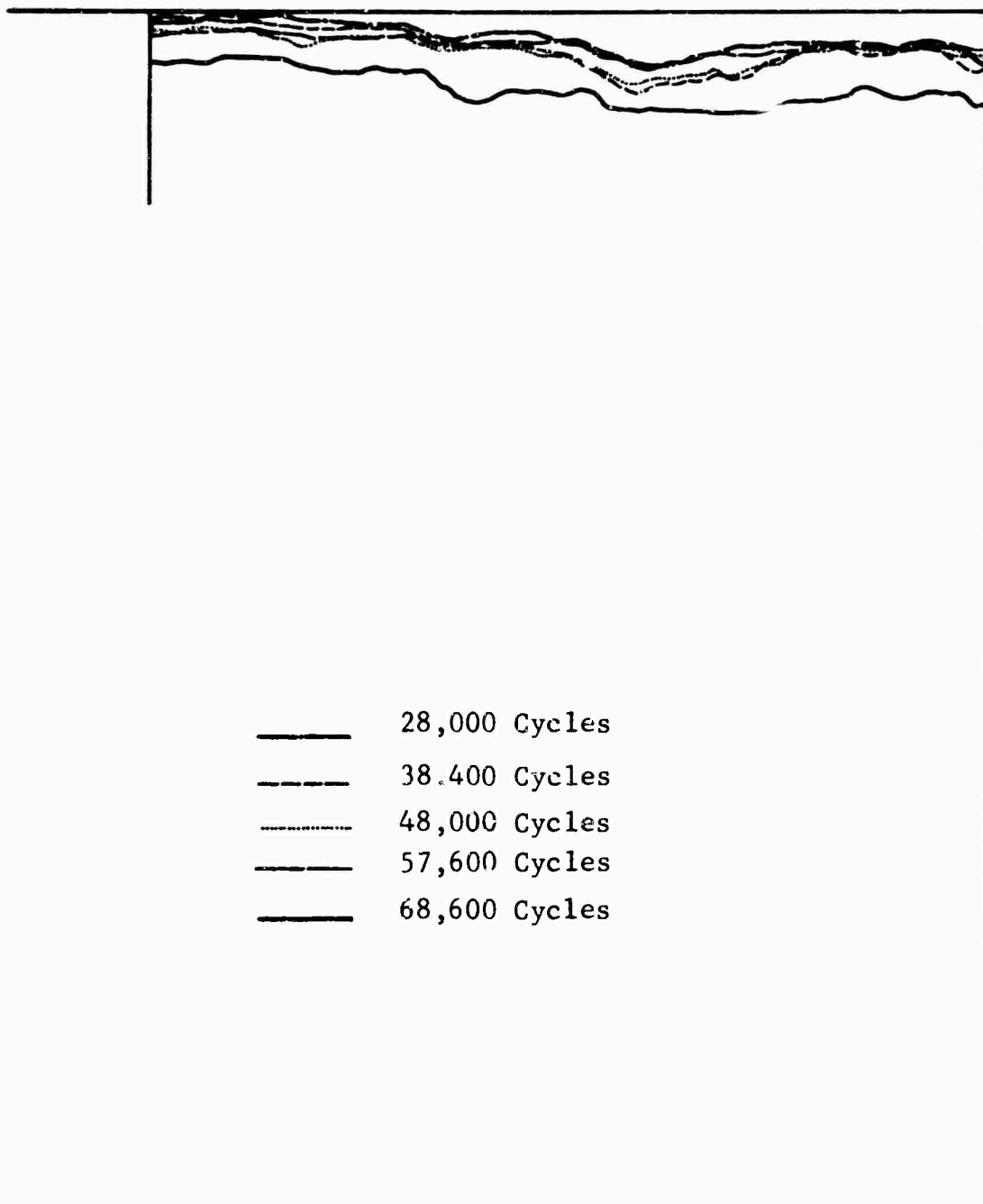


Fig. 50 ULTRASONIC INSPECTION AT DIFFERENT CYLIC LEVELS  
FOR 181S/901 GLASS CLOTH REINFORCED EPOXY SPECIMEN  
2-T-20 TESTED IN TENSION-ZERO-TENSION ( $R = 0.05$ )  
 $\sigma_{MAX} = 35,000$  PSI, FAILURE AT 205,000 CYCLES

where

$E_1$  = input unattenuated voltage

$E_2$  = attenuated voltage

Several alternatives then presented themselves for the interpretation of these attenuated signals. Each of these alternatives, their merits and liabilities, will now be discussed.

#### 1. Average Attenuation over Gage Length

In this method the area under the ultrasonic trace (see Fig. 51) bounded by straight lines AB, BC and DA and curved trace CD is integrated by means of a planimeter (or other suitable means). The area is then divided by the length of the path over which the trace has been obtained to obtain an average attenuated voltage. (The recorder scale was set at volts per inch so that the average height in inches became the average voltage numerically.) The db loss is then calculated from the equation

$$db = 20 \log (E_1/E_2)$$

given earlier for the average attenuation. The averages for each of the inspection traces are then plotted against the cycles at inspection (or percent expended life).

#### 2. Weighted Average Attenuation over Parallel Paths

For wide specimens where traces are potentially available over several parallel paths, a weighting procedure is advisable. Figure 52 shows a specimen where three paths are available and the central path (No.2) is to receive the "weighting" evaluation. Following the procedure given in Method 1, the average attenuations are then weighted as follows.

Each trace is assumed to characterize the material along its path in the specimen and to a certain distance, H, on either side of the path. Then the "area" covered consists of material, half of which is characterized by the trace along Path 1, and one-fourth of which is characterized by the trace along Path 3.

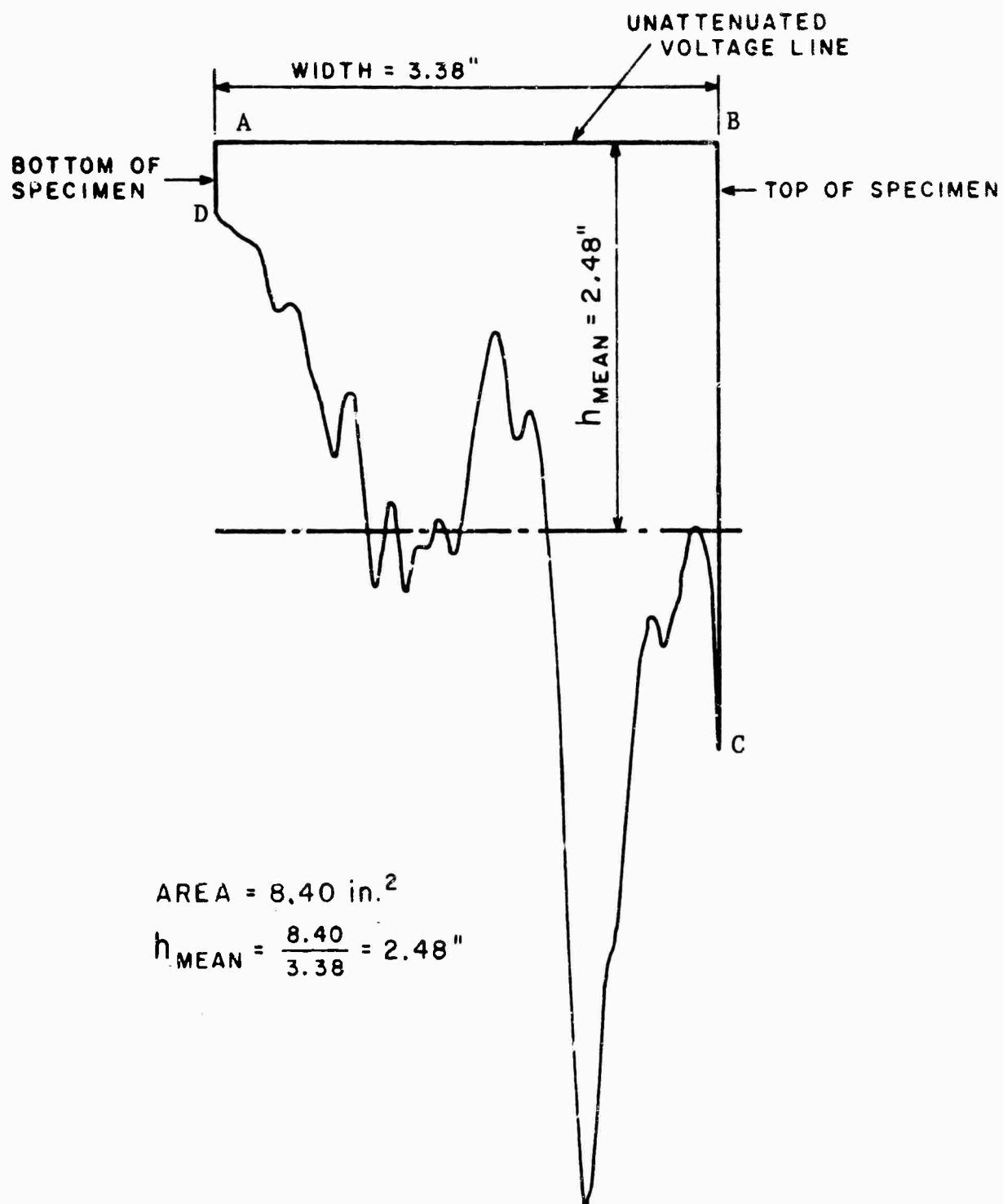


Fig. 51 AVERAGE ATTENUATION MEASUREMENT OF AN ULTRASONIC TRACE

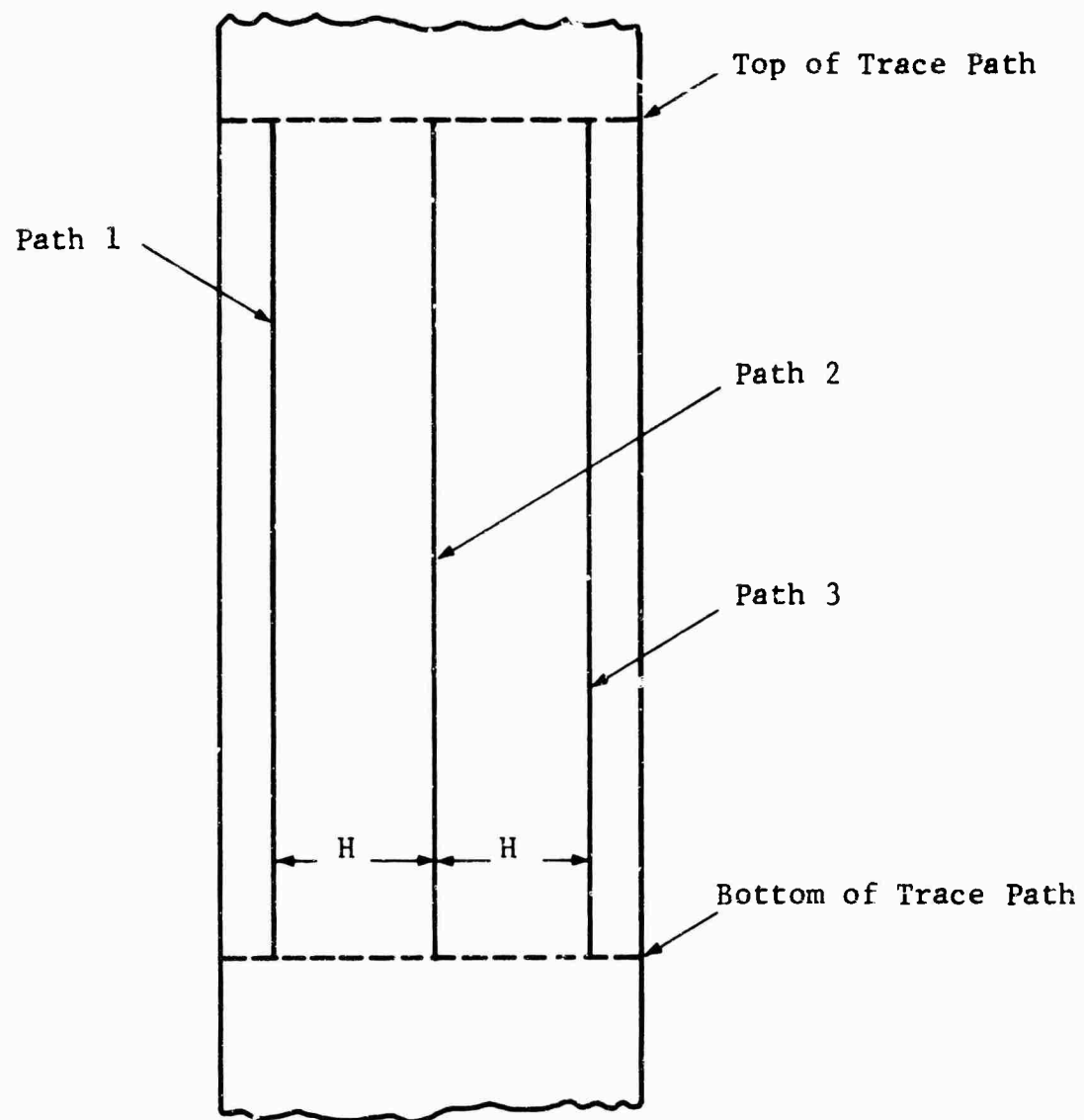


Fig. 52 WIDE SPECIMEN WITH THREE AVAILABLE TRACE PATHS TO BE USED IN WEIGHTED ATTENUATION MEASUREMENTS

The weighting formula used to obtain the weighted average attenuation  $\bar{A}$  for the section comprised of material near Path 2 is given by

$$\bar{A} = 1/4(\text{db loss})_{\text{Path 1}} + 1/2(\text{db loss})_{\text{Path 2}} + 1/4(\text{db loss})_{\text{Path 3}}$$

where the interior path trace is given double weight in accordance with the above discussion.

### 3. Maximum Attenuation Changes for Largest Apparent Flaw

Figure 53 which is typical, although exaggerated, of the behavior of the specimens tested, illustrates attenuation which occurs as the result of a single large defect area. In general, these large defect areas extend resulting in an increasing attenuation as the material degrades.

More severe than the average attenuation criterion and easier to apply, this criterion employs only the heights of the maximum voltage ( $h_{\text{max}}$ ) recorded for each trace. The attenuated voltage and db loss calculated as before can also be weighted as in Method 2, but here the most reliable method is to weight the maximum voltage change on the central path (Path 2) and the voltage change on adjacent points on the two side paths (see Fig. 54).

### 4. Weighted Maximum Attenuations for All Flaws in a Scan Path

Where several large voltage changes are recorded on a single scan path, these maximums can be recorded as described in Method 3, the db calculated for each and an average maximum attenuation obtained by dividing the number of peaks used. Figure 55 shows the method. Additional weighting may be performed where multiple parallel paths are available by using the weighting procedure described in Method 3 for each large "flaw" and averaging the results at the critical points along the central path by a formula such as was used in Method 2.

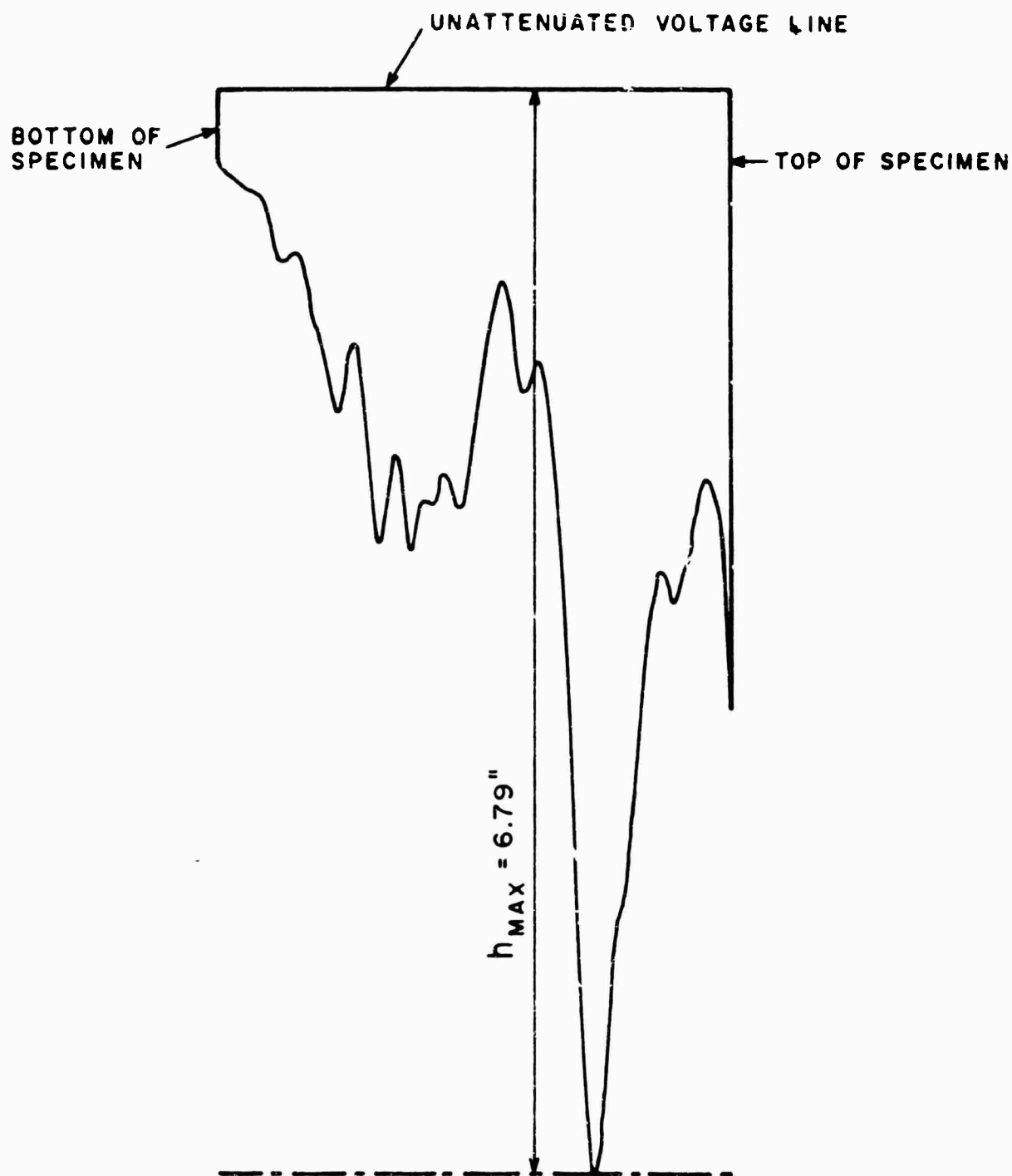


Fig. 53 MAXIMUM ATTENUATION MEASUREMENT OF AN  
ULTRASONIC TRACE

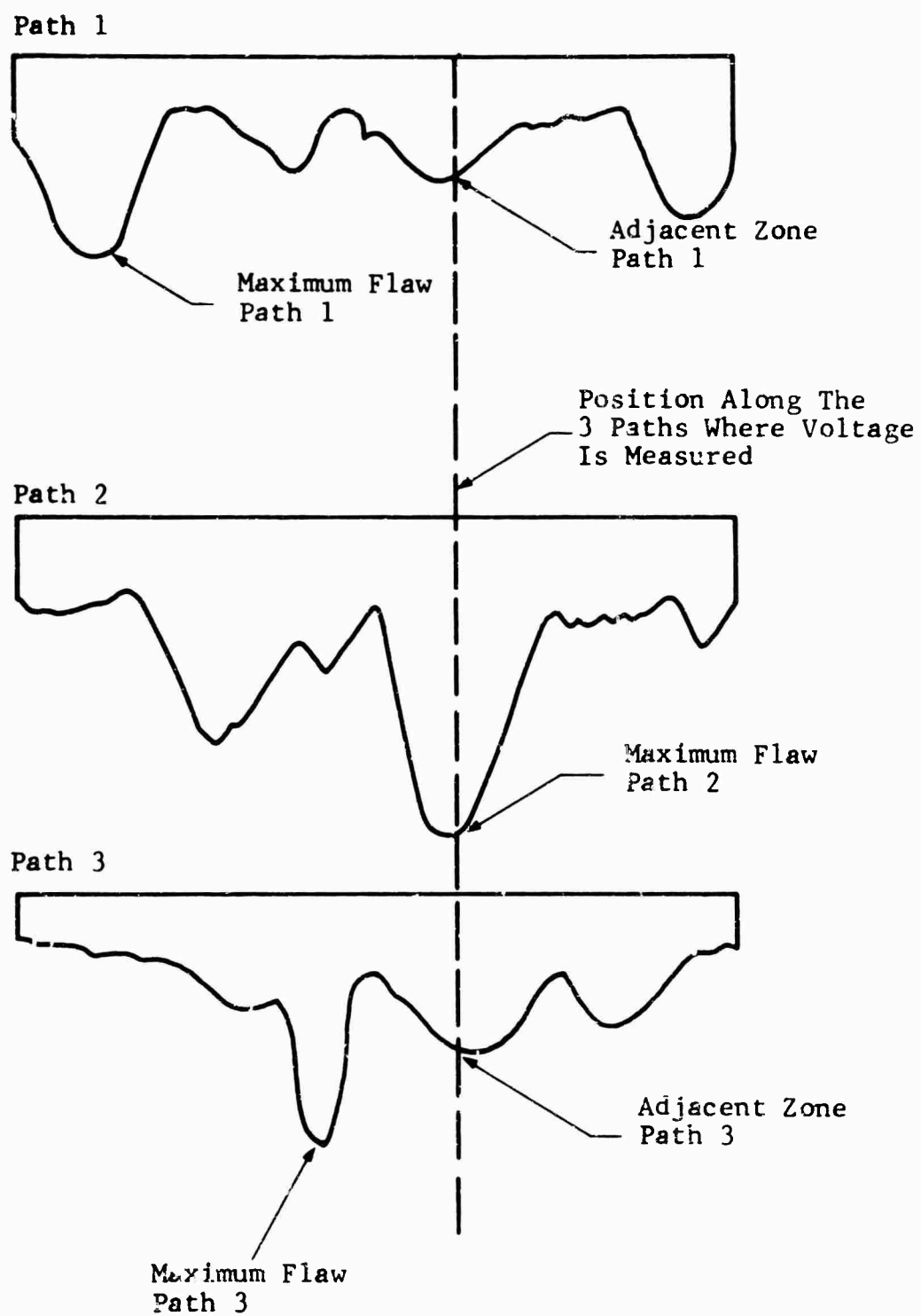
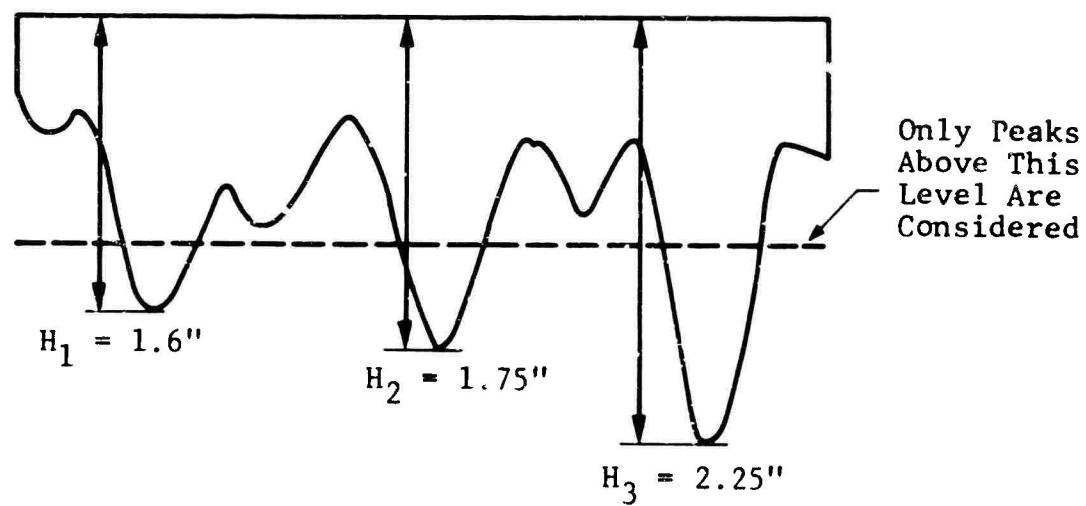


Fig. 54 WEIGHTING OF MAXIMUM ATTENUATION  
ALONG PARALLEL PATHS





$$\Sigma H_i = 5.6''$$

$$\bar{H}_{\max} = 1.87''$$

Fig. 55 EXAMPLE OF WEIGHTED MAXIMUM ATTENUATIONS  
ALONG SINGLE SCAN PATH

5. Previous Work on Examining the Various Ultrasonic Evaluation Methods and Correlation with Residual Interlaminar Shear Strength after Cycling

Hydrocyclic testing in Appendix B was performed in association with ultrasonic measurements. At various points in the testing, the specimens were sliced and tested in 3-point bending to ascertain the residual interlaminar shear strength. Some specimens were sliced prior to cycling but after an inspection. Figures 56 and 57 show the plot of residual interlaminar shear versus weighted maximum attenuation (Method 3) and weighted average attenuation (Method 2) respectively.

6. Current Ultrasonic Evaluations

Some 57 specimens were tested in tension, compression and bending as well as fully reversed fatigue and inspected ultrasonically throughout the course of the testing to determine the attenuation versus cycles inspection. Tables 37 through 41 present values for typical tensile fatigue specimens and the results are plotted in Fig. 58 as a function of the number of cycles to failure. Figure 59 presents similar results for other specimens plotted against percent of life expended.

The results shown in Fig. 58 although scant in number and apparently contradicting previous results by other investigators are worthy of additional comment. It is to be noted that no single level of attenuation could be ascribed as indicative of failure. Indeed, the curves for specimens 14-CuT-5, 15-CuT-2 and 16-CuT-1 appear to behave in reverse order. It is noted, however, that the slopes of the attenuation versus log-total cycles to failure appear to correlate. That is to say, the higher slopes in the semilog plot indicate shorter lives and decreasing slopes indicate increasingly longer lives. Figure 60 for specimen 5-T-12 shows a potential reason for this behavior. As the cyclic lives are expended, the damage curves (as expressed here by attenuation) appear to increase nonlinearly with cycles (see Appendix C). The slope increases substantially just prior to failure. Since the majority of cases described in Fig. 58 were not inspected prior to failure, linearity was apparently maintained to the last inspection. It is to be noted that as shown in Fig. 57 and 58

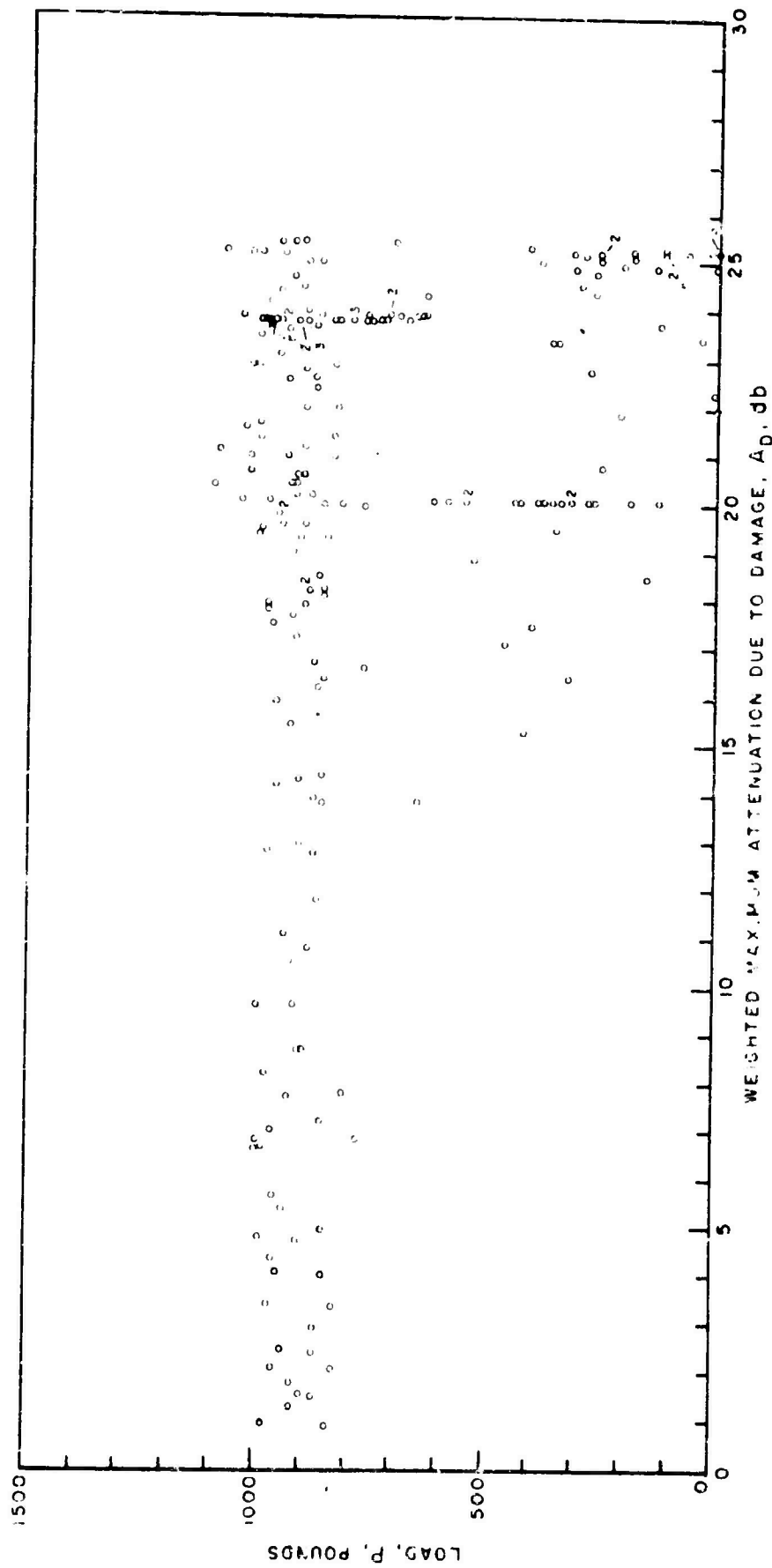


Fig. 56 SHEAR FAILURE LOAD VERSUS MAXIMUM ULTRASONIC ATTENUATION FOR 3-POINT BEAM SPECIMENS

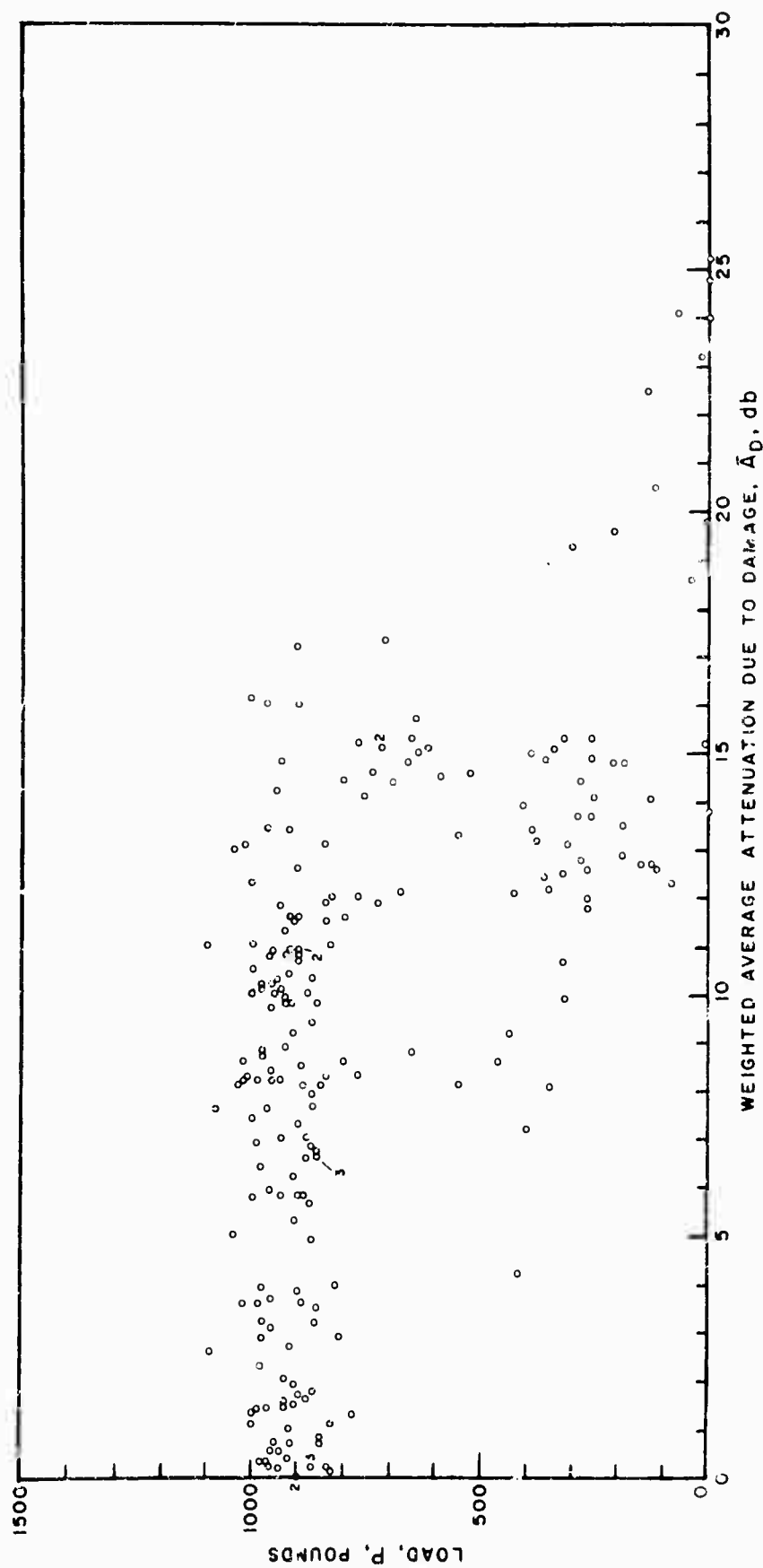


Fig. 57 SHEAR FAILURE LOAD VERSUS AVERAGE ULTRASONIC ATTENUATION  
FOR 3-POINT BEAM SPECIMENS

Table 37

MAXIMUM ATTENUATION AT A SINGLE FLAW - 181/S901 GLASS CLOTH  
 REINFORCED EPOXY SPECIMEN 9-CUT-5 TESTED IN TENSION (R=0.05)  
 FATIGUE TO  $\sigma_{MAX}$  = 43,000 PSI AT 6 CPM

Cycle	$V_o$	$V_o/V_i$	$\log \frac{V_o}{V_i}$	db
0	4.75	19.0	1.279	25.6
50	5.45	21.8	1.338	26.8
100	6.55	26.2	1.418	28.4
500	5.95	23.8	1.376	27.6

(Failure at 937 cycles)

Table 38

MAXIMUM ATTENUATION AT A SINGLE FLAW - 181/S901 GLASS CLOTH  
 REINFORCED EPOXY SPECIMEN NO. 14-CUT-3 TESTED IN TENSION  
 (R=0.05) FATIGUE TO  $\sigma_{MAX}$  = 43,000 PSI AT 6 CPM

Cycle	$V_o$	$V_o/V_i$	$\log \frac{V_o}{V_i}$	db
0	2.75	11.0	1.041	20.8
100	4.25	17.0	1.230	24.6
500	3.80	15.2	1.181	23.7
1000	4.25	17.0	1.230	24.6

(Failure at 1080 cycles)

Table 39

MAXIMUM ATTENUATION AT A SINGLE FLAW - 181/S901 GLASS CLOTH  
 REINFORCED EPOXY SPECIMEN NO. 15-CUT-2 TESTED IN TENSION  
 (R=0.05) FATIGUE TO  $\sigma_{MAX} = 43,000$  PSI AT 6 CPM

Cycle	$V_o$	$V_o/V_i$	$\log \frac{V_o}{V_i}$	db
0	0.60	2.40	0.38	7.6
100	1.50	6.00	0.778	15.6
500	2.10	8.40	0.924	18.5

(Failure at 663 cycles)

Table 40

MAXIMUM ATTENUATION AT A SINGLE FLAW - 181/S901 GLASS CLOTH  
 REINFORCED EPOXY SPECIMEN NO.16-CUT-1 TESTED IN TENSION  
 (R=0.05) FATIGUE TO  $\sigma_{MAX} = 43,000$  PSI AT 6 CPM

Cycle	$V_o$	$V_o/V_i$	$\log \frac{V_o}{V_i}$	db
0	4.95	19.8	1.247	26.0
10	6.05	24.2	1.384	27.7
50	5.05	20.2	1.305	26.1
100	5.60	22.4	1.350	27.0
500	5.15	20.6	1.314	26.5
1000	4.90	19.7	1.294	25.9

(Failure at 1550 cycles)

Table 41

MAXIMUM ATTENUATION AT A SINGLE FLAW - 181/S901 GLASS CLOTH  
REINFORCED EPOXY SPECIMEN NO. 10-CUT-4 TESTED IN TENSION  
(R=0.05) FATIGUE TO  $\sigma_{MAX} = 43,000$  PSI AT 6 CPM

Cycle	$V_o$	$V_o/V_i$	$\log \frac{V_o}{V_i}$	db
0	4.35	17.4	1.24	24.8
10	4.50	18.0	1.255	25.1
50	6.50	26.0	1.415	28.3
100	7.65	30.6	1.486	29.7
1000	7.65	30.6	1.486	29.7

(Failure at 1331 cycles)

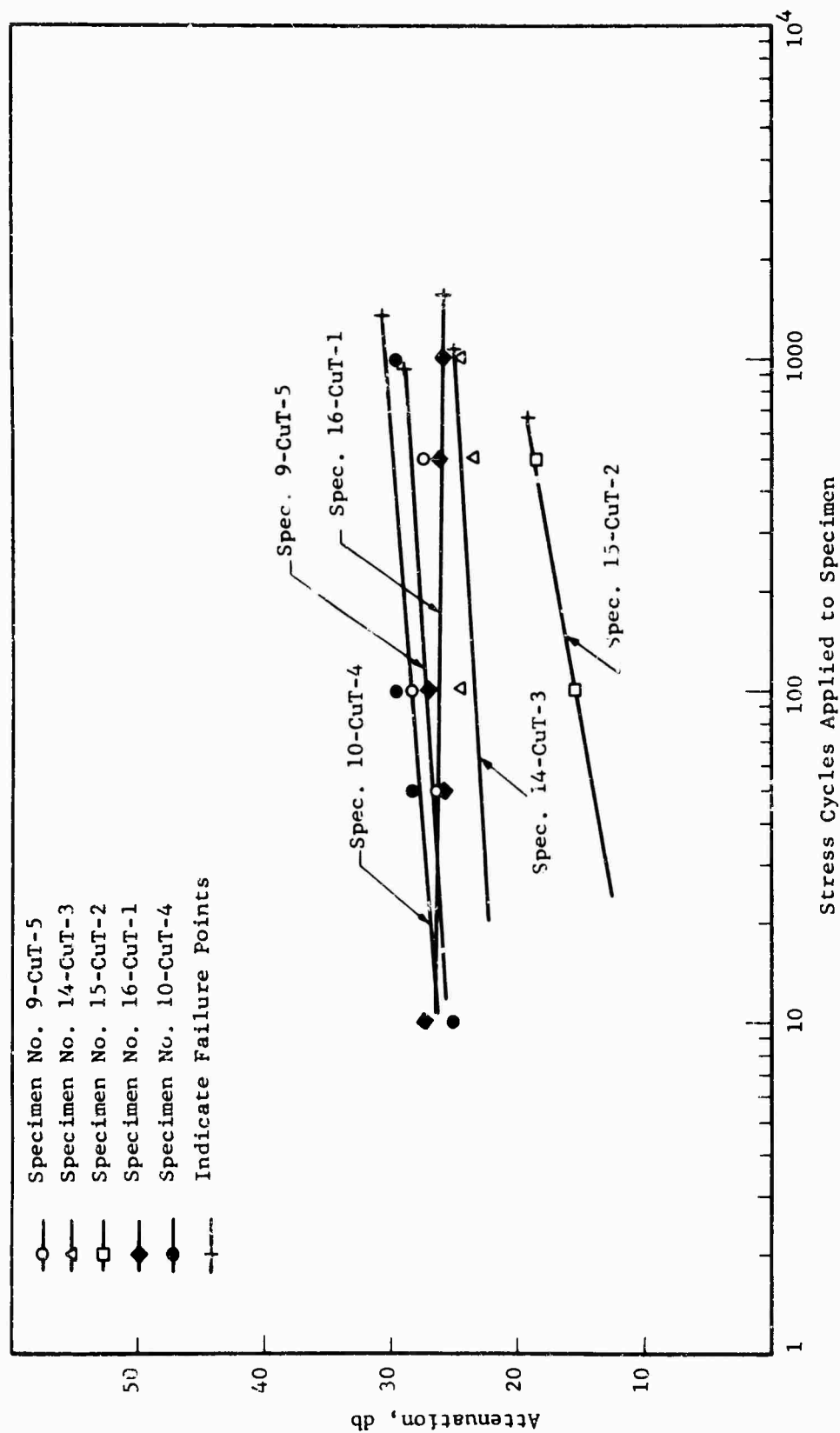


Fig. 58 ATTENUATION VERSUS STRESS CYCLES TO FAILURE FOR 181/S901 GLASS CLOTH REINFORCED EPOXY SPECIMENS TESTED IN TENSION-ZERO-TENSION ( $R = 0.05$ ) AT  $\sigma_{MAX} = 43,000$  PSI AT 6 CPM



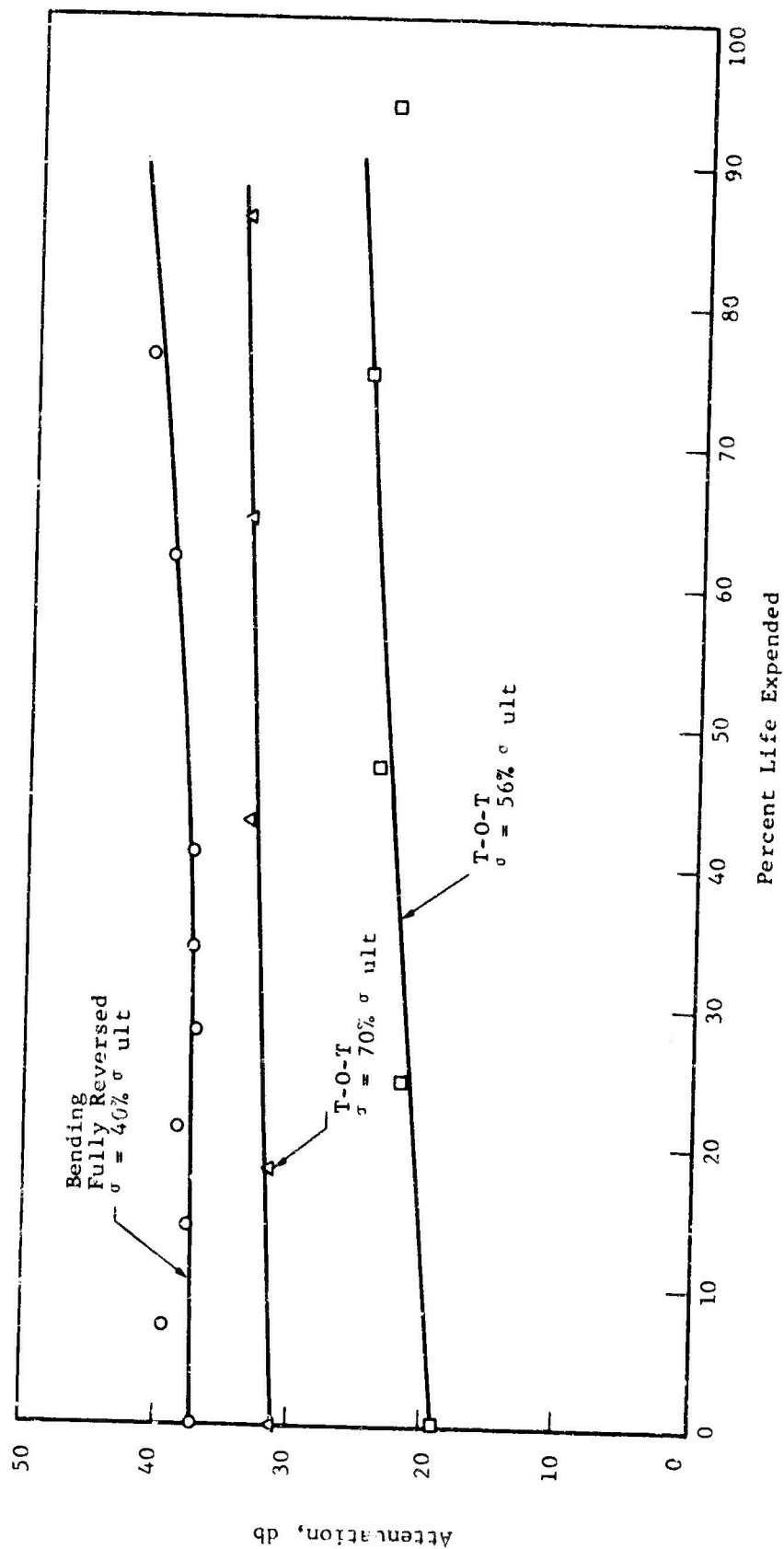


Fig. 59 ATTENUATION IN db VERSUS PERCENT OF LIFE EXPENDED FOR 181/S901 GLASS CLOTH REINFORCED EPOXY SPECIMENS TESTED IN TENSION ( $R = 0.05$ ) AND BENDING ( $R = -1$ ) FATIGUE

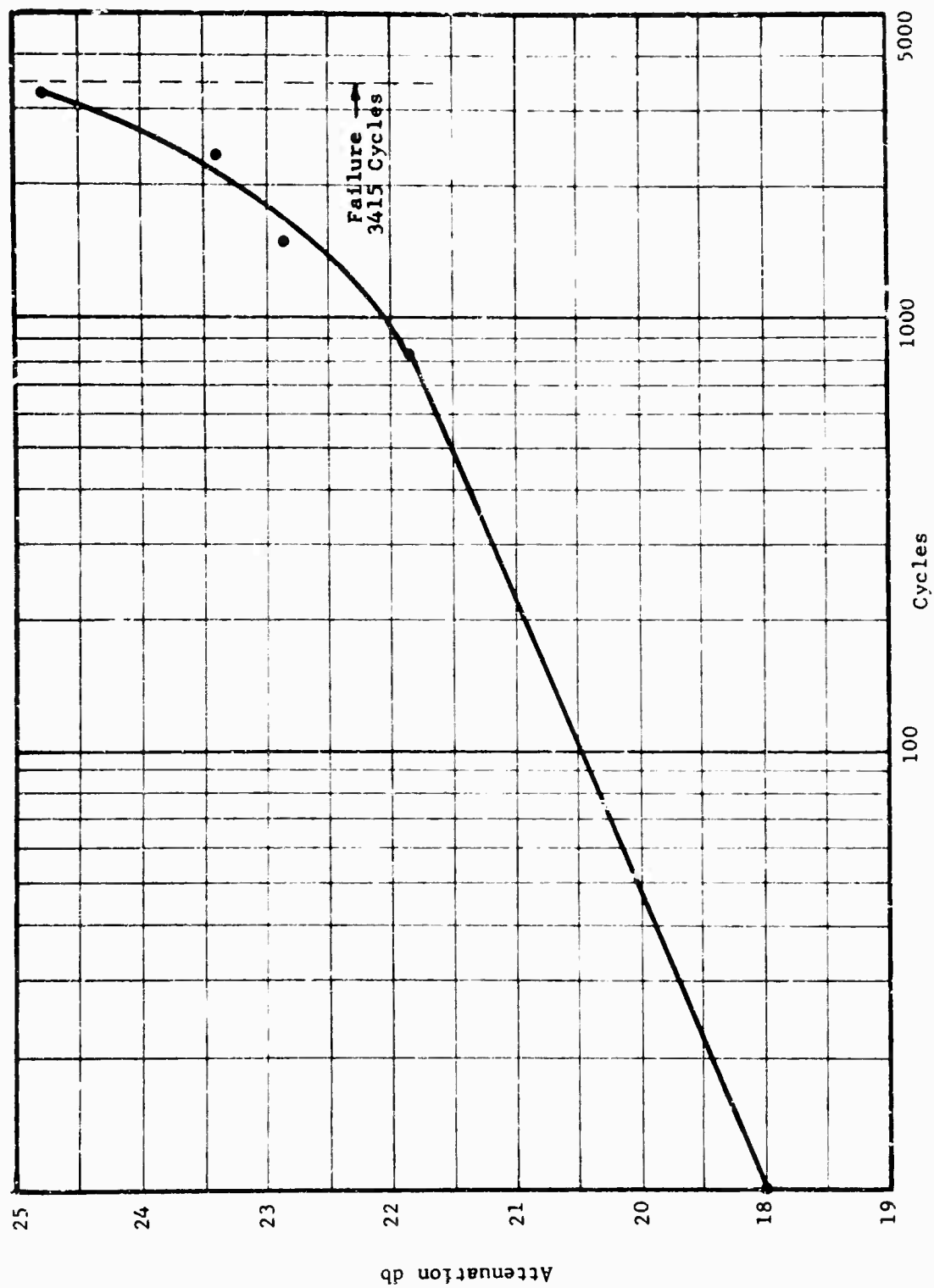


Fig. 60 ATTENUATION VERSUS CYCLES, SPECIMEN 5-T-12 181/S901 GLASS CLOTH REINFORCED EPOXY TESTED IN TENSION-ZERO-TENSION AT 47,500 PSJ

there is a sudden sharp decrease in interlaminar shear after a certain average attenuation level has been attained. It is possible then that within the region of say 8 to 16 db attenuation levels (in Fig. 56 and 57) the damage curve slope increases sharply. Considerably more evidence is needed, however, before quantitative evaluations along these lines are possible.

#### B. SEQUENTIAL AMPLITUDE STUDIES

A most desirable situation is to have an analytical expression which permits the GRP designer to give a quantitative estimate of the life of his structure from the results of tests on small coupons. Furthermore, since the cyclical loads, to which his structure is subjected, vary in amplitude with time, it is important that his analytical expression be able to set forth this "cumulative damage". Appendix C describes several such theories which have been used in the past primarily to describe cumulative damage effects for metals. To test the applicability of some of these theories for GRP, a study was initiated utilizing one of the GRP materials studies in this program, viz., 181/S901 glass cloth reinforced epoxy.

A two-step stress level type of cumulative damage test was performed on 181 cloth axial fatigue specimens (see Fig. 61). The load profile was tension-zero-tension. Both types of two-step loading patterns were used, i.e. high-low and low-high. Three specimens for each type of load pattern were employed. Initial cycling was performed to two life levels: 1/3 life and 2/3 life. A full parametric study thus demanded 12 specimens as a minimum. Tests were conducted in the 6 and 50 cpm ranges as shown in Fig. 62 since it was felt that sufficient discretion of lives at the second stress level could be ascertained for these two frequencies from the comprehensive studies described earlier.

An investigation of various cumulative damage theories (Appendix C) showed that the bases for six theories are commonly derived; but only three appear to be applicable at the present time for GRP. These three are Miner's, Corten-Dolan's and Freudenthal-Heller's theories. The results of the simple two-step stress level tests were employed in these three theories to confirm or to deny such apparent applicability.

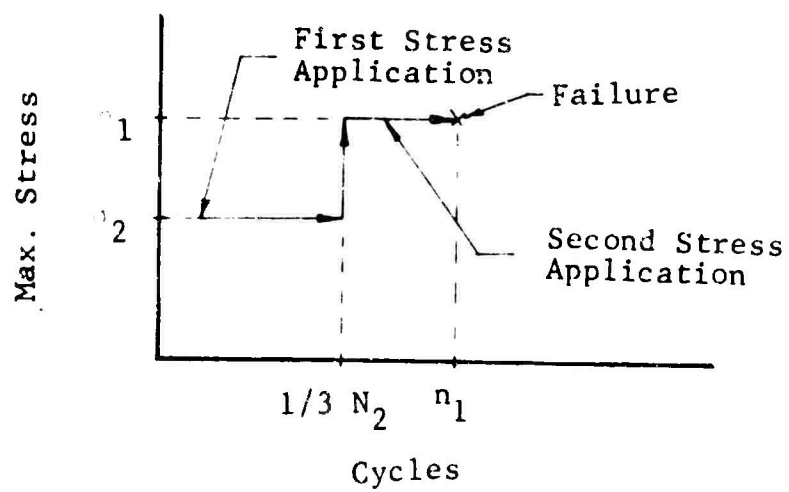
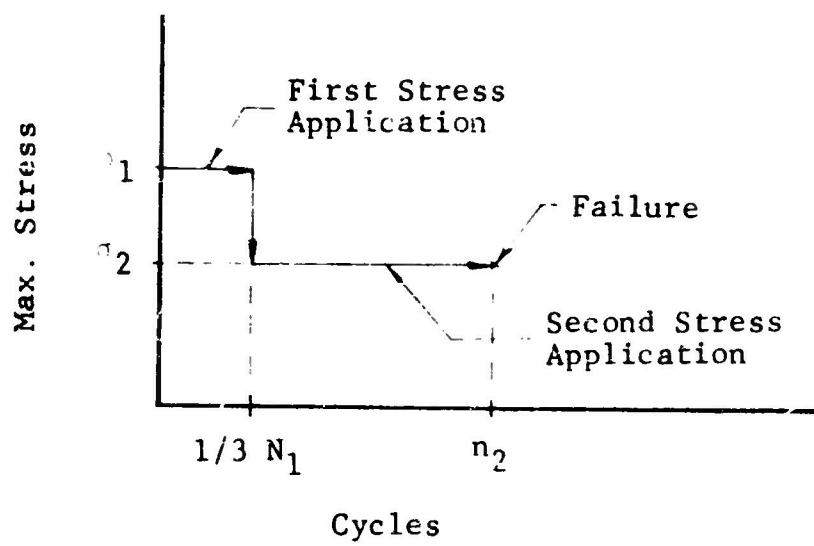
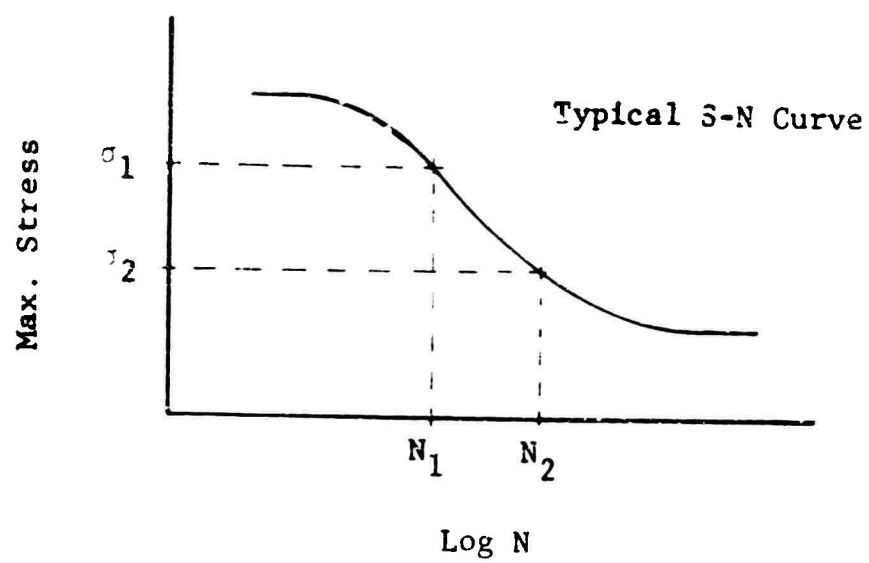


Fig. 61 TWO STRESS LEVEL CUMULATIVE DAMAGE METHOD

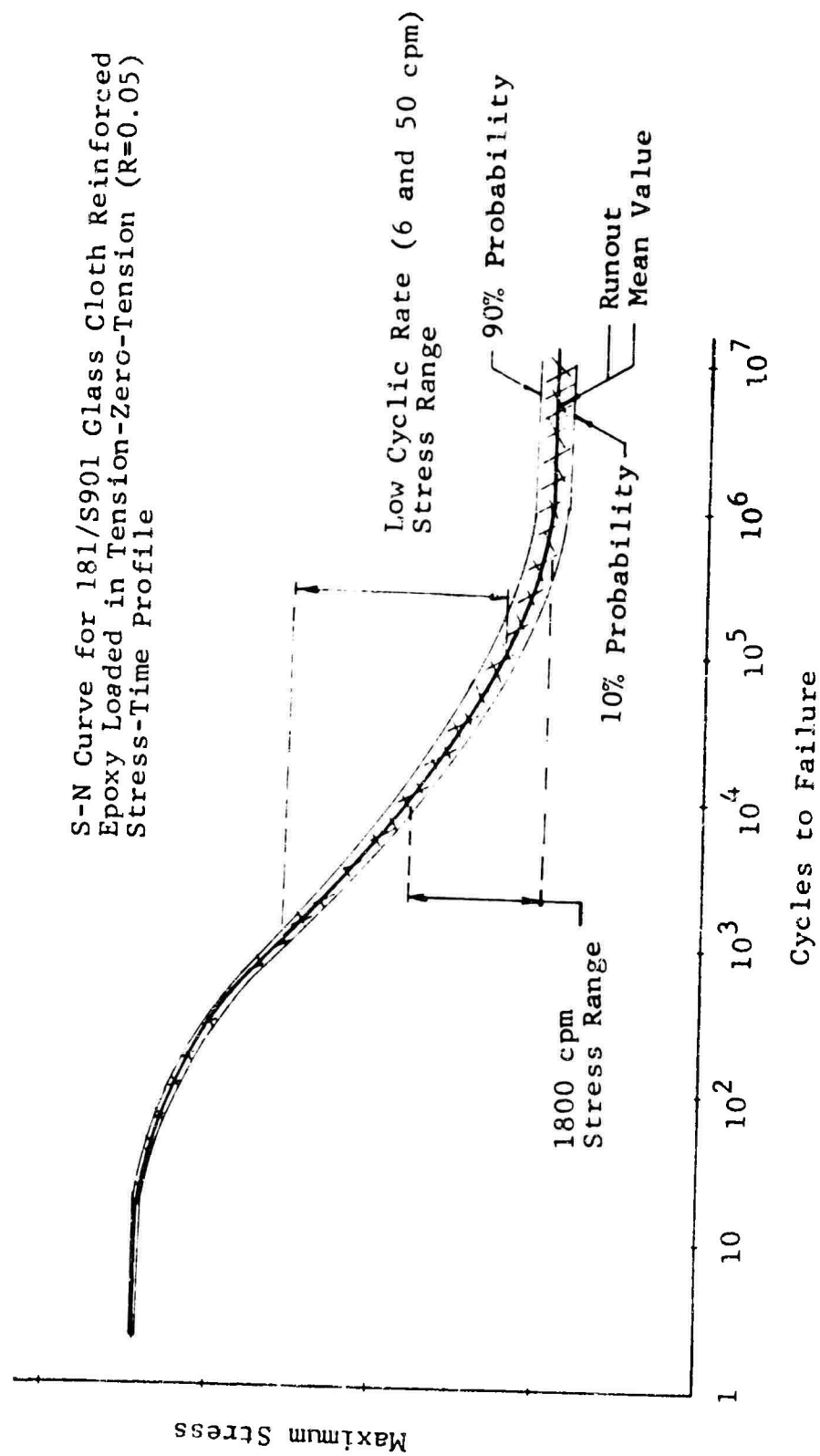


Fig. 62 RANGES FOR TWO CYCLIC RATE FATIGUE MACHINES FOR APPLICATION IN CUMULATIVE DAMAGE STUDY

## 1. Miner's Rule and the Corten-Dolan Theory

Summarizing from Appendix C, we have for two-step stress level tests

### Miner's Rule

$$\frac{n_1}{N_1} + \frac{n_2}{N_2} = 1$$

### Corten-Dolan Rule

The Corten-Dolan theory states that every material has a constant,  $d$ , which is independent of stress spectrum. This material constant can be used to construct a fictitious S-N curve for use in the linear summations.

$$N_G = \frac{N_1}{\frac{n_1}{N_1} + \frac{n_2}{N_2} \left( \frac{\sigma_2}{\sigma_1} \right)^d} d$$

here  $N_1 = \sigma_1$  life,  $N_2 = \sigma_2$  life at constant stress amplitude and  $n_1$  = cycles applied to specimen at  $\sigma_1$  stress level,  $n_2$  = cycles applied to specimen at  $\sigma_2$  stress level. It is to be noted that  $\sigma_1$  is always the larger of the two stress levels regardless of its order of appearance in the sequential loading.

The general scheme is to plot  $N_1/N_{Gt}$  versus  $d$  for experimental values of  $n_1$ ,  $N$  and  $\sigma$ . Then an average is made of  $N_1/N_{Ge}$  thus permitting the determination of  $d$  from the plot of  $N_1/N_{Gt}$  versus  $d$ . Here we have taken  $N_{Gt}$  to mean the theoretical value of  $N_G$ , and  $N_{Ge}$  to mean the experimentally derived value. As an example of the determination of  $d$  from a two-step stress level experiment, consider the following.

We start with the general Corten-Dolan expression

$$\frac{N_G}{N_1} = \left[ \frac{n_1}{N_1} + \frac{n_2}{N_2} \left( \frac{\sigma_2}{\sigma_1} \right)^d \right]^{-1}$$

With  $n_1$  and  $n_2$  experimentally determined, we can calculate  $N_{Gt}$ . Let us assume that

$$\begin{aligned}\sigma_1 &= 40,000 \text{ psi} \\ \sigma_2 &= 30,000 \text{ psi} \\ N_1 &= 20,000 \text{ cycles} \\ N_2 &= 100,000 \text{ cycles} \\ n_1 &= 6,000 \text{ cycles} \\ n_2 &= 8,000 \text{ cycles}\end{aligned}$$

then we obtain

$$\frac{N_G}{N_1} = \left[ 0.3 + 0.9 \left( \frac{\sigma_2}{\sigma_1} \right)^d \right]^{-1}$$

Plotting this as shown in Fig. 63, a curve is obtained, which when experimental values of  $N_G/N_1$  are inserted, permits us to establish  $(\sigma_1/\sigma_2)^d$  and thus obtain  $d$ .

The results of 16 two-step tests on 181/S901 glass cloth tests are shown in Table 42 with a summary appropriate to the testing of the applicability of Miner's Rule. The values shown for Miner's summation in Table 42 are generally greater than one for the high-low two-step stress level tests, which definitely represents a conservative approach to design. This does not completely tell the story since at least one value is less than 1 and 3 specimens failed prior to attaining the average life of 43,000 psi. For the low-high two-step stress level, test values of the Miner's summation were generally less than one which definitely indicates a nonconservative design approach. The average linear summation for the high-low tests is 2.09 and for the low-high tests is 0.95. An overall summation, eliminating the highest and lowest values yields 1.56. This indicates that use of Miner's Rule for this material should provide a conservative design in the majority of loading spectra.

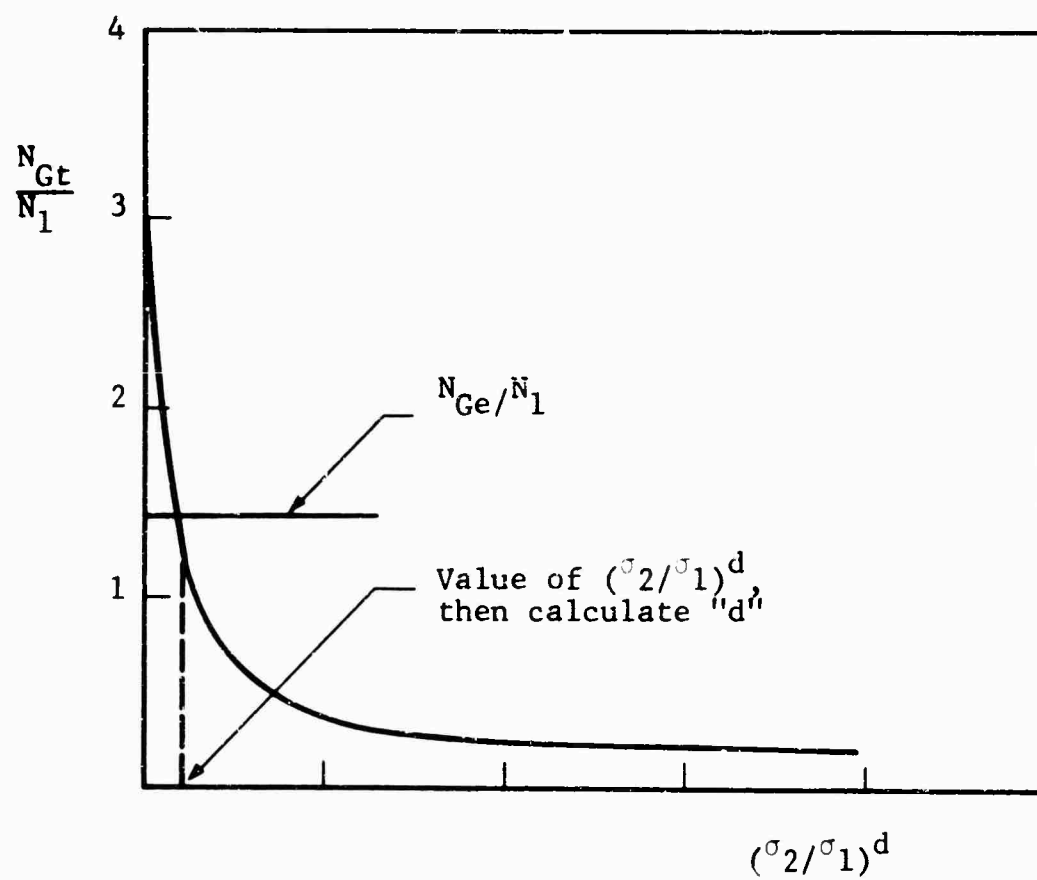


Fig. 63 EXAMPLE OF THE DETERMINATION OF  $d$  FROM EXPERIMENTAL DATA



Table 42

CUMULATIVE DAMAGE TWO STEP STRESS LEVEL TESTS RESULTS WITH MINER'S RULE SUMMATIONS -  
 181/S901 GLASS CLOTH REINFORCED EPOXY LOADED IN TENSION - ZERO TENSION ( $R = 0.05$ ) AT  
 6 CPM, (AVERAGE LIFE  $N_1$  AT  $\sigma_1 = 43,000$  PSI WAS 1150 CYCLES; AVERAGE LIFE  $N_2$  AT  $\sigma_2 =$   
 31,000 PSI WAS 29,200 CYCLES)

Specimen Number	$\sigma_1$ (psi)	$n_1$ (cycles)	$\sigma_2$ (psi)	$N_G$ Cycles to Failure	$n_2 = N_G - n_1$ Cycles	$\frac{n_1}{N_1}$	$\frac{n_2}{N_2}$	Miner's Summation $\frac{n_1}{N_1} + \frac{n_2}{N_2}$
16-Cut-1	43,000	385	31,000	118,128	117,745	0.33	3.8	4.13
3-Cut-2	43,000	383	31,000	278		0.24		
15-Cut-3	43,000	383	31,000	384		0.33		
15-Cut-4	43,000	766	31,000	728		0.632		
14-Cut-5	43,000	766	31,000	61,865	61,099	0.66	2.1	2.76
15-Cut-6	43,000	766	31,000	29,128	28,362	0.66	0.97	1.63
11-Cut-7	43,000	115	31,000	18,354	18,239	0.1	0.624	0.724
11-Cut-8	43,000	115	31,000	29,405	29,290	0.1	1.0	1.10

Spec.	$\sigma_2$	$n_2$	$\sigma_1$	N	$n_1 = N - n_2$	$\frac{n_1}{N_1}$	$\frac{n_2}{N_2}$	$\Sigma \frac{n_i}{N_i}$
9-Cut-9	31,000	9,740	43,000	3,209			0.11	
16-Cut-10	31,000	9,740	43,000	23,903	14,163	12.3	0.46	12.76
16-Cut-11	31,000	9,740	43,000	10,018	278	0.242	0.33	0.57
4-Cut-14	31,000	20,598	43,000	20,642	44	0.038	0.705	0.74
7-Cut-15	31,000	19,480	43,000	20,073	593	0.52	0.66	1.18
16-Cut-16	31,000	19,480	43,000	19,648	168	0.15	0.66	0.81

Table 43 also presents the same test results with the Corten-Dolan parameters calculated. Here, values of  $(N_{Gt}/N_{Ge})$  less than unity represent conservative design approach. The results show generally that both high-low and low-high two-step stress level tests yield conservative design values with the Corten-Dolan theory. Plotting in a log S-log N curve permits calculation of the theoretically derived b. Recall that  $(\sigma_2/\sigma_1)^b = N_1/N_2$  is an approximate expression in a log-log plot.

Thus

$$b = \frac{\log N_1 - \log N_2}{\log \sigma_1 - \log \sigma_2} = 9.2$$

The average values for Table 42 were made discarding both the highest and lowest values in accordance with standard statistical techniques.

The test results shown in Table 43 give an average value of  $d = 17.9$ . This material constant predicts less fatigue life than the mean summation (Miner's Rule) but could still be considered nonconservative. This results from the following argument. In their original assumptions, Corten and Dolan implied that a two-stress level test could be used to determine the material constant. This is in disagreement with the Freudenthal and Heller statement that the material constant is dependent on the stress spectrum. The fact that the low cyclic life used in the tests was only 29,000 cycles shows that there is a need for tests beyond this cyclic life. The reason 29,200 cycles or 31,000 psi was used in the current series of tests is that at lower stresses where the lives approach  $10^7$  cycles, the scatter in test data increases. Use of a small number of test specimens makes it difficult to ascribe statistical reliability to the method. Thus a higher stress level is more desirable experimentally. If the value of  $d = 17.2$  was used in design for a stress spectrum with the majority of stress levels below the stress spectrum used to

Table 43

CUMULATIVE DAMAGE TWO STEP STRESS LEVEL TESTS RESULTS WITH CORTEN - DOLAN EXPONENT  
 COMPRESSIONS OF THEORETICAL AND EXPERIMENTAL VALUES-181/S901 GLASS CLOTH REINFORCED  
 EPOXIES LOADED IN TENSION ZERO - TENSION ( $R = 0.05$ ) AT 6 CPM (AVERAGE LIFE AT  $\sigma_1 =$   
 43,000 PSI WAS 1150 CYCLES; AVERAGE LIFE AT  $\sigma_2 = 31,000$  PSI WAS 29,200 CYCLES)

Specimen Number	$\alpha - \frac{n_1}{N_G}$	$1 - \alpha$	$N_{Ge}$	$R^{1/a}$	$d = \frac{\log R^{1/a}}{-1.142}$	$\frac{N_{Ge}}{N_1}$	$N_{Gt}$	$\frac{N_{Gt}}{N_{Ge}}$
16-Cut-1	0.00326	0.99674	118,128	0.00975	28.5	102.5	24,200	0.205
3-Cut-2	1.00	0	278					
15-Cut-3	1.00	0	384					
15-Cut-4	1.00	0	728					
14-Cut-5	0.0124	0.9876	61,865	0.0066	27.3	53.8	12,700	0.205
15-Cut-6	0.0264	0.9736	29,129	0.0140	15.3	25.2	12,700	0.436
11-Cut-7	0.00626	0.99374	18,354	0.0572	19.7	15.9	32,400	0.691
11-Cut-8	0.00391	0.99609	29,405	0.0352	18.2	25.6	32,400	0.432
9-Cut-9	0	1.00	3,209					
16-Cut-10	0.594	0.406	23,903	-1.35	0.915	20.8	10,600	0.443
16-Cut-11	0.026	0.974	10,018	0.0914	21.2	8.7	10,600	1.060
5-Cut-12	0.272	0.728	26,798	0.218	9.4	23.2	10,600	0.396
4-Cut-14	0.055	0.945	20,642	0.00095	35.5	17.9	20,150	0.968
7-Cut-15	0.032	0.968	20,073	0.0245	7.1	18.0	20,150	1.00
16-Cut-16	0.010	0.99	19,648	0.0490	19.2	17.1	20,150	1.025
Average								

determine  $d$ , it is possible that the cyclic life predicted could be nonconservative. Therefore, a complete stress spectrum should be used to determine  $d$  according to the Freudenthal-Heller theory.

It should also be pointed out that even Miner's theory applied to a stress spectrum having stresses below the endurance limit, predicts nonconservative cumulative results

$$\left(\sum \frac{n}{N} = 0 \text{ for } N = \infty\right)$$

## 2. Freudenthal-Heller (and/or Corten-Dolan) Fictitious S-N Curve

Here the assumption is made that a fictitious S-N curve may be drawn which relates the stress intersection resulting from a spectrum loading (see Fig. 64). Using our values of  $d$  and  $b$  from the experiments, let us try to construct such a curve ( $b = 9.2$ ,  $d = 17.9$ ). Furthermore, we will use  $\sigma_{ult} = 62,000$  psi at the single cycle life as the point common to the fictitious S-N curve and the actual S-N curve for a single stress level test.

Recall that

$$\left(\begin{matrix} \sigma_2 \\ \sigma_1 \end{matrix}\right)^d = \frac{N_1^1}{N_2^1}$$

$$\sigma_1^1 = 62,000 \text{ psi}, N_2^1 = 10 \text{ cycles}, \sigma_2^1 = 43,000 \text{ psi}$$

then

$$d (\log 43,000 - \log 62,000) = \log 10 - \log N_2^1$$

$$17.9 (4.6333 - 4.799) = 1 - \log N_2^1$$

solving we obtain

$$N_2^1 = 9868$$

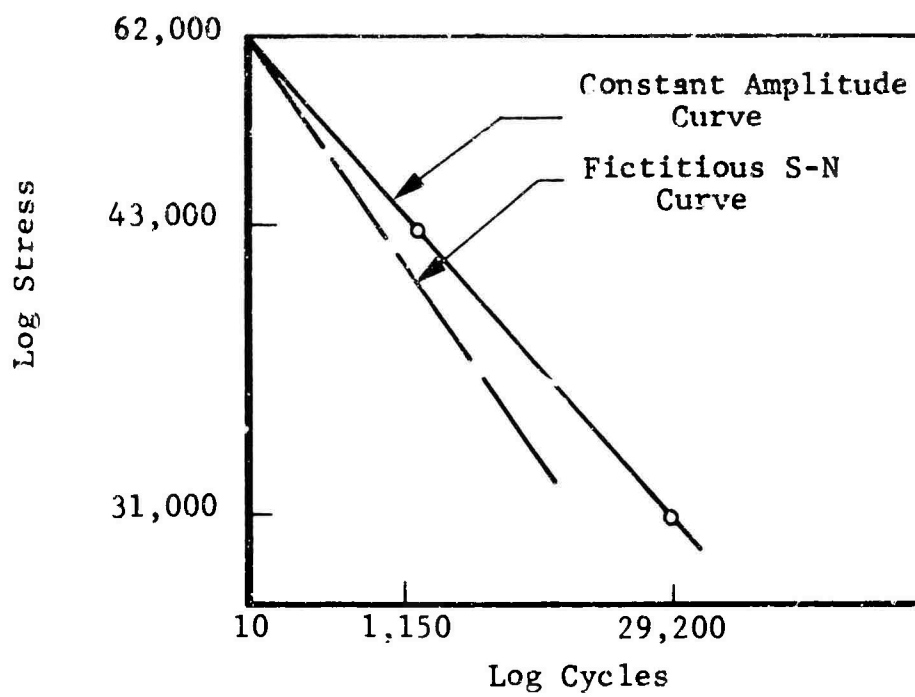


Fig. 64 EXAMPLE OF FREUDENTHAL-HELLER FICTITIOUS S-N CURVE

for  $\sigma_2 = 31,000$

$$\log N_1^1 = 1 - 17.9(4.491 - 4.799)$$

$$N_1^1 = 7.07 \times 10^6$$

This last value has been demonstrated through test to be far higher than the real value obtained in a single stress level test.

Now we assume that the point of intersection of the fictitious S-N curve is at 43,000 psi with  $N_1 = N_1^1 = 1,150$  cycles. Here we must satisfy

$$17.9(4.491 - 4.633) = 3.061 - \log N_2^1$$

$$N_2^1 = 399,000 \text{ cycles}$$

Testing this against our experimental values:

Specimen 16-CuT-1

$$n_1 = 383 \text{ cycles}, n_2 = 117,745 \text{ cycles}, n_1/N_1^1 = 0.33$$

$$n_2/N_2^1 = 0.295 \text{ and } \Sigma = 0.625$$

Specimen 14-CuT-5

$$n_1 = 766 \text{ cycles}, n_2 = 61,099 \text{ cycles}, n_1/N_1^1 = 0.66,$$

$$n_2/N_2^1 = 0.15 \text{ and } \Sigma = 0.81$$

Table 44 gives additional values for other specimens. Hence, it appears from the summations that the intersection point actually occurs at a stress level below 43,000 psi as shown in Fig. 65. This would tend to indicate that values of  $\sigma$  some distance below 43,000 psi when added cumulatively would tend to deviate the curve away from this fictitious S-N curve.

Table 44

MINER'S SUMMATIONS FOR FREUDENTHAL-HELLER FICTITIOUS S-N  
CURVE FROM TENSILE FATIGUE DATA ON 181/S901 GLASS CLOTH  
REINFORCED EPOXY.

Specimen Number	$\frac{n_1}{N_1}$	$\frac{n_2}{N_2}$	$\Sigma \frac{n_i}{N_i}$
16-Cut-1	0.33	0.29	0.62
14-Cut-5	0.66	0.15	0.81
15-Cut-6	0.66	0.07	0.73
11-Cut-7	0.10	0.045	0.145
11-Cut-8	0.10	0.073	0.173
16-Cut-10	12.3	0.0244	12.32
16-Cut-11	0.243	0.024	0.266
4-Cut-14	0.038	0.05	0.09
7-Cut-15	0.52	0.05	0.57
16-Cut-16	0.15	0.05	0.20

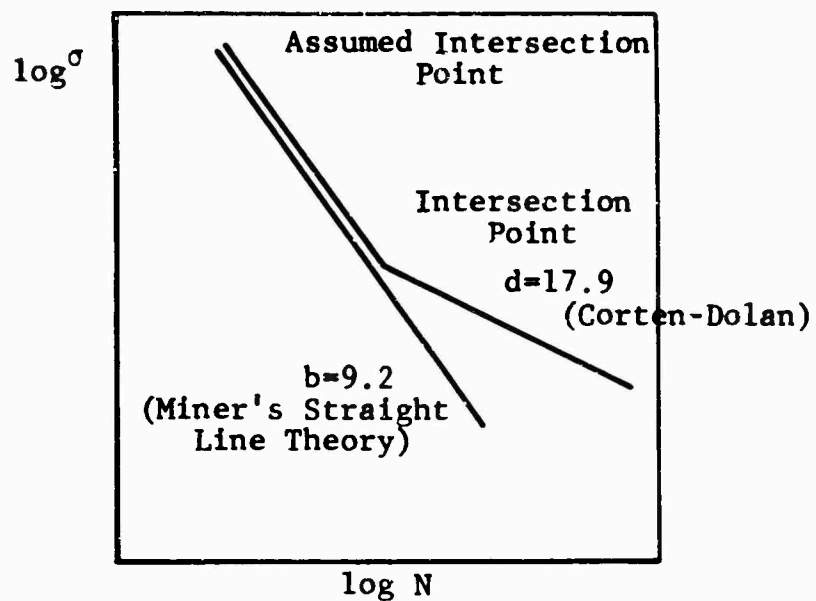


Fig. 65 INTERSECTION OF CORTEN-DOLAN AND FREUDENTHAL-HELLER FICTITIOUS S-N CURVES



Such stress levels might result in a nonconservative design if  $b = 9.2$  were used. Such a condition might be demonstrated to be inadequate if the deviation were in the other direction.

### 3. Summary and Some Previous Values for b, d, and p

Since the Miner summations have values of approximately unity, it is evident that the 9.2 value for  $b$  is reasonable. Furthermore, the fictitious S-N curve must intersect the actual curve somewhere around 10,000 cycles. This means that some interaction effect is present and that the rate of damage is nearly linear.

A value of  $d > b$  can give nonconservative estimates of fatigue life. Corten and Dolan initially assumed in their cumulative damage theory that the rate of damage accumulation is positive and that there is some stress interaction effect. This assumption could give either conservative or nonconservative results. It is further dependent on a load spectrum over the full range of stresses and cyclic lives. Even Miner's theory might predict nonconservatively if the stress spectrum contains stress below the endurance limit ( $\sum \frac{n}{N} = 0$  where  $N = \infty$ ). The Freudenthal-Heller theory appears to be quite general and to give more reliable results. The major shortcoming is its cumbersome application.

Table 45 indicates some previous values obtained for the principal parameters  $b$ ,  $d$  and  $p$  of the three cumulative damage theories as well as the values for the 181/S901 glass cloth reinforced epoxy.

### 4. Application of Miner's Cumulative Damage Rule to S994 Uniaxial Glass Roving Reinforced Epoxy

Two step stress level tests were also conducted at 1800 cpm in tension-zero-tension for S994 glass roving reinforced epoxy. The results are summarized in Table 46. With an average Miner's summation of  $\sum (n_i/N_i) = 3.20$ , it can be safely assumed that the Miner's rule provides a conservative estimate of cyclic strength for design purposes. Two S994

**Table 45**  
**COMPARISON OF CUMULATIVE DAMAGE CONSTANTS**

Material	Test Condition	Miner b	Corten- Dolan c	Freudenthal- Hellm p	Reference
7075-T6 Wire	Two Stress Level (Av)				
	$\sigma_2 =$		3.30		72
	Constant Stress				
	R = -1	4.62			72
7075-T6 Extr.	Constant Stress				
	R = -1	10.00			73
	R = 0	15.30			73
	Two Stress Level				
	$\sigma_2 = 0.8 \sigma_1$		4.17		74
	$\sigma_2 = 0.6 \sigma_1$		8.25		74
	$\sigma_2 = 0.25 \sigma_1$		1.58		74
	Spectrum Stress No. 1		10.30		74
	Spectrum Stress No. 1		8.25		75
2024-T4	Constant Stress				72
	R = -1	4.10			72
	Two Stress Level (Av)		5.788		72
2024-T4 Extr.	Constant Stress				
	R = -1	8.25			76
	R = 0	13.30			72
	Stress Spectrum (Av)			4.0 - 8.0	76
4340	Constant Stress				
	R = -1	10.00			76
	Stress Spectrum			6.0 - 9.8	76
Brite Basic Steel Wire	Constant Stress				
	R = -1	7.35			72
	Two Stress Level (Av)		5.98		72
Ti-170-A	Constant Stress				
	R = -1	306.00			73
Ti-150-A	R = -1	$\infty$			73
181/Cloth Epoxy Resin	Constant Stress				
	R = 0	11.50			
	$\sigma_2 = 0.72 \sigma_1$ (Av)		22.50		

Table 46

SUMMARY OF RESULTS OF TWO STEP STRESS LEVEL TESTS WITH MINER'S RULE APPLIED FOR S994  
UNIAxIAL GLASS ROVING REINFORCED EPOXY TESTED AT 1800 CPM IN TENSION-ZERO-TENSION (R=0.05)  
(AVERAGE LIFE AT 75,000 PSI = 9,000 CYCLES, AVERAGE LIFE AT 45,000 PSI = 2,500,000 CYCLES)

Specimen Number	First Stress (psi)	n <sub>1</sub> or n <sub>2</sub> (cycles)	$\sigma_2$ (psi)	n <sub>2</sub> = N <sub>c</sub> - n <sub>1</sub> (cycles)	$\frac{n_1}{N_1}$	$\frac{n_2}{N_2}$	Miner's Summation $\frac{n_1}{N_1} + \frac{n_2}{N_2}$
34-T-46	75,000	3,000	45,200	5,169,000	0.333	2.06	2.39
34-T-50	75,000	3,000	45,200	7,964,000	0.333	3.19	3.52
34-T-51	75,000	3,000	45,200	664,000	0.333	0.265	0.60
34-T-52	75,000	2,500	45,200	—	0.278	—	0.28
34-T-53	75,000	3,000	45,200	1,174,000	0.333	0.468	0.80
34-T-54	75,000	4,500	45,200	12,224,000*	0.500	>4.90	>5.40
34-T-55	75,000	4,500	45,200	4,000,000*	0.500	>1.60	>2.10
34-T-56	75,000	4,500	45,200	10,139,000	0.500	>4.05	>4.55
34-T-57	45,200	834,000	75,000	3,946,000	1.54	0.33	1.87
34-T-58	45,200	834,000	75,000	9,117,000	3.65	0.33	3.98
					Average**		3.20

\* Runout, specimen did not fail.

\*\* Discarding high and low values.

uniaxial roving reinforced epoxy specimens were subjected to three-step stress levels as shown in Table 47.

Because of the lack of a sound statistical base for the uniaxial  $N_1$  values, the values of Miner's summation close to unity are acceptable at this time. Although the two values are less than unity, insufficient evidence is available to indicate whether or not Miner's rule is nonconservative.

5. Residual Strength Determinations - Strength after Stress Cycling - for 181/S901 Glass Cloth Reinforced Epoxy

It is important for the designer to have an estimate of the residual strength in his material after cycling at some stress level for a period of time. Table 48 describes the results of several tests at the same stress levels used in the cumulative fatigue damage studies. The specimens were cycled for various portions of the average life at their respective stress levels. Each specimen was then removed from the fatigue machine and tested in tension to destruction on an Instron Universal Testing Machine. Five specimens failed prior to attainment of the average life at their respective stress levels which was not surprising. Residual strength calculations for those specimens were made although the interpretation of these results could be questioned. The theoretical results of such tests for the quarter cycle life/stress (ultimate tensile strength) indicate that at  $\sigma = 43,000$  after cycling for 33 percent of the life (383 cycles), the material should retain 67 percent of its original strength when in fact 75 percent was found experimentally. At 31,000 psi, the theoretical and experimental values were 67 and 57 percent of original strength respectively for cycling to 33 percent of life, and 33 and 70 percent of the original strength respectively for cycling to 67 percent of life. In general then, except in one instance, Miner's summation again provided a conservative estimate of residual strength for this 181/S901 glass cloth reinforced epoxy.

Table 47

THREE STEP STRESS LEVEL TESTS - USING MINER'S SUMMATION FOR S994 UNIAXIAL ROVING  
REINFORCED EPOXY - CYCLED IN FULLY REVERSED AND COMPRESSION AXIAL FATIGUE AT 1800 CPM

Specimen Number	$\sigma_1$ (psi)	$n_1$ (cycles)	$\sigma_2$ (psi)	$n_2$ (cycles)	$\sigma_3$ (psi)	$n_3$ (cycles)	$\Sigma = \frac{n_1}{N_1}$
17-F-31	17,500	$10^7$	22,500	$10^7$	27,500	$3.317 \times 10^6$	0.965
20-C-31	35,000	$10^7$	45,000	$10^7$	55,000	52,000	0.870

Table 48

RESIDUAL STATIC STRENGTH OF 181/S901 GLASS CLOTH REINFORCED EPOXY AFTER CYCLING IN TENSION - ZERO TENSION (R=0.05) AT 60 CPM FOR VARIOUS FRACTIONS OF THE AVERAGE LIFE AT TWO STRESS LEVELS ( $\sigma = 43,000$  PSI, N = 1150 CYCLES; FOR  $\sigma = 31,000$  PSI, N = 29,200 CYCLES) AVERAGE STATIC STRENGTH OF 181/S901 SPECIMENS WAS 90,200 PSI

Specimen Number	Stress Level (psi)	Percent Life Cycled (%)	Number of Cycles (Cycles)	Residual Strength (psi)	Percent Strength Remaining (%)
14-RT-1	43,000	33	383	76,300	85.2
10-RT-2	43,000	33	383	43,000	47.8
6-RT-3	43,000	33	383	78,300	86.9
11-RT-8	43,000	33	383	72,100	80.0
Average					75.0
8-RT-4	43,000	67	766	68,800	76.3
9-RT-5	43,000	67	766	43,000	47.8
2-RT-6	43,000	67	766	82,500	91.5
11-RT-7	43,000	67	766	63,100	70.1
Average					71.2

## SECTION IX

### SUMMARY, CONCLUSIONS AND RECOMMENDATIONS

Fatigue of GRP under cyclical load conditions is complicated by most of the usual parameters which influence the fatigue of metals, plus a great number of other parameters due to the structure-like aspect of composites. This program has examined some of these aspects in great detail and others in less detail.

Cumulative fatigue damage was examined solely through macroscopic means and an attempt was made to correlate these results to phenomenologically applicable theory. This aspect deserves some further comment. Additional work is required on the microscopic scale which should also be correlated with the macroscopic work. It is patently clear that the initiation and propagation of cracks must be studied in great detail. The size or length of the initial crack or flaw,  $a_0$  or  $L_0$ , can be of great importance in cumulative fatigue damage laws such as Valluri's and Shanley's theories. Subsequently the propagation of the crack or  $a = a(n)$  becomes important. "What parameters influence the rate,  $\frac{da}{dn}$ , of crack propagation? And which parameters influence the level of damage at failure?" are typical questions which must be answered for the particular composites studied and for all composites in general.

To find such answers, it would appear that future efforts should be concentrated on relatively few tests with great depth of study devoted to each test rather than the more common approach of studying a statistically valid and larger sample where each specimen receives less attention and consequently yields less information. Furthermore, conclusions based on a series of tests performed for one stress profile (i.e. tension-zero-tension,  $R = 0.1$ ) will yield far more basic and fundamental information about the mechanistic behavior of the system and subsequent detailed investigations could extend the base to other stress-time profiles.

Many of the crack propagation techniques developed for fracture mechanics should be investigated for potential application to GRP fatigue. The establishment of fracture toughness values for GRP together with the observations of  $a = a(n)$  could provide the basis for correlation of GRP fatigue crack growth to many of the newer fracture mechanics cumulative damage laws.



APPENDIXES

APPENDIX A  
LAMINATE BLANKING

APPENDIX B  
REVIEW OF GRP COMPOSITES FATIGUE TECHNOLOGY

APPENDIX C  
REVIEW OF CUMULATIVE FATIGUE DAMAGE THEORIES  
FOR POTENTIAL APPLICATION TO GRP MATERIALS

APPENDIX D  
TORSIONAL FATIGUE TESTING OF CARBON-FILAMENT  
REINFORCED PLASTIC TUBE

APPENDIX E  
STRAIN RATE CALCULATIONS FROM GRIP MOVEMENT  
OF THE INSTRON UNIVERSAL TESTING MACHINE

APPENDIX F  
FATIGUE MACHINES AND EQUIPMENT USED IN GRP STUDIES

APPENDIX A  
LAMINATE BLANKING

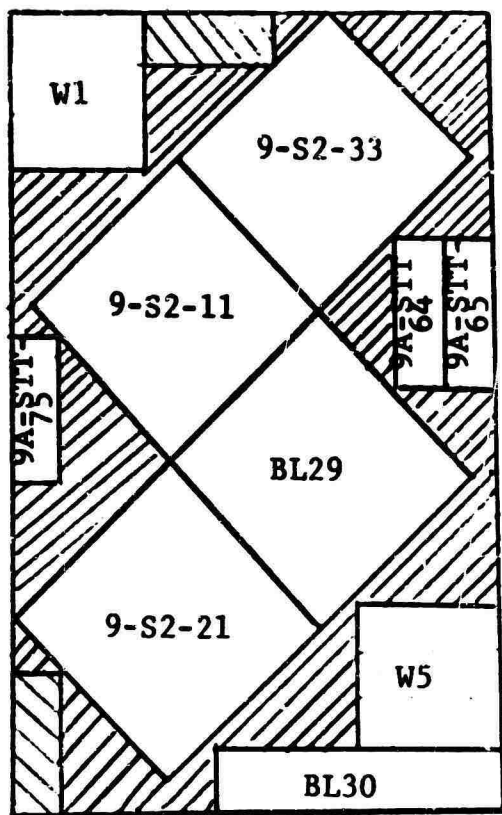
To gain a representative sampling from several laminates and at the same time to maintain control over all test specimens including location within the laminate, the laminates described earlier in Sections I and III were blanked as shown in Figs. 66 through 77. Individual specimens are shown on the sheets as identified in Section III and throughout the text.

Crosshatch sections denote areas in the plates which were not tested because of one or more of the following reasons:

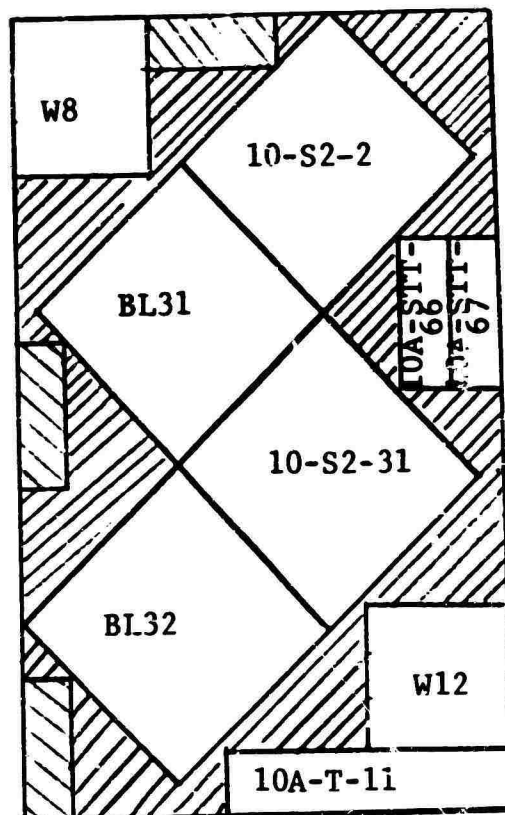
1. Area had a large visible flaw.
2. Area had delaminations at edge.
3. Specimen injured in fabrication.
4. Specimen damaged prior to test.
5. Specimen appears O.K. but ultrasonic inspection indicates problem area.
6. Specimen was used for destructive resin percent determinations.



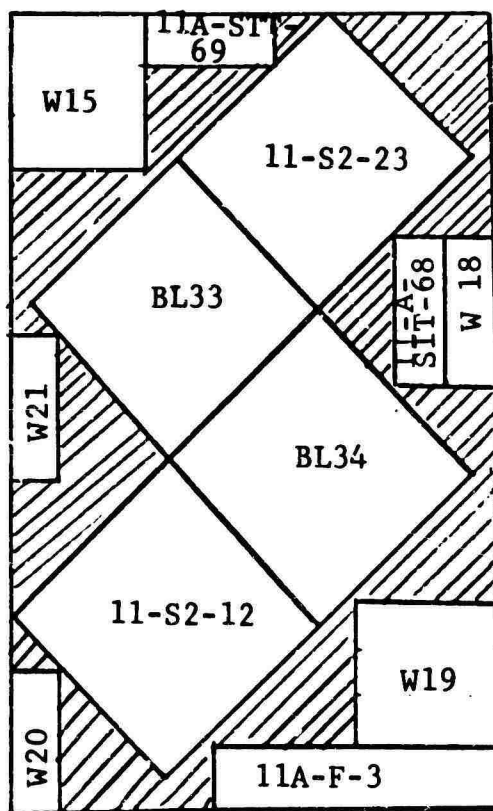




Sheet 9A

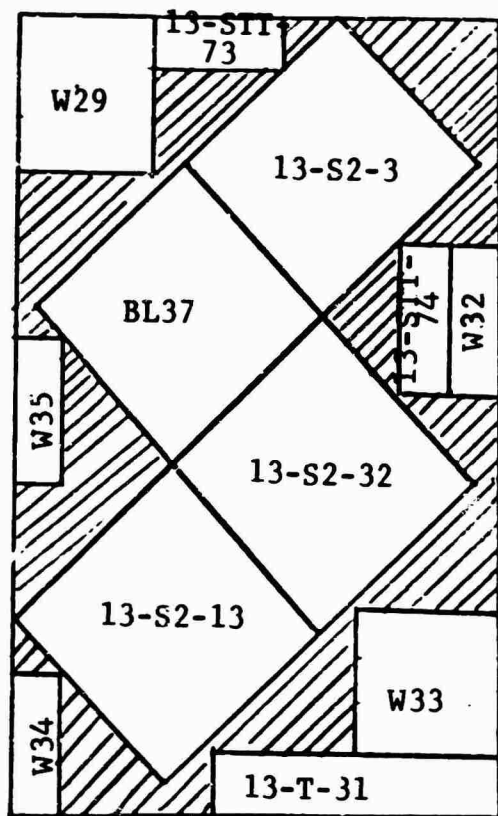


Sheet 10A



Sheet 11A

Fig. 68 LAMINATES 9A-11A, BLANKING SCHEDULE



Sheet No. 13

M32	14-T-68	14-CuF-25
14-T-49	14-F-26	14-CuF-15
M34	14-T-14	14-STT-3
14-T-49	14-C-28	14-CuT-5
14-STT-12	14-F-37	M 31
M 35	14-STT-30	
14-RT-1	14-C-14	
	14-C-12	

Sheet No. 14

15-STT-31	15-STC-6
15-CuT-3	15-STT-8
15-T-60	15-RT-11
15-F-25	15-T-62
15-F-17	15-CuF-23
15-STT-32	15-T-67
15-CuT-6	15-CuT-4
15-T-61	15-F-38
15-STT-4	15-STT-16
	15-F-39

Sheet No. 15

16-STT-9	16-CrT-17
16-CrT-16	16-CuT-10
16-STC-22	16-CrT-1
16-F-24	16-CuC-11
16-F-36	16-T-66
16-C-13	16-STT-1
16-CuT-1	16-STC-21
16-CuT-11	
16-STC-16	16-F-41
	16-STC-23
	16-STC-24

Sheet No. 16

Fig. 69 LAMINATES 13-16, BLANKING SCHEDULE



A12	23-F-40	N22	
A13	23-C-22		
N23			
23-STC-8	N25	N26	
23-C-34	23-S-31		N27
23-C-3			23-F-34
23-F-37			N29

Sheet No. 23

24-F-23	24-F-35	24-S-12	
A15	24-C-13		
A14	24-F-39		
24-STC-9	N32	N33	
24-F-36	N39		N34
24-C-35			N35
N3			N36

Sheet No. 24

25-F-25	25-C-33	25-S-3	
A17	25-C-40		
N40			
25-STC-10	N42	N43	
	N47		25-F-43
			N 45
			N 46

Sheet No. 25

A22		N49	
A21			
A20	26-C-36		
26-STC-17	26-F-42	N53	
26-C-32	26-S-23		A19
			N54
			N55

Sheet No. 26

Fig. 71 LAMINATES 23-26, BLANKING SCHEDULE



27-B2-31	27-B1-34	
27-B1-21	27-B2-23	
27-B2-35	27-B2-25	
27-B1-23	27-B2-37	
27-B2-34	27-B2-32	
27-B1-32	27-B1-33	
27-B2-33	27-B1-22	
27-B2-21	27-B2-26	
27-B2-24	27-B2-36	
27-B1-31	27-E1-39	
27-B1-35		
27-B1-36		
27-B1-37		
27-B1-38		

Sheet No. 27

28-E1-9	28-CuB1-40	
28-B2-11	28-CrB-12	
28-CrB-11	28-E1-25	
28-CuB1-33	28-CuB2-6	
28-B1-11	28-CuB1-34	
28-CuB2-4	28-E2-5	
28-CuB1-39	28-E2-8	
28-E2-1	28-E2-7	
28-B2-12	28-B1-12	
28-CuB2-5	28-CuB1-38	
28-CuB1-31		
28-B2-13		
28-E1-1		
28-B1-13		

Sheet No. 28

29-B1-12	29-B2-32	
29-B1-13	29-B2-34	
29-B1-32	29-B2-33	
29-B2-37	29-B1-31	
29-CrB-13	29-B2-31	
29-B2-36	29-CrB-12	
29-B1-34	29-CrB-11	
29-CrB-14	29-CrB-15	
29-B1-35	29-B2-35	

Sheet No. 29

30-E2-7	30-E2-2	
30-E1-7		
30-E2-5	30-E1-9	
30-E1-1	30-E2-4	
30-E2-6	30-E1-3	
30-E1-2	30-E1-4	
30-E2-3	30-E2-8	
30-E1-6	30-E2-1	
30-E1-8	30-STB-9	
30-E1-5	30-STB-8	

Sheet No. 30

Fig. 72 LAMINATES 27-30, BLANKING SCHEDULE

31-CuB2-3	31-E1-3	31-CuB2-1
31-E1-4	31-CrB-13	31-CrB-15
31-CuB1-36	31-CuB2-8	31-CuB1-37
31-E1-7	31-E1-6	31-E1-2
31-CuB2-2	31-CuB1-32	
31-E2-2	31-E1-8	
31-CrB-14	31-CuB2-7	
31-E2-3	31-E2-6	
31-CuB2-10	31-CuB1-35	
31-E2-4	31-CuB2-9	

Sheet No. 31

32-STB-11	32-STB-2	32-STB-5
32-STB-6	32-E2-10	32-STB-9
32-STB-17	32-STB-8	32-STB-13
32-E1-9	32-STB-14	32-STB-1
32-STB-3	32-E1-10	
32-STB-19	32-STB-4	
32-STB-15	32-E2-9	
32-STB-7	32-STB-16	
32-STB-39	32-STB-10	
32-STB-12	32-STB-18	

Sheet No. 32

33-STB-15	33-STB-10
33-STB-4	33-STB-7
33-STB-13	33-STB-3
33-STB-12	33-B1-11
33-STB-18	33-STB-6
33-B2-13	33-STB-16
33-STB-5	33-B2-11
33-STB-1	33-STB-2
33-STB-17	33-B2-12
33-STB-14	33-STB-11

Sheet No. 33

Fig. 73 LAMINATES 31-33, BLANKING SCHEDULE

35-B1-1	35-B1-11
35-B1-2	35-B1-12
35-B1-3	35-B1-13
35-B1-4	35-B1-14
35-B1-5	35-B1-15
35-B1-6	35-B1-16
35-B1-7	35-B1-17
35-B1-8	35-B1-18
35-B1-9	35-B1-19
35-B1-10	35-B1-20

Sheet No. 35

36-B2-1	36-B2-11
36-B2-2	36-B2-12
36-B2-3	36-B2-13
36-B2-4	36-B2-14
36-B2-5	36-B2-15
36-B2-6	36-B2-16
36-B2-7	36-B2-17
36-B2-8	36-B2-18
36-B2-9	36-B2-19
36-B2-10	36-B2-20

Sheet No. 36

37-B1-25	37-B1-32
37-B1-26	37-STB-19
37-CrB-16	37-B1-33
37-B1-27	37-B1-15
37-B1-28	37-B1-14
37-B1-29	37-B1-34
37-B2-14	37-B2-15
37-B1-30	37-B1-35
37-STB-20	37-B1-36
37-B1-31	37-B1-37

Sheet No. 37

Fig. 74 LAMINATES 35-37, BLANKING SCHEDULE

34-T-52	34-T-31
34-T-53	34-T-32
34-T-54	34-T-33
34-T-55	34-T-34
34-T-56	34-T-35
34-T-57	34-T-36
34-T-58	34-T-37
34-T-58A	34-T-38
34-T-59	34-T-39
34-T-60	34-T-40
34-T-61	34-T-41
34-T-62	34-T-42
34-T-63	34-T-43
34-T-64	34-T-44
34-T-65	34-T-45
34-T-66	34-T-46
34-T-67	34-T-47
34-T-68	34-T-48
34-T-69	34-T-49
34-T-70	34-T-50
34-T-71	34-T-51

Sheet No. 34

38-T-1	38-T-2
38-T-22	38-T-3
38-T-23	38-T-4
38-T-24	38-T-5
38-T-25	
38-T-26	38-T-6
38-T-27	
38-T-28	38-T-7
38-T-29	
38-T-30	38-T-8
38-T-31	38-T-9
38-T-82	38-T-10
38-T-83	
38-T-84	38-T-11
38-T-85	38-T-12
38-T-86	38-T-13
38-T-87	38-T-14
38-T-88	38-T-15
38-T-89	38-T-16
38-T-90	38-T-17
38-T-91	

Sheet No. 38

Fig. 75 LAMINATES 34 AND 38, BLANKING SCHEDULE

39-T-50	39-T-71
39-T-51	39-T-72
39-T-52	39-T-73
39-T-53	39-T-74
39-T-54	39-T-75
39-T-55	39-T-76
39-T-56	39-T-77
39-T-57	39-T-78
39-T-58	39-T-79
39-T-59	39-T-80
39-T-60	39-T-81
39-T-61	39-T-82
39-T-62	39-T-83
39-T-63	39-T-84
39-T-64	39-T-85
39-T-65	39-T-86
39-T-66	39-T-87
39-T-67	39-T-88
39-T-68	39-T-89
39-T-69	39-T-90
39-T-70	39-T-91

Sheet No. 39

40-STT-23	40-STT-1
40-STT-24	40-STT-2
40-STT-25	40-STT-3
40-STT-26	40-STT-4
40-STT-27	40-STT-5
40-STT-28	40-STT-6
40-STT-29	40-STT-7
40-STT-30	40-STT-8
40-STT-31	40-STT-9
40-STT-32	40-STT-10
40-STT-33	40-STT-11
40-STT-34	40-STT-12
40-STT-35	40-STT-13
40-STT-36	40-STT-14
40-STT-37	40-STT-15
40-STT-38	40-STT-16
40-STT-39	40-STT-17
40-STT-40	40-STT-18
40-STT-41	40-STT-19
40-STT-42	40-STT-20
40-STT-43	40-STT-21
40-STT-44	40-STT-22

Sheet No. 40

Fig. 76 LAMINATES 39 AND 40 BLANKING SCHEDULE

41-T-1	41-T-10	41-T-19	41-T-31
41-T-2	41-T-11	41-T-20	41-T-32
41-T-3	41-T-12	41-T-21	41-T-33
41-T-4	41-T-13	41-T-22	41-T-28
41-T-5	41-T-14	41-T-23	41-T-29
41-T-6	41-T-15	41-T-24	41-T-30
41-T-7	41-T-16	41-T-25	
41-T-8	41-T-17	41-T-26	
41-T-9	41-T-18	41-T-27	

Sheet No. 41

43-T-1	43-T-12
43-T-2	43-T-13
43-T-3	43-T-14
43-T-4	43-T-15
43-T-5	43-T-16
43-T-6	43-T-17
43-T-7	43-T-18
43-T-8	43-T-19
43-T-9	43-T-20
43-T-10	43-T-21
43-T-11	43-T-22

Sheet No. 43

42-T-1	42-T-10	42-T-19	42-T-31
42-T-2	42-T-11	42-T-20	42-T-32
42-T-3	42-T-12	42-T-21	41-T-33
42-T-4	42-T-13	42-T-22	42-T-28
42-T-5	42-T-14	42-T-23	42-T-29
42-T-6	42-T-15	42-T-24	42-T-30
42-T-7	42-T-16	42-T-25	
42-T-8	42-T-17	42-T-26	
42-T-9	42-T-18	42-T-27	

Sheet No. 42

44-T-1	44-T-12
44-T-2	44-T-13
44-T-3	44-T-14
44-T-4	44-T-15
44-T-5	44-T-16
44-T-6	44-T-17
44-T-7	44-T-18
44-T-8	44-T-19
44-T-9	44-T-20
44-T-10	44-T-21
44-T-11	44-T-22

Sheet No. 44

Fig. 77 LAMINATES 41 THROUGH 44, BLANKING SCHEDULE

## APPENDIX B

### REVIEW OF GRP COMPOSITES FATIGUE TECHNOLOGY

The history of fatigue of GRP is rather new. Not all of the problems associated with a new field of technology are solved and the fatigue testing of composite materials can hardly be called routine. Much of the data is not generally available since, in the large, it consists of closed company files. However, references 2 through 63 are part of the open literature and can be drawn upon at will by the GRP designers and investigators.

Earlier investigators relied largely upon conventional specimens such as the R. R. Moore Rotating Beam Fatigue specimens and equipment.<sup>2</sup> The choice of a constant radius flat fabric reinforced specimen for fully reversed ( $R \cong -1$ ) and tension-zero-tension ( $R = 0$ ) fatigue profiles<sup>4</sup> opened the door for general fatigue testing. In general, the equipment used was high cyclic rate (900 cpm). These early tests were performed on matrix systems which have since been reduced in importance as structural materials; i.e., the polyesters. A very important testing parameter for flat laminates was indicated almost immediately in these early tests; i.e., the importance of introducing load to the specimen through continuous contact of friction or bonded type, rather than through bolts or threads.<sup>4,5,6,7,8</sup>

Studies of fatigue resistance of GRP under various environmental and notch conditions were carried out by the early investigators. These studies, as well as those for dry, room temperature conditions indicated that composite materials did not appear to have an endurance limit in the same sense as most metals, and indeed, failures continued to occur after  $10^7$  cycles. (Normally accepted as endurance for most steels.)

Many investigators<sup>10,13</sup> began to use molded specimens similar to very early investigators<sup>2</sup> for fatigue in high speed rotating beam fatigue machines. Although more testing could be performed in the same time through the use of these machines, the results began to be suspect when it was learned of the "heating" effect on GRP.

Later, investigators<sup>10,13</sup> began investigating other matrix materials as their development came to fruition; epoxies for low temperature application and phenolics for higher temperature applications. Up to this point, however, the primary emphasis had been on glass cloth reinforcements such as 181 and 143 weaves. By 1960, investigators began studying filament and roving reinforced plastics for compressive applications.<sup>30,31,37</sup> Since the materials were primarily unidirectional and used in winding applications, an entire new round of specimen problems began. Biaxial compressive fatigue employed lower cyclic rate hydro-mechanical fatigue equipment and specimens were primarily whole cylindrical shells wound from the unwoven filaments or rovings. Fatigue S-N curves began to take on the flatter high cycle appearance representative of metal endurance.

Flat specimens for fatigue were also fabricated from these primarily unidirectional composite materials. Here the use of thicker specimens began to indicate some problem areas for high strength composite testing under compressive loads. Delaminations under the compressive cyclic stress became common.<sup>35</sup> Corollary studies on crack initiation<sup>35,38</sup> indicated breakup of the matrix parallel to the fibers and consequently a breakdown of the composite material structure. Invasion effects from environments such as water or oil were distinguished in the resulting cracks, flaws, etc.<sup>40</sup>

The concurrently developing fields of fracture mechanics and crack propagation studies in metals as well as nondestructive techniques began to be employed in the investigation of these flaw and cracks.<sup>41,53-59</sup> Of particular interest was the ultrasonic inspection of GRP for voids and flaws and its employment in Q.C. operations. A whole new perspective on notch influences was potentially available.<sup>55,56</sup>

Damping studies conducted earlier<sup>10</sup> on fabric reinforced plastics were supplemented by high frequency vibration studies and damping in unwoven reinforcements.<sup>57</sup> New specimen configurations for bending plus tension fatigue of segments of wound



composites have recently appeared<sup>58</sup> and interlaminar shear fatigue fixtures as well.<sup>60</sup> Entire GRP faced sandwich beams or panels are also being tested.<sup>61</sup>

More recently the effect of cumulative damage under spectrum type loading appears to be under way.<sup>63</sup> With the development of the new material fiber reinforcements, entirely new problems in fatigue specimens were encountered, primarily because of the relatively high moduli of the reinforcements and consequently of the composites. Tensile fatigue specimens took on a new appearance such as the straight sided tab-ended specimen.<sup>65</sup>

Table 49 summarized properties obtained by several investigators for several types of composites. The numbers refer to references at the end of the report.

Tal

SUMMARY OF SELECTED FATIGUE

Material System	Fully Reversed Axial Fatigue	Tension Axial Fatigue	Compressive Axial Fatigue	Fully Reversed Bending Fatigue	Bending Fatigue (R = 0)	Fully Reversed Shear	Shear Fatigue (R = 0)
181E-Polyester	4, 11, 55	4, 6, 11		2, 12, 55			
143E-Polyester	4						
181E-Epoxy	8, 11, 19, 42, 55			55, 57, 61			
143E & S-Epoxy			35, 38, 43				
131E Phenolic	11, 22, 36, 55	36	36				
Asbestos Mat-Phenolic	19						
181E-Silicone	11, 55						
Glass Roving-Epoxy			35, 38, 40, 41, 43	13		13	
Glass Fiber-Epoxy	19, 22, 37	37	30	55			
S-Glass Fibers-Epoxies	60		53				60

A

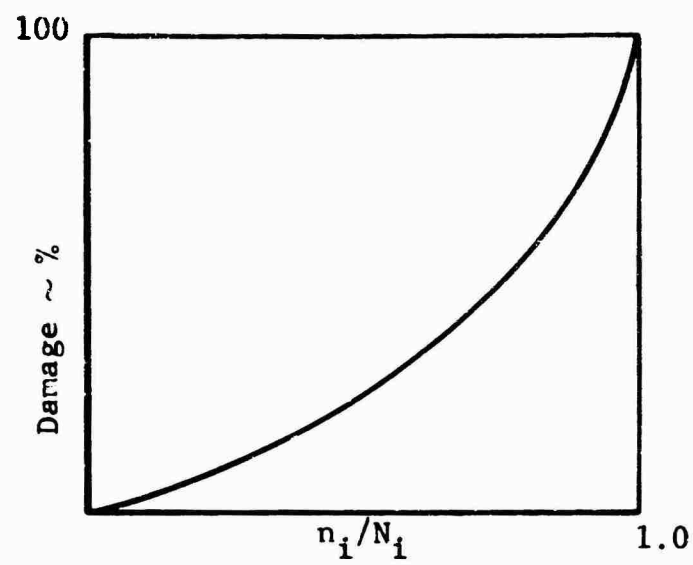
**Table 49**  
**FATIGUE AND CREEP PROPERTIES REFERENCES**

Stress Fatigue = 0)	Fatigue Test in Non-Principal Reinforcement Direction	Fatigue Various Humidity Condition	Fatigue Various Temperature Condition	Creep Tests	Strain Rate Tests	Stress Rupture Tests	Fatigue Under Notch Conditions	Bolt Hole Fatigue	Cumulative Damage
4, 11	4, 11	4, 11	2, 4, 11			2	4, 11		
8, 42	8, 11, 19	8, 11, 19	11, 55				4		
	35, 43	35, 43	11, 22, 36, 55	35		35	8, 11, 19, 55	8	42
19	19	19	11				11		
	35, 43	35, 43		35		35	19		
19, 23, 37, 55	19, 55	19, 55					11		
60	53	53					19, 55		63
									53, 54, 56, 59, 62

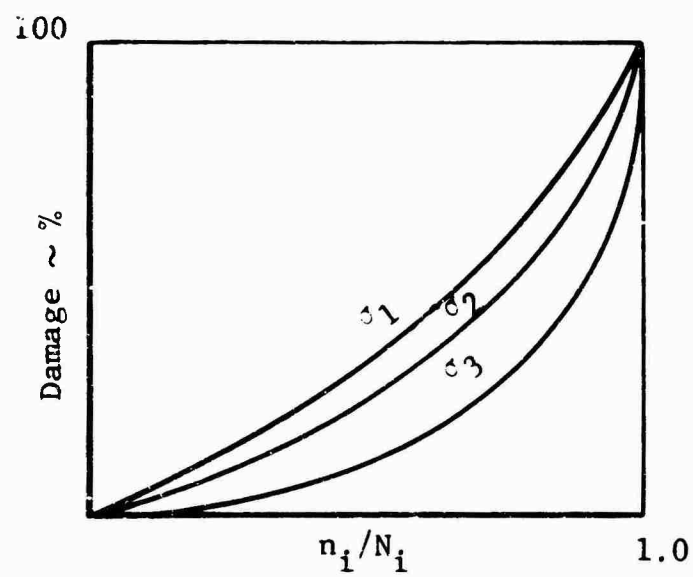
APPENDIX C  
REVIEW OF CUMULATIVE FATIGUE DAMAGE THEORIES  
FOR POTENTIAL APPLICATION TO GRP MATERIALS

In the analysis or design of a structural component subjected to cyclic loading, the engineer is faced with the problem of cumulative damage. The problem is one of predicting the useful life of a structure subjected to varying stress spectrum. Since this stress spectrum can occur in an infinite variety of ways, a single fatigue test designed to simulate actual service conditions is impractical. For this reason, cumulative damage analyses have been devised whereby the material response to spectrum loading can be predicted. Many theories have been presented starting with the most simple and popular method (Miner's Rule<sup>66</sup>) to a complicated procedure suitable only for analysis (Corten-Dolan<sup>67</sup> and Freudenthal-Heller<sup>68</sup>). This appendix enters into a brief discussion of several more useful cumulative damage theories examining each of those applicable to glass reinforced plastics but all possess such potential and consequently none should be eliminated until a great deal of test data has been assembled.

Every cumulative damage theory starts with a general relationship between damage accumulated versus cycles to failure for a constant amplitude test. There are two distinct features of these damage theories which can be used to classify them, namely stress-dependent or independent theories, and stress-interaction or interaction free theories. Stress-independence is the condition where the damage at a certain cyclic ratio ( $n_i/N_i$ ) is the same for all stress amplitudes. Stress dependence is when the damage depends on the stress amplitude applied. Stress-interaction states that the course of the damage is altered by a change in stress level. Stress-interaction-free means the course of damage is unaffected by a change in stress level. Figure 78 illustrates stress-independent and stress-dependent theories. Figure 79 illustrates stress-interaction-free and stress-interaction theories.

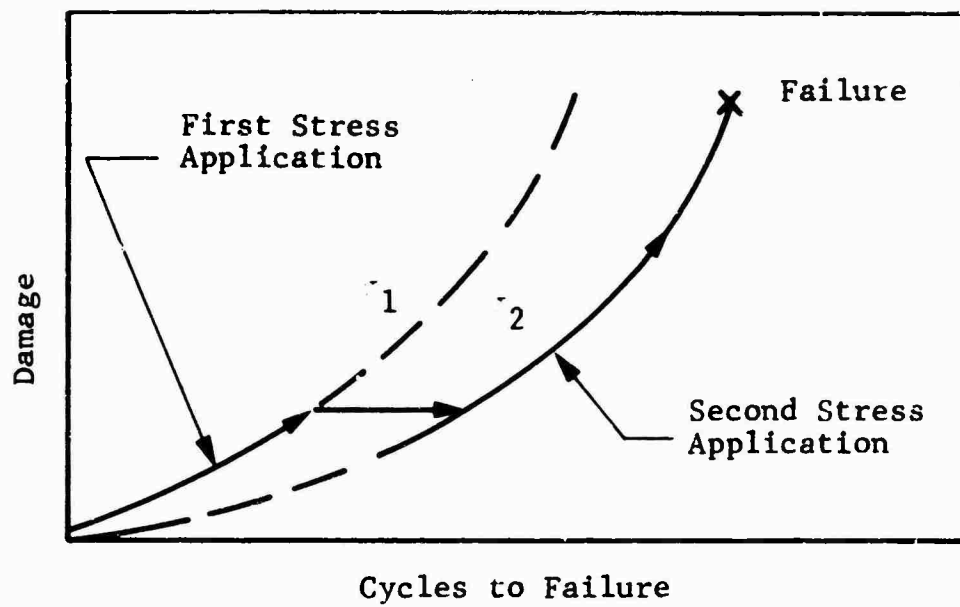


a) Stress-Independent

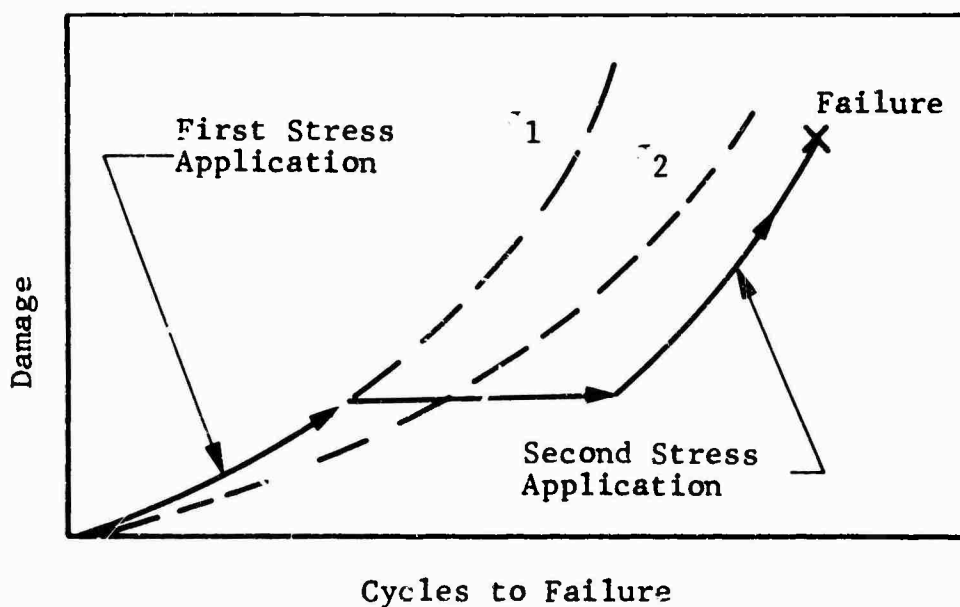


b) Stress-Dependent

Fig. 78 STRESS-DEPENDENT AND STRESS-INDEPENDENT CUMULATIVE DAMAGE THEORIES



a) Stress-Interaction-Free



b) Stress-Interaction

Fig. 79 STRESS-INTERACTION-FREE AND STRESS-INTERACTION CUMULATIVE DAMAGE THEORIES

Every cumulative damage theory begins with a general relationship between damage and cycles-to-failure or between damage and the cycle ratio ( $n_i/N_i$ ) as illustrated in Fig. 78 which is of the form

$$D = kr\phi^\gamma \quad (1)$$

where

- $D$  = damage accumulated
- $k$  = constant dependent on damage at a particular stress level
- $\phi = n_i/N_i$  = cycle ratio
- $\gamma$  = exponent which depends upon the stress level
- $r$  = a damage rate coefficient

For a two stress level test, the load application and damage accumulated will occur as shown in Fig. 80. To derive an expression for cumulative damage, let us now make the assumption that the damage produced by application of the highest stress level,  $\sigma_1$ , governs the accumulation of damage which occurs at the lower stress level,  $\sigma_2$ . Thus, the production of damage sites under the  $\sigma_2$  portion of the two-stress level process is in proportion to the constant  $k_1$  rather than  $k_2$ . This in effect assumes that new damage sites will not be formed for stress levels below  $\sigma_1$ . If these assumptions are made, the resulting cumulative fatigue damage theory involves "stress interaction". Should the  $D_3$ , damage curve, fall directly on the  $D_2$ , damage curve, the theory is said to be interaction-free.

Let us examine in closer detail what occurs in the very simplest of all multiple stress level tests. A total of  $N_G$  cycles is applied to a component in blocks of  $n$  cycles. Each block contains  $\alpha n$  cycles at  $\sigma_1$  stress level and  $(1 - \alpha)n$  cycles at  $\sigma_2$  stress level.

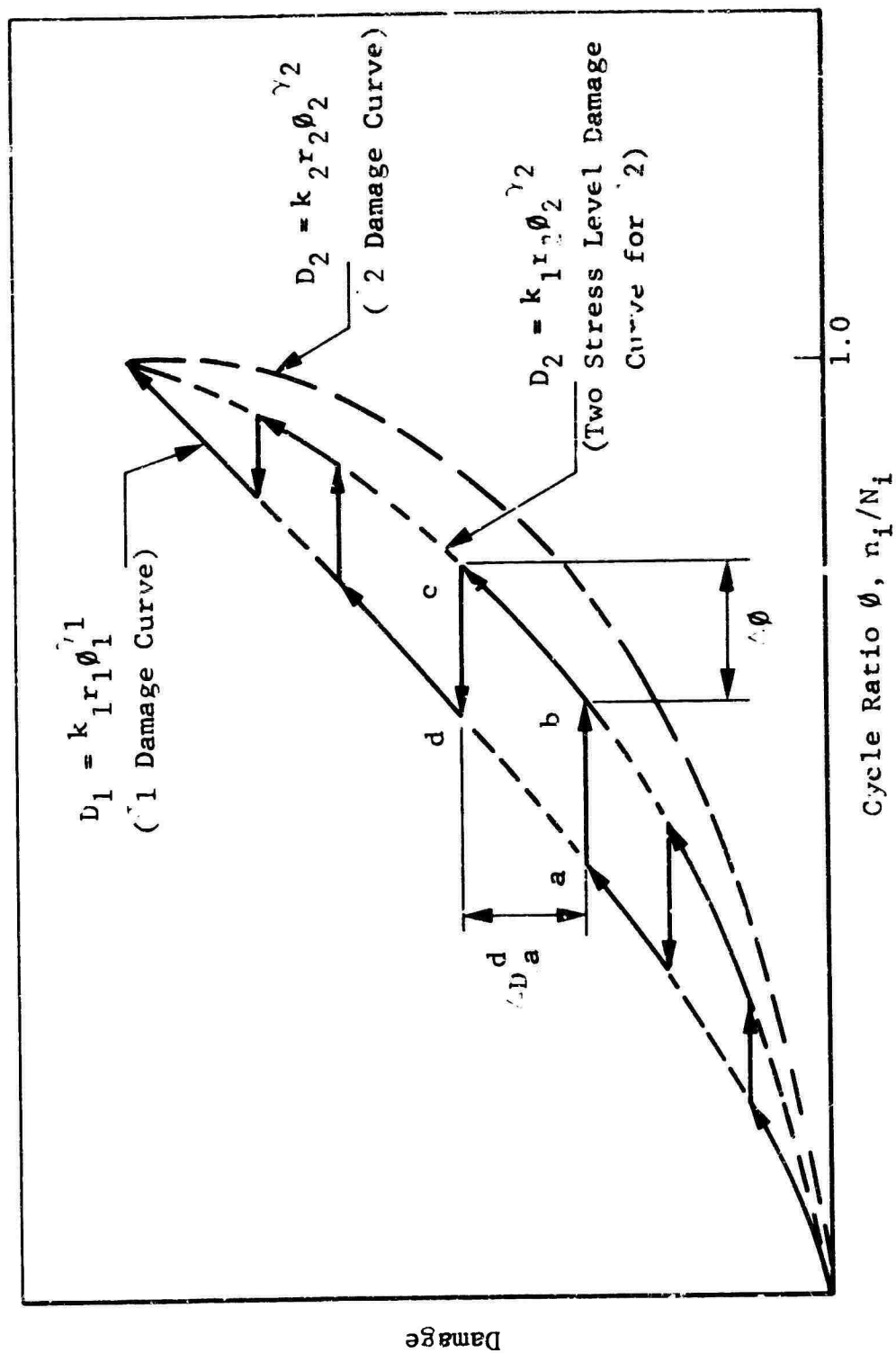


Fig. 80 TWO STRESS LEVEL CUMULATIVE DAMAGE CURVE



The damage expressions for total damage along the  $D_1$  and  $D_3$  curves respectively are

$$D_1 = k_1 r_1 \phi_1^{\gamma_1} \quad (\text{at } \sigma_1)$$

$$D_3 = k_1 r_1 \phi_2^{\gamma_2} \quad (\text{at } \sigma_2)$$

Differentiating these general damage expressions with respect to cycle ratio,  $n_i/N_i$ , we obtain

$$\frac{dD_i}{d\phi_i} = \gamma_i k_i r_i \phi_i^{\gamma_i-1}$$

Thus, an increment of damage,  $\Delta D$ , will be incurred as follows

$$\Delta D = \gamma_i k_i r_i \phi_i^{\gamma_i-1} \Delta \phi_i$$

This is further specified for the individual damage curves of interest as

$$\Delta D_1 = \gamma_1 k_1 r_1 \phi_1^{\gamma_1-1} \Delta \phi_1 \quad (2)$$

and

$$\Delta D_2 = \gamma_2 k_2 r_2 \phi_2^{\gamma_2-1} \Delta \phi_2 \quad (3)$$

Since total damage at c is equal to total damage at d

$$k_1 r_1 \phi_d^{\gamma_1} = k_1 r_2 \phi_c^{\gamma_2}$$

or

$$\phi_d^{\gamma_1} = R \phi_c^{\gamma_2} \quad (4)$$

where

$$R = r_2/r_1$$

Equating expressions (2) and (3) and rewriting them

$$\Delta\phi_1 = SR \frac{\phi_c^{\gamma_2-1}}{\phi_d^{\gamma_1-1}} \Delta\phi_2 \quad (5)$$

where

$$S = \gamma_2/\gamma_1$$

Rewriting Eq (4) we have

$$\phi_d = R^{1/\gamma_1} \phi_c^S \quad (6)$$

Replacing  $\phi_d$  in Eq (5) with Eq (6) we obtain

$$\Delta\phi_1 = SR \frac{\phi_c^{\gamma_2-1}}{\left[ R^{1/\gamma_1} \phi_c^S \right]^{\gamma_1-1}} \Delta\phi_2$$

Reducing this expression, we obtain an "equivalent damage" on the  $D_3$  curve in terms of damage on the  $D_1$  curve.

$$(\Delta\phi_1)_e = SR^{1/\gamma_1} \phi_c^{S-1} \Delta\phi_2$$

Recall now Fig. 80 where for small increments of the cycle ratio,  $\phi = n_i/N_i$ , the curves are approximately linear.

Therefore,  $\Delta\phi_1$  and  $\Delta\phi_2$  are given by

$$\Delta\phi_1 = \Delta(n_1/N_1) = \Delta \left( \frac{\alpha N_G}{N_1} \right)$$

$$\Delta\phi_2 = \Delta(n_2/N_2) = \Delta \left( \frac{(1-\alpha)N_G}{N_2} \right)$$

The total damage incurred over  $N_G$  cycles is the summation of damage increments on the  $D_1$  curve, Eq (2), plus the "equivalent damage" from the  $D_3$  curve in terms of  $D_1$  curve damage increments.

$$D = \sum \gamma_1 k_1 r_1 \phi_1^{\gamma_1 - 1} \Delta \phi_1 + \sum \gamma_2 k_1 r_2 \phi_2^{\gamma_2 - 1} \Delta \phi_2$$

$$D = \sum \gamma_1 k_1 r_1 \phi_1^{\gamma_1 - 1} \Delta \phi_1 + \sum \gamma_1 k_1 r_1 (\phi_i)_e^{\gamma_1 - 1} \Delta \phi_1$$

Setting  $D = 1$  (for 100 percent damage) and integrating we obtain, after suitable assumptions are made

$$1 = k_1 r_1 \alpha \left( \frac{N_G}{N_1} \right)^{\gamma_1} + k_1 r_2 (1 - \alpha) \left( \frac{N_G}{N_2} \right)^{\gamma_2} \quad (7)$$

where

$k_1$  = constant dependent on damage at highest stress level ( $\sigma_1$ )

$r_1, r_2$  = damage rate coefficients at  $\sigma_1, \sigma_2$  respectively

$\gamma_1, \gamma_2$  = damage exponents at  $\sigma_1, \sigma_2$  respectively

$N_1, N_2$  = cyclic lives at  $\sigma_1, \sigma_2$  respectively

$\alpha$  = decimal percent of total cycles,  $\alpha = N_1/N_G$

$N_G$  = total number of cycles

Equation (7) is a quite general cumulative damage relationship for a stress-dependent, stress-interaction theory governing the behavior when two stress levels are applied. The following is a listing of cumulative damage theories which will be discussed in the light of this relationship, where possible.

#### 1. Miner's Theory

2. Grover's Theory
3. Valluri's Theory
4. Corten-Dolan Theory
5. Freudenthal-Heller Theory
6. Shanley's Theory and 2X Method

It will be demonstrated that through the use of the constants  $k$ ,  $r$ , and  $\gamma$  in Eq (1) each of the six theories mentioned can be applied to two-step stress level tests.

#### 1. Miner's Theory

The simplest and most popular theory in practice today is Miner's. It was first published in 1945 and is stress-independent, and stress-interaction-free. This results in a linear summation of damage accumulation. Essentially the constants in Eq (7) are set equal to one. Thus,

$$\begin{aligned}\gamma_1 &= \gamma_2 = 1 \\ k_1 &= k_2 = 1 \\ r_1 &= r_2 = 1\end{aligned}$$

As a result we obtain

$$\frac{N_G}{N_1} = \frac{1}{\alpha + (1-\alpha)\frac{N_1}{N_2}} \quad (8)$$

Since  $n_1 = \alpha N_G$  and  $n_2 = (1-\alpha)N_G$ , by substituting into Eq (8) we obtain the more familiar form of Miner's Theory.

$$\frac{n_1}{N_1} + \frac{n_2}{N_2} = 1 \quad (9)$$

This particular sum is frequently called Miner's summation. In general for more than two stress levels

$$\sum \frac{n_i}{N_i} = 1$$

## 2. Grover's Theory

Grover proposed a modification to Miner's Theory which will change Eq (9) from a stress-independent to a stress-dependent criterion. Grover assumed 1) that the damage produced in the first stage of cycling is different from that produced during succeeding cycles; 2) that the amount of initial damage is constant whether or not other stress amplitudes are applied; and 3) that Miner's Theory applied to each stage of damage as illustrated in Fig. 81. As can be readily seen from Fig. 81, the initial damage  $D_0$  is not the same for all cyclic ratios, making the theory stress dependent. The general equation for Grover's Theory is of the form

$$\sum \frac{n_i}{D_i N_i} = 1$$

$$\sum \frac{m_i}{(1-D_i) N_i} = 1$$

where

$n_i$  = cycles in first damage stage

$m_i$  = cycles in second damage stage

$N_i$  = cyclic life for the  $i$  stress amplitude

$D_i$  = initial damage region for the  $i$  stress amplitude

If the initial damage is the same for all stress amplitudes at all cycle ratios, Grover's Theory will reduce to Miner's. This theory has some physical basis but at the present time it is not possible to evaluate  $D_0$ . In Grover's original paper, he defined  $D_i N_i$  as the number of cycles necessary to produce a "significant" crack.

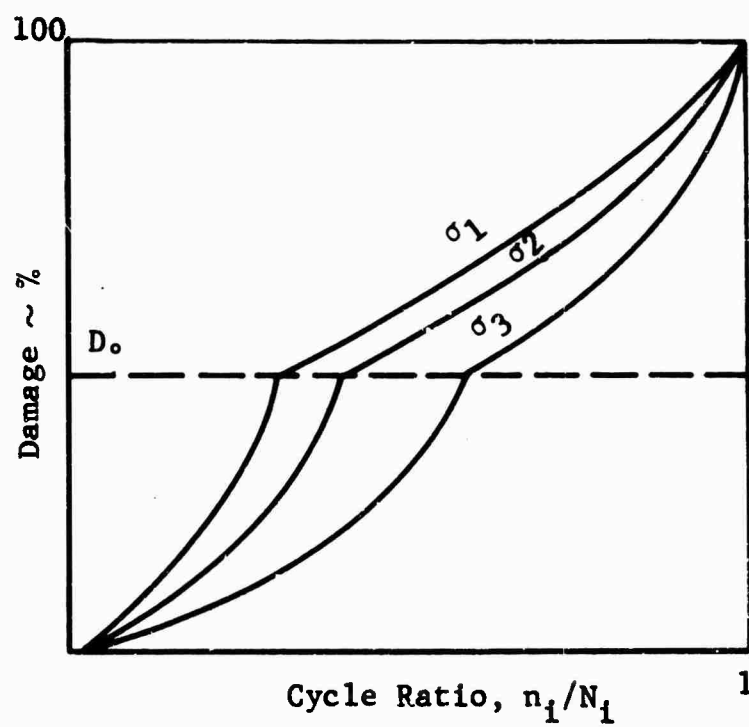


Fig. 81 GROVER'S CUMULATIVE DAMAGE THEORY

### 3. Valluri's Theory

The first departure from the use of Eq (7) will be for Valluri's Theory. This cumulative damage law is basically a crack propagation relationship which derives its basis from dislocation theory and plastic deformation at the crack tip. Obviously then, the law was derived for application to metals, but the mathematical relationship could be suitable for any material.

Starting with the ultimate strength of the material, Valluri uses that value to construct a fictitious initial crack length,  $L_0$ , from Griffith's crack theory. For each stress level (constant stress amplitude test), Valluri's cumulative damage law takes the form

$$\ln (L/L_0) = knf (\sigma_i) \quad (10)$$

where

$L$  = crack length at any time

$L_0$  = fictitious crack length derived from Griffith's crack theory

$k$  = constant

$n$  = number of cycles at same time

$\sigma_i$  = stress level

$f(\sigma_i)$  = some function of stress level, depends on geometry of loading

To obtain a cumulative damage law, Valluri assumed that the damage at each stress level was unaffected by prior stress history (similar to Miner's assumption). This then is another stress-interaction-free theory.

$L_{cr}$  is taken as the critical crack length for each stress level. Associated with this,  $L_{cr}$  is the number of cycles to attain this length,  $N_i$ , which is our familiar cyclic life at a particular stress level. Defining damage,  $D_i$ , as

$$D_i = \frac{L_i - L_0}{L_{cr} - L_0} \quad (11)$$

and by employing Griffith's crack theory to obtain the function  $f(\sigma_i)$  in Eq (10), we obtain the following expression which relates damage at any time to the number of cycles applied. Thus the expression

$$\frac{L_i}{L_0} = \left( \frac{L_{cr}}{L_0} \right)^{\phi_i} \quad (12)$$

where  $\phi_i$  is the cycle ratio together with Eq (11) provides a relationship between damage,  $D$ , and the cycle ratio,  $\phi$ .

Equations (11) and (12) form the basis of a stress-independent, stress-interaction-free law and are basically equivalent to Miner's. Thus

$$\sum \phi_i = 1$$

becomes the failure criterion. Figure 82 is a plot of Eq (11) and (12).

#### 4. Summary of Miner's, Grover's and Valluri's Cumulative Damage Laws

The similarity of Miner's, Grover's and Valluri's theories can be seen when it is realized that they are all stress-interaction-free. Miner's and Valluri's theories are stress-independent and Grover's reduces to this when the value of  $D_0$  is constant for all at stress amplitudes. Valluri's theory has the added



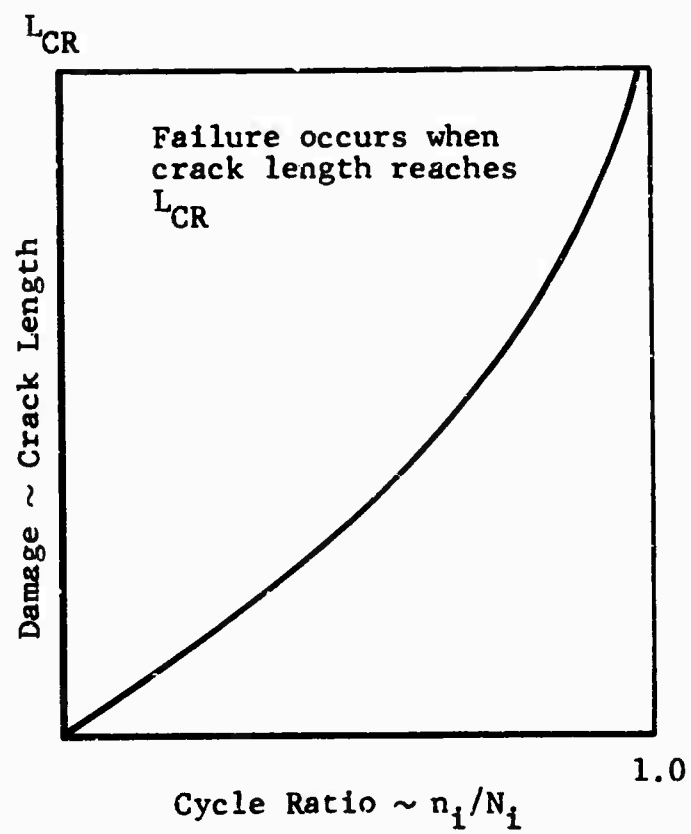


Fig. 82 VALLURI'S CUMULATIVE DAMAGE THEORY

advantage that the residual static strength, after initial fatigue cycles, can be determined. This is accomplished by calculating the crack length and using fracture mechanics to calculate the static strength. (Nominal stress at which crack will propagate.) At the present time, Grover's or Valluri's theories have not been applied to GRP; but with an advance in our understanding of the micromechanics behavior of GRP and crack propagation in GRP together with further refinements in nondestructive test techniques, these two theories could be applied. Therefore, the only cumulative damage theory which appears to be applicable to GRP on strictly a mechanistic basis is Miner's.

##### 5. Corten-Dolan Theory, Fictitious S-N Curve

Beginning with our now familiar general damage equation, Eq (1),

$$D_i = k_i r_i \phi_i^{\gamma_i}$$

we arrived at the cumulative damage law

$$1 = k_1 r_1 \alpha \left( \frac{N_G}{N_1} \right)^{\gamma_1} + k_1 r_2 (1 - \alpha) \left( \frac{N_G}{N_2} \right)^{\gamma_2}$$

for a two stress level behavior. In 1956, Corten and Dolan proposed a cumulative fatigue damage law based on a phenomenological behavior of materials which was also derived from this general damage theory. Their original investigation was concerned with a stress-independent, stress-interaction theory, but further investigation of the phenomenological aspects of the problem proved the necessity of making the theory stress-dependent.

For  $\gamma_1 = \gamma_2$  ( $S = 1$ ) Corten and Dolan arrived at the relationship (in the stress-independent form for  $\gamma_1 = \gamma_2$ )

$$N_G = \frac{N_1}{\alpha + (1 - \alpha) R^{1/\gamma_1}} \quad (13)$$

If we recall that  $R = r_2/r_1$  and that the rate coefficients are each stress level dependent, then  $R$  must be related to  $\sigma_1$  and  $\sigma_2$ , i.e.

$$R = R(\sigma_1, \sigma_2)$$

After some 700 tests, Corten and Dolan came to the conclusion that

$$R^{1/\gamma_1} = \left( \sigma_2 / \sigma_1 \right)^d$$

Where  $d$  is some material constant. As a material constant,  $d$  can be determined from a two-step stress level test.

The Corten-Dolan damage law provides a neat mathematical model for predicting cumulative damage through the use of a "fictitious S-N curve". Recalling Eq (8) and (13), we have

#### Miner's Law

$$N_G = \frac{N_1}{\alpha + (1 - \alpha) (N_1/N_2)}$$

#### Corten-Dolan Law

$$N_G = \frac{N_1}{\alpha + (1 - \alpha) R^{1/\gamma_1}}$$

In a log-log plot of  $\sigma$  versus  $N$ , Eq (8) may be seen to be approximated by

$$\frac{N_1}{N_2} = \left( \frac{\sigma_2}{\sigma_1} \right)^b$$

Where  $b$  (the Miner exponent) is a constant for a given material. Recall now that

$$R^{1/\gamma_1} = (\sigma_2/\sigma_1)^d$$

Thus we set

$$(\sigma_2/\sigma_1)^d = (N_1^*/N_2^*) \quad (14)$$

where

$N_1^*$  = fictitious cyclic life at  $\sigma_1$  stress level

$N_2^*$  = fictitious cyclic life at  $\sigma_2$  stress level

Thus, it should be possible to produce a fictitious straight-line S-N curve for cumulative fatigue damage under multiple stress levels by plotting Eq (14) in a log-log plot (similar to Miner's) and inserting the values of  $N_i$  obtained from this curve into Miner's summation to arrive at  $N_G$ , the total cycles. To start such a procedure, it is necessary only to locate one point through which the fictitious S-N curve must pass. Usually some upper bound is taken as the point such as  $\sigma_y$ , the yield stress, or  $\sigma_u$ , the ultimate stress along with the single cycle life.

#### 6. Freudenthal-Heller Theory

In 1958, Freudenthal and Heller of Columbia University completed an extensive random fatigue test program on 2024-T4 and 7075-T6 aluminum and 4340 steel. They choose three test spectrums having six stress levels each. Their conclusions based on theoretical considerations of stress-interaction and their test data resulted in a stress-interaction, stress-dependent cumulative damage theory similar to the Corten-Dolan theory.

Freudenthal and Heller initially assumed that there existed a fictitious  $\sigma$ -N curve which adequately related the stress interaction resulting from a spectrum loading. They

further assumed that the conventional  $\sigma$ -N and the fictitious  $\sigma$ -N curve were straight lines on a log-log plot. Where Corten and Dolan concluded with a fictitious  $\sigma$ -N curve, Fruedenthal and Heller began with one. The only difference between the two theories is in the definition of the exponents used in the fictitious  $\sigma$ -N curves.

#### Corten-Dolan

$$\left( \frac{\sigma_2}{\sigma_1} \right)^d = \frac{N_1^1}{N_2^1}$$

#### Fruedenthal-Heller

$$\left( \frac{\sigma_1}{\sigma_2} \right)^b = \frac{N_1^1}{N_2^1}$$

Fruedenthal and Heller defined p as a parameter dependent on stress amplitude, test specimen, and test conditions. They did not conclude that p could be obtained from a two stress level test as did Corten and Dolan.

It has been shown in subsequent fatigue tests that a two stress level test usually does not give a reliable estimate of the exponent for all test conditions and specimen configurations. Further work is required to find the exact nature of the dependence of the exponent on stress level and specimen configuration.

#### 7. Shanley's Crack Propagation Cumulative Damage Theories and 2X Method

F. R. Shanley of the Rand Corporation, in 1952, proposed three cumulative damage theories. Two of the theories are crack propagation laws and the third is a stress-interaction law familiarly known as the 2X Method.

The crack propagation laws are similar to Valluri's since a relationship is proposed relating crack growth to the cycles to failure and to the stress applied. These mathematical relationships were derived from a mechanistic consideration of the unbonding of atoms during cyclic loading. Two equations were proposed: one stress-independent and stress-interaction-free and the other stress-dependent.

The first theory starts with a crack growth relationship

$$L_i = L_{0i} \exp (C \sigma_i^x n_i)$$

where

$L_i$  = crack length at any time

$L_{0i}$  = initial crack length (produced in 1st cycle)

$C$  = constant

$\sigma_i$  = stress amplitude level

$n_i$  = number of cycles

By defining failure as the attainment of a critical crack length,  $L_{cr}$  which occurs at  $N_i$  cycles in single stress amplitude tests, and defining damage,  $D$ , as  $L_i/L_{cr}$  (at failure,  $D = 1$ ) we have

$$D = \exp \left( CK (\phi_i - 1) \right)$$

where  $K = \sigma_i^x N_i$  from single stress level test data and is a constant since the S-N curve shows  $N = K/\sigma_a^x$ .

Shanley's modification of the first theory assumes that the crack length is not a constant but depends on the stress magnitude. This gives rise to the relationship

$$D = \exp \left( C \sigma_i^x N_i (\phi_i - 1) \right)$$

Here  $\sigma_i^* N_i$  is not a constant and the S-N curve can be written as

$$D = \exp \left( C \sigma_i^x N_i (\phi - 1) \right)$$

Here  $\sigma_i^* N_i$  is not a constant and the S-N curve can be written as

$$N = \frac{k_1 (1 - k_2 \log \sigma)}{\sigma^x}$$

where  $k_1$  and  $k_2$  are both constants.

Since the stress-independent theory is in essence the same as Valluri's theory, it will reduce to Miner's rule under the conditions previously mentioned in the discussion of Valluri's theory. The stress-interaction theory states that initial damage occurs in the first few cycles of the highest stress in the spectrum and subsequent damage at lower stress will continue from this initial damage. Figure 83 is a graphical representation of this theory. If the initial damage is then defined as

$$D_{o,i} = \frac{L_{0,i}}{L_{cr}} = \exp(-C \sigma_i^x N_i)$$

the expression for damage becomes

$$D_i = \left( D_{o,i} \right)^{(1 - \phi_i)}$$

Because of the initial damage, the cycles to failure are shifted by some amount,  $n^*$ , and we employ a modified cycle ratio,  $\bar{\phi}$ , where  $\bar{N}_i = N_i - n_i^*$  and  $\bar{n}_i = n_i - n_i^*$  and  $\bar{\phi}$  is defined as

$$\bar{\phi} = \frac{\bar{n}_i}{\bar{N}_i} = \frac{\left( \frac{n}{N} \right)_i - \left( \frac{n}{N} \right)_i^*}{1 - \left( \frac{n}{N} \right)_i}$$

the damage relationship becomes

$$D_i = D_{o,i}^{(1 - \bar{\phi})}$$

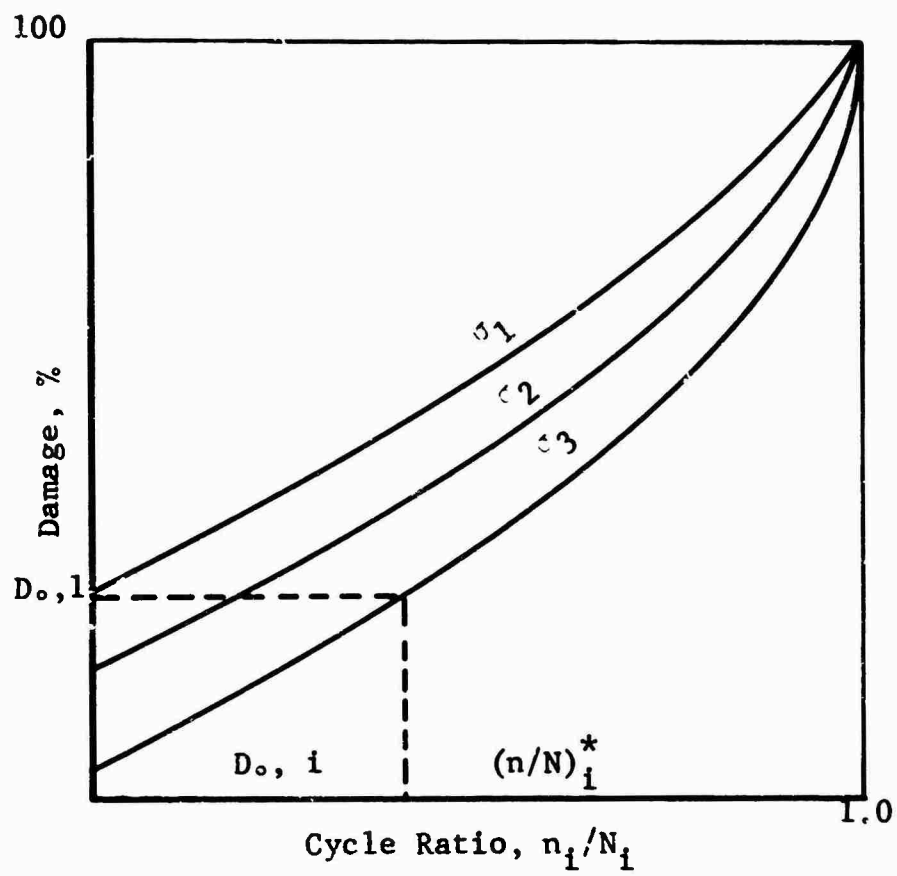


Fig. 83 SHANLEY'S STRESS-DEPENDENT INTERACTION CUMULATIVE DAMAGE THEORY



This theory then revises the damage and  $\sigma$ -N curves by the amount  $1 - \frac{n^*}{N}$ . At the present time, this theory cannot be used since the initial damage has to be determined for each stress amplitude.

Shanley's 2X Method is an interaction theory with the concept of initial damage omitted. The presence of stress interaction occurs primarily at high stresses, causing greater damage than low stresses. Shanley's derivation produces an equation of the form

$$\sigma_r = \left[ \frac{\sum dn_i \sigma_i^{2x}}{\sum dn_i} \right]^{1/2x} \quad (14)$$

where

$\sigma_r$  = constant stress amplitude that will produce the same number of cycles to failure as the stress spectrum

$dn_i$  = number of cycles at the  $i^{\text{th}}$  stress amplitude

The equation for the  $\sigma$  - N curve is

$$N_G = \frac{K}{\sigma_{ar}^x} \quad (15)$$

From equation (14) and (15) we obtain

$$\left( \frac{K_1}{N_G^{1/x}} \right)^{2x} \sum dn_i = \sum dn_i \sigma_i^{2x}$$

for a two stress level test

$$\sum dn_i \sigma_i^{2x} = \alpha N_G \left( \frac{K_1}{N_1^{1/x}} \right)^{2x} + (1 - \alpha) N_G \left( \frac{K_1}{N_2^{1/x}} \right)^{2x}$$

and with

$$\sum dn_1 = N_G, \sum dn_1 = \alpha N_G, \sum dn_2 = (1 - \alpha) N_G$$

we obtain

$$\left( \frac{K_1^{1/x}}{N_G} \right)^{2x} N_G = \alpha N_G \left( \frac{K_1^{1/x}}{N_1} \right)^{2x} + (1 - \alpha) N_G \left( \frac{K_1^{1/x}}{N_2} \right)^{2x}$$

which reduces to

$$\frac{1}{N_G^2} = \frac{\alpha}{N_1^2} + \frac{(1 - \alpha)}{N_2^2}$$

By a small amount of manipulative algebra, a familiar general form emerges

$$\frac{N_G}{N_1} = \left[ \frac{1}{\alpha + (1 - \alpha) \left( \frac{N_1}{N_2} \right)^2} \right]^{1/2}$$

## 8. Conclusion

Of the six cumulative damage theories discussed, the ones which appear to be most applicable to GRP at the present time are Miner's, Corten-Dolan and Freundenthal-Heller. With advances in our understanding of the micromechanics of failure of GRP and in nondestructive testing, Valluri's, Grover's and Shanley's methods could be applied. The most versatile method in terms of analysis techniques, scope of stress spectrum and structural configuration appears to be the Freundenthal-Heller theory. The disadvantage of this method is its cumbersome design procedure. By a similar argument, Miner's rule becomes the most advantageous method for design purposes.

It is obvious that there is not at present an adequate cumulative damage theory for analysis or design purposes. Until further research into the effects of mean stress, stress spectrum, structural configuration, and stress concentrations has been performed, cumulative damage theories will continue to be inadequate. To illustrate this, we refer to Table 45 in the text which lists various materials, test conditions, and cumulative damage theories.

## APPENDIX D

### TORSIONAL FATIGUE TESTING OF CARBON-FILAMENT REINFORCED PLASTIC TUBE

A carbon-filament reinforced plastic tube delivered to IITRI by Navy BuWeps was tested in torsional fatigue. The dimensions of the tube and final specimen configuration are shown in Fig. 84. The ends of the tube were overwound with eight layers of S-glass filament tape containing Hysol Epoxy No. 0151 clear. Following this operation, the ends of the specimen were ground flat to final specimen dimensions. The specimen was subsequently tested in shear-zero-shear ( $R = 0.1$ ) torsional fatigue in the torsional fatigue machine described earlier in Section V. The static shear strength of the tube was given as 12,000 psi. The test was performed cycling the specimen from 800 to 8,000 psi in pure shear. This called for torquing from 262 to 2,650 in-lb to insure that the specimen did not go into zero torque. The specimen failed after sustaining 1,596 cycles of torque.

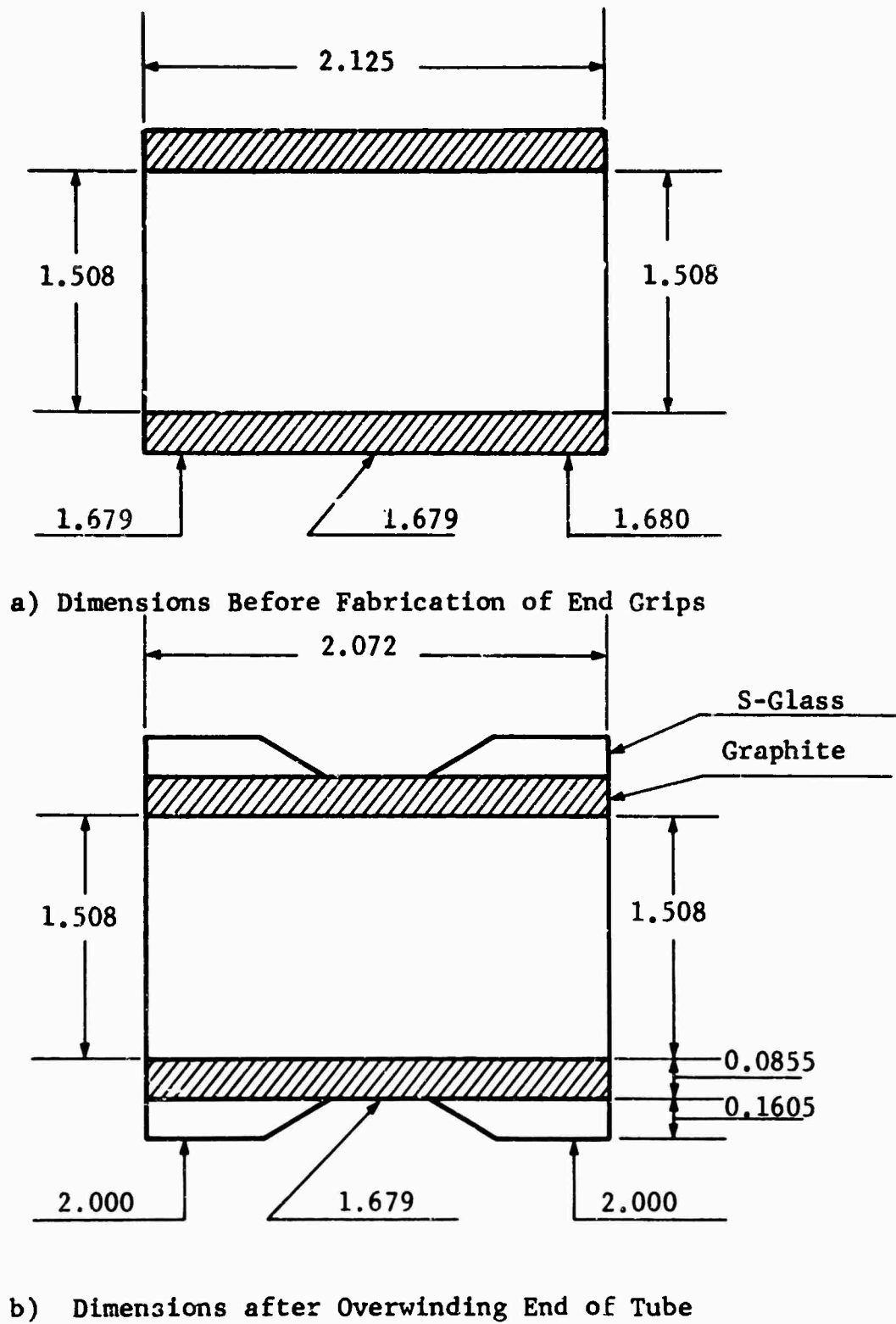


Fig. 84 FABRICATION OF CARBON-FILAMENT TORSIONAL FATIGUE SPECIMEN

APPENDIX E  
STRAIN RATE CALCULATIONS FROM GRIP MOVEMENT  
OF THE INSTRON UNIVERSAL TESTING MACHINE

A. TENSILE TEST

In the tensile test for the 181/S901 glass cloth reinforced epoxy, the effective gage length is approximately 2.0 in. Then

$$\dot{\epsilon} = 0.0083 \dot{\delta}$$

where

$$\dot{\epsilon} = \text{strain rate, in./in./sec}$$

and

$$\dot{\delta} = \text{grip displacement rate, in./min}$$

An exact expression for  $\dot{\epsilon}$  can be obtained by relating  $\dot{\epsilon}$  to  $\dot{\delta}$  for the particular shape of this tensile specimen. In Fig. 85 the effective length constant radius specimen is shown. Then

$$w = w_0 + 2R (1 - \cos \theta)$$

$$\frac{x}{R} = \sin \theta$$

$$\cos \theta = \sqrt{1 - \left(\frac{x}{R}\right)^2}$$

$$\therefore w = w_0 + 2R \left[ 1 - \sqrt{1 - \left(\frac{x}{R}\right)^2} \right]$$

$$\Delta \delta = \frac{P \Delta x}{AE}$$

$$\Delta \delta = \frac{P \Delta x}{wtE}$$

$$\Delta \delta = \frac{P \Delta x}{tE \left\{ w_0 + 2R \left[ 1 - \sqrt{1 - \left(\frac{x}{R}\right)^2} \right] \right\}}$$

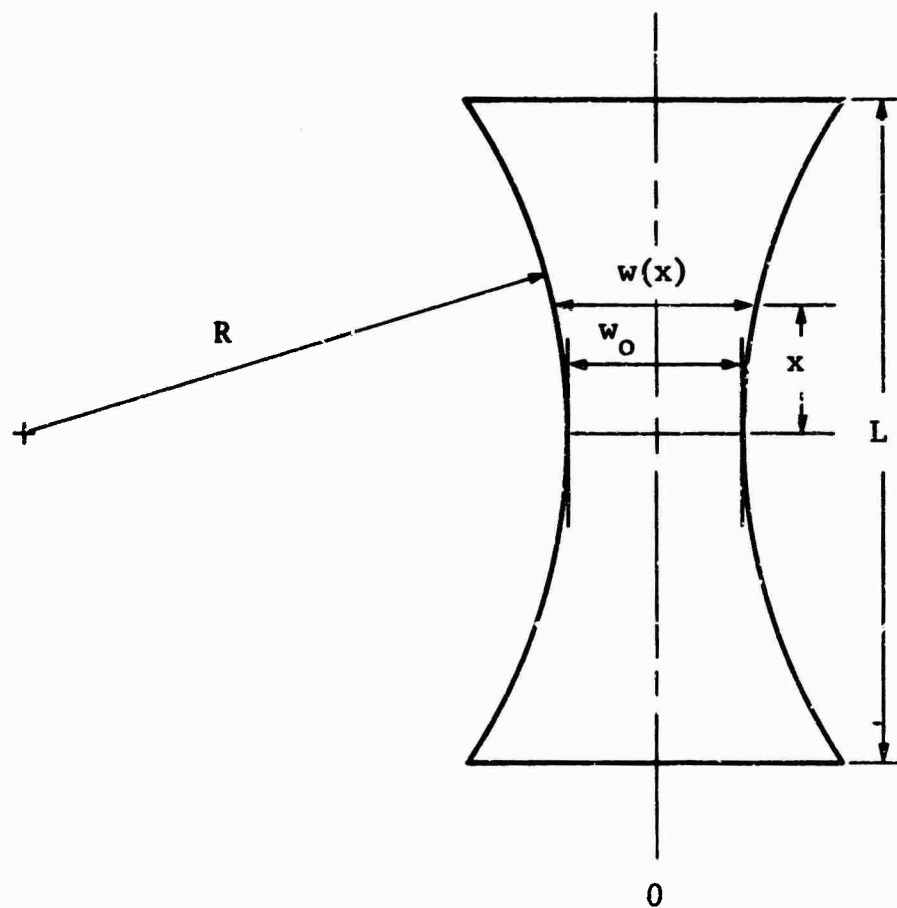


Fig. 85 CONSTANT RADIUS TENSILE SPECIMEN GAGE SECTION  
(USED TO EVALUATE 180/S901 GLASS CLOTH REIN-  
FORCED EPOXY)

In the limit

$$\delta = 2 \int_0^{L/2} \frac{P dx}{\left\{ w_0 + 2R \left[ 1 - \sqrt{1 - \left(\frac{x}{R}\right)^2} \right] \right\}}$$

By placing a strain gage at the center of the specimen and automatically recording strain versus load, it was determined that

$$\epsilon = 3.95 P$$

where

$$\epsilon = \text{gage strain, } \mu - \text{in./in.}$$

$$P = \text{load, lb}$$

then

$$\dot{\delta} = \frac{0.509 \dot{\epsilon}}{Et} \int_0^{L/2} \frac{dx}{w_0 + 2R \left[ 1 - \sqrt{1 - \left(\frac{x}{R}\right)^2} \right]}$$

The integration was never carried out for this program.

Similarly, the S994 uniaxial glass roving reinforced epoxy tensile specimens with an exposed gage length of 6 in. resulted in a relationship of

$$\dot{\epsilon} = 0.00278 \dot{\delta}$$

where

$$\dot{\epsilon} = \text{strain rate, in./in./sec}$$

$$\dot{\delta} = \text{grip displacement rate, in./min}$$



## B. COMPRESSION TESTS

In compression, the 2 in. long rectangular specimen used for both 181/S901 glass cloth and the S994 uniaxial roving reinforced epoxies led to the relationship

$$\dot{\epsilon} = 0.00831 \dot{\delta}$$

where

$$\dot{\epsilon} = \text{strain rate, in./in./sec}$$

$$\dot{\delta} = \text{grip displacement rate, in./min}$$

## C. BENDING TESTS

Figure 86a shows the beam under constant bending moments with grips and supports. Then

$$\epsilon = \frac{\sigma}{E} = \frac{Wac}{EI}$$

The displacement of point o shown in Fig. 86b was found in Roark to be

$$\delta = - \frac{Wa^2}{3EI\ell} = \left[ \frac{3\ell^2}{2} - 2a\ell \right]$$

which leads to the relationship

$$\epsilon = \frac{3c\ell}{a \left[ \frac{3\ell^2}{2} - 2a\ell \right]} \dot{\delta}$$

with  $c = 1/8$  in.,  $a = 1$  in.,  $\ell = 5$  in.,  $\epsilon$  in in./in./sec and  $\dot{\delta}$  in in./min.

We have

$$\dot{\epsilon} = 0.00114 \dot{\delta}$$

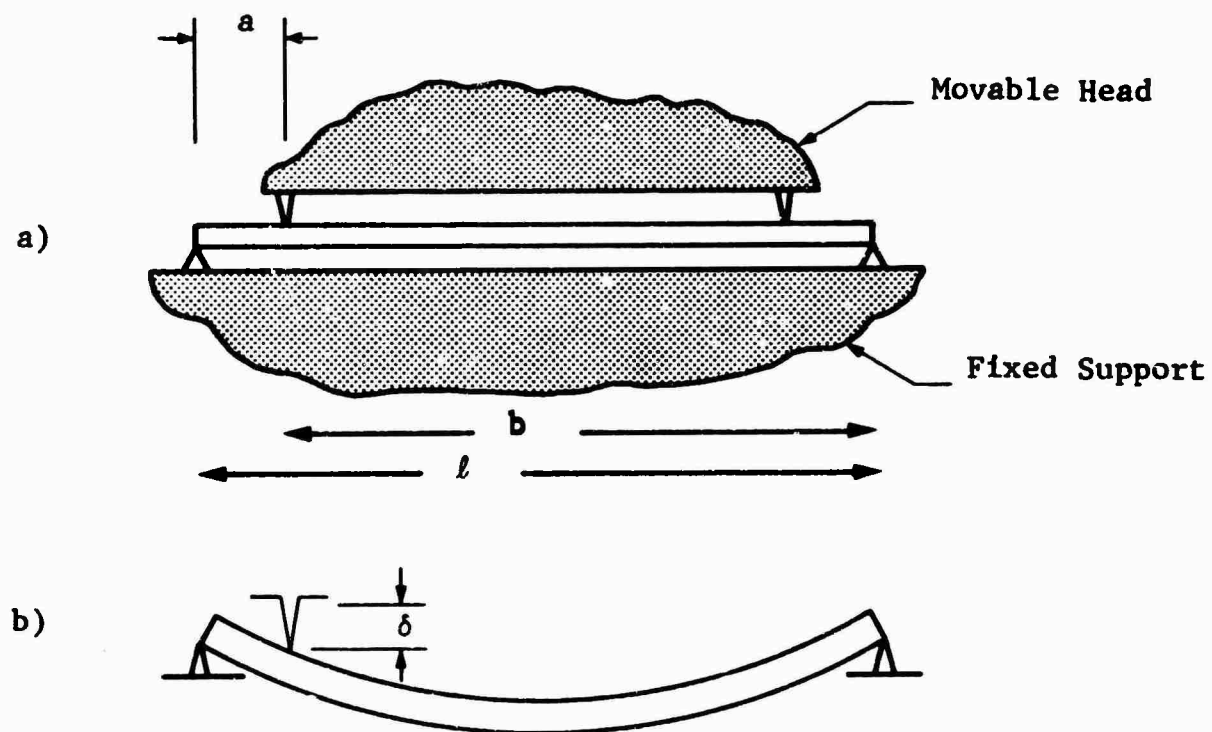


Fig. 86 TEST BEAM UNDER CONSTANT MOMENT IN CENTER GAGE SECTION

APPENDIX F  
FATIGUE MACHINES AND EQUIPMENT USED IN GRP STUDIES

Both hydraulic-mechanical and electromechanical prime mover systems were employed in the course of the fatigue studies. A description of their construction, purpose, and utility follows.

A. AXIAL FATIGUE LOADERS

High cyclical rate fatigue tests were performed on 1800 cpm eccentric weight dynamic load applicators. The units were two BLH SF-1-U and a SF-10-U. The driver is alternately moved up and down by an eccentric weight driven by an electric motor. Load axiality is maintained through the use of flex plates on the system. Static load is applied to the specimen through the extension or compression of calibrated springs and is automatically compensated for any material creep. For any tests requiring loads greater than 1,000 lb, a 5:1 multiplier was used.

As mentioned earlier, a most important parameter in control of fatigue tests is gripping and fixturing arrangements used. Figure 87 shows a SF-1-U with the 4-point bending fixture. This fixture applies the load at quarter points thus producing pure bending in the gage section and has swivel supports which eliminate load which might occur as a result of specimen deflection. A detail of the bending fixture is shown in Fig. 88. Figure 89 shows the SF-1-U with the 5:1 multiplier and the grips used for uniaxial tension and compression loading of the 181/S901 glass cloth materials. The uniaxial grips are two 3 x 2 in. angles machined parallel and square with a slot machined on one side for specimen alignment. The specimen is clamped together with four carefully spaced bolts at each end of the specimen.

Fatigue tests at the other two cyclic rates (6 and 50 cpm) were performed using hydraulic-mechanical prime movers. The units employed hydraulic rams, pumps, accumulators, and solenoid or air

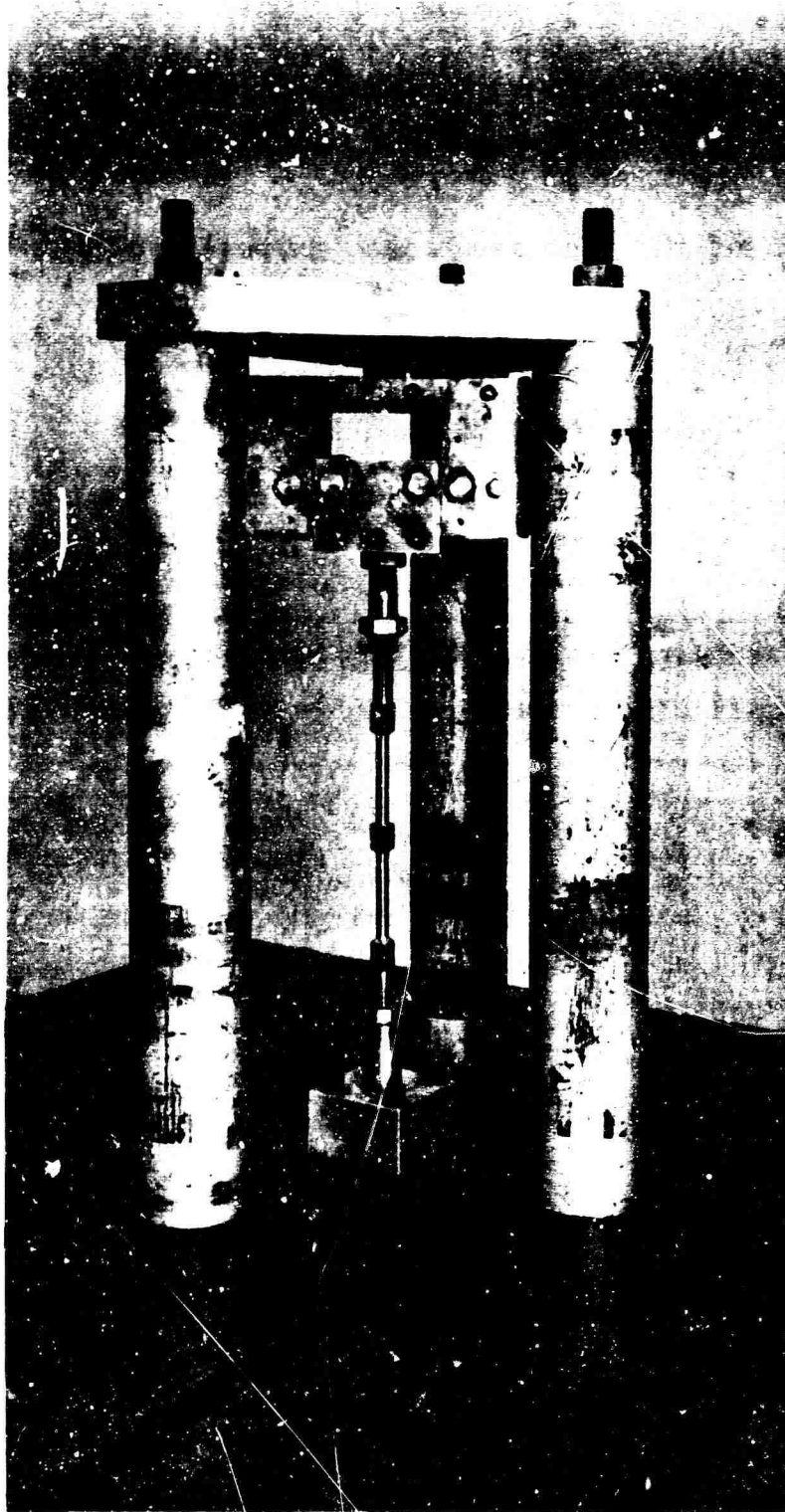


Fig. 87 SONNTAG SF-1-U FATIGUE MACHINE AND 4-POINT BENDING FIXTURE

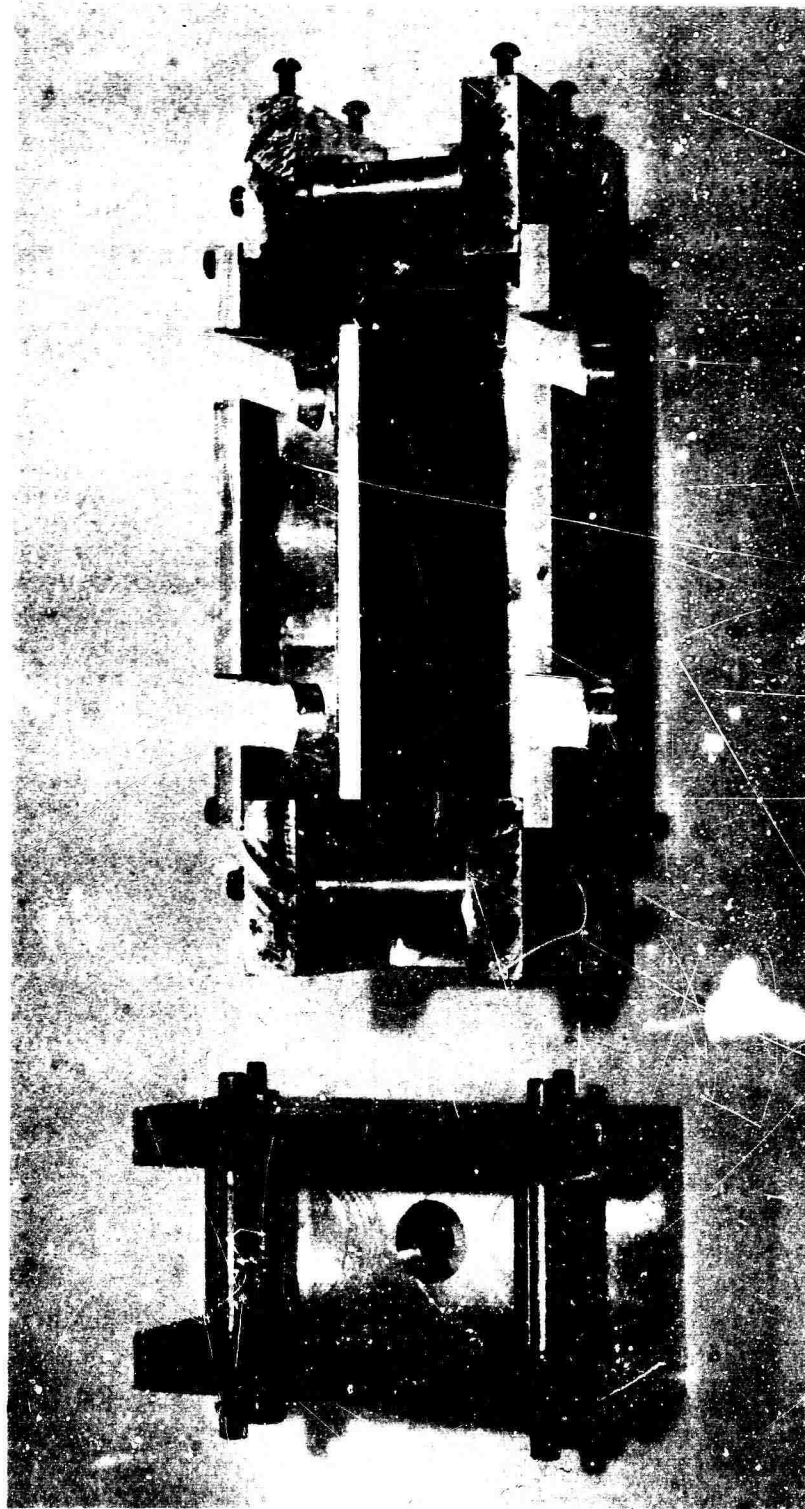


Fig. 88 BENDING FIXTURE FOR FATIGUE OF 181/S901 GLASS CLOTH  
AND S994 UNIAXIAL ROVING REINFORCED EPOXIES



Fig. 89 UNIAXIAL TENSION AND COMPRESSION FATIGUE GRIPS USED  
FOR TESTING SHEET COUPONS OF 181/S901 GLASS CLOTH  
REINFORCED EPOXIES

actuated valves. Five of these units were designed and assembled for use on the program. The following is a list of these units and their capabilities.

1. Constant axial stress or strain at cyclic rates from 6 to 60 cpm. The double acting ram has a load capability of  $\pm 10,000$  lb which can be applied with a mean load up to 10,000 lb. See Fig. 90.
2. A 6 cpm constant stress fatigue machine used for flexural fatigue studies using a double acting ram with a load capability of  $\pm 1,000$  lb with a zero mean load. See Fig. 91.
3. A 6 cpm constant stress or strain amplitude fixture which is moved by a double acting ram which can support a mean load equal to the alternating load, the load capability is  $\pm 10,000$  lb. See Fig. 92.
4. A constant alternating axial load, 6 to 100 cpm machine with a 40,000 lb capacity. This unit is capable of bending large structural sections of composites or of applying a tension-zero-tension force of 40,000 lb to a composite. See Fig. 93.
5. A constant torque or rotary angle fatigue machine capable of applying 8,000 in.-lb of torque at 0.1 to 100 cpm. A varying load profile may also be applied. This machine will be described later in greater detail and is shown in Fig. 90.

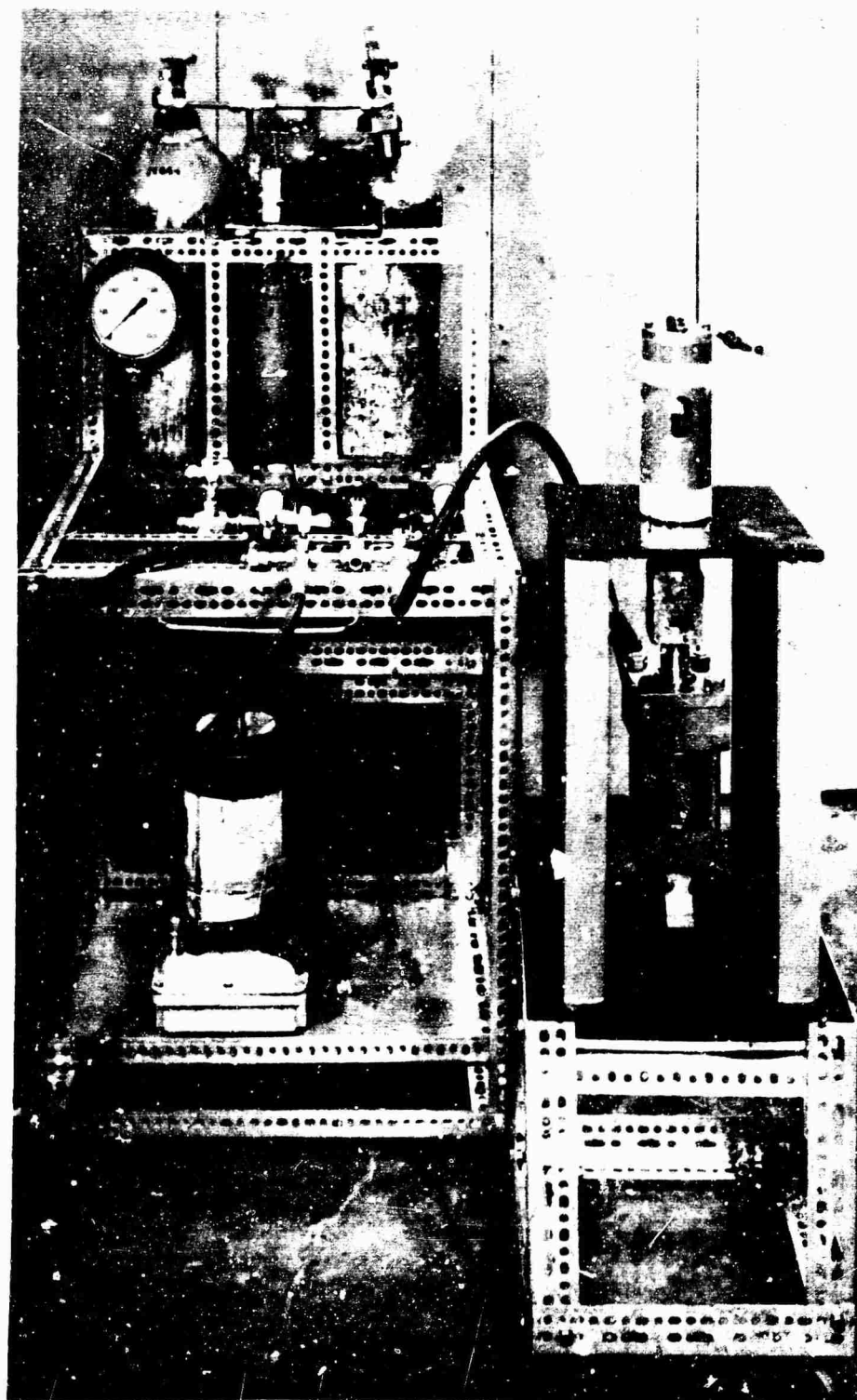


Fig. 90 HYDRAULIC-MECHANICAL PRIME MOVER CAPABLE OF 6 TO 60 CPM  
AND + 10,000 LB ALTERNATING LOAD AT A MEAN LOAD OF FROM  
0 TO 10,000 LB



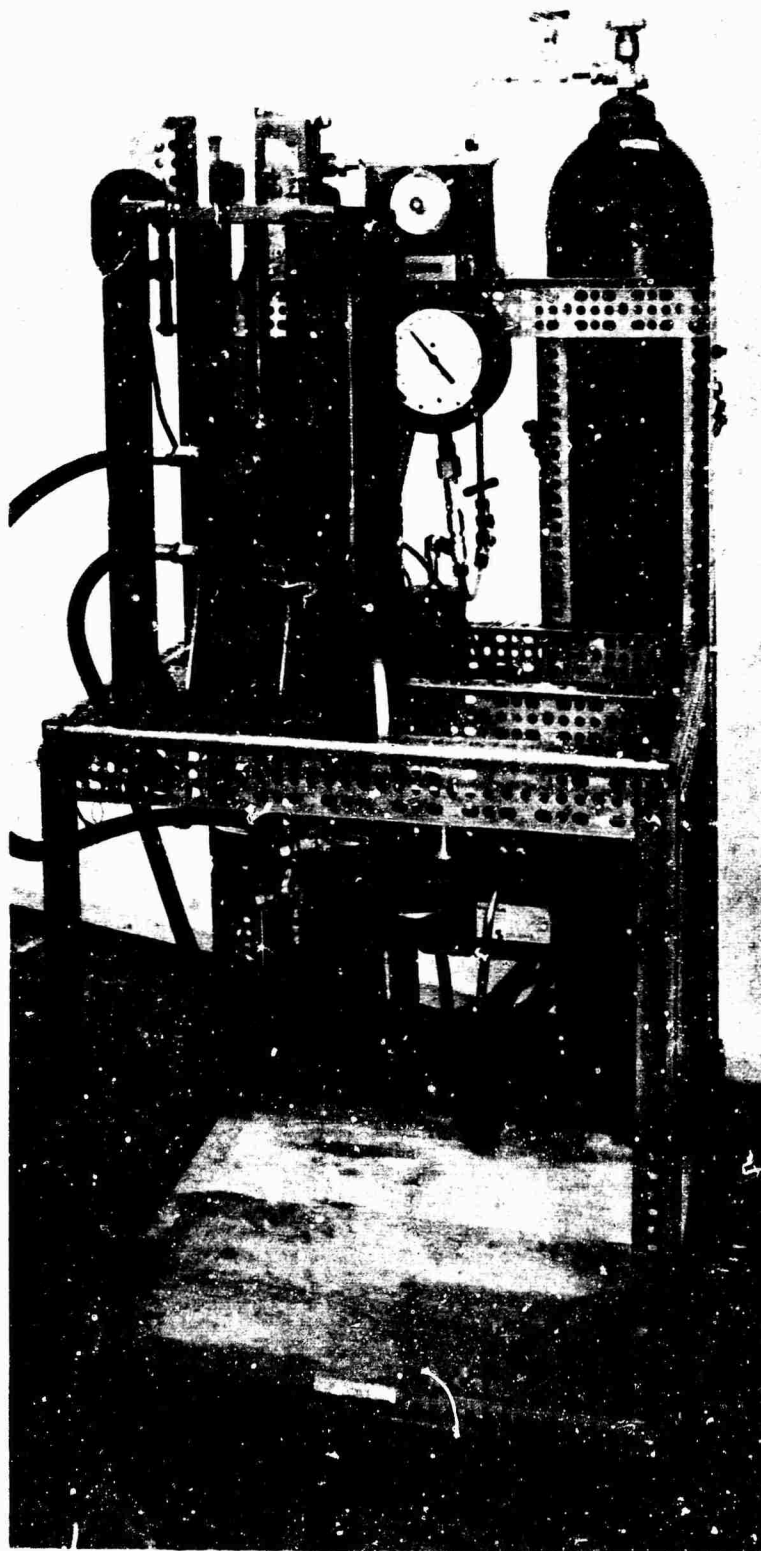


Fig. 91 LOW CYCLIC RATE FLEXURAL FATIGUE CONSOLE  
LOAD CAPABILITIES ARE  $\pm 1,000$  LB

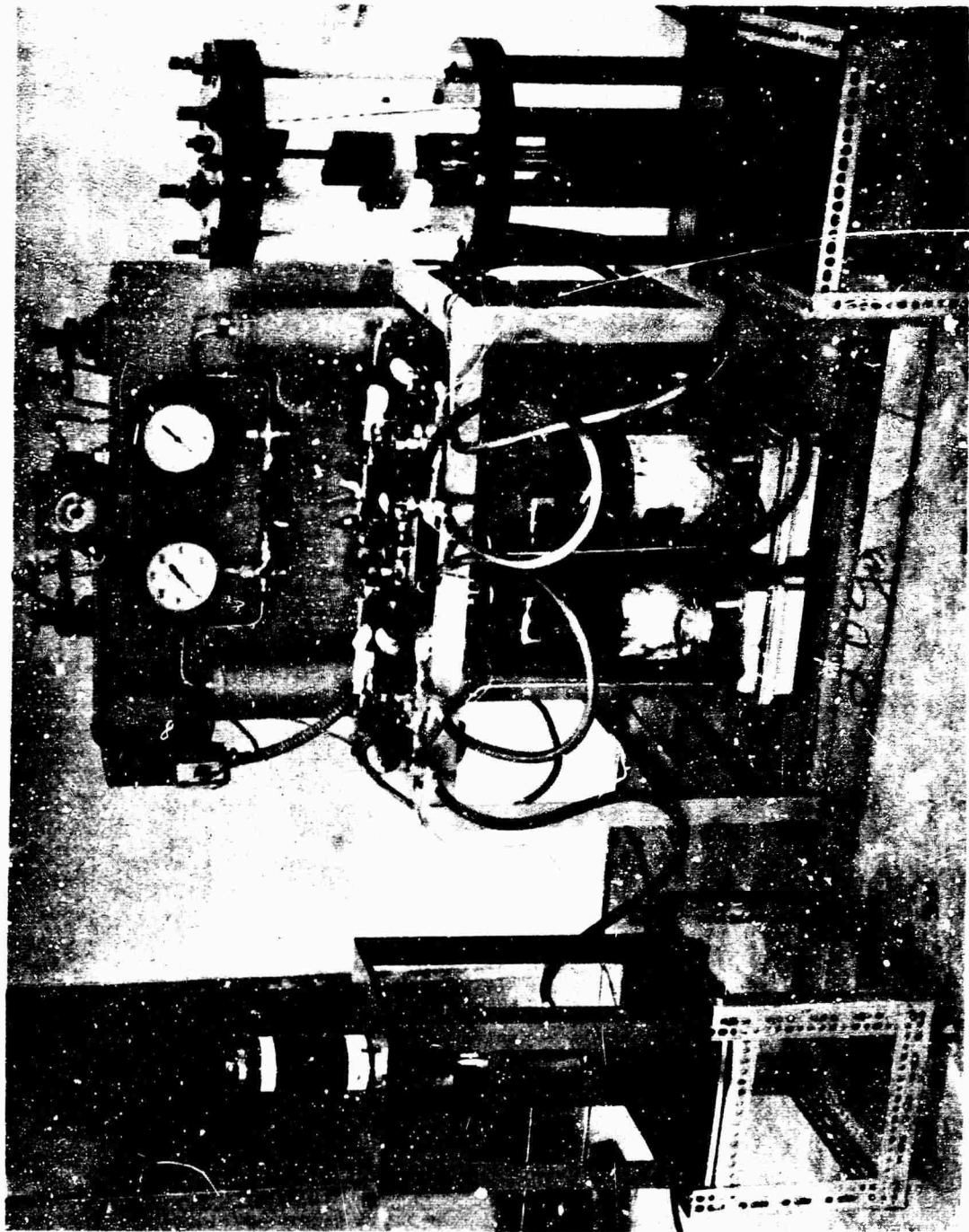


Fig. 92 HYDRAULIC-MECHANICAL FATIGUE MACHINE CAPABLE OF BOTH CONSTANT STRESS AND CONSTANT STRAIN AMPLITUDES TO  $\pm 10,000$  LB LOAD

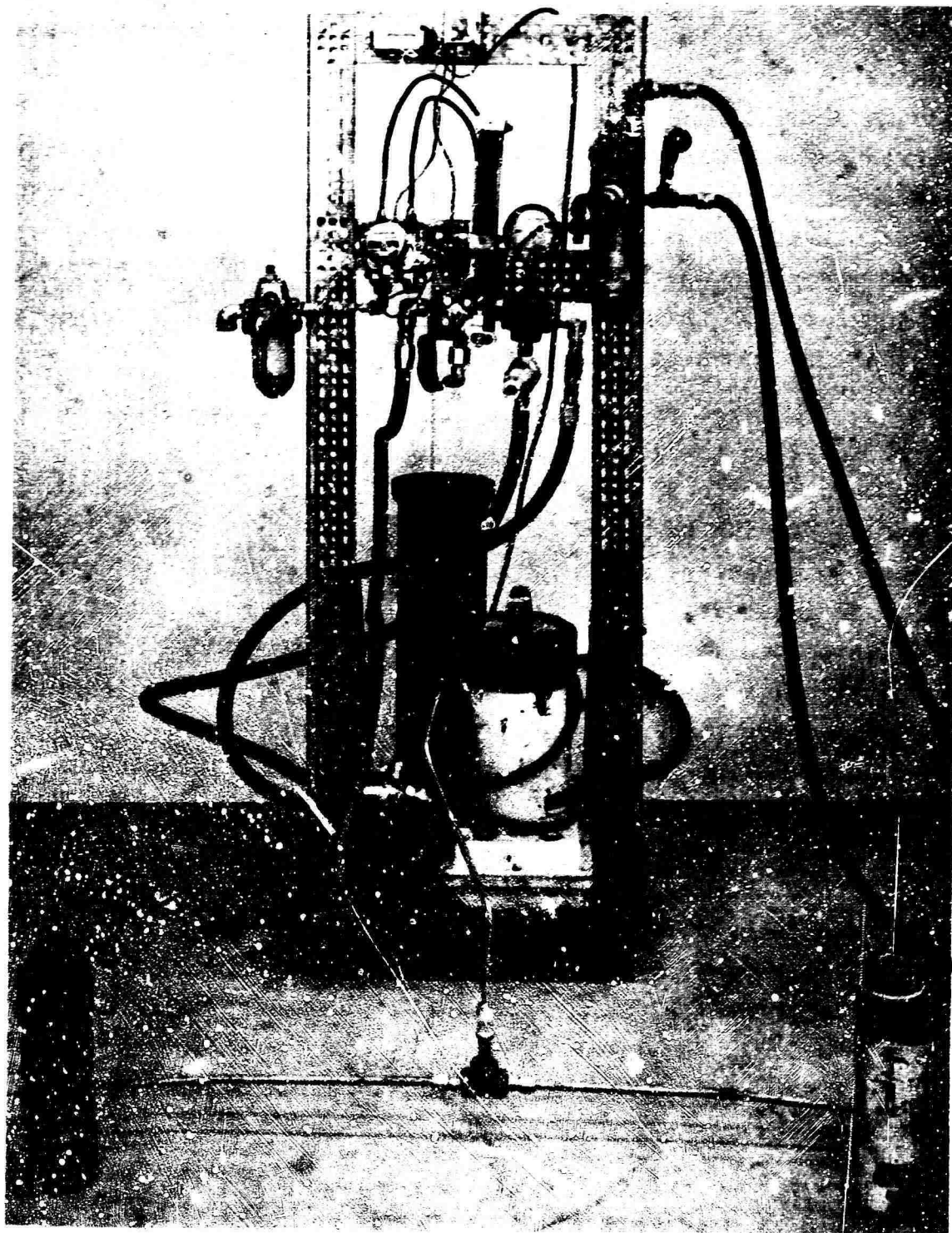


Fig. 93 HYDRO-MECHANICAL BEAM FATIGUE MACHINE-POWER SUPPLY AND RAMS

The principle of operation for the first four units is basically the same and is shown schematically in Fig. 94. As can be seen, a constant load is maintained in the nitrogen backed accumulator by a hydraulic pump. Fluid at this pressure is valved to the ram by a valve arrangement sequenced by a timer motor. The timer motor determines the cyclic rate at which the prime mover can operate. Load is monitored by a load cell located in the reaction frame. On occasion a precalibrated pressure gage in the line can also be used for that purpose.

The grips used for applying tensile and compressive axial loads to the 181/S901 glass cloth reinforced epoxy specimens were in principle an extension of the hydraulic ram piston. A bronze bushing was used to provide specimen load axiality. Figure 95 shows the means of aligning the specimen and grips prior to insertion in the load frame. To check alignment, a steel specimen was fitted with electrical resistance foil gages and statically tested. Three strain gages in the longitudinal direction were used on each of the specimens. Strains were monitored and recorded at various load levels. The gage locations and test results are shown in Figs. 96 and 97. The test results showed that deviation from the true stress due to specimen bending never exceeded 10 percent. In addition to this, the strain-gaged specimen was tested to destruction in fatigue to check the overall alignment of the grips and reaction frame for the first hydraulic-mechanical fatigue machine. The test results in Fig. 98 show relatively excellent agreement with the static test. Closeups of the grips employed in testing the 181/S901 glass cloth and the S994 uniaxial glass roving reinforced epoxies are shown in Fig. 99.

All low cyclic rate fatigue fixtures and equipment were calibrated by steel specimens which had been strain-gaged and tested in an Instron static load machine. Figure 100 shows an oscilloscope trace of a typical tension-zero-tension loading cycle for the hydraulic-mechanical fatigue machines.

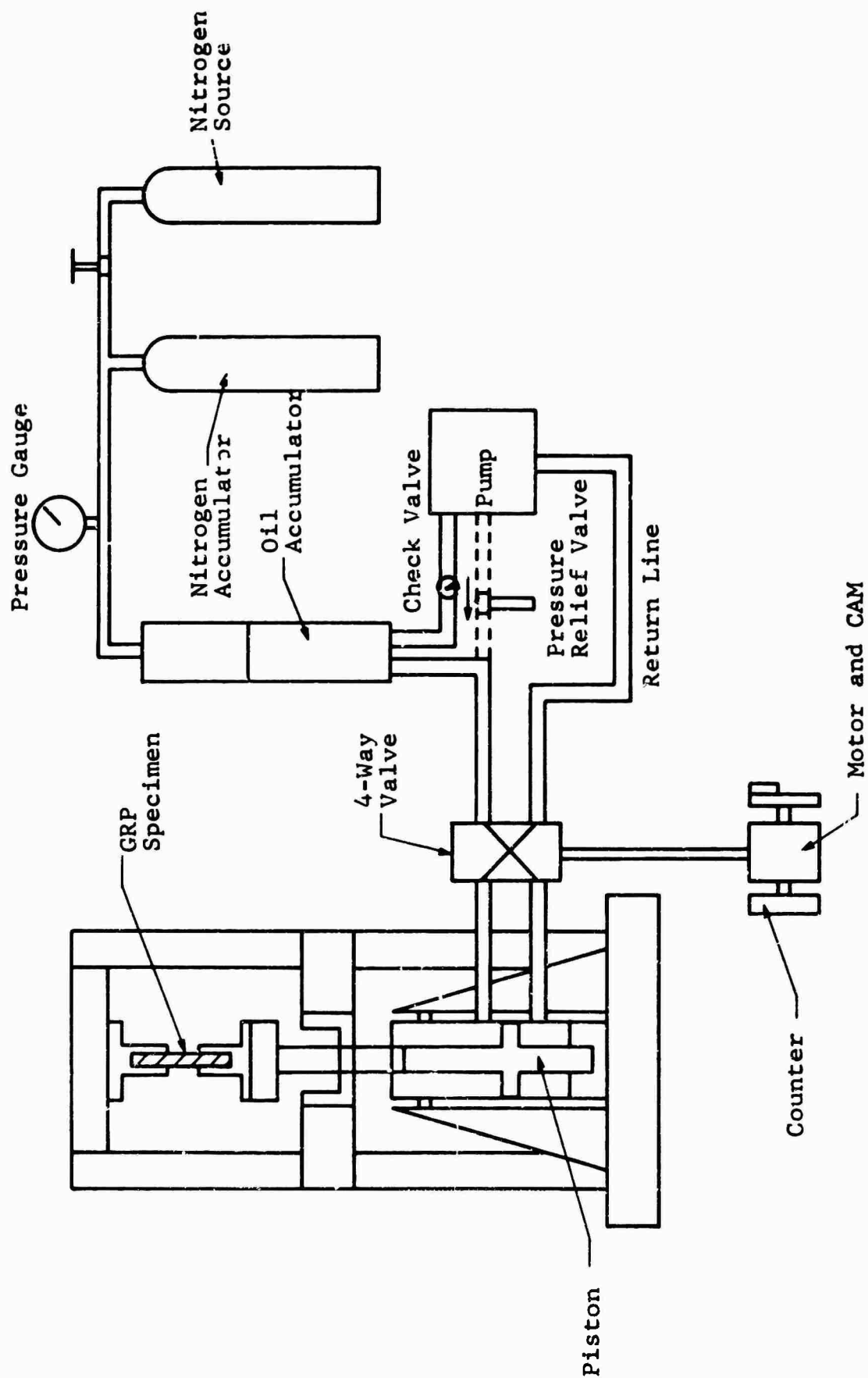


FIG. 94 SCHEMATIC OF HYDRAULIC MECHANICAL PRIME MOVERS

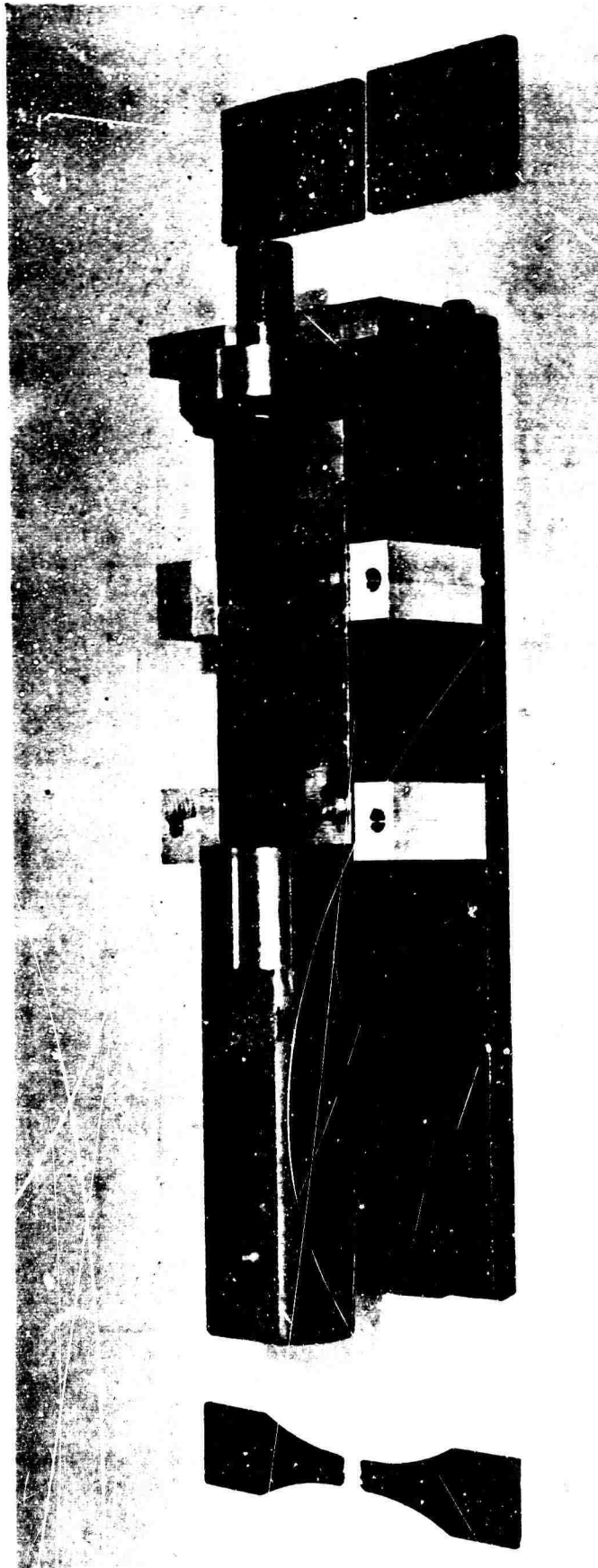


Fig. 95 UNIAXIAL FATIGUE GRIPS WITH OPTIMUM 181/S901 GLASS CLOTH REINFORCED  
EPOXY TENSILE SPECIMEN AND ALIGNMENT FIXTURE

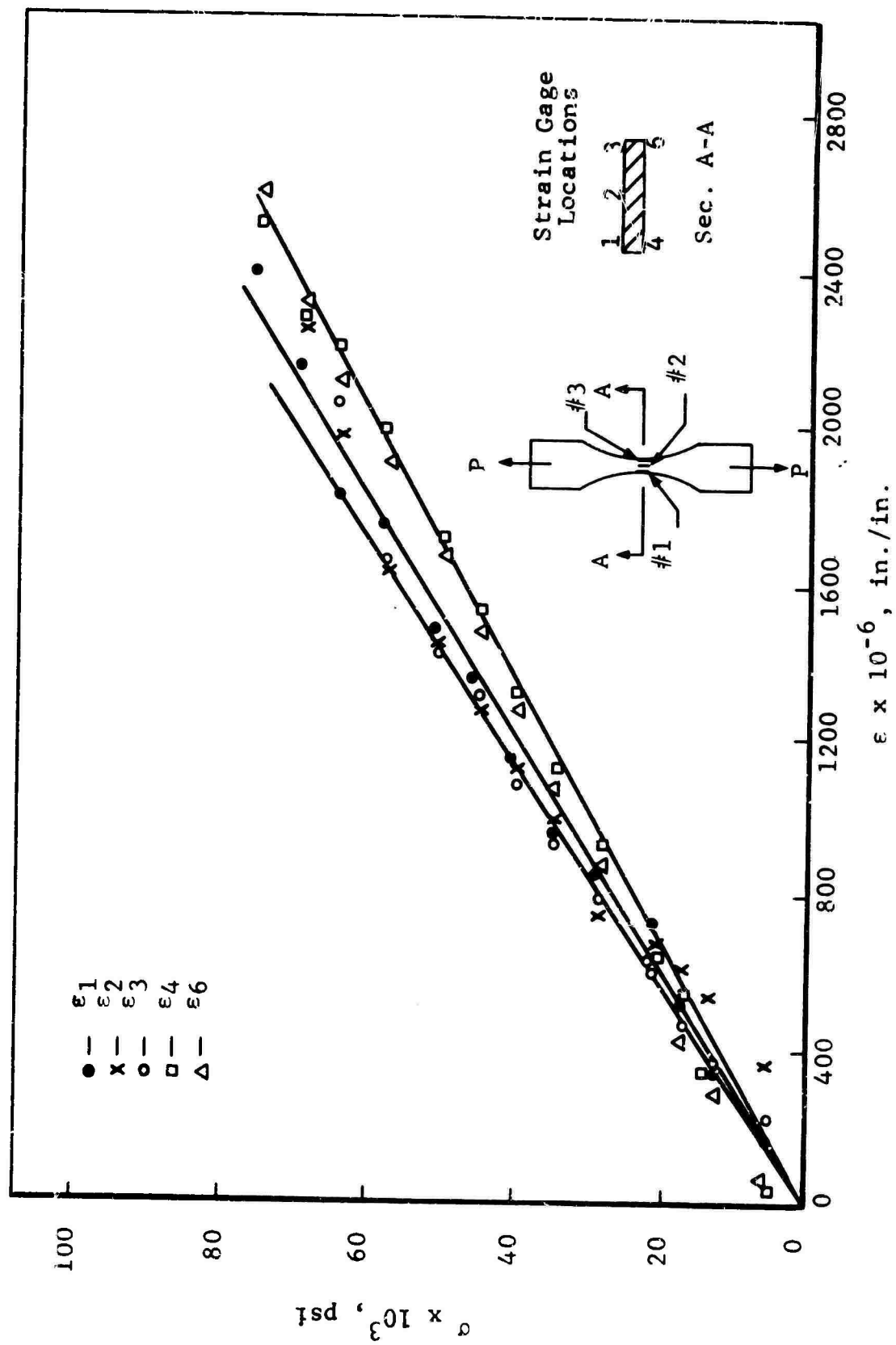


Fig. 96 TEST RESULTS, FATIGUE FIXTURE CALIBRATION

From Fig. 1 for  $\sigma = 69,600$  psi

$$\begin{aligned}\epsilon_1 &= 2160 \times 10^{-6} \text{ in./in.} \\ \epsilon_2 &= 2261 \times 10^{-6} \text{ in./in.} \\ \epsilon_3 &= 2484 \times 10^{-6} \text{ in./in.} \\ \epsilon_4 &= 2290 \times 10^{-6} \text{ in./in.} \\ \epsilon_6 &= 2307 \times 10^{-6} \text{ in./in.}\end{aligned}$$

$$\epsilon_5 = \frac{\epsilon_4 + \epsilon_6}{2} = 2298 \times 10^{-6} \text{ in./in.}$$

1. Pure Axial Strain,  $\epsilon_A$ :

$$\epsilon_A = \frac{\epsilon_2 + \epsilon_5}{2} = 2279 \times 10^{-6} \text{ in./in.}$$

$$\therefore E = \frac{\sigma}{\epsilon_A} = 30.5 \times 10^6 \text{ psi}$$

2. Stress Due to Bending in Strong Direction,  $M_1$ :

$$\sigma_1 = E \frac{(\epsilon_1 + \epsilon_4)}{2} = \frac{30.5 \times 10^6 (2261 \times 10^{-6})}{2} = 69,500 - 1,600 \text{ psi}$$

3. Stress Due to Bending in Weak Direction,  $M_2$ :

$$\sigma_2 = E \epsilon_2 - \sigma = 30.5 \times 10^6 (2261 \times 10^{-6}) - 69,600 = -600 \text{ psi}$$

4. Maximum Stress,  $\sigma_T$ :

$$\sigma_T = \sigma + \sigma_1 + \sigma_2 = 71,800 \text{ psi} = 3.16\% \text{ error}$$

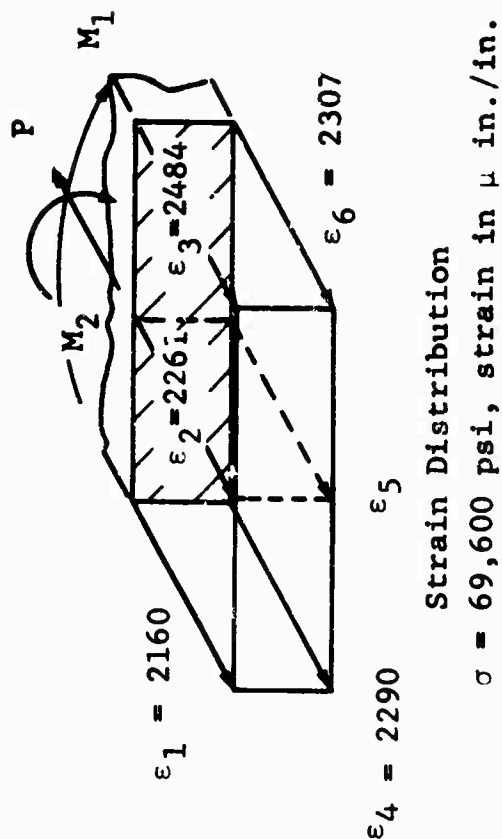


Fig. 97 STRAIN DISTRIBUTION OVER SPECIMEN CROSS SECTION AS PRODUCED BY HYDRAULIC-MECHANICAL FATIGUE MACHINE NO. 1



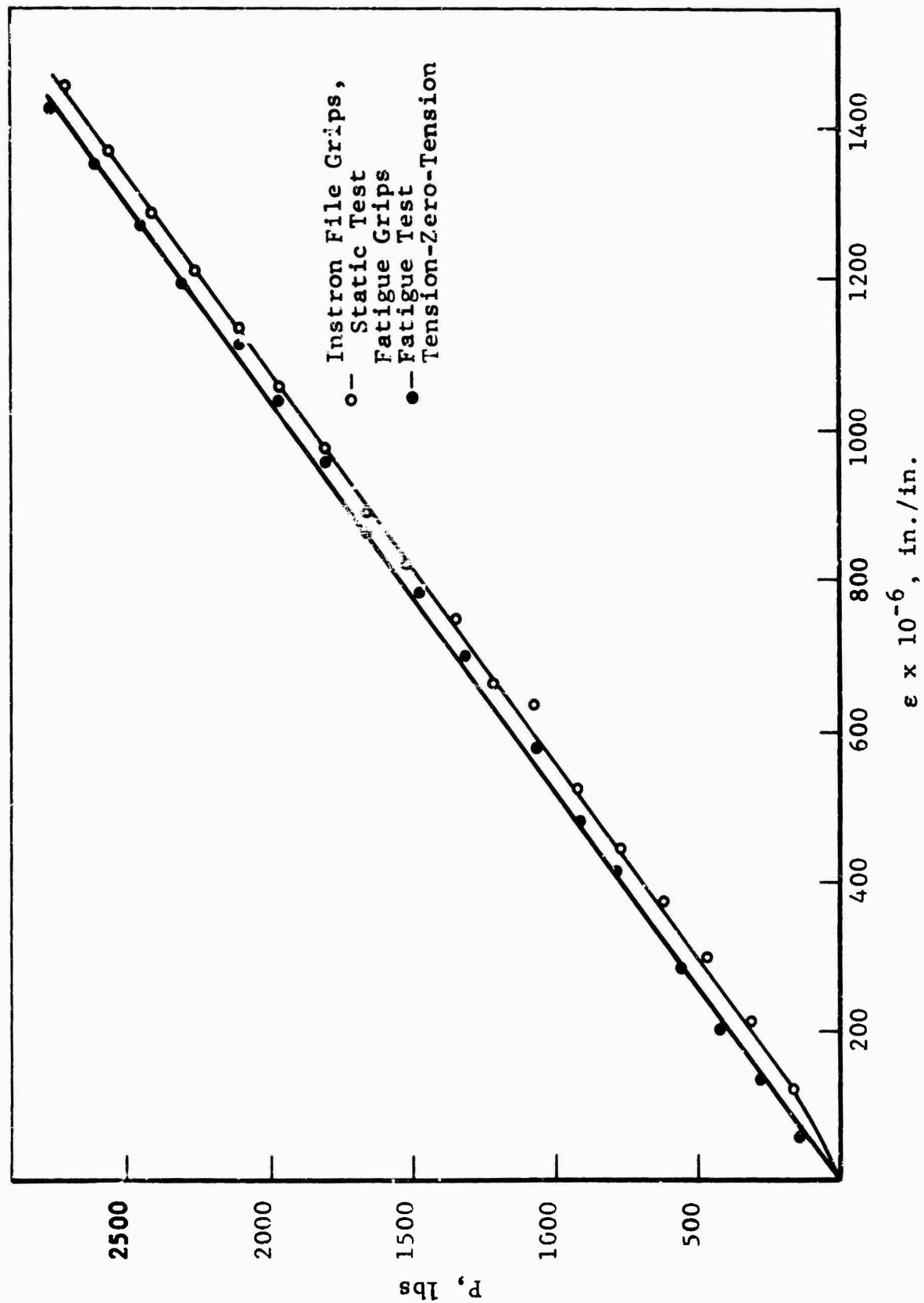
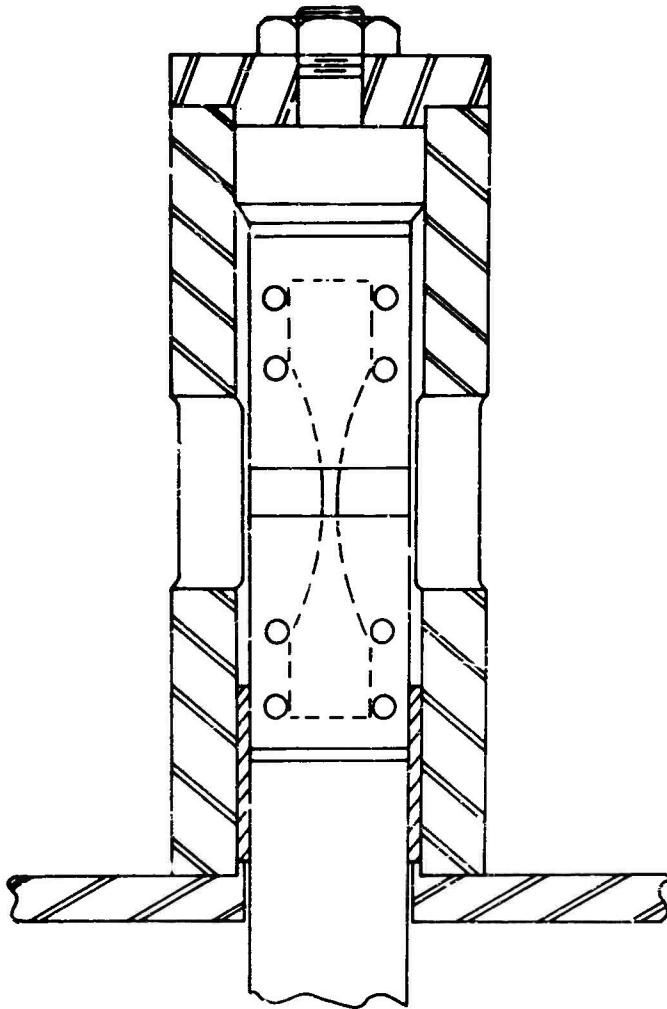
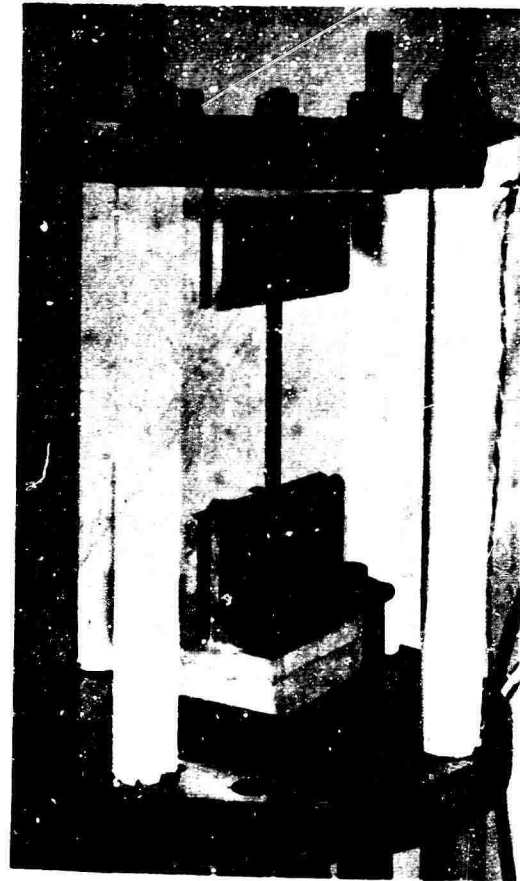


Fig. 98 TEST RESULTS, FATIGUE CONSOLE CALIBRATION

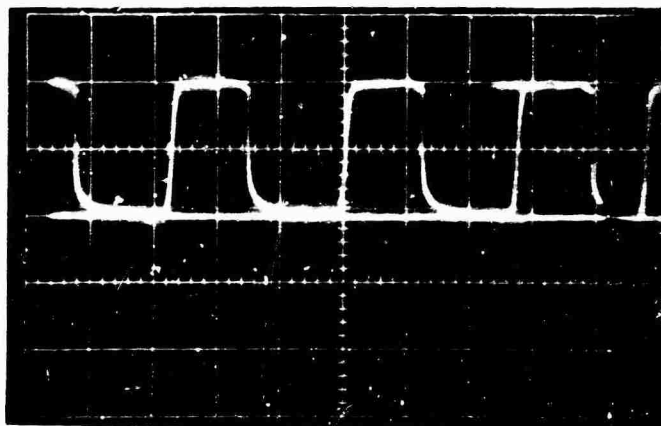


a) 181/S901 Glass Cloth Specimen

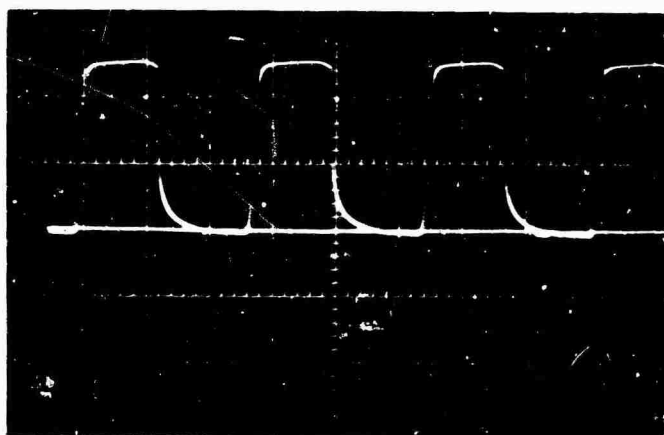


b) S994 Glass Roving Specimen

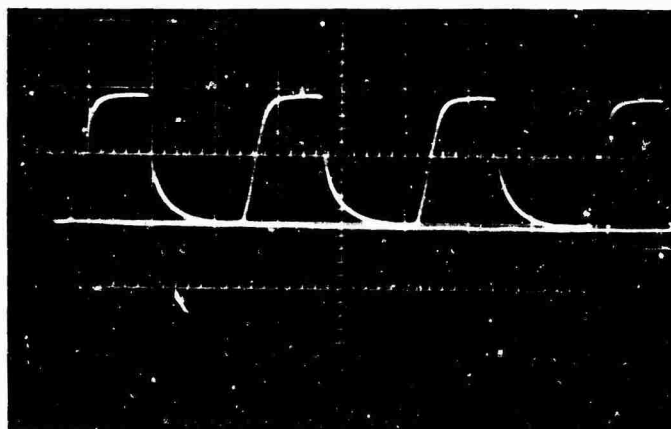
**Fig. 99 CLOSEUPS OF UNIAXIAL GRIPS EMPLOYED IN TESTING  
181/S901 GLASS CLOTH AND S994 ROVING REINFORCED  
EPOXIES IN LOW CYCLIC RATE FATIGUE MACHINES**



1900# 6. cpm  $500 \times 10^{-6}$  in./in. per div.



950# 6. cpm  $200 \times 10^{-6}$  in./in. per div.



315.# 6. cpm  $100 \times 10^{-6}$  in./in. per div.

Fig. 100 LOAD CYCLES, TENSION-ZERO-TENSION

## 1. Basic Prime Mover and System

As mentioned earlier, a hydraulic-mechanical power supply and prime mover unit was assembled to apply torque cyclically to specimens. This servo-hydraulic testing machine system was used to evaluate torsional fatigue life of an epoxy resin uniaxial glass roving composite. The system was composed of three basic subsystems shown schematically in Fig. 101.

- a. A hydraulic power supply unit comprised of a pump that operates to a maximum pressure of 10,000 psi and a 50 gal sump tank.

The high pressure side of the system operates at 3,000 psi. Figure 102 is a photograph of the entire system. The pump and sump tank are to the left. The 10,000 psi pump is regulated to the desired 3,000 psi level by means of a pressure relief bypass valve. At 3,000 psi, the pump output is approximately 5 gpm. This pressure flow rate is compatible with all other components of the system. The sump provides a reservoir for hydraulic oil as the demand changes throughout a test. It should be mentioned that there is a very important aspect of holding reserve oil in a container such as this. With the large amount of energy placed in the oil by the pump and no efficient means to dissipate this energy other than producing heat, the oil returns to the sump with its temperature increased. Oil in the elevated temperature state is not conducive to proper lubrication of the pump in operation. The viscosity of the oil is reduced to such a point that the lubricating film that generally

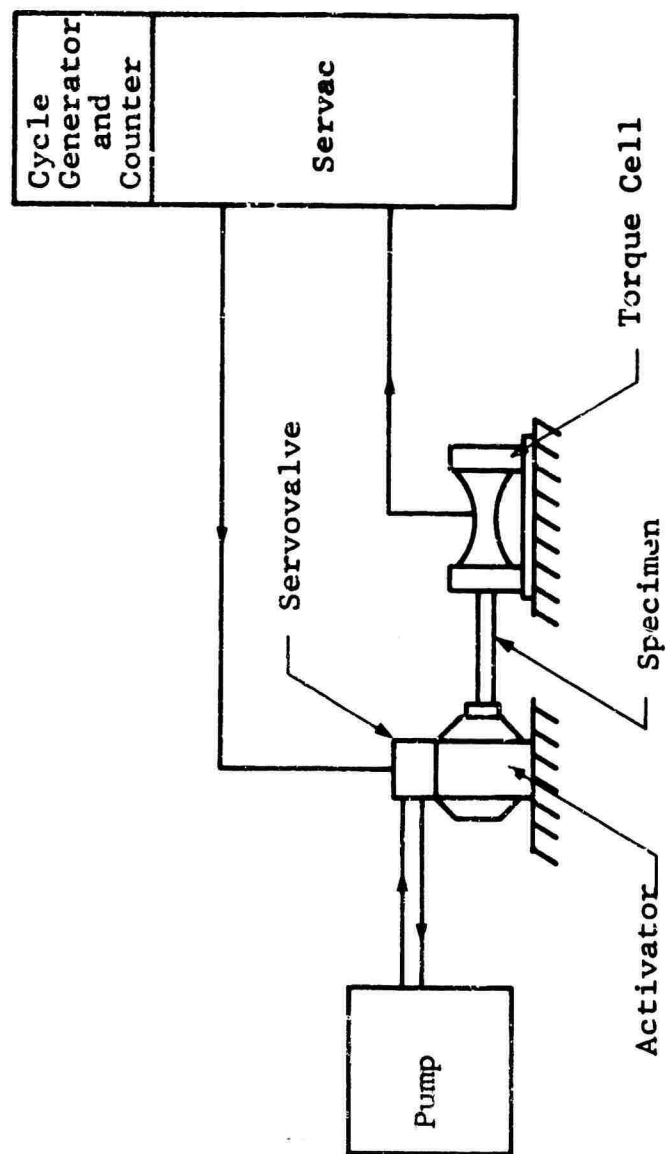


Fig. 101 SCHEMATIC OF TORSION FATIGUE EQUIPMENT

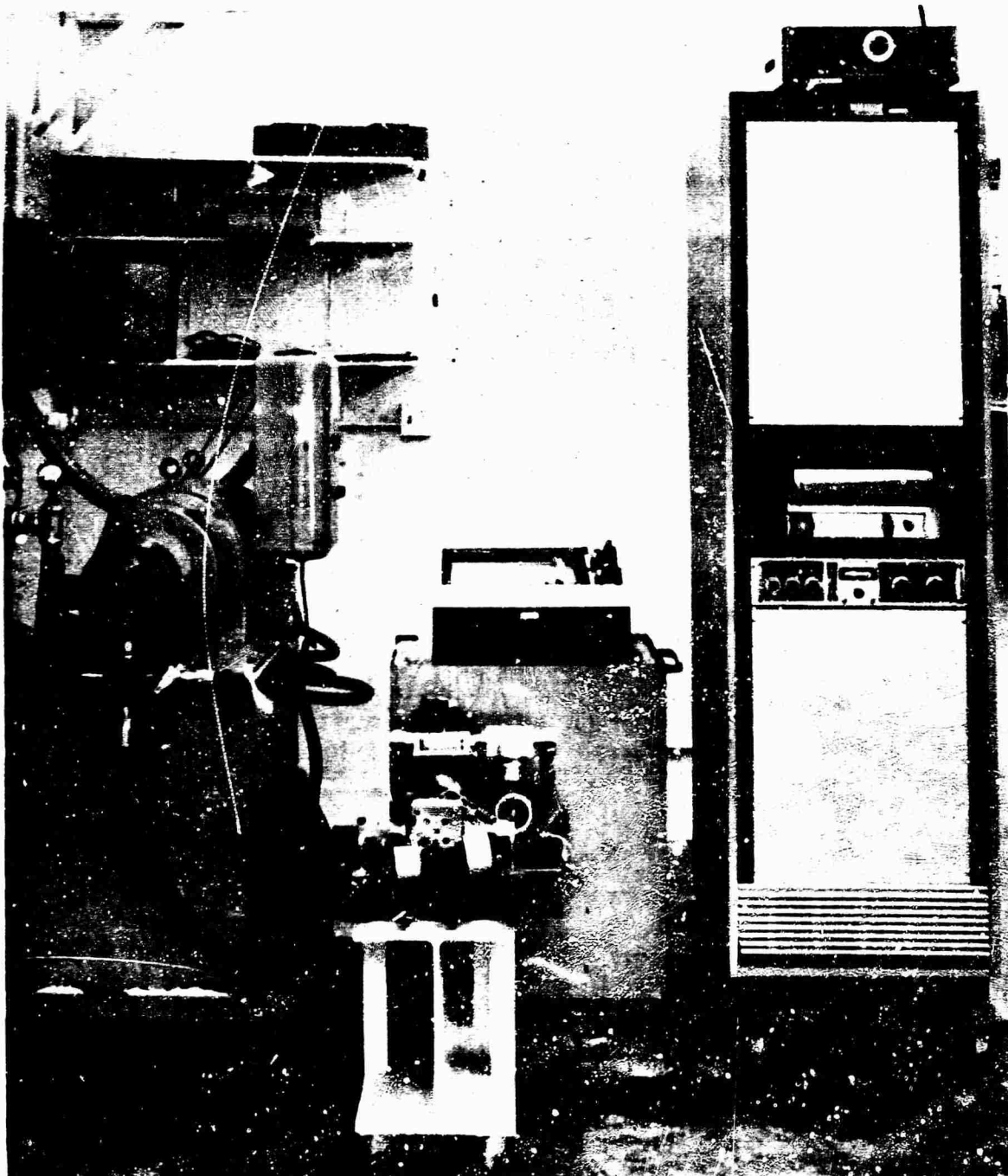


Fig. 102 POWER SUPPLY, TEST STANDARD PRIME MOVER, AND SERVAC CONTROL SYSTEM FOR HYDRAULIC-MECHANICAL TORSIONAL FATIGUE OF EPOXY-GLASS COMPOSITES

added to the sump. Turns of copper tubing may be placed into the tank and cold water circulated through the tubing to remove the heat that would otherwise build up in the tank. A large volume of reserve oil then increases the efficiency of such a heat exchange system.

- b. A prime mover connected to one end of a test specimen and a load sensing member attached to the other end compose the second subsystem.

The prime mover of the torsion testing machine is a rotary actuator. The actuator is constructed with vanes of a fixed area inside a pressure tight housing. Figure 103 is a 3/4 top view of the actuator, specimen, and load frame. A differential pressure is applied between the front and back surfaces of the vanes causing motion of a splined shaft which extends from the pressure housing. To this rotating shaft, a specimen grip is attached. The material being investigated is fabricated into a specimen as shown in Fig. 104 to be held and tested for both static and fatigue evaluation. The other end of the test sample is fixed to a load measuring structure, a statically indeterminate frame used to resist the moment applied by the actuator. Electrical resistance foil strain gages are affixed to the horizontal members of the frame and serve as the load monitoring sensor. The load resisting frame and the actuator housing are both bolted to a common base plate that serves as the plane of reference. The plate was designed with a stiffness factor that would not allow the base to rotate more than 0.01 percent of the total rotation in the system.

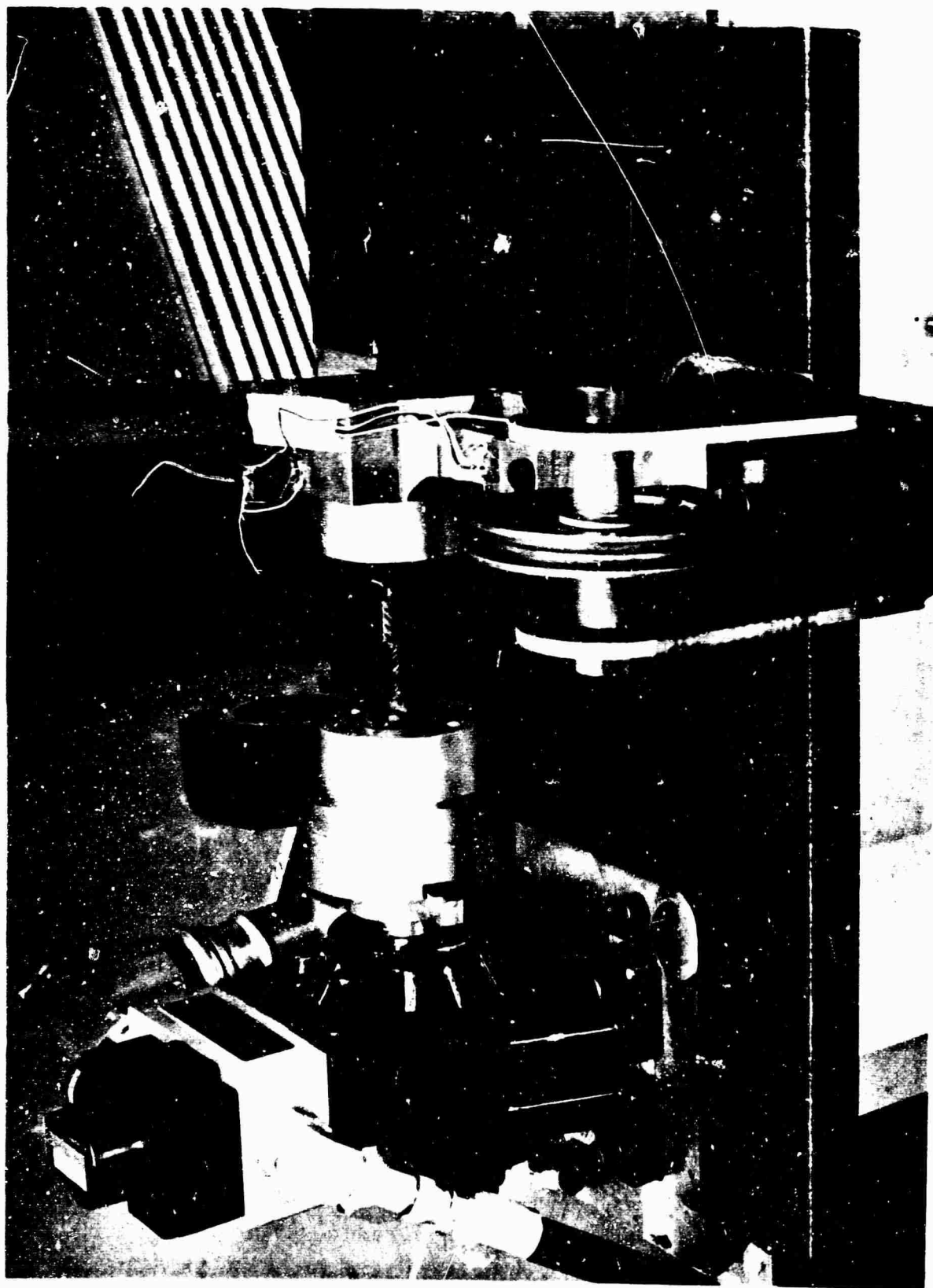


Fig. 103 ACTUATOR TEST SPECIMEN AND LOAD FRAME - TORSIONAL FATIGUE OF EPOXY-GLASS COMPOSITE



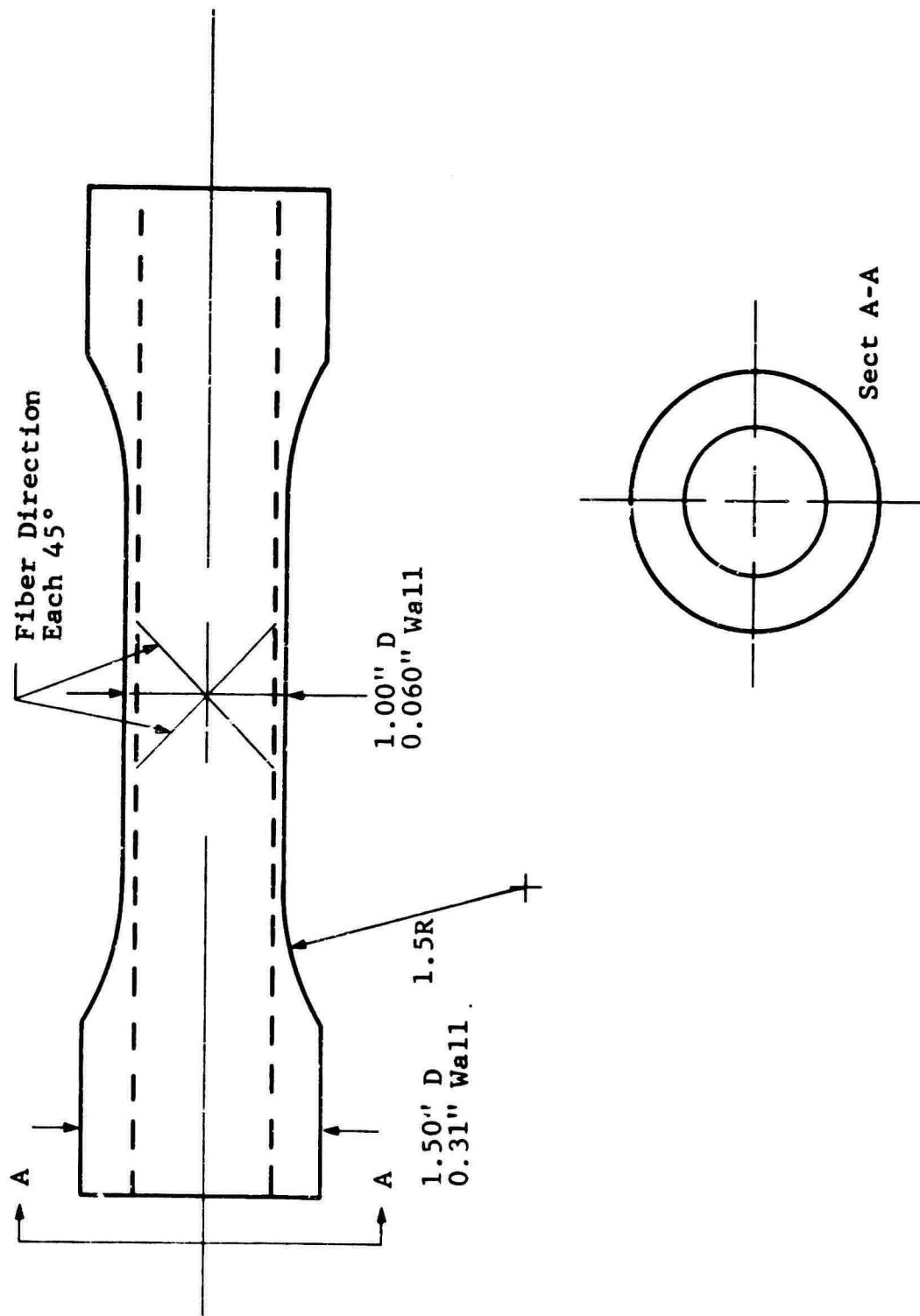


Fig. 104 EPOXY-WOVEN GLASS ROVING COMPOSITE TORSIONAL SPECIMEN

- c. A control unit that monitors and regulates the load in the specimen as the test is in progress is the third subsystem.

The last and probably most important system is the servo-hydraulic control unit. This unit can be broken down into four basic stages.

Stage 1 A differential output signal amplified to drive a servo-control valve.

Stage 2 An electro-hydraulic servo-valve that regulates the oil to drive the actuator.

Stage 4 A generated control signal of the desired frequency of amplitude for the test program of the specimen.

The actual servo-control unit which houses the control signal generator and the differential output signal amplifier is composed of three modules.

Module 1 An input module that acts as a signal conditioning unit between the load sensing element and the differential amplifier. In addition to this, it conditions the signal between the control signal generator and the same differential amplifier.

Module 2 A differential amplifier that compares and puts out an electrical pulse proportional to the difference between the control signal and the feedback.

Module 3 A control signal generator that creates a signal of the same magnitude as the feedback device.

## 2. Calibration of the Hydraulic-Mechanical Torsion Equipment

To obtain a meaningful calibration of the system, a dead weight loading arrangement is used. In order to impart pure moment to the resisting frame, a jig was used that loads the frame with parallel forces in opposite directions. Figure 105 shows the jig with the weights in position.

The feedback signal produced by the strain gages attached to the load resisting frame is calculated from the following relations:

The strain  $E$  on the arm is

$$E = \frac{M}{SE}$$

This strain is also related to the input and output voltages as follows:

$$E = \frac{E_o}{FV}$$

Where

- $M$  = moment of structure
- $S$  = section modulus of member
- $E$  = modulus of elasticity
- $E_o$  = output voltage from strain gages
- $F$  = gage factor
- $V$  = input voltage to strain gages

The moment is then determined at the point where the strain gages are affixed to the arm and this moment, and consequently, the deliverable torque is related directly to the strain gage output signal. The signal can be monitored as in the calibration setup or used as the servac control during actual testing.

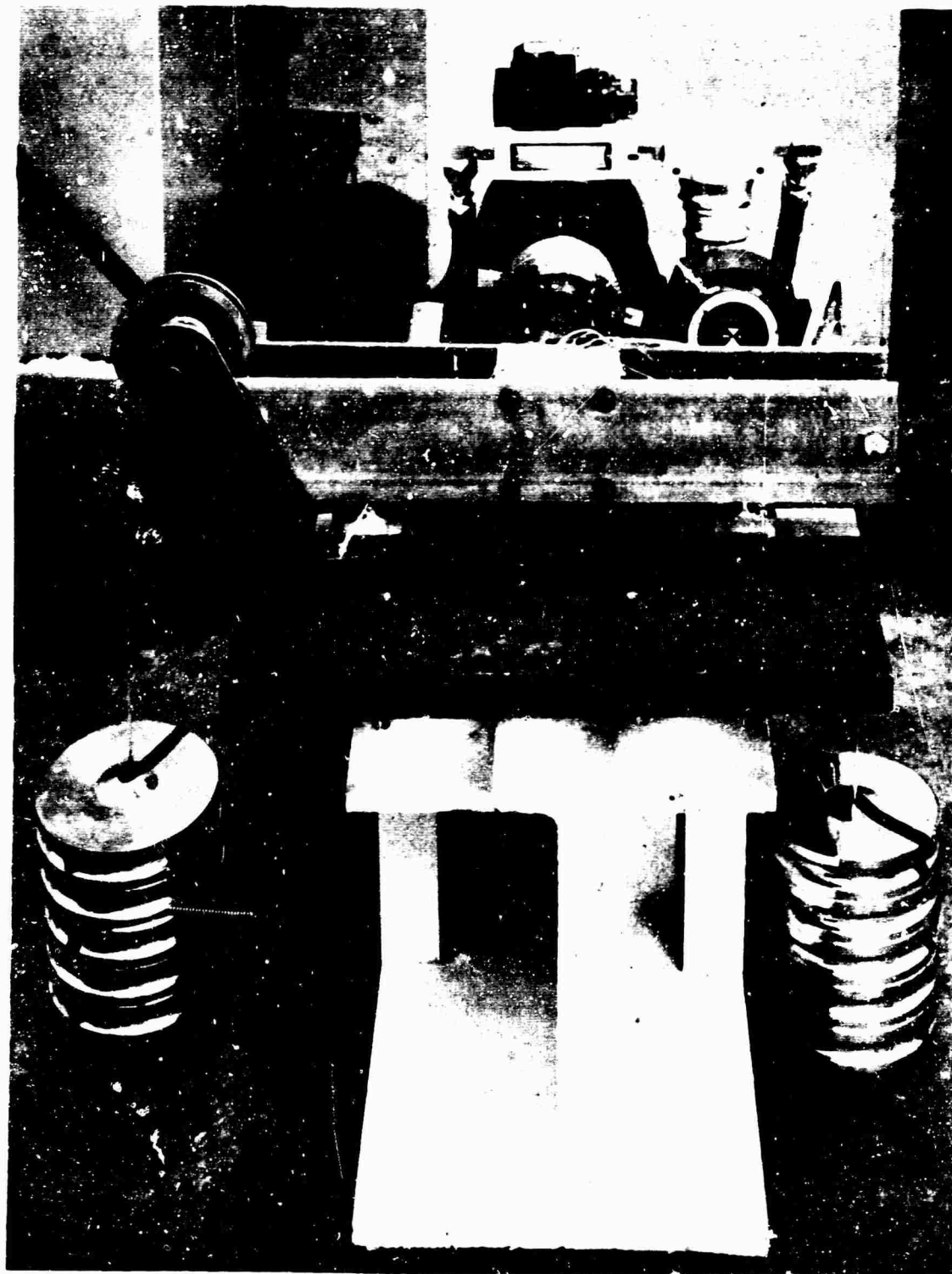


Fig. 105 DEAD WEIGHT CALIBRATION SYSTEM FOR TORSIONAL FATIGUE SYSTEM

## REFERENCES

1. Peterson, R. E., Stress Concentration Design Factors, John Wiley and Sons, 1953, p. 66.
2. Findley, W. N. and Worley, W. J., "The Elevated Temperature Creep and Fatigue Properties of a Polyester Glass Fabric Laminate," SPE Journal, April 1951.
3. Werren, F., Fatigue of Sandwich Construction for Aircraft, FPL Report 1559-J, April 1952.
4. Boller, K. H., Fatigue Tests of Glass-Fabric-Base Laminates Subjected to Axial Loading, FPL Report No. 1823, 1952 (also reviewed 1958).
5. Freas, A. D., "Effect of Preloading and Fatigue on Mechanical Properties of Glass-Cloth Plastic Laminates," Trans ASME, May 1953.
6. Boller, K. H., Supplement to Fatigue Tests of Glass-Fabric-Base Laminates Subjected to Axial Loading, FPL Report 1823-A, April 1954, and reviewed May 1960.
7. Breunich, T. R., "Fatigue Testing Fixtures," Product Engineering, June 1954.
8. Werren, F., Supplement to Fatigue Tests OC Glass Fabric Base Laminates Subjected to Axial Loading, FPL Report No. 1823-B, August 1956.
9. Boller, K., Fatigue Properties of Various Glass-Fiber-Reinforced Plastic Laminates, WADC TR-55-389, 1956.
10. Lazar, L. S., "Accelerated Fatigue of Plastics," ASTM Bulletin, February 1957.
11. Boller, K. H., "Fatigue Properties of Fibrous Glass-Reinforced Plastic Laminates Subjected to Various Conditions," Modern Plastics, June 1957.
12. Hooper, R. C., "Molding Finish Interactions in Fatigue of Glass-Reinforced Polyester Resins," Plastics Technology, August 1957.
13. Calvert, N. G., "Fatigue Tests on Glass-Fibre Reinforced Plastics," 1957.
14. Fried, N., Fatigue Strength of Reinforced Plastics, Proc. 12th Annual SPI Conference, RPD Section 5-A, 1957.

15. Boller, K. H., Fatigue Properties of Glass-Fibre-Reinforced Plastic Laminates Subjected to Various Conditions, Proc. 12th Annual SPI Meeting, Section 5-B, 1957.
16. Pusey, B. B., Flexural Fatigue Strengths of Reinforced Thermosetting Laminates, Proc. 12th Annual SPI Meeting, Section 5-C, 1957.
17. Nara, H. R., Some Fatigue Characteristics of Glass-Reinforced Plastics, Proc. 12th Annual SPI Meeting, Section 5-D, 1957.
18. Lazar, L. S., Accelerated Fatigue of R. P., Proc. 12th Annual SPI Meeting Section 5-E, 1957.
19. Stevens, G. H. and Boller, K. H., Effect of Type of Reinforcement on Fatigue Properties of Plastic Laminates, WADC TR 59-27, Sept. 1958, Reprint and May 1959.
20. Kimball, K. E., Supplement to Fatigue Tests of Glass-Fabric-Base-Laminates Subjected to Axial Loading - Effect of Notches, FPL Report No. 1823-C, 1958.
21. Freudenthal, A. M., Fatigue Sensitivity and Reliability of Mechanical Systems, Especially Aircraft Structures, WADD 61-53, July 1961.
22. Stevens, G. H., Fatigue Tests of Phenolic Laminates at High Stress Levels and Elevated Temperature, FPL Report 1884, August 1961.
23. Keer, L. and Lazar, B. J., Damping and Fatigue Properties of Sandwich Configurations in Flexure, ASD TR 61-646 Nov. 1961.
24. Stevens, G. H., Fatigue Tests of Phenolic Laminates Reinforced with Unwoven Glass Fibers, ASD-TDR-62-464, 1962.
25. Crichlow, W. J., Young, L., Melcor, M. A., An Engineering Evaluation of Methods for the Prediction of Fatigue Life in Airframe Structures, ASD-TR-61-434, March 1962.
26. Peterson, G. P., Engineering Properties of High-Modulus Reinforced Plastics, Proc. 17th Annual SPI Conference, RPD, Section 1-A, 1962
27. Hagerup, E., Flexural Fatigue Testing of Polyesters, Proc. 17th Annual SPI Meeting, Section 1-C, 1962.
28. Pflederer, F. R., Cycle Pressure Testing of Reinforced Plastic Pipe, Proc. 17th Annual SPI Meeting, Section 1-D, 1962.

29. Fatigue Strength of Fiberglass Plastics, Translation of Russian Text, 1962.
30. Palermo, P. M., Cyclic Loading Tests of Two Glass-Reinforced Plastic Cylinders, DTMB Report 1653, S-F013-01-03, Nov. 1962.
31. Boller, K. H., Resume of Fatigue Characteristics of Reinforced Plastic Laminates Subjected to Axial Loading, ASD-TDR-63-768, July 1963.
32. Cote, M. J., Structural Design for Accoustical Fatigue, ASD-TDR-63-820, October 1963.
33. Anderson, J. A., McCarthy, J. A., Prepare Reinforced Plastics in Fatigue Applications, Proc. 18th Annual SPI Conference, RPD, Section 8-C, 1963.
34. Broutman, L. J., Failure Mechanisms for Filament Reinforced Plastics Subjected to Static Compression Creep and Fatigue, Proc. 19th Annual SPI Conference, RPD Section 9-L, 1963.
35. Cornish, R. H., Nelson, H. R., Broutman, L. J., Abbott, B. W., An Investigation of Material Parameters Influencing Creep and Fatigue Life in Filament Wound Laminates, 6th Quarterly Progress Report, December 1963, Contract No. 6S 86461.
36. Stevens, G. H., Fatigue Strength of Phenolic Laminates from 1 to 10 Million Cycles of Repeated Load, FPL Report 027, January 1964.
37. Boller, K. H., Effect of Mean Stresses on Fatigue Properties of Plastic Laminates Reinforced with Unwoven Glass Fibers, ML-TDR-74-86, June 1964.
38. Cornish, R. H., Nelson, N. R., and Dally, J. W., Compressive Fatigue and Stress Rupture Performance of Fiber-Reinforced Plastics, Proc. 19th Annual Technical and Management Conference RPD, Section 1-E, January 1964.
39. Anderson, R. C., Compilation and Analysis of Test Data on Fiberglass-Reinforced Plastics, TRECOM TR 64-9, March 1964.
40. Cornish, R. H., Abbott, B. W., Cole, C. K., An Investigation of Material Parameters Influencing Creep and Fatigue Life in Filament Wound Laminates, IITRI Final Report No. M251, Contract No. NObs 86461, May 1964.
41. Cornish, R. H., Abbott, B. W., Cole, C. K., Effect of Cycle Profile on the Biaxial Compressive Fatigue Performance of Filament Wound Laminates, IITRI Project No. M6081, Report Contract NObs 90329, August 1964.

42. Boller, K. H., Effect of Precyclic Stresses on Fatigue Life of Plastic Laminates, ML-TDR-64-168, September 1964.
43. Nelson, H. R., Effect of Environment on Uniaxial Compressive Fatigue Performance of Glass Filament Reinforced Plastic Laminates, IITRI Project M6081, Contract No. NObs 90329, November 1964.
44. Davis, J. W., McCarthy, J. A., Schurb, J. N., "The Fatigue Resistance of Reinforced Plastics," Materials in Design Engineering, December 1964.
45. Wilson, F. M., Development of Fatigue-Resistant Filament-Wound Emergency Air Storage Bottles, Proc. 19th Annual Technical and Management Conference, RPD, Section I-E, 1964.
46. Meyers, N. C., Lee, G. D., Investigation of Structural Problems with Filament-Wound Deep Submersibles, Proc. 19th Annual Technical and Management Conference RPD, Section 9-F, 1964.
47. Brink, N., Mechanical Behavior of Reinforced Plastics at Cryogenic Temperatures, Proc. Soc. Plastics Engineers, 20th Annual Technical Conference, Section 15-2, 1964.
48. Outwater, J. O., Effect of Repeated Loading on Filament Wound Internal Pressure Vessels, Proc. 20th Annual SPE Convention, Section 19-4, 1964.
49. Young, R. E., Filament Wound Structures, Proc. 67th Annual Meeting ASTM, June 1964.
50. Boller, K. H., Fatigue Strength of Unwoven S-Glass Laminates, ML-TR-64-403, 1965.
51. Boller, K. H., "List of Reports on Fatigue Properties of Plastic Laminates," January 12, 1965.
52. Shibley, A. M., Winans, R. R., "Bibliography of Fatigue Properties of Fiberglass Reinforced Plastics," Plastech, May 1965.
53. Abbott, B. W., Cornish, R. H., Cole, C. K., Effect of Cycle Profile on the Biaxial Compressive Fatigue Performance of Filament Wound Laminates, IITRI Report No. M6081, Contract No. NObs 6S 90329, January 1965.
54. Cole, C. K., Cornish, R. H., Abbott, B. W., Effect of Cumulative Damage on the Biaxial Compressive Fatigue Performance of Filament Wound Laminates, 1st QPR Extension Phase, June 1965.



55. "Reinforced Plastic is the Superior Material for Fatigue Applications," Reinforced Plastics, May-June 1965.
56. Cole, C. K., Cornish, R. H., Elliott, J. P., Effect of Cumulative Fatigue Damage on the Biaxial Compressive Fatigue Performance of Filament Wound Laminates, IITRI Project No. M6081, Report No. 4, August 1965.
57. Nordby, G., Cusiman, W. C., Bert, C. W., Dynamic Elastic, Damping and Fatigue Characteristics of Fiberglass-Reinforced Sandwich Structure, USA AVLABS Tech. Report 65-60, October 1965.
58. Kinna, M. A., Prosen, S. P., A Multiaxial Fatigue Test for Evaluation of Plastic Composite Materials, NOLTR 65-191, February 1966.
59. Cole, C. K., Zoiss, M. H., Effect of Cumulative Damage on the Biaxial Compressive Fatigue Performance of Filament Wound Laminates, IITRI Project No. M6081, Report No. 6, February 1966.
60. Boller, K. H., Fatigue Characteristics of two New Plastic Laminates Reinforced with Unwoven "S" Glass Fibers Under Cyclic Axial or Shear Loading, AFML-TR-66-54, May 1966.
61. Nordby, G. M., Crisman, W. C., "Fatigue Characteristics of an R. P. Sandwich Structure," Modern Plastics, June 1966.
62. Cole, C. K., Effect of Cumulative Damage on the Biaxial Compressive Fatigue Performance of Filament Wound Laminates, IITRI Program M6081. Report No. 7, July 1966.
63. Boller, K. H. Effect of Single Step Change in Stress on Fatigue Life of Plastic Laminates Reinforced with Unwoven "E" Glass Fibers, AFML-TR-66-220, September 1966.
64. Pinckney, R., et. al., Attachment Techniques and Dynamic Properties of High Modulus Filament Reinforced Composites, Ist Q.P.R. on Contract AF-33-(615)-3319, Boeing Report D8-0340, March 1966.
65. Hofer, K. E., "Fatigue Testing of Boron Reinforced Composite Materials," in Application of Advanced Fibrous Reinforced Composite Materials to Airframe Structures, Vol. II, AFML-TR-66-313, September 1966.
66. Miner, M. A., "Cumulative Damage in Fatigue," Jour. Appl. Mech., Vol. 12, No. 3, September 1945.

67. Corten, H. T. and Dolan, T. J., Cumulative Fatigue Damage. Proc. Int. Conf. on Fatigue of Metals, Session 3, Paper Z, IME, London 1956.
68. Freudenthal and Heller, On Stress Interaction in Fatigue and a Cumulative Damage Rule - Part I - 2024 Al and 4340 Steel, WADC T.R. 53-69, June 1958,
69. Grover, H. J., Cumulative Damage Theories, (In Proceedings of the Symposium on Fatigue of Aircraft Structures) WADC Tech. Report 49-507, pp 207-225, August 1959.
70. Valluri, R. A., A Theory of Cumulative Damage in Fatigue, Falcit SM 61-2 Douglas Aircraft Company.
71. Shanley, R. R., A Theory Fatigue Based on Unbonding During Reversed Slip, The Rand Corporation. Report P-350-1, 11 November 1952.
72. Liu, H. W. and Corten, H. T., Fatigue Damage During Complex Stress Histories, NASA TN D-256, November 1959.
73. Grover, H. J., Gordon, S. A. and Jackson, L. R., The Fatigue of Metals and Structures, Bureau of Naval Weapons, 1954.
74. Mordfin, L. and Halsey, N., Programmed Maneuver - Spectrum Fatigue Tests of Aircraft Beam Specimens, ASTM STP No. 338, 1962.
75. Rosenfeld, M. S., Aircraft Structural Fatigue Research in the Navy, ASTM STP No. 338, 1962.
76. Freudenthal, A. M. and Heller, R. A., On Stress Interaction in Fatigue and a Cumulative Damage Rule, Jour. of the Aero-Space Sciences, 1959.

Unclassified

Security Classification

DOCUMENT CONTROL DATA - R&D		
(Security classification of title, body of abstract and indexing annotation must be entered when the overall report is classified)		
1. ORIGINATING ACTIVITY (Corporate author) IIT Research Institute 10 W. 35th St., Chicago, Ill.		2a. REPORT SECURITY CLASSIFICATION U
		2b. GROUP N/A
3. REPORT TITLE "An Investigation of the Fatigue and Creep Properties of Glass Reinforced Plastics for Primary Aircraft Structures"		
4. DESCRIPTIVE NOTES (Type of report and inclusive dates) Final Report May 1, 1965 through December 1, 1966		
5. AUTHOR(S) (Last name, first name, initial) Hofer, K.E., Jr. Clsen, E.M.		
6. REPORT DATE April 1967	7a. TOTAL NO. OF PAGES 236	7b. NO. OF REFS 76
8a. CONTRACT OR GRANT NO. NOW-65-0425-F	9a. ORIGINATOR'S REPORT NUMBER(S) M6104	
b. PROJECT NO.	9b. OTHER REPORT NO(S) (Any other numbers that may be assigned this report) N/A	
c.		
d.		
10. AVAILABILITY/LIMITATION NOTICES Distribution of this report is unlimited.		
11. SUPPLEMENTARY NOTES		12. SPONSORING MILITARY ACTIVITY Naval Air Systems Command Washington D.C., 20360
13. ABSTRACT <p>Fatigue of glass reinforced epoxy composite materials is examined from several points of view. High cycle and low cycle fatigue and the effects of frequency, moisture, and state of stress on the fatigue life are included. The effects of creep and strain rate are also studied with a view toward their effect on fatigue life. Cumulative fatigue damage studies include nondestructive ultrasonic techniques applied to damage levels and application of phenomenological theory to the results of two stress level testing. Appendices accompanying the report include 1) a survey of GRP fatigue literature, and 2) a survey of existing cumulative fatigue damage theories with potential application to GRP. Two types of reinforcement were used, uniaxial roving and glass cloth.</p>		

DD FORM 1473  
1 JAN 64

Unclassified

Security Classification

Unclassified

Security Classification

14 KEY WORDS	LINK A		LINK B		LINK C	
	ROLE	WT	ROLE	WT	ROLE	WT
Composites, Fatigue, Cumulative Damage Creep, Strain Rate, Environmental Effects						

**INSTRUCTIONS**

**1. ORIGINATING ACTIVITY:** Enter the name and address of the contractor, subcontractor, grantee, Department of Defense activity or other organization (corporate author) issuing the report.

**2a. REPORT SECURITY CLASSIFICATION:** Enter the overall security classification of the report. Indicate whether "Restricted Data" is included. Marking is to be in accordance with appropriate security regulations.

**2b. GROUP:** Automatic downgrading is specified in DoD Directive 5200.10 and Armed Forces Industrial Manual. Enter the group number. Also, when applicable, show that optional markings have been used for Group 3 and Group 4 as authorized.

**3. REPORT TITLE:** Enter the complete report title in all capital letters. Titles in all cases should be unclassified. If a meaningful title cannot be selected without classification, show title classification in all capitals in parentheses immediately following the title.

**4. DESCRIPTIVE NOTES:** If appropriate, enter the type of report, e.g., Interim, progress, summary, annual, or final. Give the inclusive dates when a specific reporting period is covered.

**5. AUTHOR(S):** Enter the name(s) of author(s) as shown on or in the report. Enter last name, first name, middle initial. If military, show rank and branch of service. The name of the principal author is an absolute minimum requirement.

**6. REPORT DATE:** Enter the date of the report as day, month, year, or month, year. If more than one date appears on the report, use date of publication.

**7a. TOTAL NUMBER OF PAGES:** The total page count should follow normal pagination procedures, i.e., enter the number of pages containing information.

**7b. NUMBER OF REFERENCES:** Enter the total number of references cited in the report.

**8a. CONTRACT OR GRANT NUMBER:** If appropriate, enter the applicable number of the contract or grant under which the report was written.

**8b, 8c, & 8d. PROJECT NUMBER:** Enter the appropriate military department identification, such as project number, subproject number, system numbers, task number, etc.

**9a. ORIGINATOR'S REPORT NUMBER(S):** Enter the official report number by which the document will be identified and controlled by the originating activity. This number must be unique to this report.

**9b. OTHER REPORT NUMBER(S):** If the report has been assigned any other report numbers (either by the originator or by the sponsor), also enter this number(s).

**10. AVAILABILITY/LIMITATION NOTICES.** Enter any limitations on further dissemination of the report, other than those imposed by security classification, using standard statements such as:

- (1) "Qualified requesters may obtain copies of this report from DDC."
- (2) "Foreign announcement and dissemination of this report by DDC is not authorized."
- (3) "U. S. Government agencies may obtain copies of this report directly from DDC. Other qualified DDC users shall request through \_\_\_\_\_."
- (4) "U. S. military agencies may obtain copies of this report directly from DDC. Other qualified users shall request through \_\_\_\_\_."
- (5) "All distribution of this report is controlled. Qualified DDC users shall request through \_\_\_\_\_."

If the report has been furnished to the Office of Technical Services, Department of Commerce, for sale to the public, indicate this fact and enter the price, if known.

**11. SUPPLEMENTARY NOTES:** Use for additional explanatory notes.

**12. SPONSORING MILITARY ACTIVITY:** Enter the name of the departmental project office or laboratory sponsoring (paying for) the research and development. Include address.

**13. ABSTRACT:** Enter an abstract giving a brief and factual summary of the document indicative of the report, even though it may also appear elsewhere in the body of the technical report. If additional space is required, a continuation sheet shall be attached.

It is highly desirable that the abstract of classified reports be unclassified. Each paragraph of the abstract shall end with an indication of the military security classification of the information in the paragraph, represented as (TS), (S), (C), or (U).

There is no limitation on the length of the abstract. However, the suggested length is from 150 to 225 words.

**14. KEY WORDS:** Key words are technically meaningful terms or short phrases that characterize a report and may be used as index entries for cataloging the report. Key words must be selected so that no security classification is required. Identifiers, such as equipment model designation, trade name, military project code name, geographic location, may be used as key words but will be followed by an indication of technical context. The assignment of links, rules, and weights is optional.

Unclassified

Security Classification